NUREG/CR-6822
BNL-NUREG-71355-2003

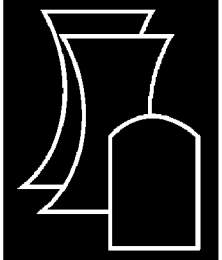

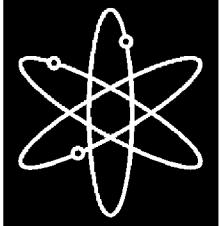

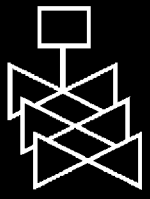

Collaborative Study of NUPEC Seismic Field Test Data for NPP Structures

Brookhaven National Laboratory

U.S. Nuclear Regulatory Commission
Office of Nuclear Regulatory Research
Washington, DC 20555-0001

NUREG/CR-6822
BNL-NUREG-71355-2003

Collaborative Study of NUPEC Seismic Field Test Data for NPP Structures

Manuscript Completed: June 2003
Date Published: June 2003

Prepared by
J. Xu, C. Costantino, C. Hofmayer

Brookhaven National Laboratory
Upton, NY 11973-5000

S. Ali, NRC Project Manager

Prepared for
Division of Engineering Technology
Office of Nuclear Regulatory Research
U.S. Nuclear Regulatory Commission
Washington, DC 20555-0001
NRC Job Code W6081

ABSTRACT

The Nuclear Power Engineering Corporation (NUPEC) conducted a multi-year test program for the Ministry of Economy, Trade and Industry (METI) of Japan to investigate different aspects of the soil-structure interaction (SSI) effect. The program, consisting of both field and laboratory tests, was developed to address various SSI aspects, including the dynamic cross interaction (DCI) effect on the seismic response of NPP structures built in close proximity to each other. The program also was performed to verify the adequacy of the available analytical tools for predicting the SSI effect. As part of collaborative efforts between the United States and Japan on seismic issues, the US Nuclear Regulatory Commission (NRC) and Brookhaven National Laboratory (BNL) participated in a program to apply the industry practice to predict the structural response to recorded earthquake events, including the DCI effect, and to interpret the observed data. The overall objectives of the US-Japan collaboration on the DCI issue were, through the exchange of mutual knowledge and useful information on the DCI test data, to gain valuable insights into understanding the complex phenomena and dynamic response mechanism of DCI effects under earthquake ground motions. Another objective was to validate, confirm, and capture the limitations of analytical methods or computer codes, which may lead to improvements of the existing analysis methods, and remove unnecessary conservatism in seismic design. BNL has completed its study of the field test data as provided by NUPEC. This report summarizes the BNL study and the insights drawn from the comparisons of the BNL analysis results and the NUPEC field recorded earthquake responses.

TABLE OF CONTENTS

TABLE OF CONTENTS

List of Figures

List of Figures (Cont'd)

List of Figures (Cont'd)

List of Figures (Cont'd)

List of Figures (Cont'd)

List of Figures (Cont'd)

List of Figures (Cont'd)

List of Figures (Cont'd)

List of Tables

EXECUTIVE SUMMARY

It is widely recognized that multiple structures built in close proximity exhibit different dynamic behaviors from those of a single structure under earthquake ground motions. With multiple structures involved, the dynamic cross interaction (DCI) effect through soils becomes a much more complex phenomenon. In 1994, the Nuclear Power Engineering Corporation (NUPEC) initiated a multi-year test program for the Ministry of Economy, Trade and Industry (METI) of Japan. The program, consisting of both field and laboratory tests, was developed to address the DCI effect on the seismic response of NPP structures built in close proximity to each other. The NUPEC program provided the first large-scale experimental data for studying the DCI phenomenon and should prove to be of great value to the engineering community. The program also provided another opportunity to validate current analytical methods for evaluating the soil-structure interaction (SSI) effect on the seismic response of NPP structures.

The test site for the field tests was located in Aomori Prefecture in northern Japan, a region which experiences frequent seismic activities. Large-scale models with dynamic characteristics similar to typical NPP structures were constructed on soils representative of actual NPP sites. The DCI field test considered three building construction conditions: a) a single reactor as reference for comparison purposes, b) closely spaced twin reactors, and c) a reactor and a turbine building in close proximity to each other. The field tests also consider both excavated and embedded foundations and two types of loading conditions: 1) forced vibrations and 2) observations of the structural response to real earthquake ground motions. The latter was accomplished by pre-installed seismometers in the structures and free field. To complement the field tests, laboratory tests were also performed by NUPEC using a shaking table and smaller scaled DCI soil-structure models. The laboratory tests were used by NUPEC for detailed investigation of DCI effects under strong earthquake motion, which could not be achieved in the field tests.

As part of collaborative efforts between the United States and Japan on seismic issues, the US Nuclear Regulatory Commission (NRC) and Brookhaven National Laboratory (BNL) participated in a program to apply the industry practice to predict the structural response to recorded earthquake events, including the DCI effect, and to interpret the observed data. The overall objectives of the US-Japan collaboration on the DCI issue were, through the exchange of mutual knowledge and useful information on the DCI test data, to gain valuable insights into understanding the complex phenomena and dynamic response mechanism of DCI effects under earthquake ground motions. Another objective was to validate, confirm, and capture the limitations of analytical methods or computer codes, which may lead to improvements of the existing analysis methods, and remove unnecessary conservatism in seismic design.

The BNL study consisted of two parts: 1) free-field analyses, and 2) SSI response analyses. Four elements were included in the free-field analyses including: 1) Arias intensity analysis, 2) low-strain best estimate soil profile analysis, 3) selection of the appropriate strain degradation model, and 4) probabilistic site identification analysis to determine the strain dependent soil profiles and the surface input motions for the SSI response analyses. BNL has applied the current practice for performing free-field analyses and correlated the analytical results with the recorded data provided by NUPEC. The analyses documented in this report have generally demonstrated the conservatism of the current practice.

The SSI response analyses performed in this study covered three structural configurations, which include the single reactor building, twin reactor buildings and reactor-turbine buildings. BNL analyzed these configurations for both the excavated and embedded conditions. By applying the

current approach for the SSI analyses of the NPP structures, BNL performed the seismic response calculations in terms of the mean, mean minus sigma and mean plus sigma values to account for uncertainties in the soil properties (sigma represents the lognormal standard deviation of the soil profile in terms of shear modulus, G_s). As described in this report, the BNL SSI response results either closely matched or exceeded the recorded responses, which further substantiated the conservatism in the analytical procedures as many have suggested. Based on the BNL analyses and comparisons between the analysis results and the recorded earthquake responses, the following conclusions were drawn:

1. The BNL analyses have demonstrated the application of the current approach for addressing uncertainties for SSI analyses. The consideration of soil uncertainties in the SSI analyses is necessary to assure conservatism in the computed structural response.

2. Most of the earthquake data used in this study involved recorded earthquake motions in the range of 0.01g-0.03g and for these earthquakes, the BNL analyses generally enveloped the in-structure response spectra generated from the test data for all configurations.

3. Two (2) moderate size earthquakes: No. 63 (0.1g) and No. 89 (0.13g) were analyzed for both the excavated and embedded single-reactor model (field test data for other configurations were not available). For the embedded case, the analysis enveloped the in-structure response spectra generated from the test data for both No. 63 and No. 89. For the excavated case, the analysis enveloped the in-structure response spectra generated from the test data for No. 63, but did not envelop No. 89. However, by adjusting the soil property for the 0.5m thin layer under the basemat, the analysis was able to match closely No. 89. The effect of the disturbed soil in close proximity to the foundation was found to be an important aspect in the SSI analysis for the excavated cases.

4. Based on the comparison of recorded spectral data, Dynamic Cross Interaction (DCI) effects were observed to be important. For the earthquake data studied, some show that the DCI effects cause amplification in response with respect to the single reactor configuration, while some suggested a reduction of response when compared with the single reactor configuration. The analytic results generally showed conservative estimates of the DCI effect when considering soil uncertainty in the calculations.

5. An increase in frequency at the spectra peak was also observed from the recorded motions with the DCI effect. No similar shift in frequency was noted in the computations.

6. The exceedances caused by the DCI effect were lower for the fully embedded configuration as compared to the excavated configuration.

7. It is not clear that current approaches to SSI response analysis adequately capture potential DCI effects. Additional studies may be required to investigate the impact of this effect on peak structural response.

Based on the BNL analyses, the evaluation of the NUPEC recorded data and the conclusions described above, the following recommendations are made:

1. In light of the smaller earthquake data investigated in this study, the issues related to the DCI effect need to be confirmed for larger magnitude earthquakes comparable to the SSE

level for typical NPP safety related structures, systems, and components. The U.S.-Japan collaboration effort should be continued to investigate the availability of other relevant SSI data from strong earthquakes and simulation experiments such as shaking table tests, as well as the possibility of data from future blast tests at a strip mine.

2. The investigation performed in this study indicated the importance of the DCI effect on seismic response, especially the findings concerning the amplifications induced by the DCI effect as compared with situations without the DCI effect. It is recommended that the implication of the findings of this study regarding the DCI effect be assessed with respect to the industry practice and the regulatory guidelines for performing SSI analyses.

3. As the results of this study indicated, some significant influences of the DCI effect on the SSI calculations may be associated with inherent uncertainties in structural properties which may not be adequately captured by the analytical models; e.g, the frequency shift in the twin reactor response. It is recommended that further study be performed to investigate the modeling aspects of SSI analysis for treating adjacent structural effects. As discussed in Section 5.4, the higher mode relative responses between the two identical adjacent structures may be responsible for the frequency shift as seen in the recorded data. Small uncertainty in the analytical modeling parameters (mass, cg location, etc.) may need to be introduced into the analysis to determine if such higher mode response is significant.

ACKNOWLEDGMENTS

The research program described in this report was sponsored by the Office of Nuclear Regulatory Research of the U.S. Nuclear Regulatory Commission. The authors would like to express their gratitude to Dr. Syed Ali and Dr. Andrew Murphy, NRC Project Managers, for the technical and administrative support they have provided in performing this study.

This research program was performed as part of the Implementing Agreement Between the U.S. Nuclear Regulatory Commission and the Nuclear Power Engineering Corporation of Japan in the Area of Seismic Engineering Research. This agreement is an item of the Implementing Arrangement Between the United States Nuclear Regulatory Commission and the Nuclear and Industrial Safety Administration of Japan for Cooperation in the Field of Nuclear Regulatory Matters and Nuclear Safety Research and Development (1997-).

All of the test results and information about the test models included in this report were provided by NUPEC and are greatly appreciated. The authors especially thank Dr. Yoshio Kitada, Program Manager of the Seismic Engineering Center of NUPEC, for his support and technical guidance throughout the collaborative study. The authors also wish to acknowledge the helpfulness and cooperation provided by Mr. Kazuhiro Kusama of NUPEC, Mr. Atushi Suzuki and Dr. Yukio Naito of Kajima Corporation and Mr. Tsutomu Hirotani of Shimizu Corporation.

The authors also express special thanks to Ms. Susan Signorelli for her secretarial help throughout this program and in the preparation of this report.

1. INTRODUCTION

1.1 Background

It is widely recognized that multiple structures built in close proximity exhibit different dynamic behaviors from those of a single structure under earthquake ground motions. With multiple structures involved, the dynamic cross interaction (DCI) effect through soils becomes a much more complex phenomenon. In 1994, the Nuclear Power Engineering Corporation (NUPEC) initiated a multi-year test program for the Ministry of Economy, Trade and Industry (METI) of Japan. The program, consisting of both field and laboratory tests, was developed to address the DCI effect on the seismic response of NPP structures built in close proximity to each other. The NUPEC program provided the first large-scale experimental data for studying the DCI phenomenon and should prove to be of great value to the engineering community. The program also provided another opportunity to validate current analytical methods for evaluating the soil-structure interaction (SSI) effect on the seismic response of NPP structures.

The test site for the field tests was located in Aomori Prefecture in northern Japan, a region which experiences frequent seismic activities. Large-scale models with dynamic characteristics similar to typical NPP structures were constructed on soils representative of actual NPP sites. The DCI field test considered three building construction conditions: a) single reactor as reference for comparison purposes, b) closely spaced twin reactors, and c) a reactor and a turbine building in close proximity to each other. The field tests also consider both excavated and embedded foundations and two types of loading conditions: 1) forced vibrations and 2) observations of the structural response to real earthquake ground motions. The latter was accomplished by pre-installed seismometers in the structures and free field. To complement the field tests, laboratory tests were also performed by NUPEC using a shaking table and smaller scaled DCI soil-structure models. The laboratory tests were used by NUPEC for detailed investigation of DCI effects under strong earthquake motion, which could not be achieved in the field tests.

As part of collaborative efforts between the United States and Japan on seismic issues, the US Nuclear Regulatory Commission (NRC) and Brookhaven National Laboratory (BNL) participated in this program to apply the industry practice to predict the structural response to recorded earthquake events, including the DCI effect, and to interpret the observed data. The overall objectives of the US-Japan collaboration on the DCI issue were, through the exchange of mutual knowledge and useful information on the DCI test data, to gain valuable insights into understanding the complex phenomena and dynamic response mechanism of DCI effects under earthquake ground motions. Another objective was to validate, confirm, and capture the limitations of analytical methods or computer codes, which may lead to improvements of the existing analysis methods, and remove unnecessary conservatism in seismic design.

1.2 Scope and Objectives

The objectives of the NRC/BNL research activity in the US-Japan collaboration on DCI issues are: 1) to verify the current industry methods for performing soil-structure interaction analysis by comparing analysis results produced using the industry practice with the actual earthquake observation data provided by NUPEC, 2) to determine the technical significance of the NUPEC data related to the DCI effect on the overall methodology used for performing SSI analysis, and 3) to analyze and interpret the NUPEC test results and provide insights that can be clearly understood and utilized by NRC staff and stakeholders.

The DCI effect is a complex phenomenon, and to address such a phenomenon requires state-of-the-art methods and computer programs. As in typical SSI solutions, a two-step analysis is required to be performed: 1) free-field analysis, and 2) seismic response analysis including the DCI effect. This report describes the methods used and summarizes the results obtained from the free-field and seismic response analyses. The analyses results were compared to the field test data and did not attempt to address the laboratory test data.

The scope of the free-field analysis was to apply methods used by the nuclear industry to address issues related to free-field wave propagations, and to identify the in-situ soil properties, both the low-strain profile and the strain dependent modulus degradation relationships, which can produce the free-field response that best matches the recorded data supplied by NUPEC. Two locations were used to record the free-field response. These are referred to as the old and new free-field points, and the recorded data supplied by NUPEC were grouped accordingly. The BNL free-field analysis examined the recorded data associated with each free-field point separately, which lead to two different soil profiles.

The scope of the seismic response analyses was to apply the sub-structuring approach to performing the SSI analyses for the various structural configurations, and via comparisons with test data, to address the adequacy of the numerical method and also to address a variety of SSI issues. The sub-structuring method is a widely accepted approach by the nuclear industry for computing seismic responses of NPP structures including the SSI effects. It was also used for seismic predictions in the Taiwan (Lotung and Hualien) field test programs. The Taiwan tests involve a single quarter scale model reactor containment building with embedment. These tests addressed certain SSI issues such as embedment and SSI frequencies, but did not address issues related to adjacent building effect. In commercial nuclear power plants, the reactor building is usually constructed adjacent to other structures such as a turbine building and auxiliary building, and in some plants, two reactor containments may exist next to each other. Therefore, understanding the dynamic characteristics of the adjacent building effect (or DCI effect) and determining quantitatively the impact on the seismic response of a structure, especially NPP type structures, are important aspects which could improve and potentially advance the design and analysis techniques for NPP structures subjected to seismic loads.

The NUPEC field test program includes structural configurations of a single reactor building, two adjacent reactor buildings and a reactor building adjacent to a turbine building. For these test configurations, earthquake responses were recorded for a decade or so and for both embedded and excavated situations. Hence, these recorded earthquakes enable the study of the SSI phenomena related to the adjacent building interaction or the DCI effect, in addition to the traditional SSI effect such as embedment and SSI frequencies. Furthermore, recognizing that large uncertainties exist in the test data, the field soil properties, and the numerical models, the objective of the seismic response analyses is not to achieve a one-to-one match for the seismic responses; instead, the mean, and plus and minus one standard deviations (15^{th} and 84^{th} percentiles) responses are computed and compared with the recorded responses. Such an exercise could provide insights into the adequacy of the state of the practice in the seismic response analyses accounting for uncertainties in soil properties.

1.3 Report Organization

This report is organized in seven chapters. Chapter 2 describes the NUPEC field test program and the earthquake test data that was made available for the collaboration activities. Chapter 3 describes the analysis methods employed by BNL in this study. It discusses the methods used for the free-field analyses, including the use of Arias intensity to characterize energy transmission, the use of Fourier ratios with the Levenburg-Marquat non-linear least square fitting algorithm to predict the low strain best estimate soil profiles, and the probabilistic sampling method for developing the motion dependent soil profile. It also discusses the SASSI substructure method used for the SSI response. Chapter 4 presents the analysis of the free-field data. It discusses the examination of the free-field records using Arias intensity, the free-field analyses for determining the best estimate low strain soil profile, the basis for determining the soil modulus degradation relationships, and the probabilistic based strain-dependent soil profiles. Chapter 5 presents the SSI analysis of the NPP models to earthquake motions. Furthermore in Chapter 5, discussion is provided with respect to the potential DCI effect through comparisons of the SSI responses between multi-structure configurations and the single structure configuration. It describes the SSI models for the excavated and embedded structures and compares the SSI analysis results to the recorded earthquake motions. Chapter 6 summarizes the conclusions and recommendations from this study. Chapter 7 includes a complete listing of the references to this report.

2.0 DESCRIPTION OF NUPEC FIELD TEST PROGRAM

The Nuclear Power Engineering Corporation (NUPEC) of Japan has conducted a series of large-scale field tests for the Ministry of Economy, Trade and Industry (METI) of Japan to address various aspects of the soil-structure interaction (SSI) effect on the seismic response of nuclear power plant (NPP) structures. The experimental studies used scaled models of nuclear power plant buildings constructed on field sites typical of an actual NPP site. The following programs have been conducted since 1980:

1. Model Tests on Dynamic Interaction Between Reactor Building and Soil (1980-1986) (Iguchi, 1987).

2. Model Test on Embedment Effect of Reactor Building (1986-1994) (Nasuda, 1991).

3. Model Test on Dynamic Cross-Interaction Effects of Adjacent Structures (1994-2002) (Kitada, 2001).

The field tests for the second and third programs listed above were performed at the same site which is located in Aomori Prefecture in northern Japan as shown in Figure 2-1, a region which experiences frequent seismic activities. Large-scale models with dynamic characteristics similar to typical NPP structures were constructed on the soils at this site which are representative of actual NPP sites. The third program, which is the subject of this collaborative study, made use of some of the buildings from the second program. Some of the recorded earthquake motions from the second program were also made available for use in this collaborative study to investigate the embedment effect.

The Dynamic Cross-Interaction (DCI) tests were carried out by NUPEC as an 8-year project from Japanese fiscal year 1994 to 2002 (each fiscal year in Japan starts on April 1 of that year). The tests considered three building construction conditions: a) single reactor as reference for comparison purposes, b) closely spaced twin reactors, and c) a reactor and a turbine building in close proximity to each other. The field tests also considered both excavated and embedded foundations and two types of loading conditions: 1) forced vibrations and 2) observations of the structural response to real earthquake ground motions. The latter was accomplished by pre-installed seismometers in the structures and free field. Figure 2-2 shows the overall plan for the field tests.

To supplement the field tests, laboratory tests were also performed by NUPEC using a shaking table and smaller scaled DCI soil-structure models. The distance between adjacent buildings and the adjacent effect of three closely constructed buildings were the main test parameters for these tests. These tests were carried out using 1/230-scale building models made of aluminum and an artificial ground model made of silicone rubber. The evaluation of these tests was not included in this collaborative study. Further information on these tests can be obtained in papers by Kitada (2001) and Hirotani (2001).

Figure 2-3 shows a plan layout of the NUPEC DCI field test models. The single reactor building is designated as Model AA, the closely constructed twin reactor buildings are designated as Models BAN and BAS, and the reactor and turbine building models are designated as Models DA and DF, respectively.

Although three different model-building configurations were utilized in the NUPEC tests, there are only two structurally distinct model buildings, namely, the reactor building and the turbine

building. The reactor building is a three-story reinforced concrete structure ($1/10^{th}$ scale of the typical reactor building in a commercial NPP in Japan). The building has dimensions of 8m by 8m in plane and 10.5m in height and weighs about 660 metric tons. The turbine building is a two-story reinforced concrete structure and is 6.4m by 10m in plan and 6.75m high and weighs about 395 metric tons. A cross section of the reactor and turbine building models is shown in Figure 2-4. The single reactor building is situated in the base of a pre-excavated pit of trapezoidal shape as shown in Figures 2-3 and 2-5. For the single reactor building, the excavated pit is 10m by 10m in plan at the base and 20m by 20m in plan at the ground surface. The base of the pit is 5m below the ground surface with the sidewalls inclined at a 45-degree angle with the ground surface. The excavated pit for the twin-reactor building is located to the east of the single reactor building and has a rectangular opening of 10m by 18.6m at the base and 20m by 28.6 at the ground surface, and is 5m deep. The longer side of the pit is in the north-south direction (x-axis). As shown in Figure 2-3, the twin-reactor buildings are situated in the north-south direction at the base center of the pit with a gap of 0.6m between the two reactor buildings. The reactor-turbine buildings are situated in an excavated pit, which is located to the north of the twin reactor buildings and has an opening of 11m by 17.2m at the base and 19m by 25.2m at the surface. The pit is 4m deep and the basemat of the reactor building is embedded into the base foundation by 1m as indicated by Figure 2-4. As shown in this figure, the gap between the reactor and the turbine buildings is 0.1m.

Photographs of the NUPEC field test models, both with and without embedment, are shown in Figures 2-6 through 2-11.

During the period between 1989-1999, the test site experienced 27 earthquake events with maximum free-field accelerations exceeding 10 gal (Note: 980 gal = 1g). Two of these events had recorded maximum free-field accelerations of over 100 gal. As part of the US-Japan collaboration effort to investigate the DCI phenomenon, NUPEC provided the seismometer measurements of responses in both structures and free fields from eight earthquake events, including two major events with maximum free-field accelerations of 109 and 174 gal. Table 2-1 summarizes these events with respect to their occurrence time, source location, magnitude, epicenter and focal distances from the site, as well as maximum acceleration induced in the free field.

Two free-field locations were installed with down-hole seismometers, and are named the old and new free-field points, as shown in Figure 2-12. Figure 2-12 also shows the locations of the down-hole seismometers. Earthquake Nos. 34, 63 and 89 occurred before the down-hole seismometers were installed at the new free-field point and, therefore, were recorded only at the old free-field point. Earthquake Nos. 131, 139, 157, 164, and 172 were recorded at both the old and new free-field points. As shown in Figure 2-12 for the down-hole seismometer arrangement in the old free-field point, there are four recording stations: one station is near the surface (Gl – 1.5m), one station was built in the rock (Gl – 34.3m), and two stations were placed in between. For the seismometer arrangement in the new free-field point, as depicted in Figure 2-12, five stations were installed, with one near the surface (Gl – 3m) and one well into the rock (Gl – 53m), and the rest spread in between.

The site geological features consist of primarily weathered-pyroclastic and pyroclastic rocks overlain by a 5-8m layer of overburden comprised of weathered sandstones and diluvial loams. The site water table is located between 7-10m from the ground surface. Ultrasonic wave tests were performed at the locations where the test models were built. In addition, the site geological features were examined. The locations of the boring points under the building models are shown in Figures 2-13 and 2-16. The soil profiles under the buildings, as shown in Figures 2-14 through 2-16, indicate fairly horizontal uniformly layered soils across the site.

Table 2-1. Earthquake Events Selected for Collaboration

Earthquake No.	Earthquake Occurrence Time	Source Location East Longitude	Source Location North Latitude	Earthquake Magnitude (M)	Epicenter/Focal Distance (km)	Max old free field point acceleration GL-1.5m (gal) NS	Max old free field point acceleration GL-1.5m (gal) EW	Max new free field point acceleration GL-3.0m (gal) NS	Max new free field point acceleration GL-3.0m (gal) EW
34	03-05-1991	141'41.0	41'16.0	4	28/46	15.8	9.6		
89	12-28-1994	143'43.3	40'27.1	7.5	213/213	123.0	174.0		
131	02-17-1996	141'23.0	40'47.0	4.6	43/45	15.9	17.3	15.1	13.3
139	02-20-1997	142'52.0	41'45.0	5.6	140/146	9.3	8.9	11.4	11.6
157	01-03-1998	142'04.0	41'28.0	5.1	66/89	28.5	26.7	20.8	30.2
63	01-15-1993	144'23.0	42'51.0	7.8	294/310	109.0	98.0		
164	11-07-1998	142'03.0	41'34.0	4.6	71/95	8.9	8.5	6.3	10.8
172	05-11-1999	143'55.0	42'57.0	6.4	288/305	13.5	13.6	13.3	10.8

Note: 980 gal = 1g

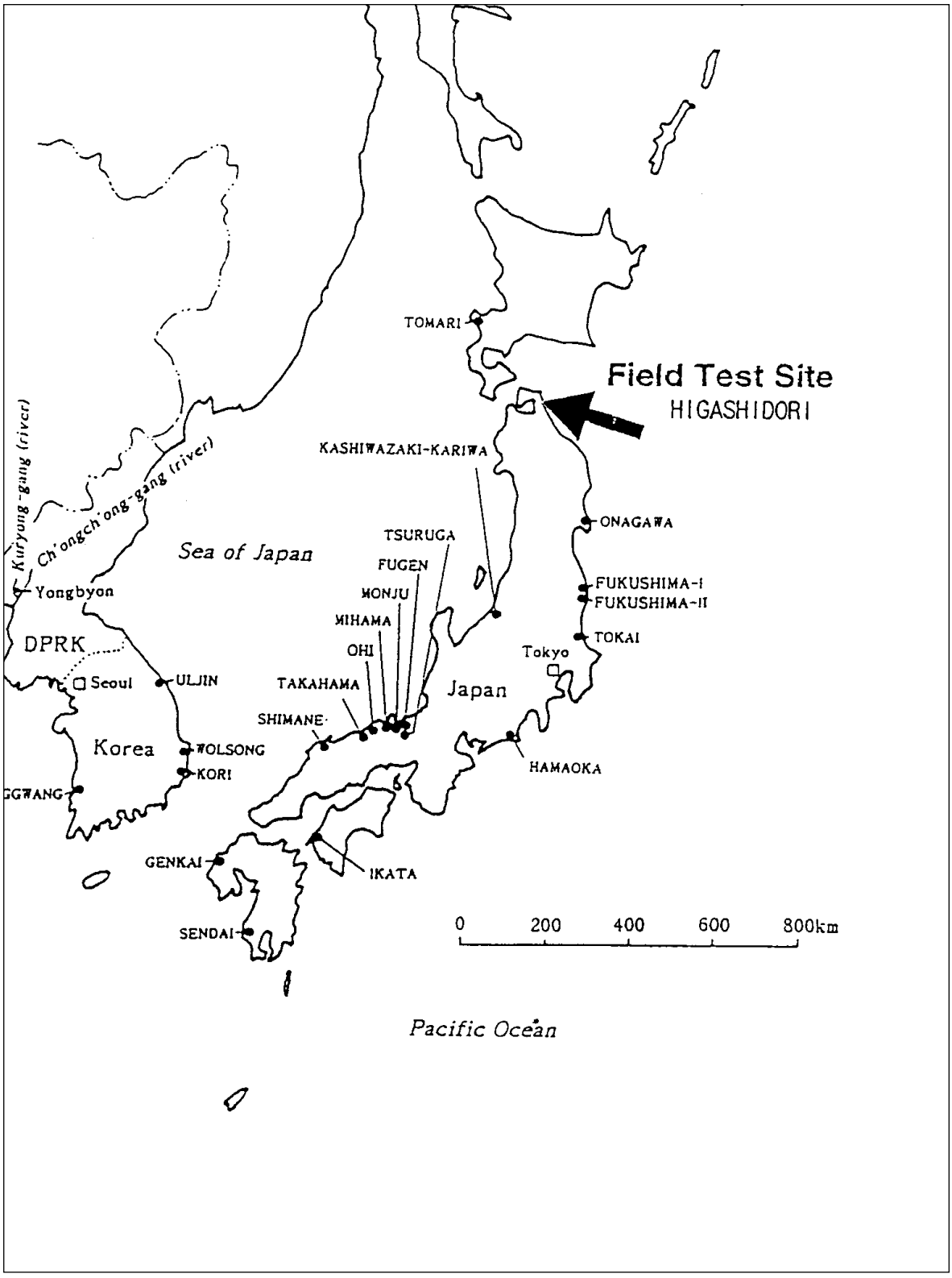

Figure 2-1. Location of NUPEC Field Test Site in Japan

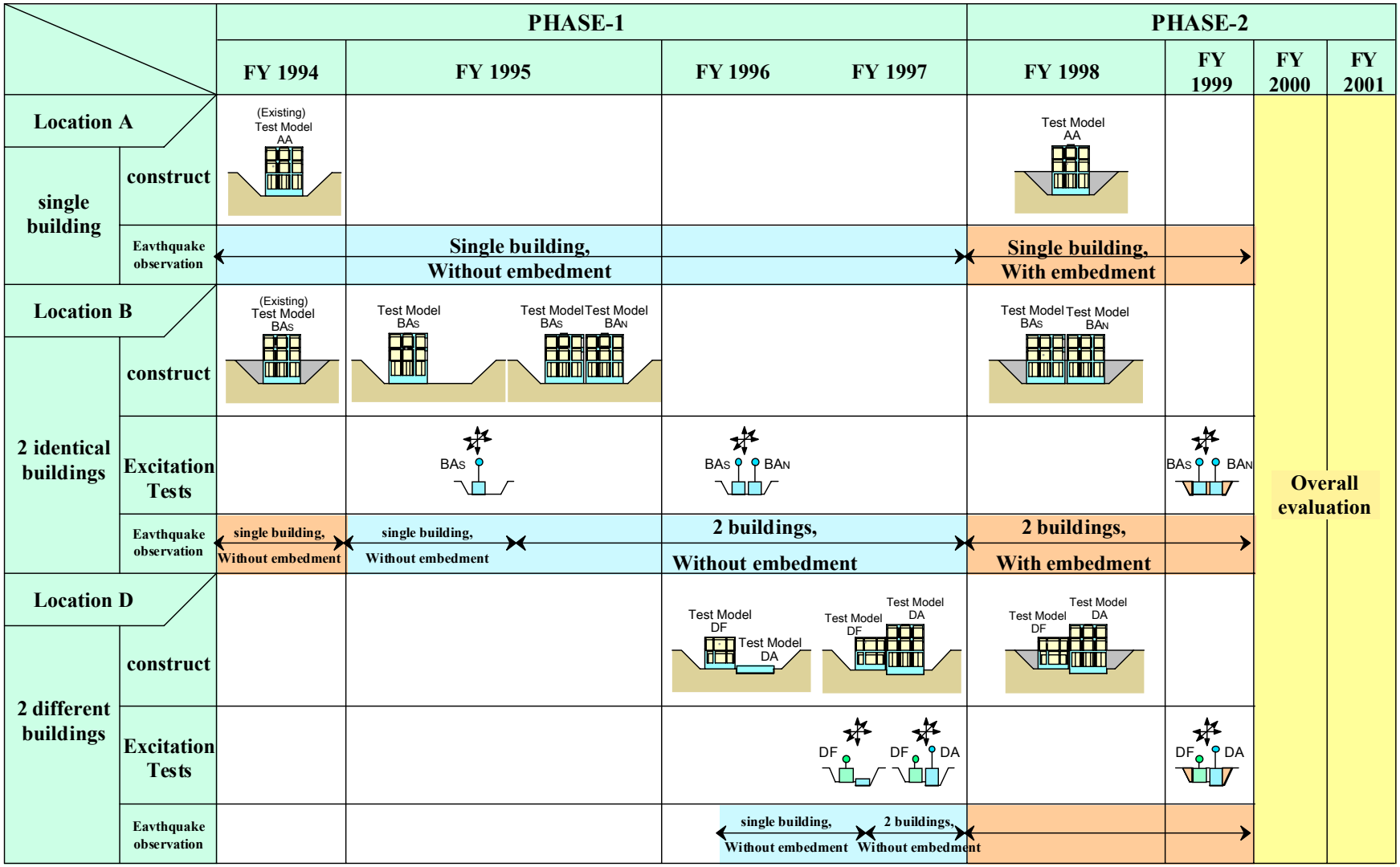

Figure 2-2. Overall Plan for NUPEC Field Tests
(NOTE: Each fiscal year in Japan starts on April 1 of that year)

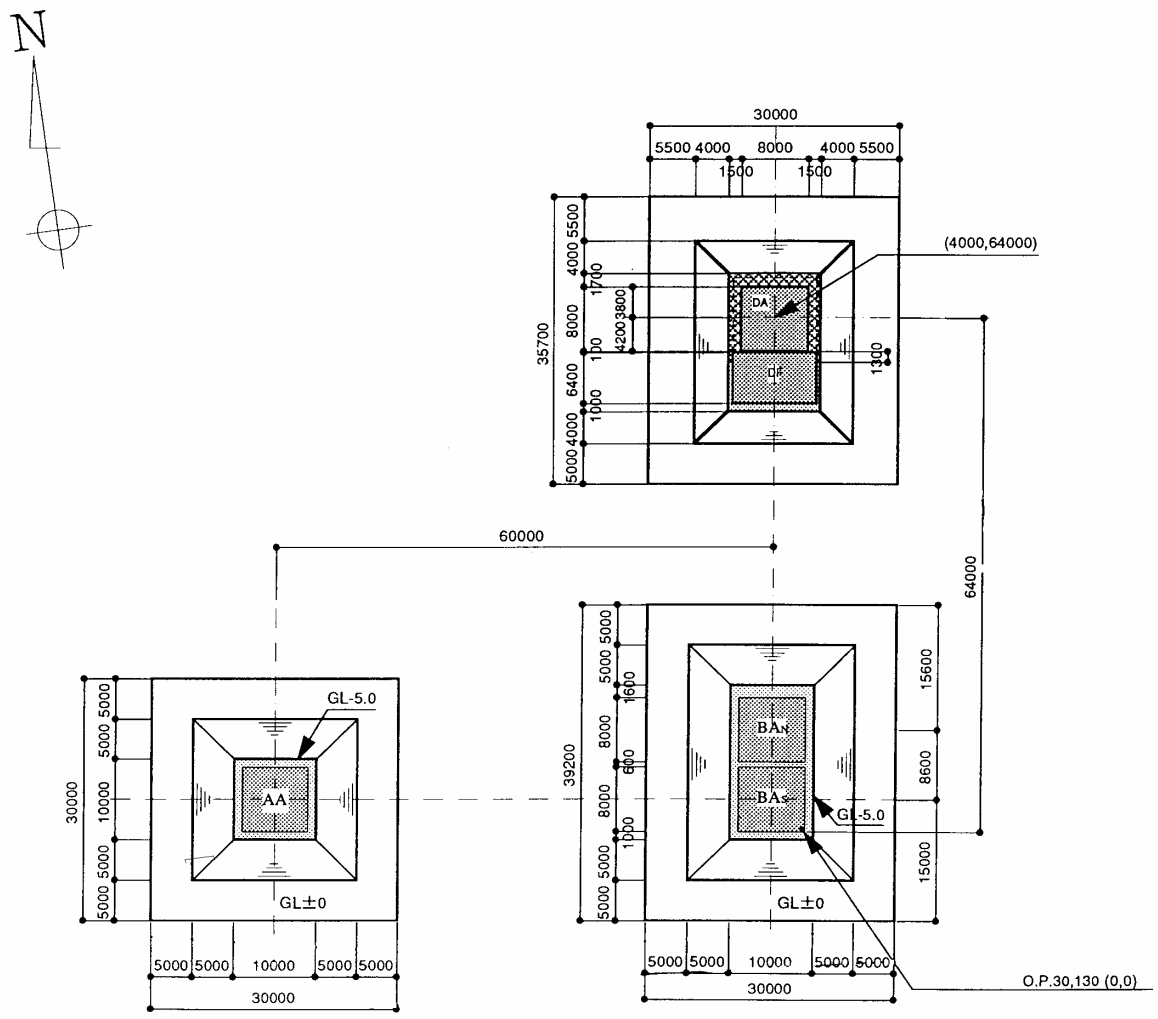

Figure 2-3. Layout of Models at NUPEC Field Test Site

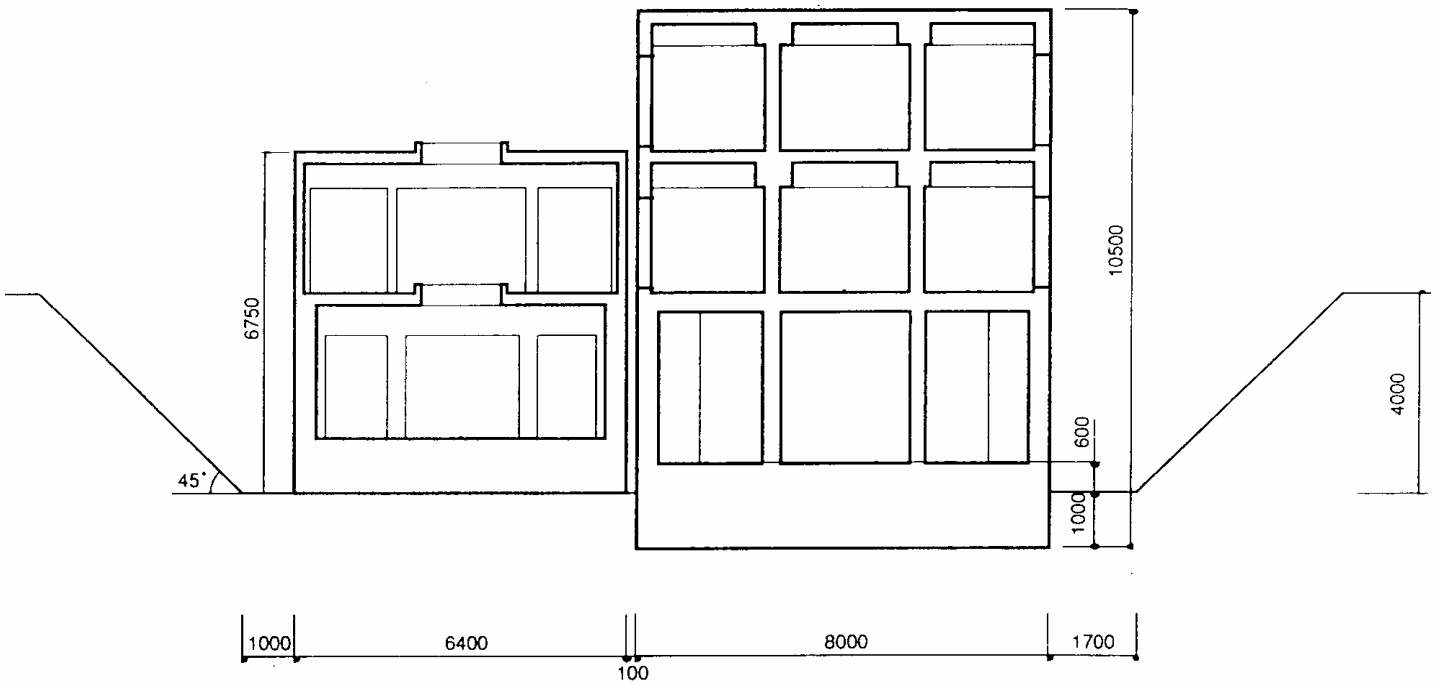

Figure 2-4. Cross Section of Reactor and Turbine Building Models

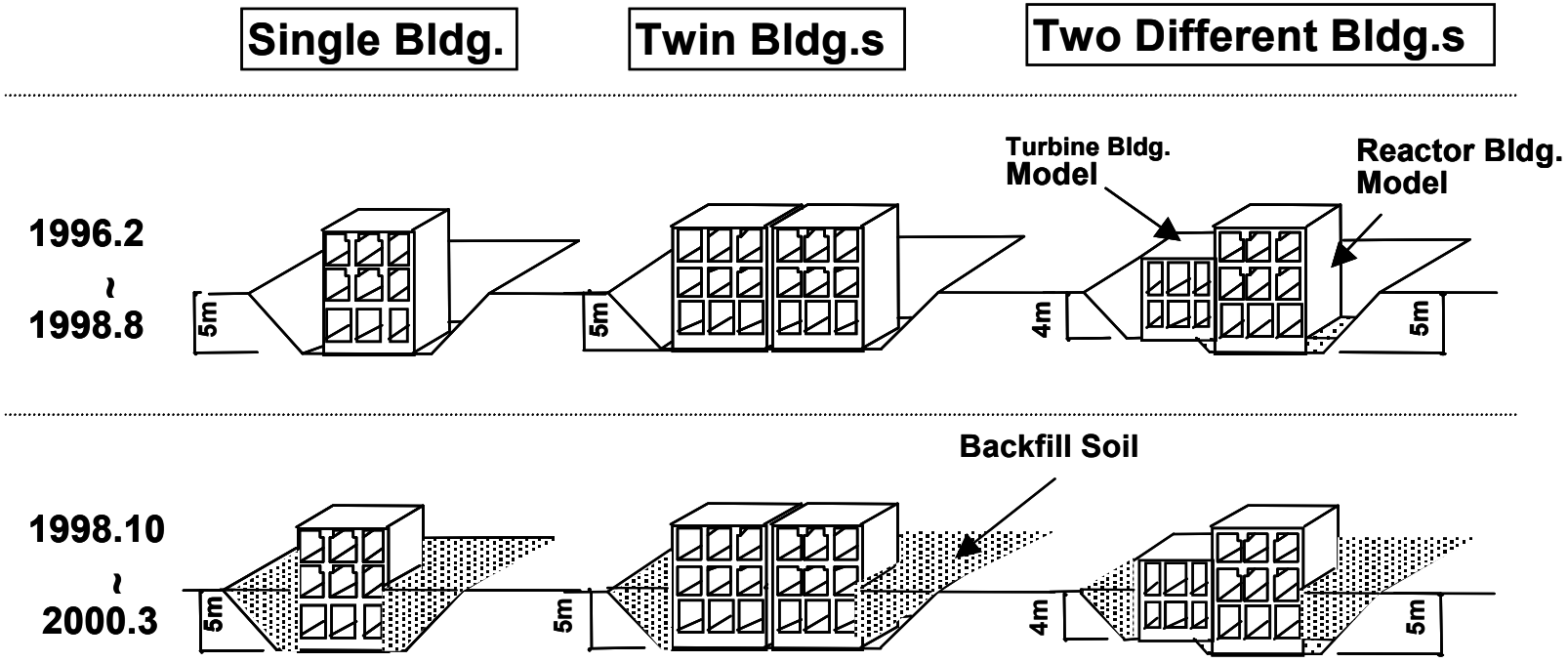

Figure 2-5. Embedment Conditions for the Building Models

Figure 2-6. NUPEC Field Test Model of Reactor Building Without Embedment

Figure 2-7. NUPEC Field Test Model of Adjacent Twin Reactor Buildings Without Embedment

Figure 2-8. NUPEC Field Test Model of Adjacent Reactor -Turbine Buildings Without Embedment

Figure 2-9. NUPEC Field Test Model of Reactor Building with Embedment

Figure 2-10. NUPEC Field Test Model of Adjacent Twin Reactor Buildings with Embedment

Figure 2-11. NUPEC Field Test Model of Adjacent Reactor-Turbine Buildings with Embedment

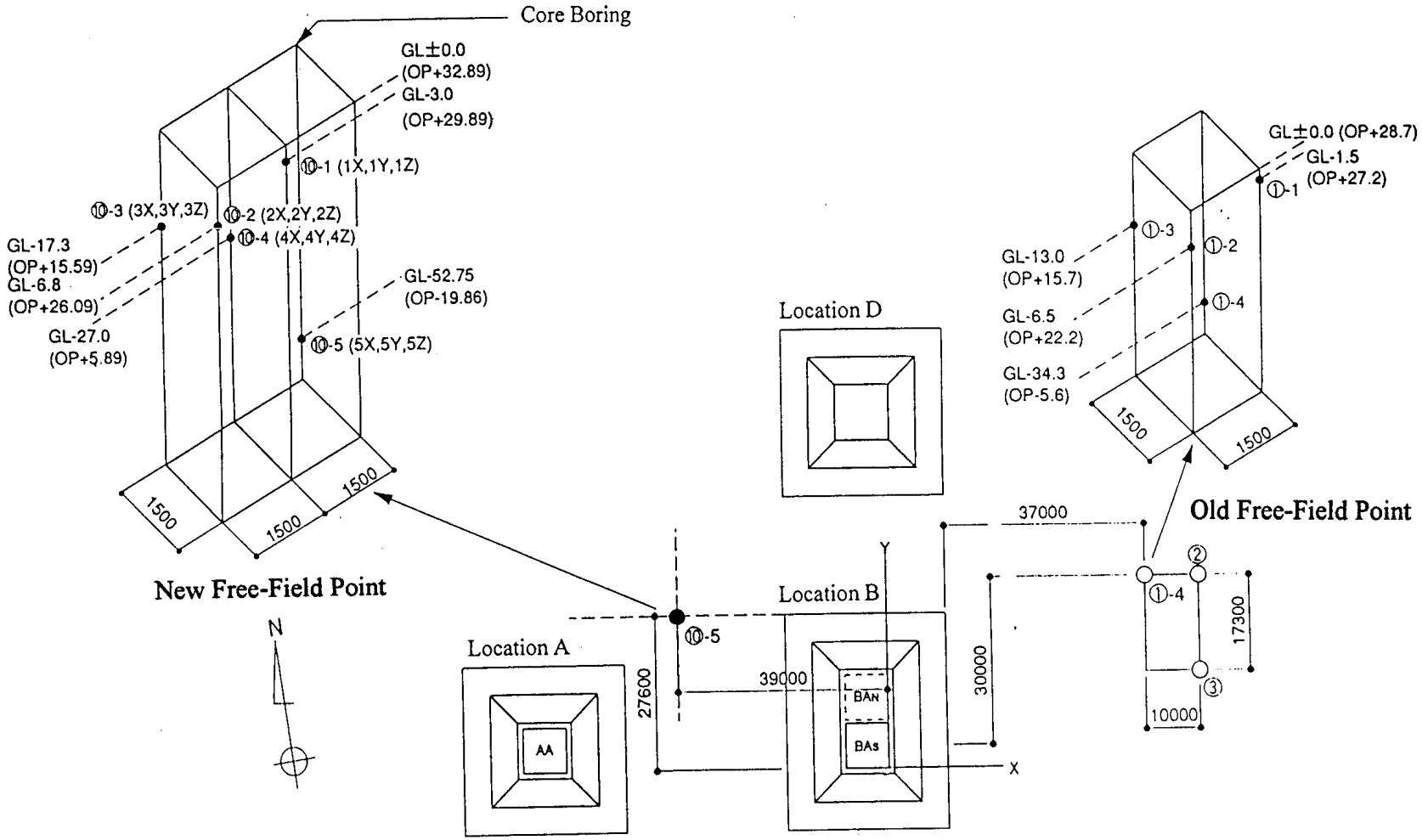

Figure 2-12. Layout of Seismometers in Free-Field Down-Hole Arrays

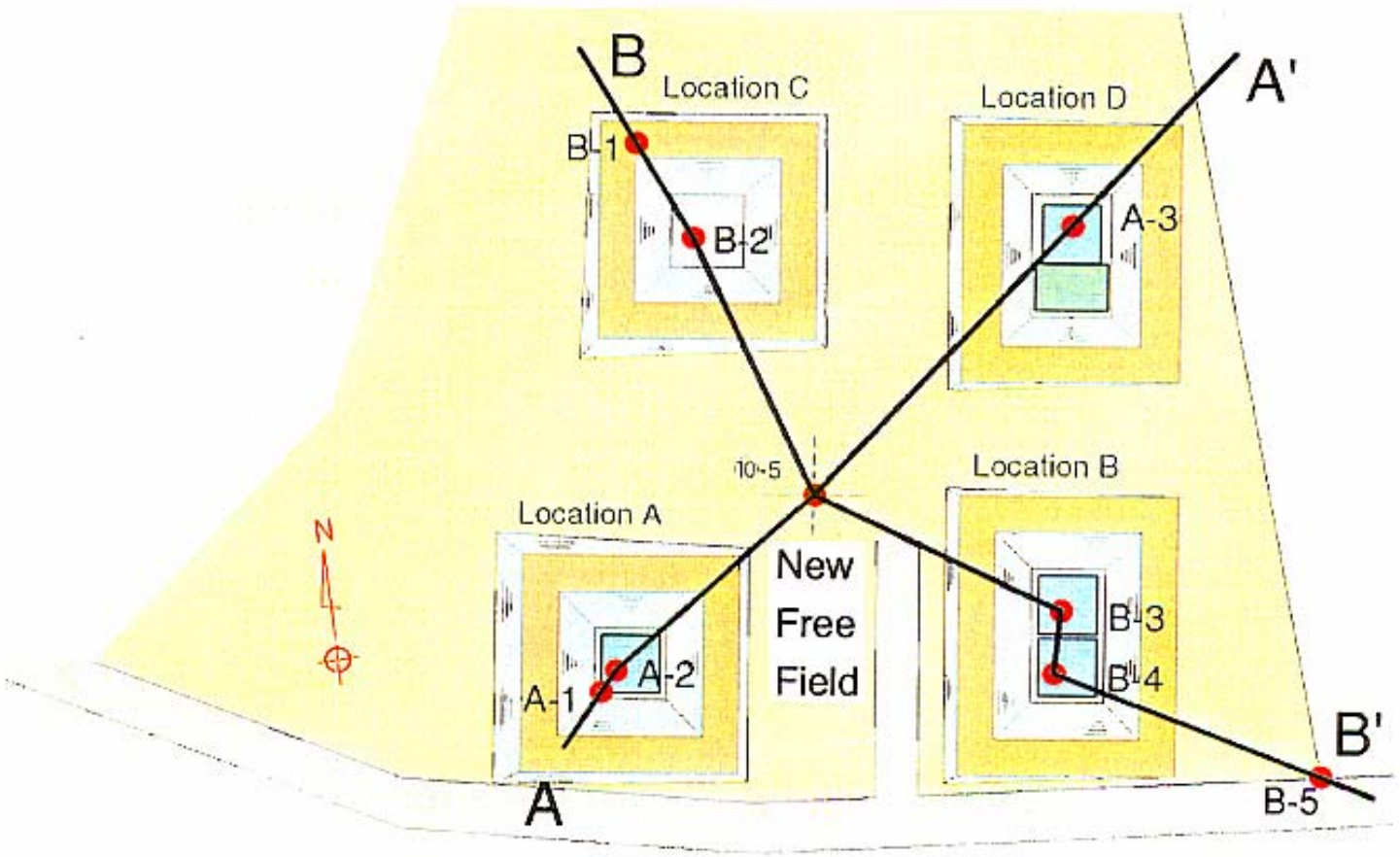

Figure 2-13. Location of Boring Points Under Building Models and Cross Sections for Soil Profiles

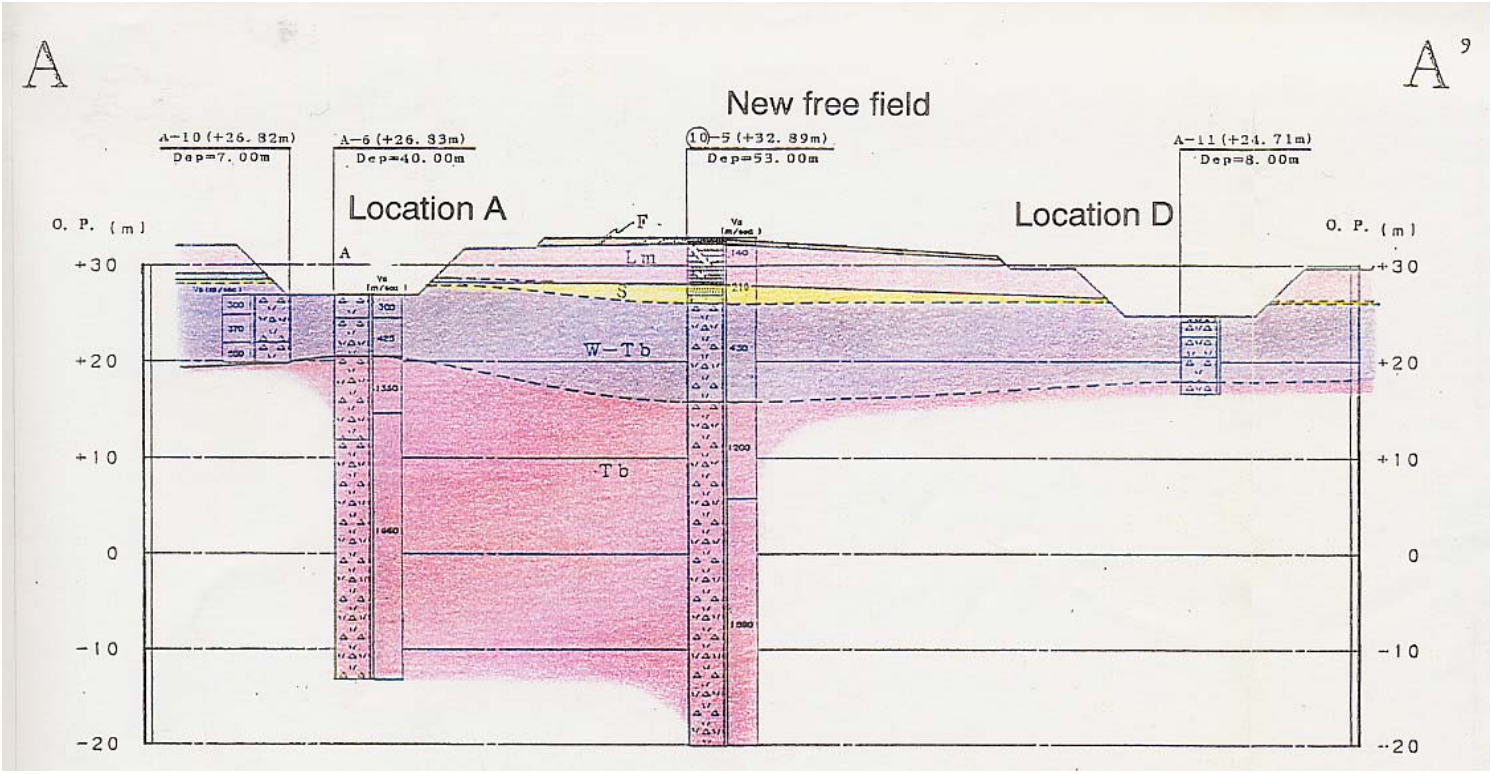

Figure 2-14. Soil Profile for Section A-A
(Refer to Figure 2-13 for Section Location)

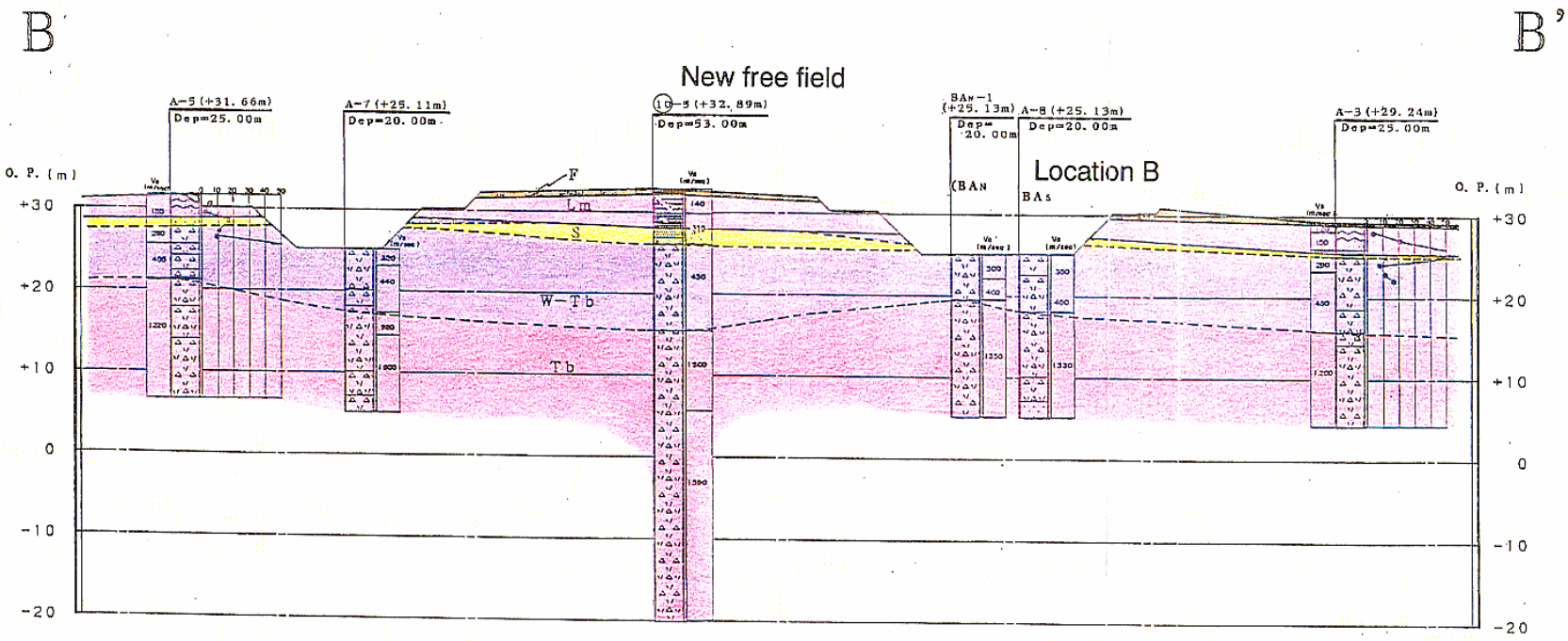

Figure 2-15 Soil Profile for Section B-B (Refer to Figure 2-13 for Section Location)

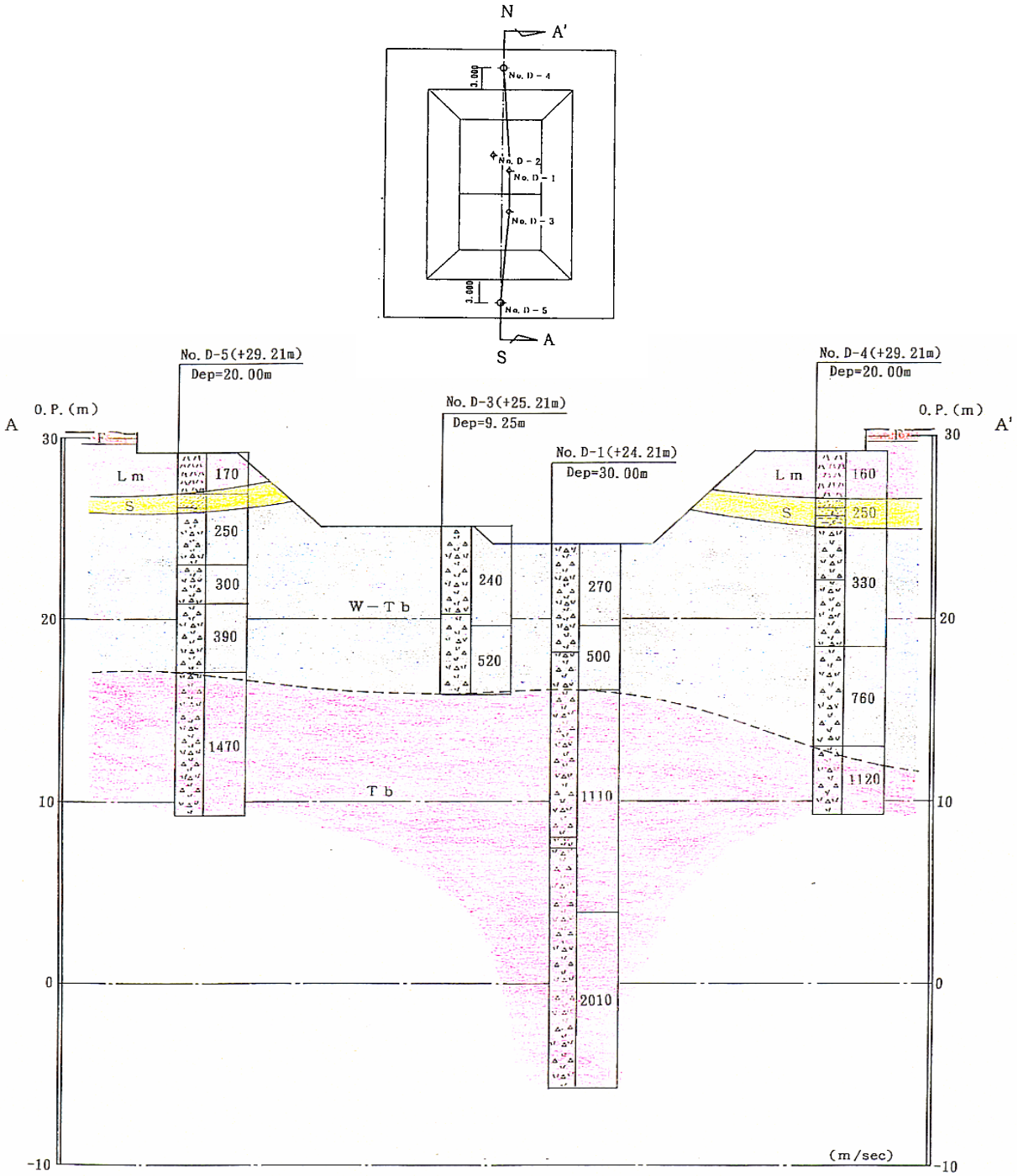

Figure 2-16. Soil Profile for Reactor-Turbine Buildings

3.0 DESCRIPTION OF ANALYSIS METHODS EMPLOYED BY BNL STUDIES

Broadly speaking, for structures founded on soils, the seismic analyses are performed in two steps: the free-field analysis and the soil-structure interaction (SSI) analysis. The free-field analysis uses the ground motion input appropriate for the site, derived either from a site-specific study or site-independent sources such as USNRC Regulatory Guide 1.60. Various analytical tools and available geotechnical information are applied to determine the site soil properties, generally characterized by strain-dependent shear wave velocity and hysteretic damping, and the control motion input for the subsequent SSI analysis. The SSI analysis incorporates the interaction effect between the structure and the soil and computes the dynamic response of the structure subjected to the prescribed ground motion input.

Procedures to develop ground motion inputs at soil sites are based upon either deterministic or probabilistic approaches. Both approaches attempt to account for uncertainty in soil properties (epistemic uncertainty) as well as expected randomness in wave fields (aleatoric uncertainty) by using procedures that are felt to lead to conservative estimates of design ground motions. In the deterministic approach, as described in USNRC's Standard Review Plan (NUREG-0800), the surface ground motion has typically been determined from generic soil attenuation models using empirical data where available. SSI effects are then determined using bounding estimates of soil properties generated from local site data. Deconvolution methods are used to generate strain-iterated bounding soil properties in the SSI calculation. Care must be exercised when using this approach to ensure that soil property definitions (low strain shear properties and soil degradation models) are appropriate for the (typically) broad-banded surface response spectra selected for the design.

In recent years, proposals have been made to modify the deterministic approach to eliminate these deficiencies in the calculational models. The current recommendations of the USNRC (USNRC, 1997 and NUREG/CR-6728, 2001) and the DOE (DOE-STD-1023-95) generate the design response spectrum based upon probabilistic rock hazard evaluations. This is significantly different from that having been typically used in deterministic convolution studies wherein a best estimate (BE) soil profile is selected together with a potential lower bound (LB) profile and an upper bound (UB) profile. The properties of the LB and UB profiles are simply scaled from the BE profile, eliminating the potential effect of layer-to-layer variability on the mean spectral response on the surface spectrum. It has been shown (Costantino, 2001) that at deep soil sites, this layer-to-layer variability can lead to exceedances with respect to the surface spectrum calculated with the deterministic approach, particularly at frequencies higher than the fundamental frequency of the soil column.

As described in the previous section, the NUPEC test site consists of two free-field locations, each having a down-hole array with a series of seismometers installed at different stations along the array, and three structural sites where the model structures with different configurations were built. Seismometers were also installed at various locations within the model structures to record the seismic response to earthquake motions. The objective of BNL's study is to apply the current practice in the seismic analyses for nuclear power plant structures to predict both the test site soil properties using the seismometer recordings and the seismic response of the model structures. This section of the report describes the analysis methods employed by BNL for performing the free-field analysis and the SSI analysis.

3.1 Evaluation of Primary Wave Propagation Mechanisms

Where ground motions are specified as rock outcrop motions, convolution methods of analysis, assuming upward propagating SH waves, have been used to generate bounding estimates of the soil surface ground motion. When the broad-banded rock spectrum is used as input to this free-field calculation, the nonlinear behavior of the soil tends to lead to excessive soil strain, changing the effective frequency of the soil column and therefore the calculated surface motion, particularly at higher input acceleration levels.

At the NUPEC test site, a series of seismometers were placed at different depths along two down-hole arrays in the free field (referred to as the old and new free-field points) to record the free-field response to earthquake events that traveled across the site. In this study, BNL used the one-dimensional (1D) vertical propagating shear wave model (validated by many studies such as those of Seed and Idriss, 1969; Joyner, 1976, 1981; Idriss, 1991) for the free-field response calculations. The recorded free-field seismometer data were therefore examined for their primary propagating wave types in the free field to evaluate their consistency with the 1D propagating model employed. To identify the primary wave propagating mechanism associated with the earthquake, one could examine the energy content of the down-hole seismometer data and establish the energy movement along the down-hole array, therefore verifying the consistency with the assumed upward propagation for the 1-D site model. It is proposed that the Arias intensity be used as a measurement of the energy content of these seismometers. The Arias intensity (Arias, 1970) is defined by the following function

$$I_g(t) = \frac{\pi}{2g} \int_0^t \ddot{x}_g^{\,2}(\tau)\, d\tau \qquad (1a)$$

Where, $\ddot{x}_g(\tau)$ represents a seismometer measurement recorded at a down-hole station and the g is gravitational acceleration.

To simplify the numerical calculation, the Arias Intensity is rewritten as:

$$I_g^*(t) = \frac{2g}{\pi} I_g(t) \qquad (1b)$$

Note that $I_g^*(t)$ is used in the numerical calculations presented in this report.

To confirm an upward propagating motion for the earthquake event under consideration, the Arias intensities for the down-hole seismometers located between rock and ground surface in the free field are first computed and then plotted versus time. This Arias intensity plot should show in time an initial built-up of energy in the rock seismometer and gradually increasing energy in seismometers moving toward the surface. Eventually the domination of energy should be established in the surface seismometer. For earthquake events with strong surface wave characteristics, which are usually associated with epicenter distances of more than 100m, the Arias intensity plots for the down-hole seismometers would not show a clear upward energy movement. Based on the examination of the Arias intensity for the down-hole seismometer data associated with the recorded earthquake events at the NUPEC test site, BNL screened out those records that are inconsistent with the 1D site model.

3.2 Method for Free-Field Analysis

The purpose of the free-field analysis is 1) to identify the NUPEC test site soil properties, and 2) to determine the ground motion input appropriate for the subsequent SSI analysis. The site soil properties as characterized by the shear wave velocity and hysteric damping were determined using the seismometer data from recorded earthquakes.

The Fourier ratio method with a non-linear least square fitting technique was applied to predict the free-field low-strain soil properties by correlating the analytical site amplification with the amplification computed using the recorded seismometer data. Similar approaches were also applied in the Lotung (Chin, 1998) and Port Island experiments (Kurita, 1997). A number of published laboratory tests (GEI, 1983; Lee, 1996; Geomatrix, 1991; EPRI, 1993) were examined and convolution analyses performed to identify the strain-dependent modulus degradation relationship suitable for the test site.

Recognizing the probabilistic nature of the soil behavior controlled by the peak strains induced by earthquake motions, which can be characterized by stochastic processes, the uncertainty inherent in the soil properties should be considered and incorporated into the soil profile identification and the ground motion input to the SSI analysis. To accomplish this, BNL performed a probabilistic analysis using a Monte Carlo process in conjunction with equivalent linear convolution analyses. The BNL probabilistic analysis produced the free-field soil properties in terms of the mean, median and various fractiles at the test site, and the corresponding surface motions, which can be readily applied to the SSI analysis.

In the context of the 1D site model assumed for the BNL free-field analysis, the wave propagating mechanisms associated with the recorded free-field seismometer data need to be appropriately identified in order to screen out those records with wave types that are inconsistent with the 1D site model assumption. The remaining records are analyzed using the Fourier ratios with the Levenburg-Marquadt (Fletcher, 1971) non-linear least square fitting algorithm. In the following subsections, the techniques used to compute the low-strain soil property predictions are first described, followed by a description of BNL's method for the probabilistic site analysis.

3.2.1 Fourier Ratios with the Levenburg-Marquadt Non-Linear Least Square Fitting Algorithm

The Fourier ratio technique has been used extensively in studies for Treasure Island and Taiwan (Lotung and Hualein) sites for predicting the in-situ soil properties (Chin, 1998). It was also employed by investigators in Japan (Kurita, 1997) to identify the site soil properties at Port Island, Japan. The technique involves matching the theoretical transfer function for the 1-D site model to the actual amplifications in terms of Fourier spectral ratios computed directly from the down-hole seismometer recordings. The least square algorithm is used for back-calculating the soil properties by iteration. It should be noted that this procedure was intended for determining the low strain soil properties in this study, although it could also be applied to identify strain-dependent properties, in which case both the shear wave velocity and hysteretic damping values associated with the soil column should be considered. A brief description of the Fourier ratio technique and its computer implementation for use in the free-field analysis is provided below.

Assuming that the laboratory tests are used as an initial estimate of the soil column property, the identification process of the actual dynamic characteristics of the soil deposits can be formulated as a conditional non-linear least square minimization problem, which is stated as

$$\underset{v_s \subset V^{L_N},\zeta \subset Z^{L_N}}{\text{Minimum}} \frac{1}{2} \sum_{\omega_n \subset \Omega} \sum_{l_m \subset L_M} F_{nm}(v_s,\zeta)^2 \quad (2)$$

in which,

- v_s Vector containing shear wave velocities associated with the L_N layers of a soil column,
- V^{Ln} Bounds for v_s defined as: $v_{sBE}/(1+COV) < v_s < v_{sBE}(1+COV)$, v_{sBE} is the best estimate from laboratory tests (median values) and COV represents variability of the tests (COV = 0.5 is used in this study),
- ζ Vector containing hysteretic damping values associated with the L_N layers of a soil column,
- Z^{Ln} Bounds for ζ and for low strain properties ζ is set at ζ_i = 1.5% constant for this study,
- ω_n Circular frequency,
- Ω The analysis frequency range,
- L_M Set of Fourier spectral ratios being considered.

The target function in Equation (2) is defined as:

$$F_{nm}(v_s,\zeta) = R_{l_m}(\omega_n) - H_{l_m}(\omega_n, v_s, \zeta) \quad (3)$$

in which,

- $R_{lm}(\omega_n)$ Fourier ratios computed from the accelerometer recordings between the rock and the location l_m,
- $H_{lm}(\omega_n,v_s,\zeta)$ Theoretical transfer function between the rock and the location l_m.

The theoretical transfer function is computed using the 1-D wave propagation theory.

The conditional non-linear least square minimization problem, as defined in Equation (2), was solved using the modified Levenberg-Marquardt algorithm, which has been discussed extensively in the literature (Fletcher, 1971). A brief description of the modified Levenberg-Marquardt algorithm is provided below.

Equation (2) is rewritten in the following matrix form:

$$\underset{x \subset R^n}{\text{Minimum}} \frac{1}{2} F(x)^T F(x) \quad (4)$$

where $x = (v_s,\zeta)$, $R^n = (V^{Ln}, Z^{Ln})$, and $F(x)$ is the vector whose components are comprised of $F_{nm}(v_s,\zeta)$. The initial value is set at $x_i = (v_{sBE},\zeta_i)$ to start up the algorithm, and the trust region approach is used to search for a new point x that minimizes $F(x)$. For instance, from any current point x_c, the trust region approach searches for a new point x by performing:

$$\underset{x \subset R^n}{\text{Minimum}} \left\| F(x_c) + J(x_c)(x - x_c) \right\|_2 \quad (5)$$

subject to $||x - x_c||_2 < \delta_c$

and the new point is computed as

$$x = x_c - \left\langle J(x_c)^T J(x_c) + \mu_c I \right\rangle^{-1} J(x_c)^T F(x_c) \qquad (6)$$

where $\mu_c = 0$ if $\delta_c > ||\{J(x_c)^T J(x_c)\}^{-1} J(x_c)^T F(x_c)||_c$ and $\mu_c > 0$ otherwise. $F(x_c)$ and $J(x_c)$ are the target function and its Jacobian evaluated at the current point x_c. This procedure is repeated until the stopping convergence criteria are satisfied.

The Fourier ratio technique, as described above, has been implemented into the CARES program (Costantino, 1999), in which $x = (v_s)$ and $\zeta = \zeta_i$ (set at 1.5% constant), and was used for identification of the low strain shear wave velocities of both the old and new free-field points. As will be discussed later in this paper, the strain-dependent modulus degradation relationships are determined by fitting the free-field records to several available laboratory tests by performing the equivalent-linear convolution analysis.

In order to compare the recorded soil amplifications with the theoretically computed smooth transfer function, the Fourier ratios of the surface to rock seismometer recordings were smoothed with a triangular window function, which is defined below:

$$A_s(f_m) = \frac{1}{\text{SUM (i)}} \sum_{\substack{\text{All i} \\ |f_i - f_m| \le \Delta f_m / 2}} \alpha_i \, A_r(f_i) \quad , m=1, M \qquad (7)$$

and,

$$\alpha_i = \frac{4}{\Delta f_m}[f_i - (f_m - \Delta f_m/2)], \quad f_m - \Delta f_m/2 \le f_i \le f_m$$

$$\frac{4}{\Delta f_m}[(f_m + \Delta f_m/2) - f_i], \quad f_m < f_i \le f_m + \Delta f_m/2$$

where,

Δf_m	Width of the applied frequency window (0.5 Hz used for this study)
$A_s(f_m)$	Smoothed Fourier ratios
$A_r(f_i)$	Fourier ratios of recorded motions.

3.2.2 Probabilistic Sampling Method for Motion Dependent Profiles

Conventional probabilistic analysis consists of steps, including: 1) identification of random variables and their associated distributions; 2) modeling of probabilistic process for developing various statistical data which characterize the random variables under consideration; 3)

assessment of uncertainties associated with the quantification of the random variables. In this process, soil column properties (layer thicknesses, low strain shear wave velocities (V_s), and strain degradation and damping data) all have inherent randomness in their measurements, and therefore could all be selected as random variables in order to try to capture the full range of response that would be expected from this soil site. The probabilistic process established based on all soil properties and the associated uncertainties could be rather complicated and requires significant effort to simulate. However, since the SSI effect is primarily influenced by the shear wave velocity of soils, BNL selected low-strain V_s to be the random variable in order to simply the analysis. The measurement of the other properties could be improved through the application of better techniques and instruments. The soil damping is characterized through the GEI modulus degradation model (GEI, 1983), which has been established to be suitable for the NUPEC test site.

The BNL analysis assumes a lognormal distribution for V_s. The probability density function (PDF) of V_s, therefore, assumes the following form:

$$f_{V_s}(v_s) = \frac{1}{\sqrt{2\pi}\beta v_s} \exp\left[-\frac{1}{2}\left(\frac{\ln v_s - \ln v_{smed}}{\beta}\right)\right] \quad (8)$$

where v_{smed} represents the median estimate of V_s and β is the lognormal standard deviation of V_s characterizing the uncertainty for the v_{smed} estimate. The low-strain v_{smed} is determined using the Fourier ratio method with a non-linear least square fitting technique for correlating the analytical site amplification with the amplification computed using the recorded seismometer data. The BNL estimate (Xu, 2001) of the low strain v_{smed} is determined using the techniques described in the previous sub-section. The lognormal standard deviation is determined using the guidelines of the current version (NUREG-0800) of the USNRC Standard Review Plan (SRP) and the ASCE 4-86 standard. These documents suggest that the 1.5G and G/1.5 variations may be used in SSI analyses to account for the free-field soil uncertainties. Where, G represents the best estimate of the shear modules of soils. The range of uncertainties determined by 1.5G and G/1.5 is about the 15th to 85th percentiles, corresponding to the mean+β and mean-β estimates. With the aid of the relation, $V_s = (G/\rho)^{1/2}$, and the following equation:

$$\beta = \ln \frac{v_{.85}}{v_{med}} \quad (9)$$

the lognormal standard deviation β for V_s is readily calculated to be 0.2.

In order to apply the Monte Carlo method, random sampling of the low strain V_s of the free-field profile needs be performed. This is done by using the uniform distribution for sampling and the cumulative distribution function (CDF) of V_s with the lognormal model as given in Eq. (8). The set of free field sample profiles thus generated are each subsequently used in the convolution analyses, which in turn are iterated with a modulus degradation model and a rock outcrop input earthquake motion until the strain compatible soil properties are identified. The convolution analyses are performed using an in-house CARES program (Costantino, et al, 1999) based on one-dimensional shear wave propagation theory. The results of this simulation process are a sample set of strain compatible free-field profiles, including V_s, the corresponding final strains,

and soil damping. The corresponding surface motions can also be calculated in terms of response spectrum, which may be used as input to SSI analyses.

3.2.3 Modulus Degradation Model

To determine the appropriate model for modulus degradation relationships for the NUPEC site, three well publicized and documented test models were used. They are: GEI (GEI, 1983), Geomatrix (Geomatrix, 1991) and EPRI 93 (EPRI, 1993). These models were developed primarily for soils with geological features representative of the Western United States. Parametric analyses are performed to generate the free-field responses using the BNL estimated low-strain profiles and the three modulus-degradation models for both the new and old free-field points. Earthquake records that are large enough to induce the strain-degradation effect in the soil properties will be used in the parametric analysis and the calculated free-field response at various stations along the down-hole array will be compared with the recorded response. The degradation model that produces the best match in the free-field response between the calculated results and recorded data will be selected for the NUPEC site.

3.3 SASSI Sub-structuring Method for SSI Responses

The BNL study for the SSI analysis uses the sub-structuring method as implemented in SASSI developed by Lysmer and his team at U.C. Berkeley (Lysmer, 1981 and 1999). The SASSI program has gone through extensive improvement in the past ten years, especially SASSI 2000. In addition to the sub-structuring methods such as the flexible volume, flexible boundary and rigid boundary methods as in the previous versions, SASSI 2000 implemented a new subtraction method, which the BNL study used to carry out the SSI response calculations. Given the overwhelming amount of SSI calculations required for the BNL study, it would have been an insurmountable task without using the subtraction method, which has proven to be quite an efficient algorithm with no compromise for quality for the SSI response calculations. This sub-section describes briefly the basic approach in the sub-structuring methods, with special emphasis on the subtraction method. The material used in the following discussion was drawn primarily from the SASSI 2000 theoretical manual (Lysmer, 1999).

The sub-structuring approach divides the SSI problem into several sub-problems including: 1) the site response problem (the free field with no presence of structure), 2) the scattering problem, 3) the impedance problem, and 4) the structural response problem. For the rigid and flexible boundary methods, since the embedment is explicitly modeled in the free field, all four sub-problems are required to be solved. While for the flexible volume and subtraction methods, the scattering problem is not required due to the use of superposition to avoid explicit modeling of the embedment in the free field; although the other three sub-problems are still needed to be solved. However, the treatment of impedance analysis for the flexible volume and subtraction methods is quite different from the rigid and flexible boundary methods. The impedance is computed for the rigid and flexible boundary methods in the free field with the indentation of the structural embedment. For the flexible volume and subtraction methods, the impedance is calculated in the free field without the indentation of the structural embedment, therefore significantly simplifying the SSI problem.

In contrast to the impedance treatment for the flexible volume method which computes the impedance at every nodal point within the embedment, the newly implemented subtraction method recognizes that the soil-structure interaction takes place only at the common boundary of the soil and the structure, and formulates the dynamic equations of motion in such a way that the interior nodes of the embedment are eliminated. Therefore, for the subtraction method, the

impedance is computed only for the interfacing nodes of the soil and the structure, resulting in significant savings in computing time. In addition, the site response calculation for the subtraction method is performed only for the interaction nodes as opposed to all nodes within the embedment for the flexible volume method. This results in additional savings for the subtraction method. For a more detailed description, the reader is referred to the SASSI 2000 theoretical manual (Lysmer, 1999).

For SSI calculations, the Monte Carlo approach to free-field site response was incorporated by performing Monte Carlo evaluations of initial or low strain shear wave velocities. Convolution calculations were performed using the equivalent linear method of analysis with the CARES computer program (Costantino, et al, 1999) to generate the mean surface ground motion compatible with the ground motion recorded at depth. For the Old Free-Field soil column, this ground motion was typically selected at the lowest seismometer placed in rock at a depth of 34.3m, while for the New Free-Field soil profile, this recording was typically selected at a depth of 53m.

The first step in this process was to determine the rock outcrop motion corresponding to the recorded in-column ground motion at depth. This was performed using the CARES Code together with the best estimate soil profile for the two sites as described in Section 3.2.2. This modified ground motion was then used as the rock outcrop motion in the Monte Carlo site response calculations to generate the mean estimate of the soil surface ground motion. The variability in potential soil layer velocities was selected to satisfy the recommendations of NUREG-0800. The plus/minus one sigma values of the layer shear moduli were selected to yield values at 2 times and one-half the best estimate values, assuming a log-normal distribution of shear data. For each earthquake evaluated, a set of thirty (30) site response calculations were made from which soil surface motions were generated.

The input response spectrum at the soil surface was then selected as the mean spectrum for use in the SSI calculations. To provide input to the SASSI calculations, an artificial accelerogram was then generated to closely match this mean spectrum, using the spectral phasing and strong motion duration appropriate to the recorded surface ground motion. From the resulting set of thirty soil columns, the plus/minus one sigma profiles were calculated from the iterated shear wave velocities of each soil layer of the profile. The soil profiles used in the SSI calculations were then selected as the mean, plus one sigma and minus one-sigma shear wave velocity profiles.

4.0 BNL ANALYSIS OF FREE-FIELD DATA

This section of the report describes and discusses the BNL analysis of the free-field data recorded at the NUPEC test site. The free-field data consist of a series of ground motion accelerometer measurements recorded at stations pre-arranged along two vertical down-hole arrays in the free field. The purpose of the BNL analysis of these free-field data is to evaluate the current industry methods for the free-field analysis by comparing the numerical results computed using the current practice with the recorded data. Two aspects of the free-field analysis were examined: 1) free-field soil properties and 2) derived ground inputs suitable for the SSI analyses. The approach for performing the free-field analysis follows the methods described in Section 3.

Sub-section 4.1 provides the BNL examination of the aspect of free-field data which characterizes the seismic wave transmitting mechanism of the earthquake motions traveling across the test site. The BNL analyses for determining the best estimate low strain soil profiles for both the old and new free-field points are described in Sub-section 4.2, and the basis for the use of soil modulus degradation models is discussed in Sub-section 4.3. Finally, the uncertainties inherent in the soil properties are accounted for using a probabilistic analysis, as described in Sub-section 4.4. This analysis also determines the ground motion input at the surface suitable for the SSI analysis as will be discussed in Section 5.0.

4.1 Examination of Free-Field Records Using Arias Intensity

As described in Section 2, eight earthquakes recorded at the two free-field locations were provided to BNL by NUPEC as summarized in Table 2-1. To apply the method as described in Section 3 for confirming an upward propagating motion, the Arias intensity computed for the down-hole seismometers located between rock and ground surface in the free field should follow an initial built-up of energy in the rock seismometer with energy increasing as it propagates upward. Eventually the domination of energy should be established in the surface seismometer.

As discussed in Section 2, Earthquake Nos. 34, 63 and 89 occurred before the down-hole seismometers were installed at the new free-field point and, therefore, were recorded only at the old free-field point. Earthquake Nos. 131, 139, 157, 164, and 172 were recorded at both the old and new free-field points. In order to apply the field data for the correlation analysis, it should first be confirmed that the transmission wave types associated with these earthquake events are consistent with the 1D site model to be utilized for the convolution analysis. As discussed in Section 3, the seismic propagation through the site could be examined by computing the Arias intensity for the down-hole accelerometer recordings to trace the energy movement in the free field. The following sub-sections describes the BNL analysis which applied this technique to the recorded earthquake motions at both the old and new free-field points for selecting the motions that are consistent with the 1D site model.

4.1.1 Old Free-Field Point

The free-field coordinate system is defined by two orthogonal horizontal axes: x- and y- axes, respectively, coincident with the NS and EW directions, and the vertical direction represented by the z-axis. The NS direction (x-axis) is in the alignment of the multiple structures for which the dynamic cross interaction (DCI) effect is of a major interest in this study. Therefore, although the Arias intensity versus time relationship is computed and plotted for both x and y components, the primary focus would be on the x-component of the down-hole seismometer recordings, which were then examined to identify the energy movement of the earthquake motion in the free field.

Figures 4-1 and 4-2 show the Arias intensity plots for Earthquake No. 34. For the x-component, an initial built-up of the intensity is seen in the rock (GL - 34.3m), and the intensity is gradually built-up towards the surface, therefore establishing an upward energy movement of the motion. A similar observation can be made for the y-component. It can reasonably be concluded that Earthquake No. 34 consists primarily of upward propagating body waves, which could be approximated with the 1D site model.

For Earthquake No. 89, the Arias intensity plots, which are presented in Figures 4-3 and 4-4, showed a pattern that could not be used to establish a clear upward intensity build-up to support the rock to surface energy movement, especially for the x-component, which indicates similar intensities for both rock and surface responses that are consistent with surface waves. This observation is supported by the information of the seismic events provided in Table 2-1, which shows the zero depth of the source location for the Earthquake No. 89, and equal epicenter and focal distances. Therefore, Earthquake No. 89 may not be appropriate for the convolution analysis using the 1D site model, and was not utilized in this study for deriving the best estimate of the site low strain soil properties.

For Earthquake No. 131, the Arias intensity plots were presented in Figures 4-5 and 4-6. In these plots, most stations appear to support the upward intensity build-up, except for the intensities computed from the station at GL – 13m, which seem inconsistent compared to other stations. Since the upward movement of energy could not be clearly established, Earthquake No. 131 may, therefore, not be a suitable candidate for the correlation study using the 1D site model, and not considered for the identification of the best estimate of the site low strain soil properties.

Earthquake No. 139, whose intensities were plotted in Figures 4-7 and 4-8, also does not appear to be dominated by upward propagated body waves. As evidenced in Figure 4-7 for the x-component Arias intensity, the energy in the rock motion appears to maintain its strength and higher magnitude compared to the surface motion throughout the entire duration, and therefore does not support the assumption of the 1D site model. Consequently, Earthquake No. 139 was removed for use in the free-field analysis for determining the best estimate of the low strain profile.

Figures 4-9 and 4-10 show the Arias intensity plots for Earthquake No. 157, which indicate an upward energy movement similar to Earthquake No. 34. Therefore, Earthquake No. 157 is consistent with the assumption for the 1D site model and therefore considered in the free-field analysis for determining the best estimate of the low strain profile.

Since Earthquake No. 63 was received after the free-field analysis was completed, it was not considered in the site profile calculation. However, the Arias intensity was calculated for the x-component of Earthquake No. 63, which is shown in Figure 4-11. As this figure depicts, the Arias intensity plots for Earthquake No. 63 are also consistent with an upward propagating wave.

In addition, the site amplification factors calculated as the ratio of maximum surface to rock Arias intensities were computed for the six earthquake events, and presented in Table 4-1.

Table 4-1. Site Amplification Factors for the Old Free-Field Point

	Earthquake Events					
	No. 34	No. 89	No. 131	No. 139	No. 157	No. 63
X-component	46.37	12.05	28.48	0.04	33.2	9.62
Y-component	36.92	1.12	27.55	10.47	12.95	-

4.1.2 New Free-Field Point

For the new free-field point, three earthquake events were provided by NUPEC for the free-field analysis, as designated by No. 131, No. 139 and No. 157. After the BNL free-field analyses were completed, two new earthquakes were also made available by NUPEC, which are referred to as No.164 and No. 172. The analysis using the Arias intensity to determine the energy movement of these seismic events in the free field, similar to the process utilized for the old free-field point, was performed for the new free-field point. Figures 4-12 and 4-13 present the Arias intensity plots of the free-field responses recorded at five stations along a down-hole array at the new free-field point for Earthquake No. 131. An upward energy movement of these seismic waves in the free field is clearly demonstrated by these plots, consistent with the 1D site model.

Figures 4-14 and 4-15 show the Arias intensity plots for Earthquake No. 139 at the new free-field point, and they also indicate an upward energy movement from rock to surface. A similar upward propagating wave pattern was also confirmed for Earthquake 157 as shown in Figures 4-16 and 4-17. Therefore, these three earthquake events were utilized for the correlation study for determining the low strain best estimate soil properties of the new free-field point.

In addition, the newer earthquakes, Nos. 164 and 172, were also checked for their wave propagating patterns across the test site. Figures 4-18 and 4-19 present the Arias intensity plots in the x-direction at the new free-field point for these two earthquakes, which clearly confirmed the upward energy movement for these earthquakes.

Finally, the site amplification factors, similar to the ones calculated for the old free-field point, were computed for the new free-field point. These factors are given in Table 4-2.

Table 4-2. Site Amplification Factors for the Few Free-Field Point

	No. 131	No. 139	No. 157	No. 164	No. 172
X-component	76.23	20.37	40.78	41.38	14.23
Y-component	33.62	14.28	42.81	-	-

4.2 Free-Field Analyses for Determining Best Estimate Low Strain Soil Profiles

The BNL approach for determining low-strain soil properties utilizes the Fourier ratio technique with the modified Levenburg-Marquadt least square algorithm, as described in Section 3. The NUPEC laboratory estimated soil properties as shown in Figure 4-20 were used to calculate the initial estimate of the soil transfer function (rock to surface), with 1.5 percent constant damping assumed for the low-strain soils. The modified Levenburg-Marquadt least square minimization algorithm was then applied in conjunction with the convolution analyses performed with the CARES program to correlate the predicted soil transfer function with the target Fourier ratio of the surface to rock seismometer recordings for an earthquake event. The iteration continued until a satisfactory correlation convergence at the resonant frequency of the soil column was achieved. The predicted soil properties were back calculated by the CARES program. The following sub-sections describe the BNL analyses for the best estimate of low strain soil profiles for both the old and new free-field points.

4.2.1 Old Free-Field Point

For the old free-field point, Earthquake No. 34, x-component was used for the target soil amplification. Applying the Fourier ratio technique, the rock-to-surface amplification was computed using convolution analysis. The computed amplification was then compared to the Fourier ratio of the surface to rock seismometer recordings, as shown in Figure 4-21. As noted in this figure, the recorded surface/rock Fourier ratios are jagged and were smoothed using a 0.5 Hz triangular window function as described in Section 3. The smoothed Fourier ratios of the recorded amplification were entered into the modified Levenburg-Marquadt least square minimization algorithm as the target. As displayed in Figure 4-21, the BNL calculated amplification matched very well with the smoothed Fourier ratios of the recorded amplification at the major peak near the soil frequency about 6.0 Hz. Although the BNL calculation did not predict well at the second peak in the transfer function (primarily due to the fact that a clearly defined second peak does not exist in the smoothed target soil amplification), the BNL calculation is believed to be adequate for computing the soil properties, since the soil response is primarily controlled by the first major peak in the transfer function.

The low strain soil profile for the old free-field point in terms of shear wave velocity was back calculated from the computed transfer function and compared to the NUPEC laboratory data, as shown in Figure 4-22. As indicated in this figure, the BNL predicted profile is slightly stiffer than the NUPEC laboratory data for soils below GL -5m and a thin layer near the ground surface, and for soils in-between Gl –1.5m and 5m, the BNL prediction is slightly softer than the NUPEC laboratory results.

With the predicted low strain profile and the degradation model by GEI (Geotechnical Engineers, Inc.), convolution analysis using the CARES program was performed to compute the free-field response in terms of response spectra. Figures 4-23 to 4-25 show the free field response comparisons between the BNL computed spectra and the field recordings at the various elevations along the down-hole array at the old free-field point. As noted in these figures, the BNL predicted responses compared well with the recordings, especially for the near surface station (GL-1.5m). This is because the transfer function tends to match better near the surface than other locations in the column. The free-field responses were also computed for Earthquakes No. 34, y-component and No. 157, both x and y components. The response comparisons with the corresponding recordings are plotted in Figures 4-26 to 4-28. As shown in these figures, although these records were not directly used in the calculation of the transfer function for the soil column, fairly good comparisons were obtained between the computed response and the corresponding field recordings.

Further, the Arias intensity for the computed motion near the ground surface (GL-1.5m) was calculated for Earthquake Nos. 34 and 157, and compared with the corresponding Arias intensities calculated from the recorded motions. The comparisons are shown in Figures 4-29 to 4-32. As noted in these figures, the computed motions are more energized in the low and high ends of the time history, but have good matches in the middle section, especially for Earthquake No. 34, x-component.

4.2.2 New Free-Field Point

A similar process was used to develop the best estimate low-strain soil profile for the new free-field point. For the new free-field point, three seismic events, namely, Earthquake Nos. 131, 139 and 157, were used for the free-field analyses. Two new earthquakes, namely Earthquake Nos. 164 and 172, respectively, were provided by NUPEC after the BNL free-field analyses were

completed. Although these new data were not used in the development of the best estimate low strain soil profile for the new free-field point, the convolution analysis was performed for these earthquakes to ensure that the soil profile developed based on the other three earthquakes would also be consistent with the free-field responses recorded for these two new earthquakes.

After careful examination of the Arias intensity calculations from the free-field data for Earthquake Nos. 131, 139 and 157, it was concluded that Earthquake No. 139, x-component, was best suited and selected for the computation of the low strain soil profile at the new free-field point using the Fourier ratio technique (Earthquake No. 139, x-component, exhibits one clearly defined resonant peak in the rock-to-surface amplification, while others appear lacking such resonance characteristics). Figure 4-33 shows the comparison of the BNL calculated rock to surface amplification and the surface/rock Fourier ratios calculated from the recordings for Earthquake No. 139, x-component. Similar to the procedure used for the old free-field point, the recorded jagged surface/rock Fourier ratios for the new free-field point were also smoothed using a 0.5 Hz triangular window function as indicated by the solid line in Figure 4-33. The modified Levenburg-Marquadt least square minimization algorithm was then applied in conjunction with the convolution analyses performed with the CARES program to produce the low-strain soil profile for the new free-field point. The BNL calculated rock to surface transfer function as the dotted line in Figure 4-33 was compared with the recorded amplification (solid line in Figure 4-33). In this figure, the BNL predicted resonant peak is slightly shifted towards a higher frequency relative to the peak calculated from the recorded motion. However, when comparisons were made in terms of the free-field response spectra, as shown in Figures 4-34 and 4-35 for Earthquake No. 139, x-component at the stations located at GL. -3m and GL. -6.5m, excellent agreement was observed between the BNL calculations and the free-field recordings. The new free field low strain soil profile in terms of shear wave velocity was back calculated from the modified Levenburg-Marquadt least square minimization algorithm and compared to the NUPEC laboratory estimate as plotted in Figure 4-36. As indicated in this figure, the BNL predicted profile is about the same as the NUPEC laboratory data for rock, while for the soil overburden with a thickness of about 17m, the BNL predicted soil properties are mostly stiffer than the laboratory data, except for a thin layer near the surface where the BNL prediction is slightly softer than the NUPEC laboratory results.

Using the BNL predicted low strain soil profile for the new free-field point in conjunction with the GEI degradation model, convolution analyses were performed for Earthquake No. 139, y-component. Figures 4-37 and 4-38 provide the response comparisons for Earthquake No. 139, y-component. In this case, the response calculated using the BNL estimated soil properties produced slightly lower response than the recorded response. It is noted that Earthquake No. 139, y-component, was not used in the correlation analysis due to fact that the amplification calculated for Earthquake No. 139, y-component, did not delineate a major resonance peak as seen in conventional transfer functions.

Using a process similar to that applied to the old free-field point, the Arias intensities of the computed versus recorded surface motions were compared for the new free-field point, and plotted for Earthquake No. 139, both x and y-components in Figures 4-39 and 4-40. The energy transmission rates as characterized by the slope in the Arias intensity function show good agreement between the BNL calculation and the recordings.

4.3 Basis for Determining Soil Modulus Degradation Relationships

In order to determine the modulus degradation relationships for both the new and old free-field points, three well publicized and documented test models were selected, which are: GEI,

Geomatrix and EPRI 93 models. Figures 4-41 and 4-42 plot the soil shear modulus degradation and the soil hysteretic damping ratios as a function of the soil strain. These models were developed using the soil samples with geological features representative of the Western United States. BNL performed the convolution analyses to generate the free-field responses using the BNL estimated low strain soil profiles and the three modulus-degradation models for both the new and old free-field points. The computed free-field responses were then compared with the responses induced by the recorded events. Earthquake Nos. 34 and 157 were used in the comparisons for the old free-field point, and Earthquake Nos. 139 and 157 for the new free-field point.

For the old free-field point, Figures 4-43 to 4-46 show the comparisons between the responses from the BNL convolution analysis with the three modulus-degradation models and the corresponding recorded free-field responses. In these comparisons, responses calculated using both GEI and EPRI 93 degradation models appear very close to each other and both are comparable to the recorded responses, while the response generated with the Geomatrix model appears less comparable to the recorded responses in both frequency content and amplitudes.

Similar observations were also made for the new free-field point. Comparisons between the computed free-field responses and the recorded motions are provided in Figures 4-47 to 4-52. These figures indicate that both GEI and EPRI 93 models could be used to develop comparable free-field response to the recorded motions, while the Geomatrix model appears less suitable for the NUPEC site. These comparisons lead to the conclusion that either GEI or EPRI 93 can be selected as the degradation model for the free-field analysis. The BNL study employed the GEI modulus degradation model for the subsequent SSI analyses.

4.4 Probabilistic Based Strain-Dependent Soil Profiles

The purpose of the free-field analysis presented in this section is 1) to develop the high confidence strain-dependent free field soil profiles for the earthquake data, and 2) to generate the mean surface ground input motions from the bedrock free field seismometer data for the SSI response analyses. Recognizing that inherent uncertainties exist, a probabilistic sampling analysis was performed using the Monte Carlo method as described in Section 3. This subsection presents the results of the BNL probabilistic site identification analyses.

To apply the Monte Carlo method, the soil profile in terms of shear wave velocity is assumed to have a lognormal distribution. The best estimate of the low strain soil profiles as developed in the previous section using the Fourier ratio technique is used as the median low strain free-field profile. Figure 4-53 shows the BNL computed low strain profiles for both the old and the new free-field points. As indicated in this figure, the soil at the new free-field point appears slightly stiffer than the soil at the old free-field point, which reflects the location variability of the soil properties at the site. Furthermore, the data for the old free-field point are available up to 34m below grade, while the data for the new free-field point are available up to 53m below grade. From the site plan view as shown in Figure 2-12, the new free-field point is located near the center of the test site, while the old free-field point is located to the east of the test site. Given the above discussion, the BNL study selected the best estimate of the low strain soil profile for the new free-field point to be the median low strain free-field profile for the probabilistic sampling analysis.

The BNL probabilistic site identification analysis involves the following steps: 1) development of rock outcrop motion by convolving the recorded free field bedrock motion to the surface, then de-convolving it to rock outcrop; 2) generation of an ensemble of low strain free-field profiles by

randomly sampling the soil profiles with a lognormal distribution; 3) development of the strain dependent ensemble by performing convolution analyses using the low strain ensemble of the soil profiles and the rock outcrop inputs; and 4) performing convolution analyses to generate ground surface motions suitable for the SSI response analyses.

The lognormal standard deviation of 0.2 was assumed based on the code practice for accounting for soil property uncertainties, such as ASCE 4-86 and Section 3.7 of the USNRC SRP. A set of randomly sampled low strain profiles with the lognormal distribution was then developed; BNL generated a total of thirty sample profiles. Figure 4-54 shows the low strain V_s distributions for the median, mean, plus and minus one-standard deviation. It is shown in this figure that the mean profile, though slightly stiffer, is fairly close to the median, suggesting that 30 samples are appropriate for this simulation.

Convolution analyses were performed for each of the 30 low strain profiles and a rock outcrop from each earthquake. The rock outcrop was calculated by first convolving the in-column recorded rock motion to generate a surface motion. The surface motion was then deconvolved to generate a bedrock outcrop motion. Figure 4-55 shows the final strain compatible V_s profiles in terms of the mean, and associated maximum and minimum V_s for each layer generated from Earthquake No. 139x. Since Earthquake No. 139x is a small earthquake, with the maximum acceleration of about 9 gal induced at ground surface, it is expected that V_s should stay in the low strain regime through the entire motion. This is evident in Figure 4-55, which shows that the iterated mean is coincident with the low strain mean. Figures 4-56 and 4-57 show the soil strains and the soil damping in terms of the mean, maximum and minimum. Figure 4-58 provides the computed surface response spectra from Earthquake No. 139x plotted in terms of the mean, mean+1sigma and mean-1sigma (sigma stands for standard deviation) together with the outcrop input. The surface mean response spectrum can then be used as input to an SSI analysis to compute the mean SSI response. One could also use a series of percentile spectra as inputs and propagate through the SSI analyses to generate a series of percentile SSI responses. A statistical analysis would then be performed to generate the mean response.

Finally, the sampling distribution of the strain-dependent soil profiles and hysteretic damping were plotted for Earthquake Nos. 89x, 63x, 131x, 157x, 164x and 172x in Figures 4-59 to 4-70. These strain-dependent soil properties together with the corresponding surface inputs were used in the SSI response analyses, which are discussed in the next section.

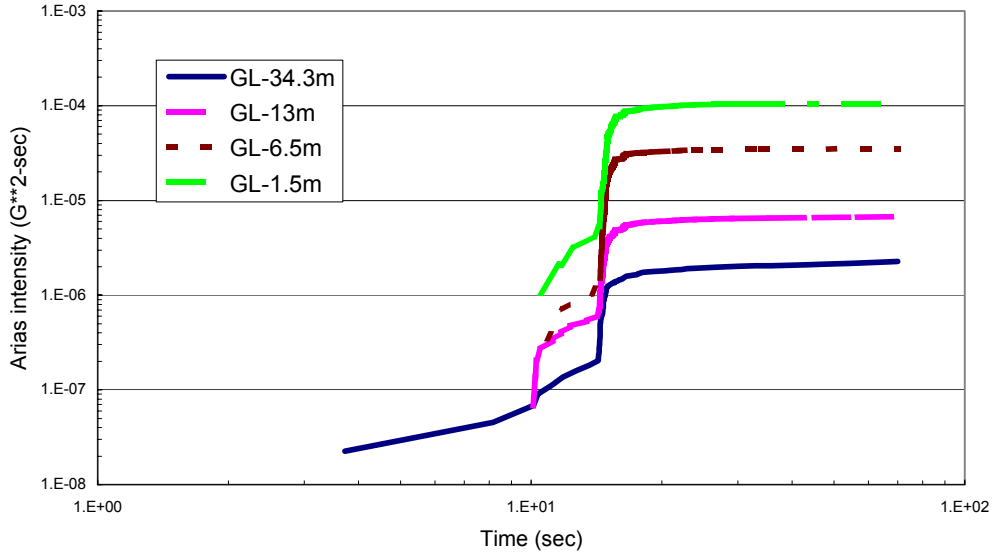

Figure 4-1. Arias intensities for the down-hole array for Earthquake 34x at Old Free-Field Point.

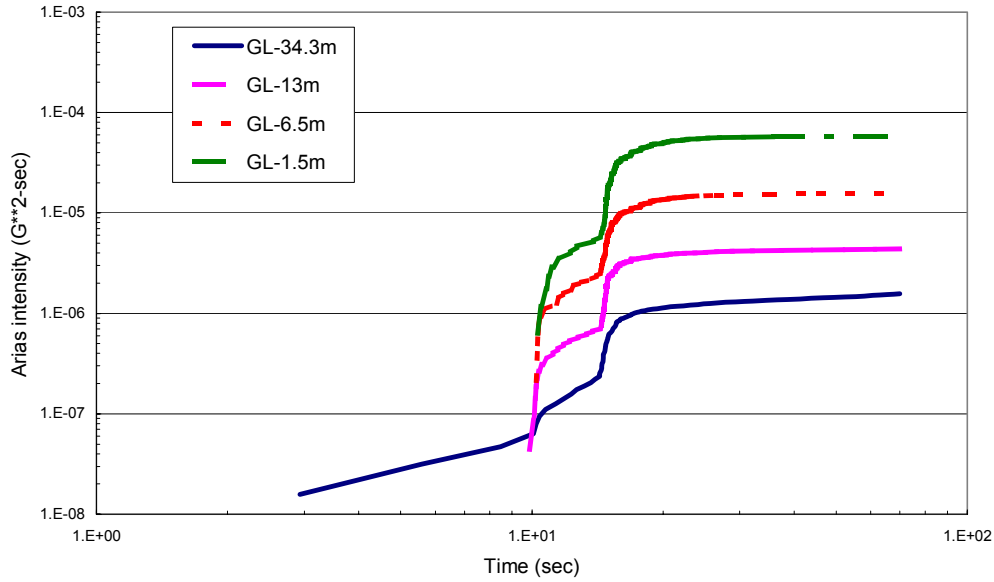

Figure 4-2. Arias intensities for the down-hole array for Earthquake 34y at Old Free-Field Point.

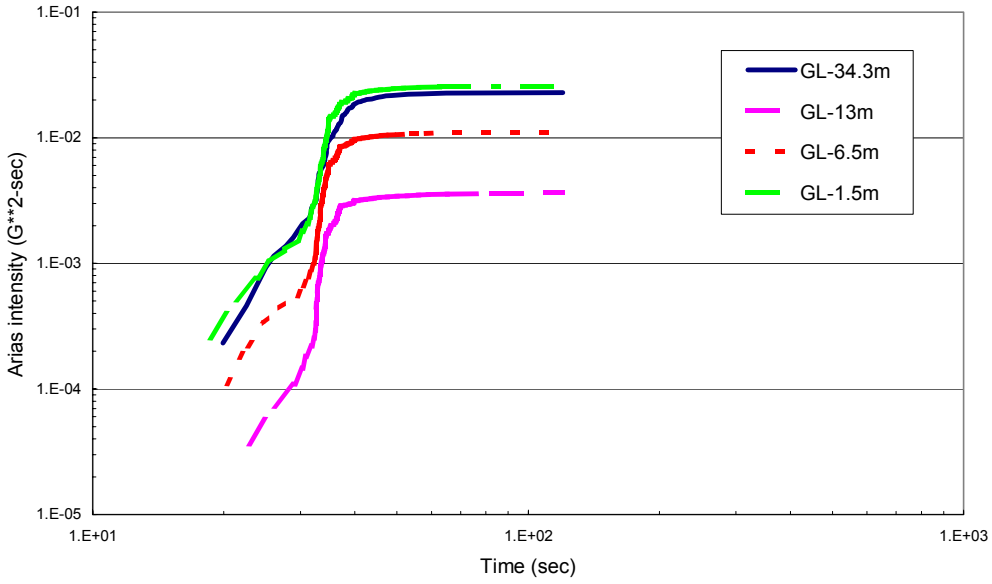

Figure 4-3. Arias intensities for the down-hole array for Earthquake 89x at Old Free-Field Point.

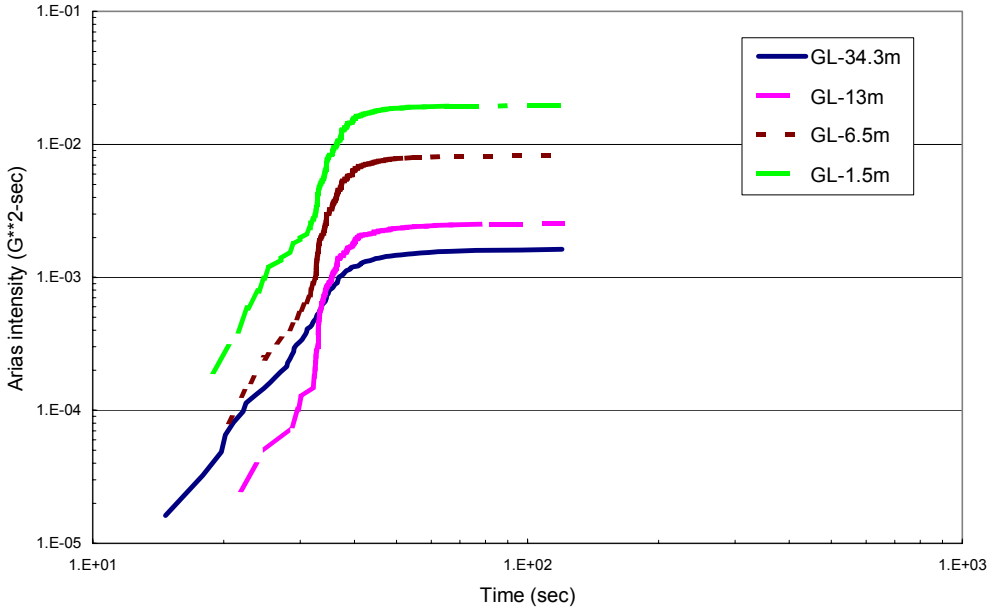

Figure 4-4. Arias intensities for the down-hole array for Earthquake 89y at Old Free-Field Point.

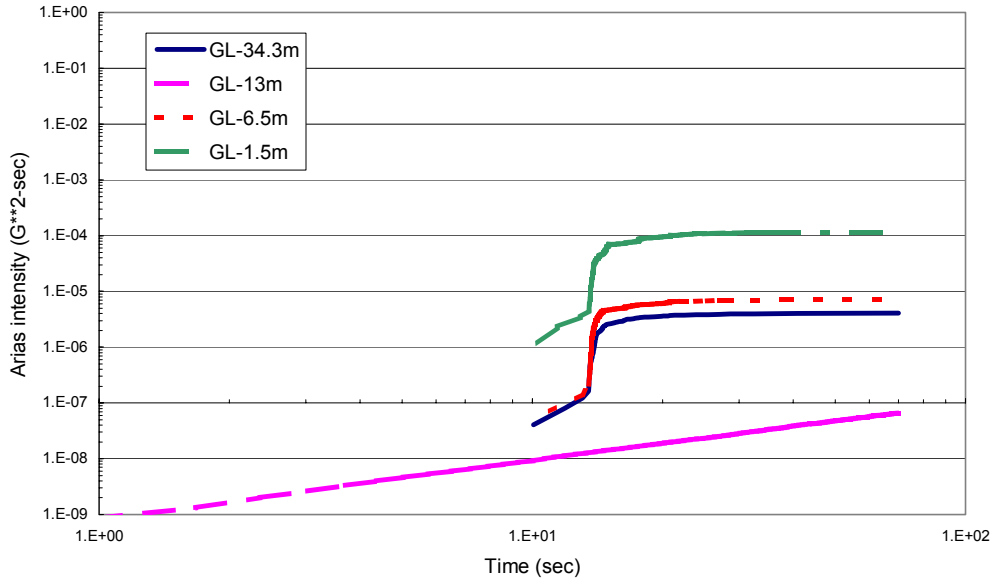

Figure 4-5. Arias intensities for the down-hole array for Earthquake 131x at Old Free-Field Point.

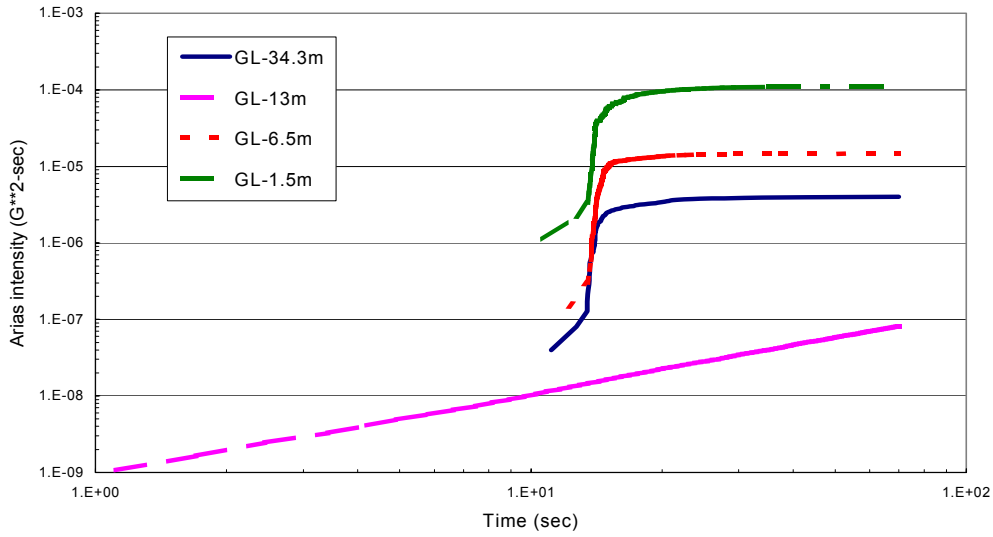

Figure 4-6. Arias intensities for the down-hole array for Earthquake 131y at Old Free-Field Point.

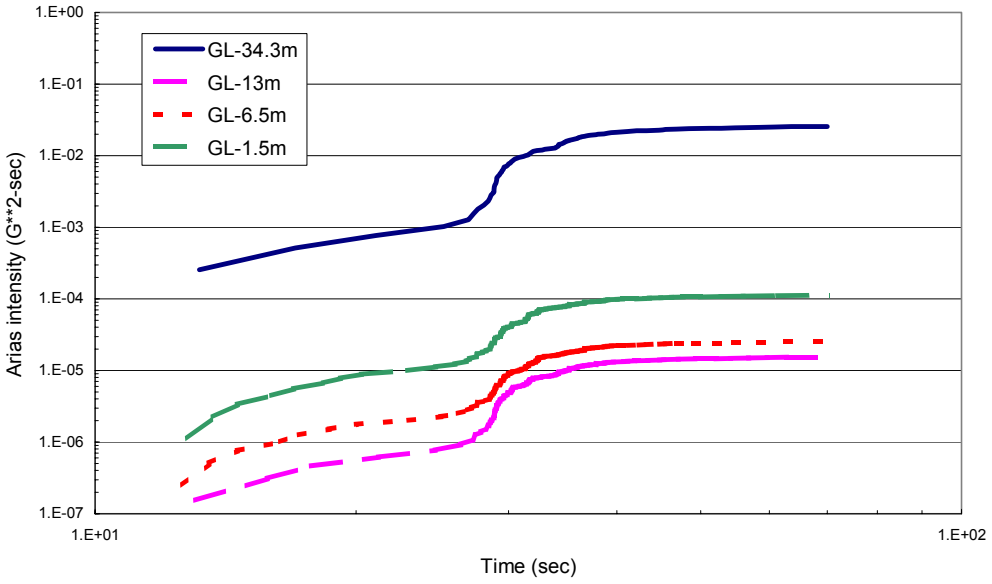

Figure 4-7. Arias intensities for the down-hole array for Earthquake 139x at Old Free-Field Point.

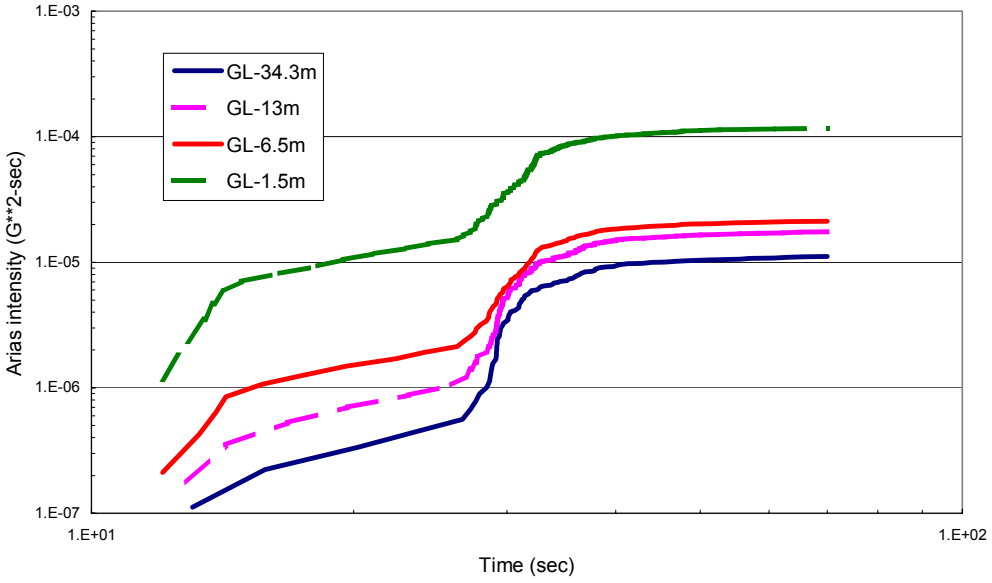

Figure 4-8. Arias intensities for the down-hole array for Earthquake 139y at Old Free-Field Point.

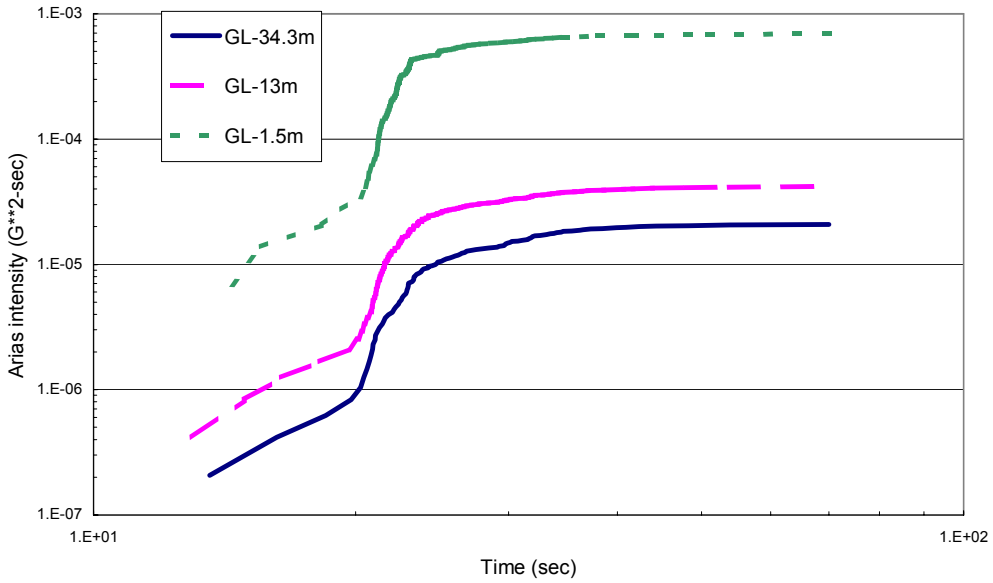

Figure 4-9. Arias intensities for the down-hole array for Earthquake 157x at Old Free-Field Point.

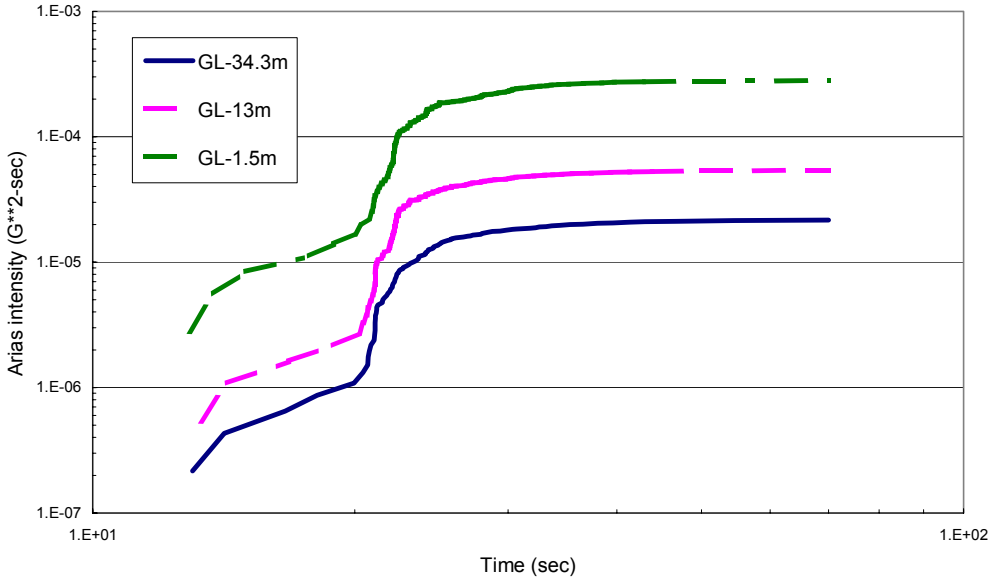

Figure 4-10. Arias intensities for the down-hole array for Earthquake 157y at Old Free-Field Point.

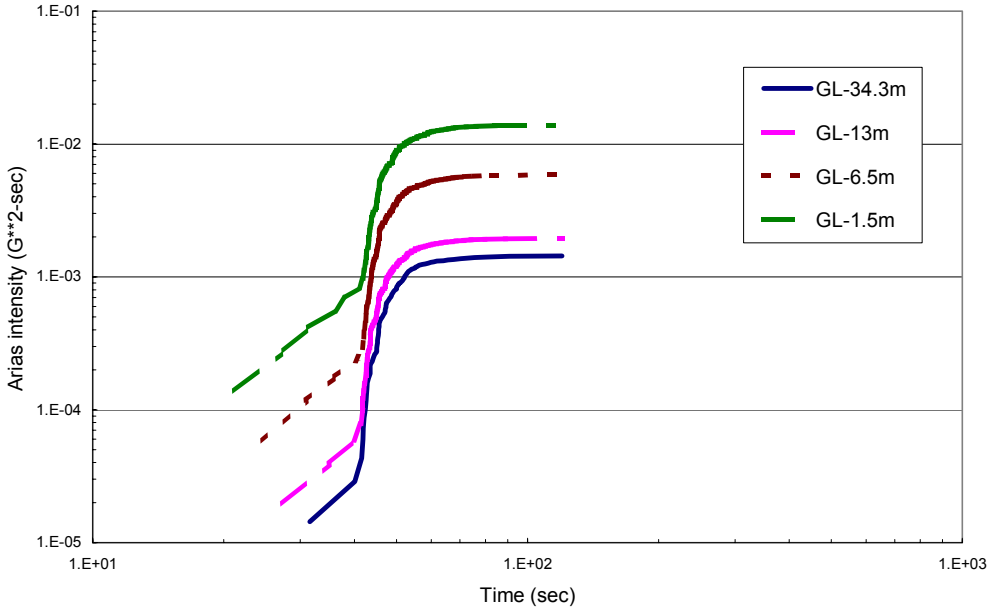

Figure 4-11. Arias intensities for the down-hole array for Earthquake 63x at Old Free-Field Point.

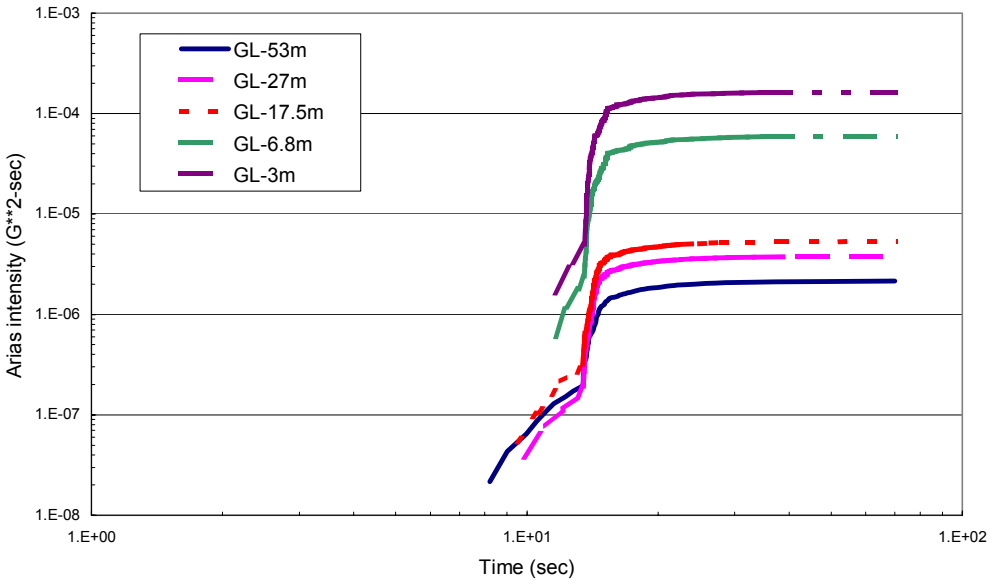

Figure 4-12. Arias intensities for the down-hole array for Earthquake 131x at New Free-Field Point.

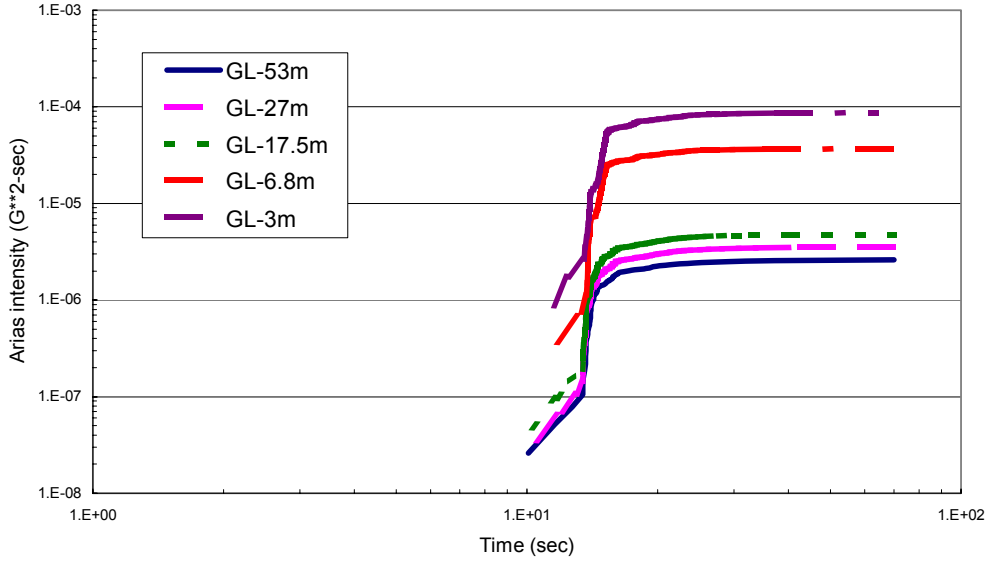

Figure 4-13. Arias intensities for the down-hole array for Earthquake 131y at New Free-Field Point.

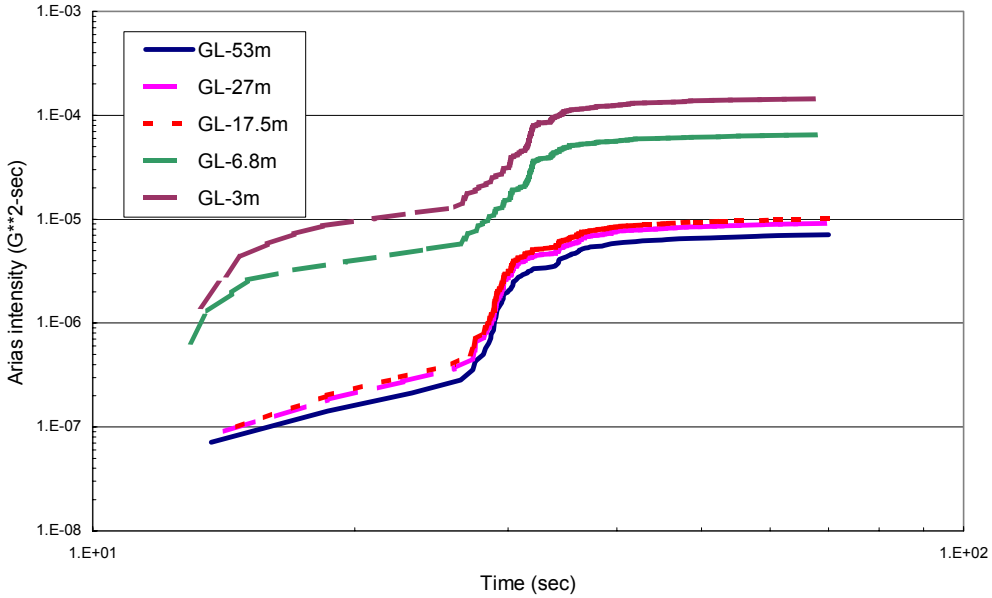

Figure 4-14. Arias intensities for the down-hole array for Earthquake 139x at New Free-Field Point.

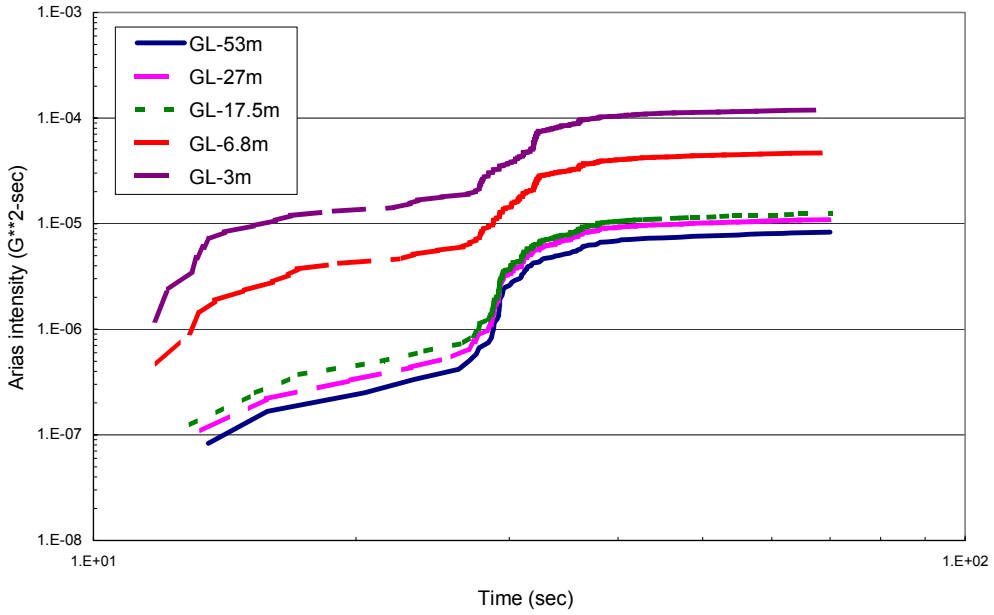

Figure 4-15. Arias intensities for the down-hole array for Earthquake 139y at New Free-Field Point.

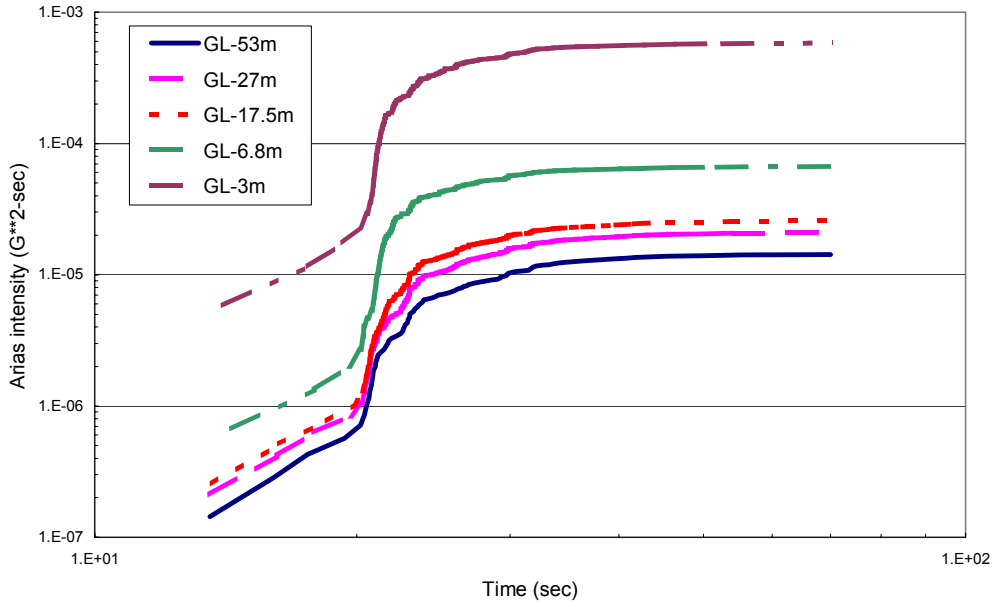

Figure 4-16. Arias intensities for the down-hole array for Earthquake 157x at New Free-Field Point.

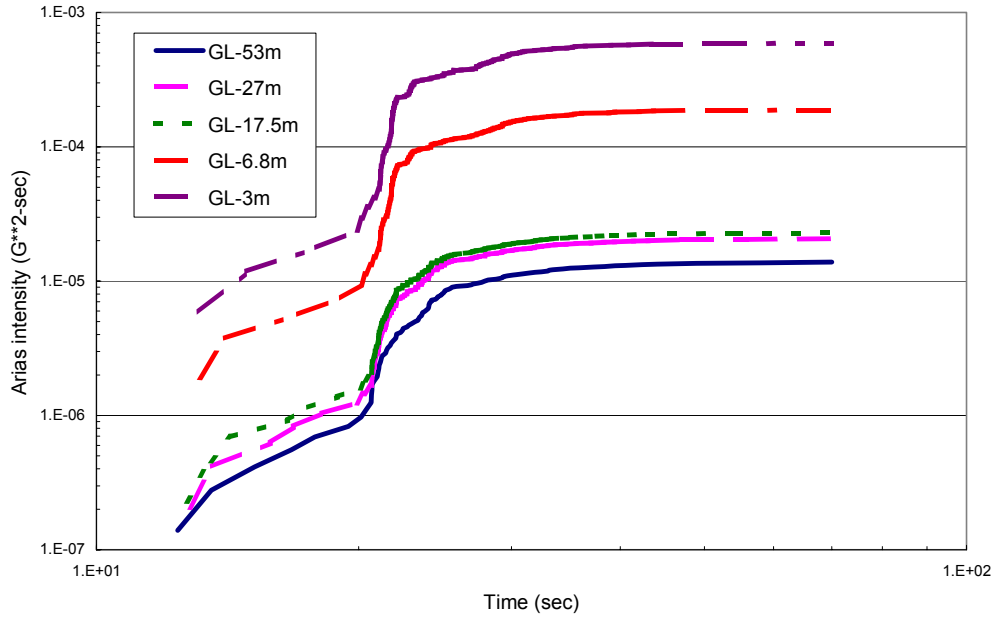

Figure 4-17. Arias intensities for the down-hole array for Earthquake 157y at New Free-Field Point.

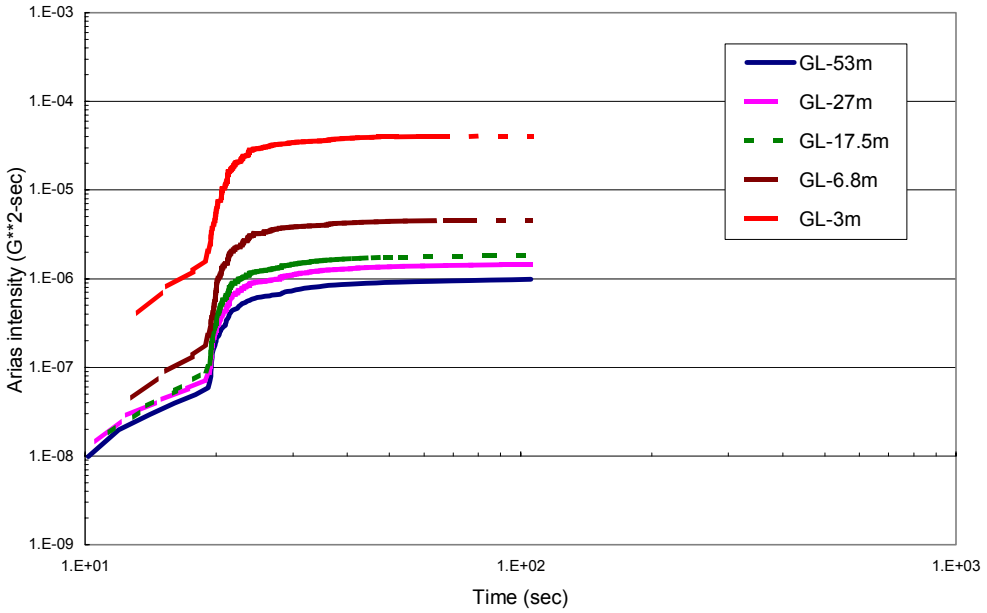

Figure 4-18. Arias intensities for the down-hole array for Earthquake 164x at New Free-Field Point.

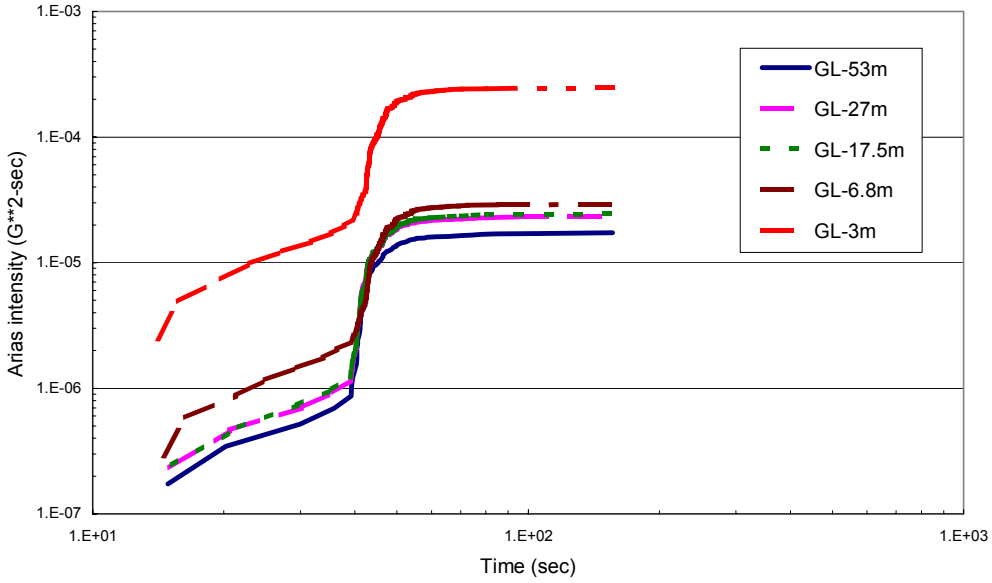

Figure 4-19. Arias intensities for the down-hole array for Earthquake 172x at New Free-Field Point.

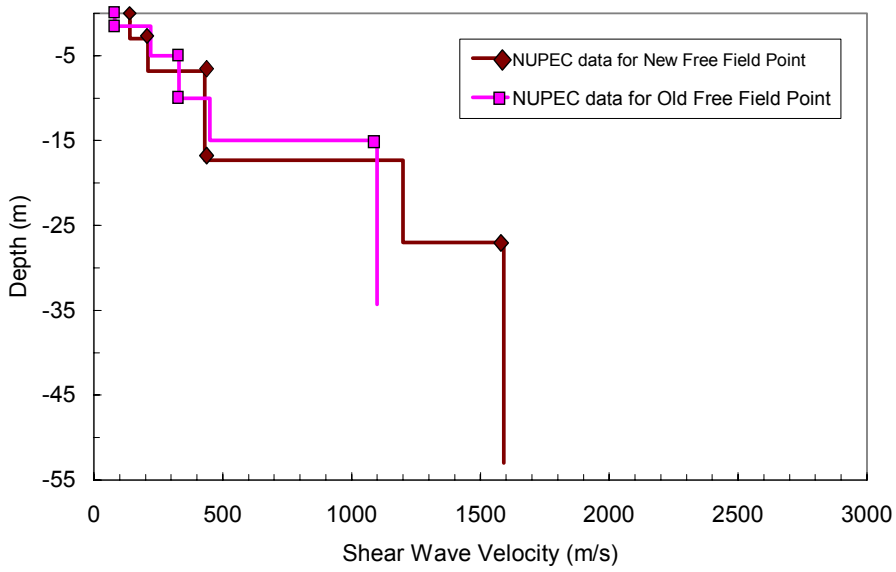

Figure 4-20. Laboratory best estimate of low strain free-field profiles.

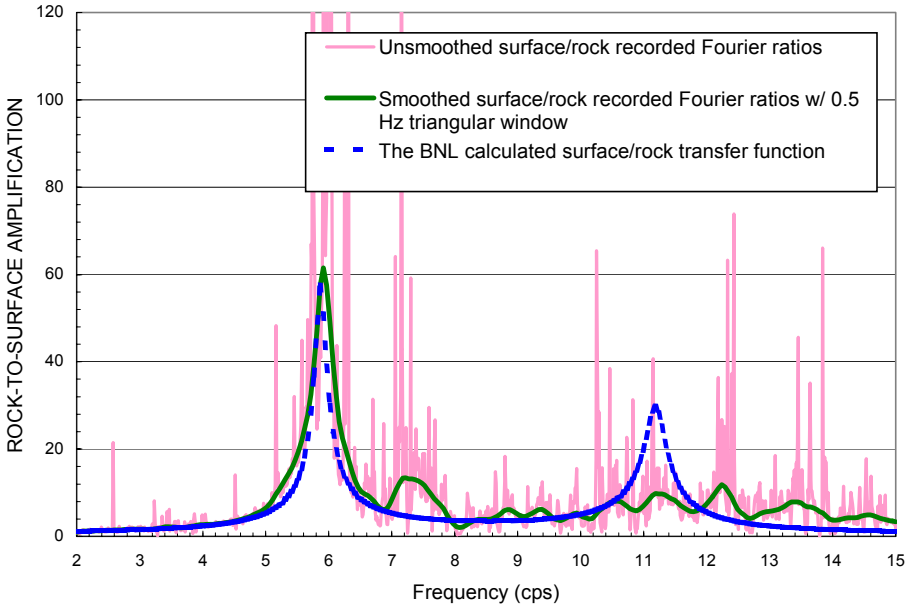

Figure 4-21. Computed surface/rock transfer function at the old free-field point.

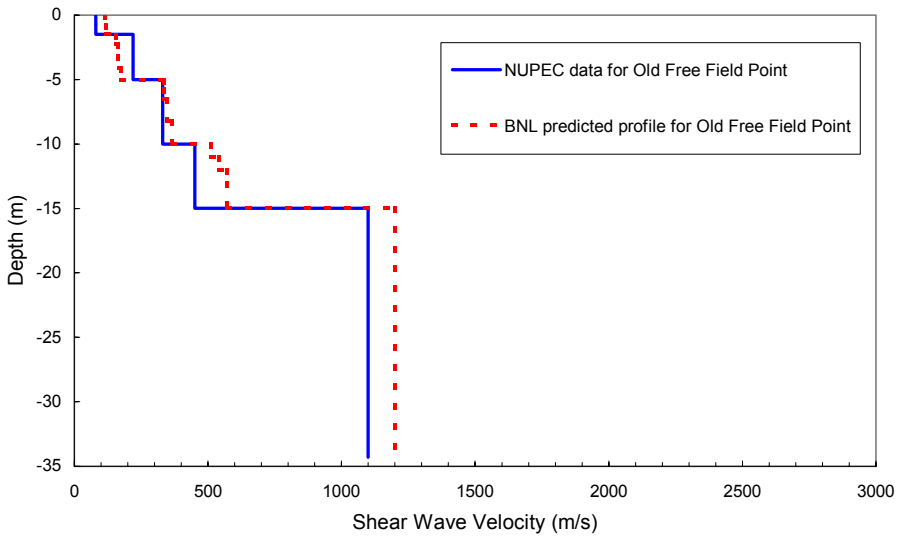

Figure 4-22. Comparison between the BNL computed low strain soil profile and the NUPEC Laboratory estimate for the old free-field point.

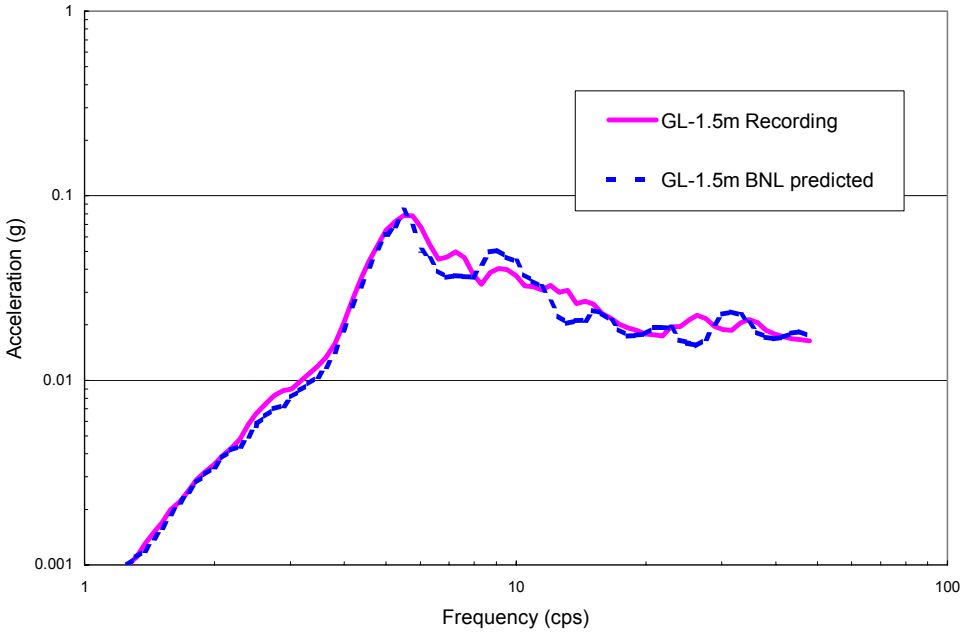

Figure 4-23. BNL predicted response spectrum at GL-1.5m, compared to the recorded response for Earthquake 34x at the old free-field point.

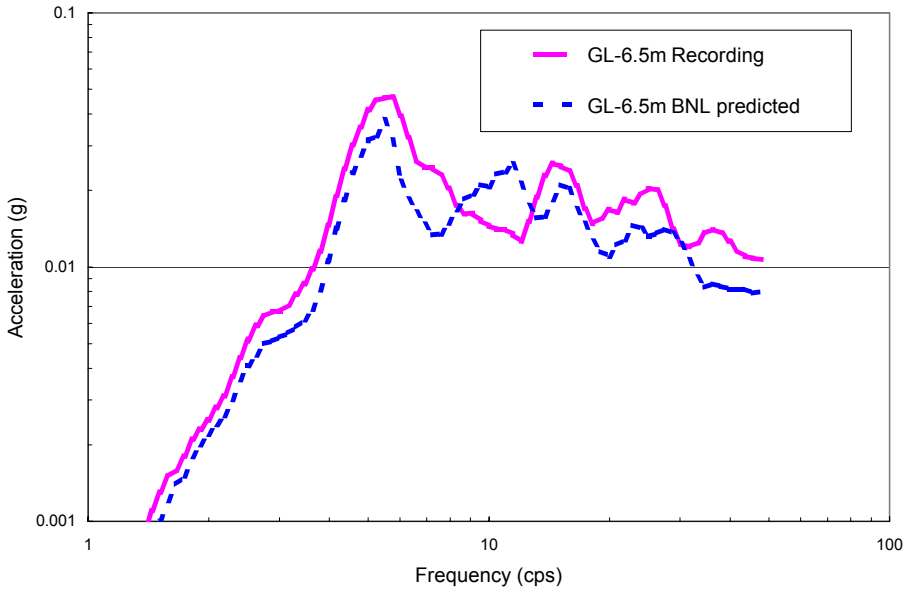

Figure 4-24. BNL predicted response spectrum at GL-6.5m, compared to the recorded response for Earthquake 34x at the old free-field point.

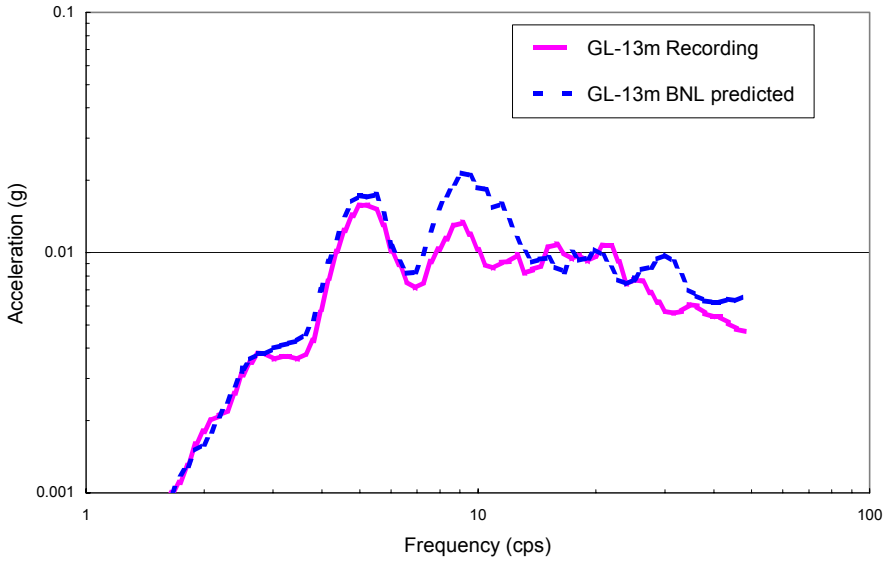

Figure 4-25. BNL predicted response spectrum at GL-13m, compared to the recorded response for Earthquake 34x at the Old Free-Field Point.

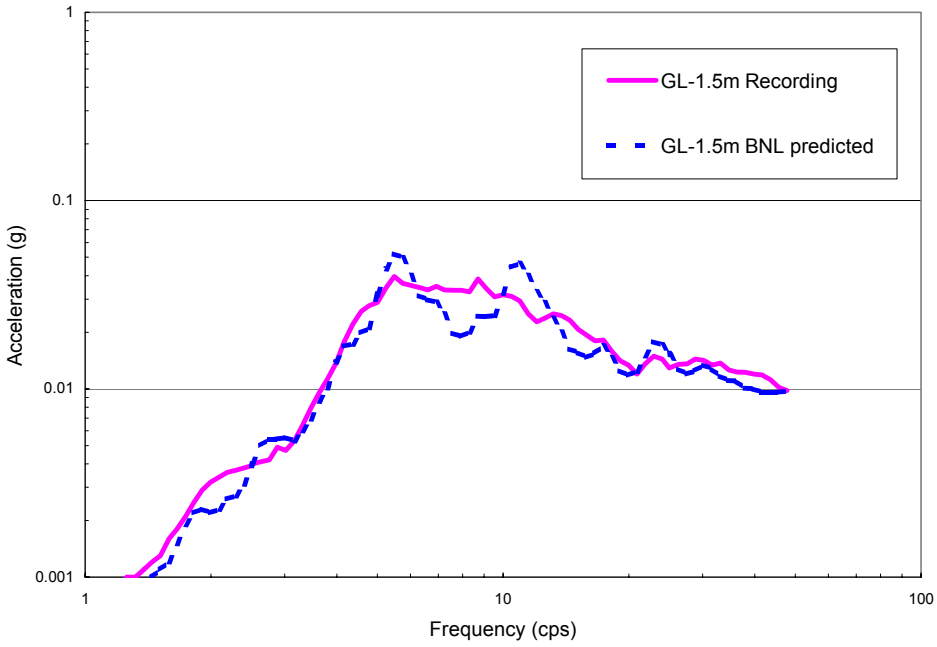

Figure 4-26. BNL predicted response spectrum at GL-1.5m, compared to the recorded response for Earthquake 34y at the Old Free-Field Point.

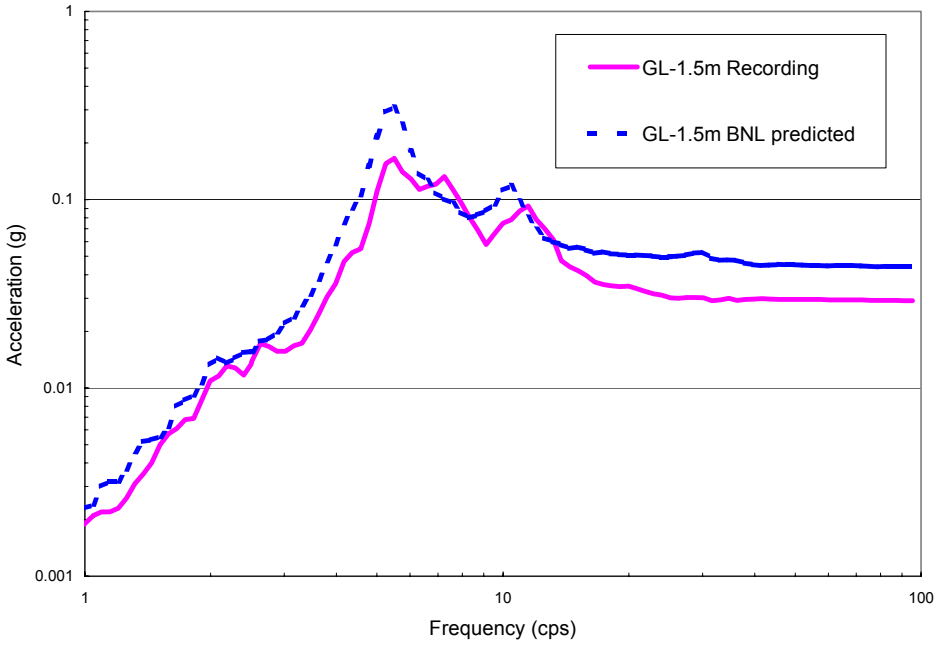

Figure 4-27. BNL predicted response spectrum at GL-1.5m, compared to the recorded response for Earthquake 157x at the Old Free-Field Point.

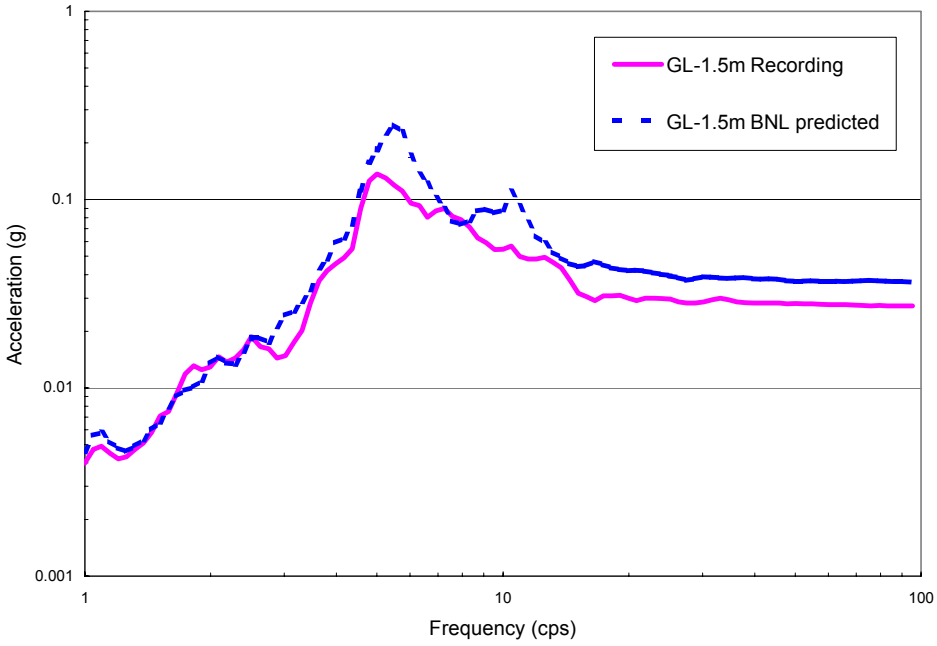

Figure 4-28. BNL predicted response spectrum at GL-1.5m, compared to the recorded response for Earthquake 157y at the Old Free-Field Point.

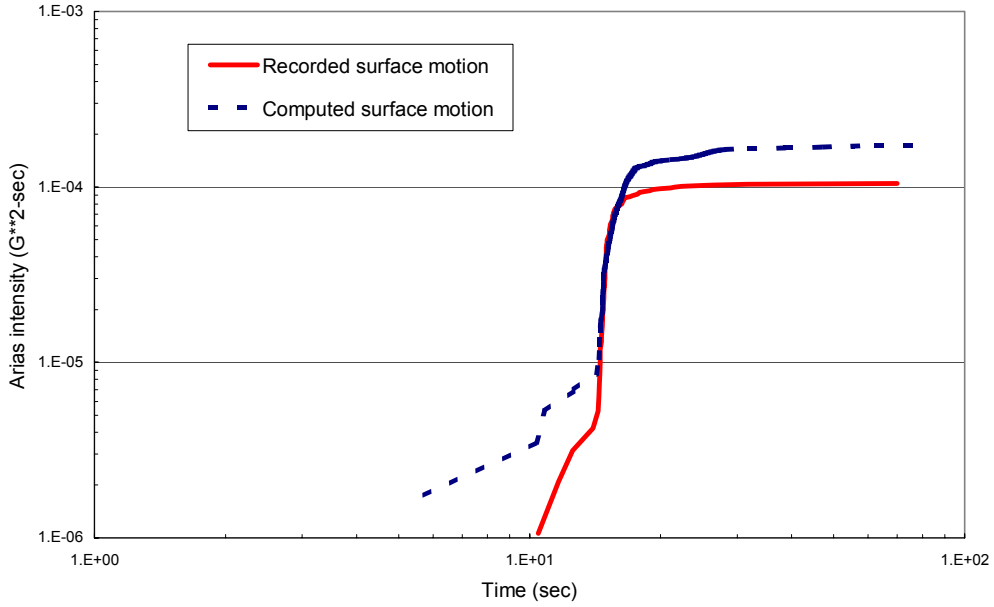

Figure 4-29. Comparison of Arias intensities between computed and recorded surface responses for Earthquake 34x at the Old Free-Field Point.

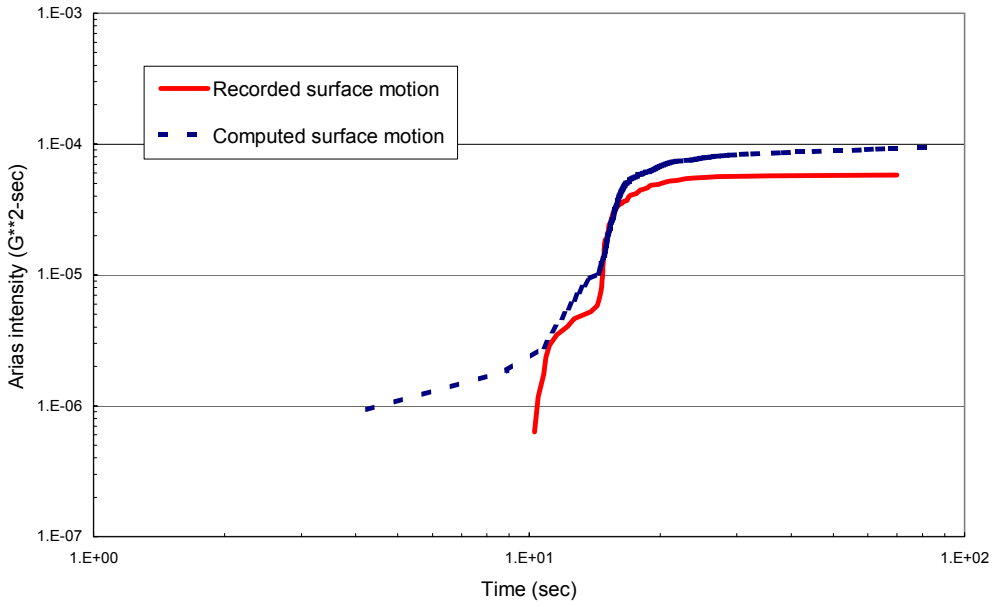

Figure 4-30. Comparison of Arias intensities between computed and recorded surface responses for Earthquake 34y at the Old Free-Field Point.

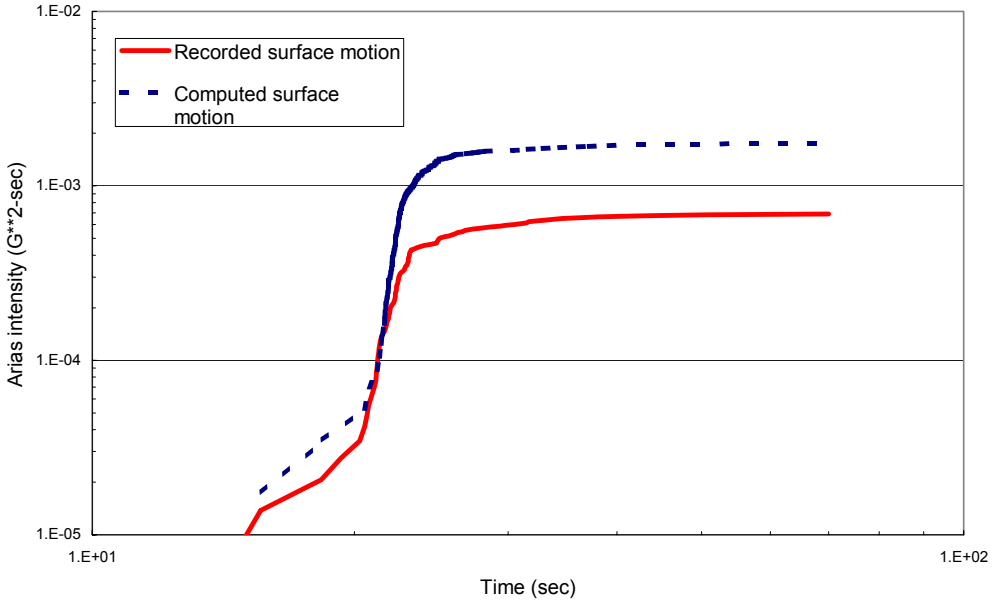

Figure 4-31. Comparison of Arias intensities between computed and recorded surface responses for Earthquake 157x at the Old Free-Field Point.

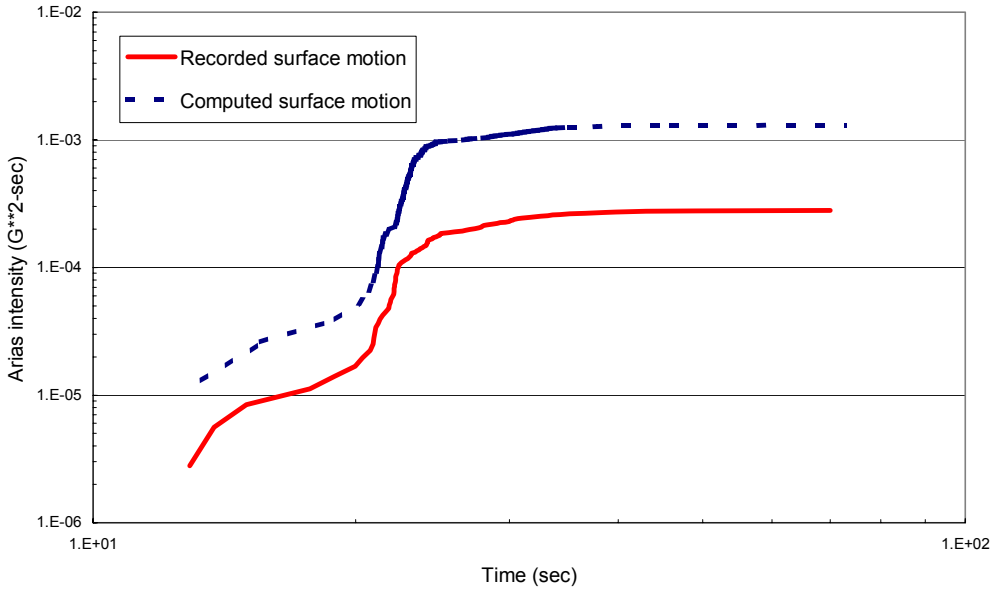

Figure 4-32. Comparison of Arias intensities between computed and recorded surface responses for Earthquake 157y at the Old Free-Field Point.

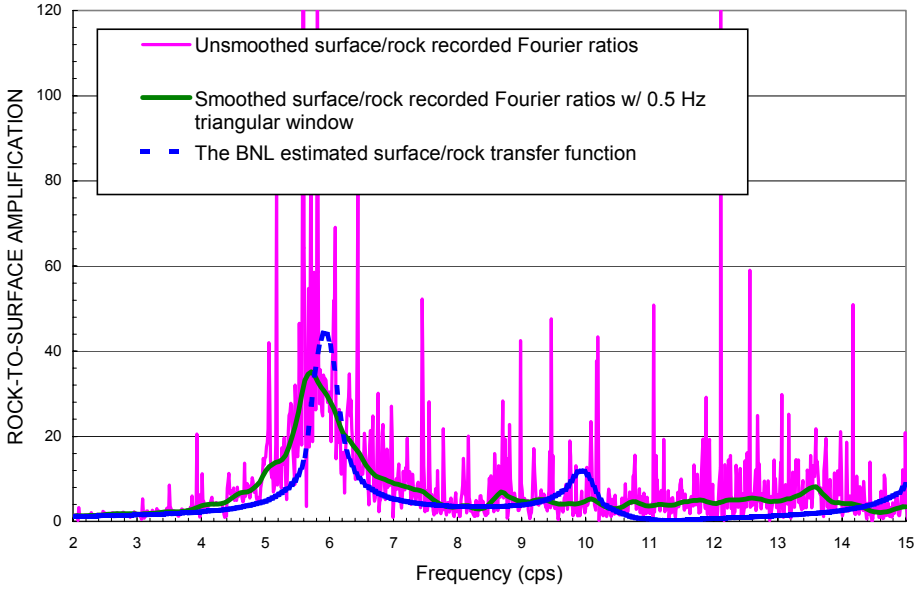

Figure 4-33. Computed surface/rock transfer function at the new free-field point.

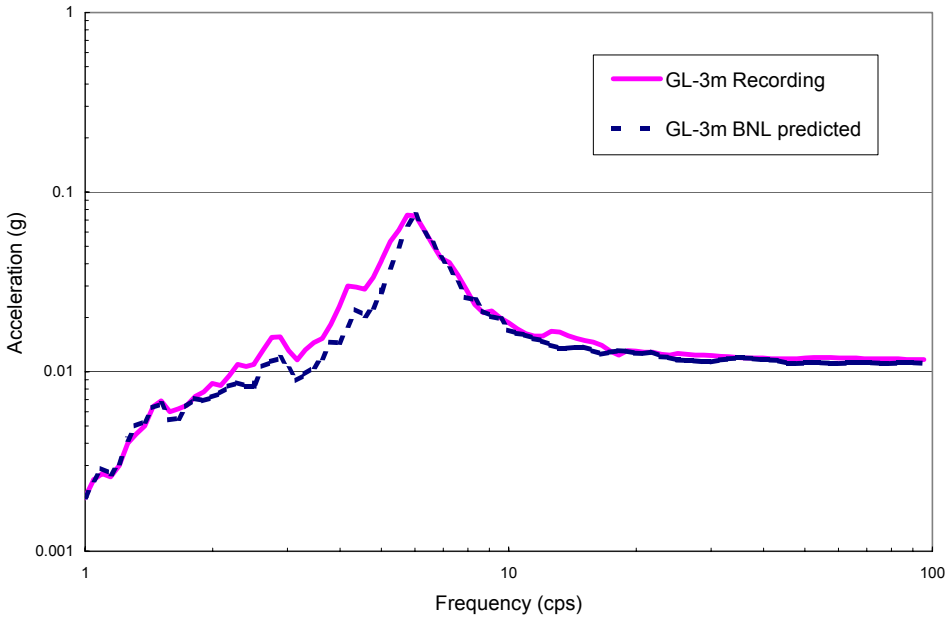

Figure 4-34. BNL predicted response spectrum at GL-3.0m, compared to the recorded response for Earthquake 139x at the new free-field point.

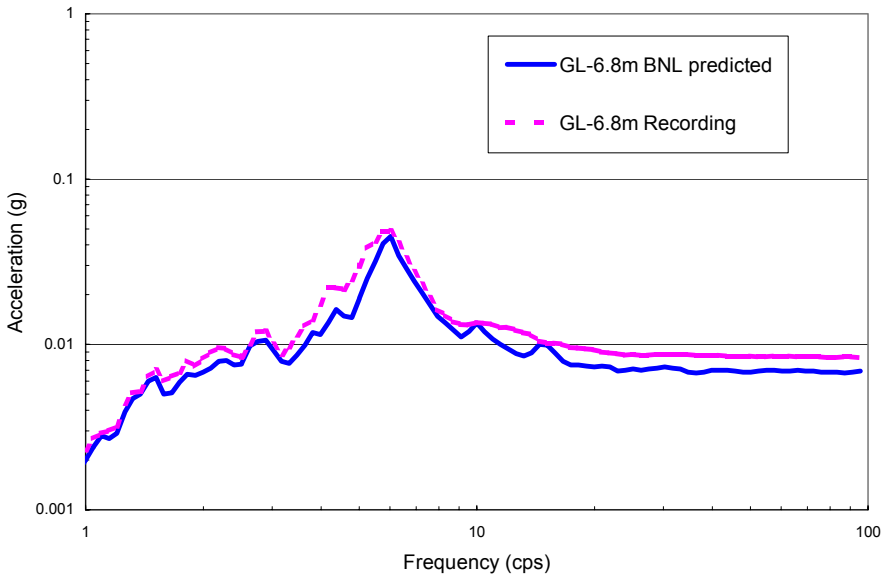

Figure 4-35. BNL predicted response spectrum at GL-6.8m, compared to the recorded response for Earthquake 139x at the New Free-Field Point.

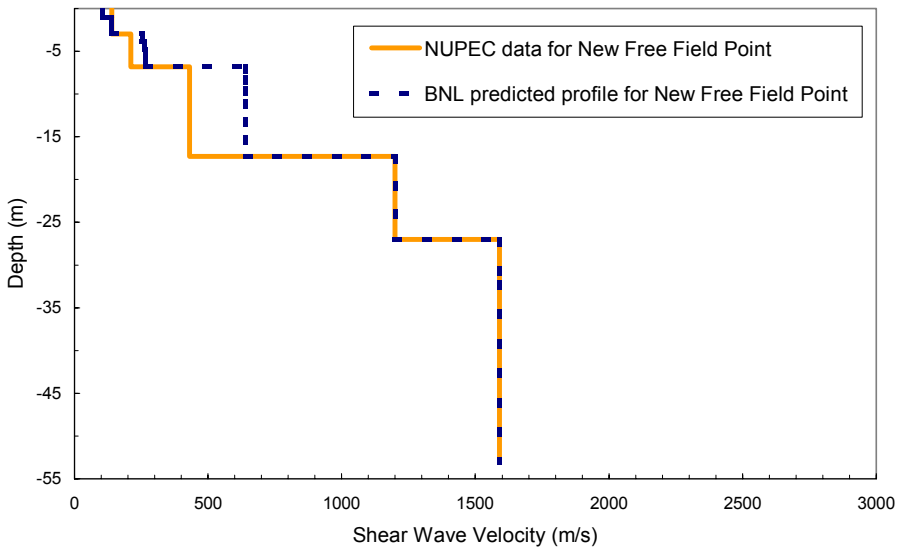

Figure 4-36. Comparison between the BNL computed low strain soil profile and the NUPEC laboratory estimate for the New Free-Field Point.

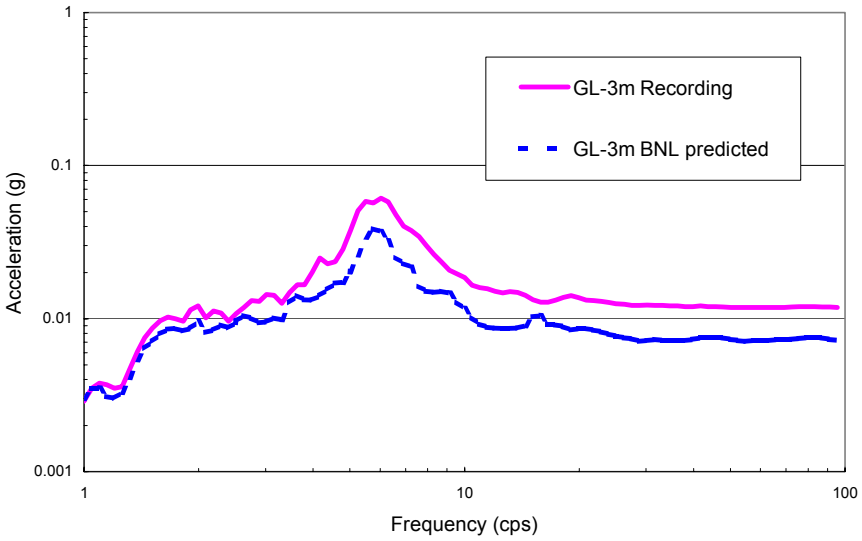

Figure 4-37. BNL predicted response spectrum at GL-3m, compared to the recorded response for Earthquake 139y at the New Free-Field Point.

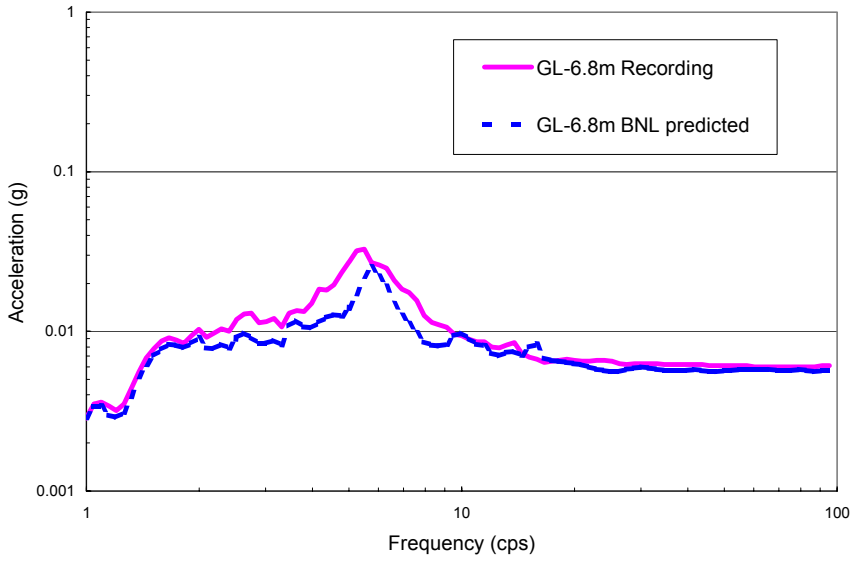

Figure 4-38. BNL predicted response spectrum at GL-6.8m, compared to the recorded response for Earthquake 139y at the New Free-Field Point.

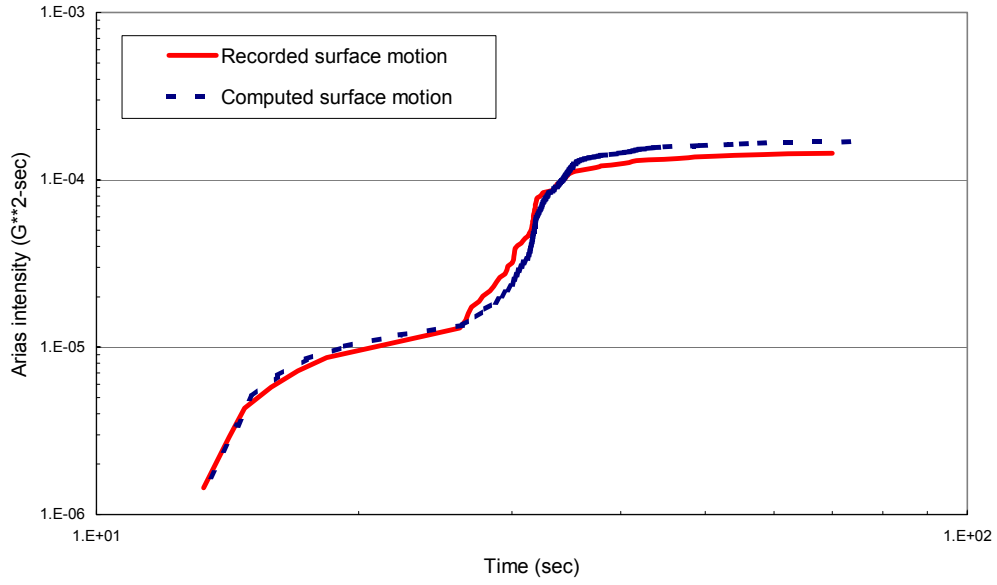

Figure 4-39. Comparison of Arias intensities between computed and recorded surface responses for Earthquake 139x at the New Free-Field Point.

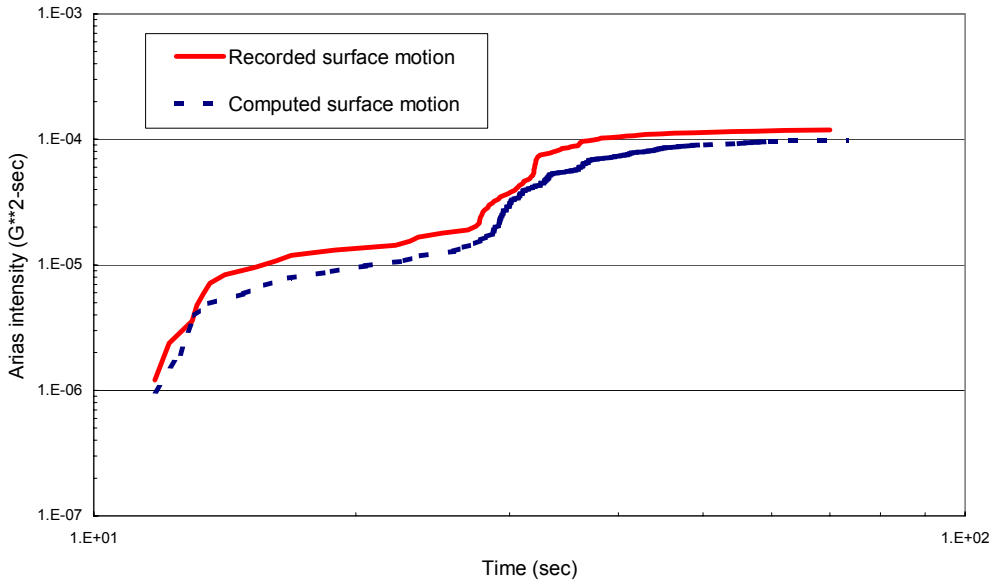

Figure 4-40. Comparison of Arias intensities between computed and recorded surface responses for Earthquake 139y at the New Free-Field Point.

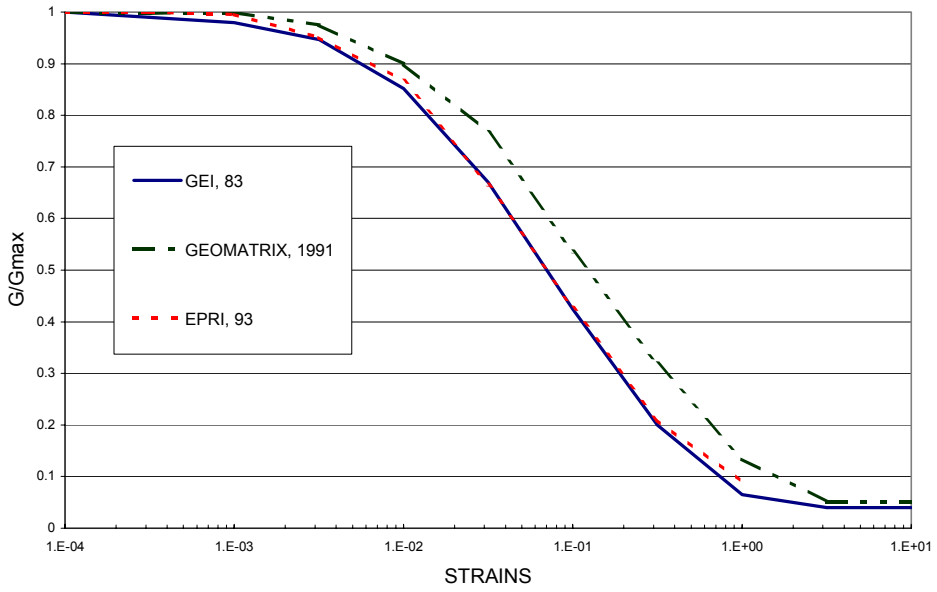

Figure 4-41. Soil modulus strain degradation relationships.

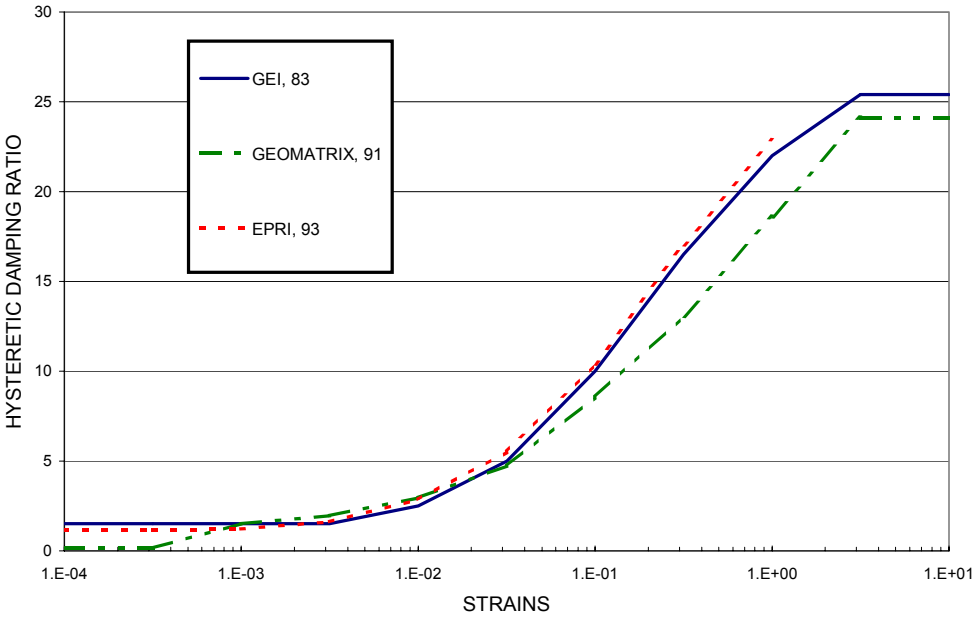

Figure 4-42. Soil hysteretic damping ratios as function of soil strain.

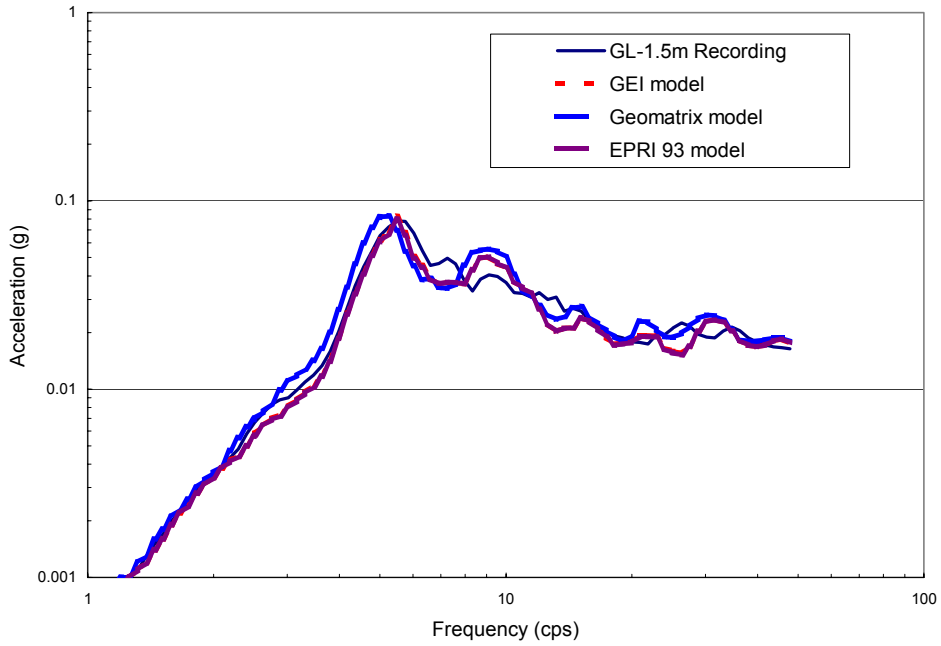

Figure 4-43. Comparison of the use of different degradation models for the old free-field point using Earthquake 34x.

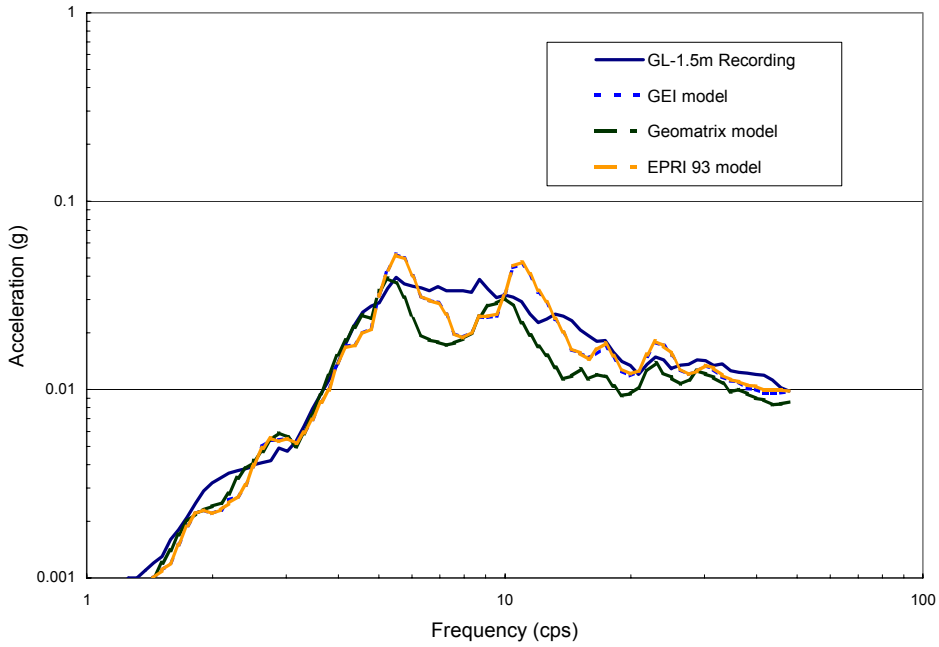

Figure 4-44. Comparison of the use of different degradation models for the old free-field point using Earthquake 34y.

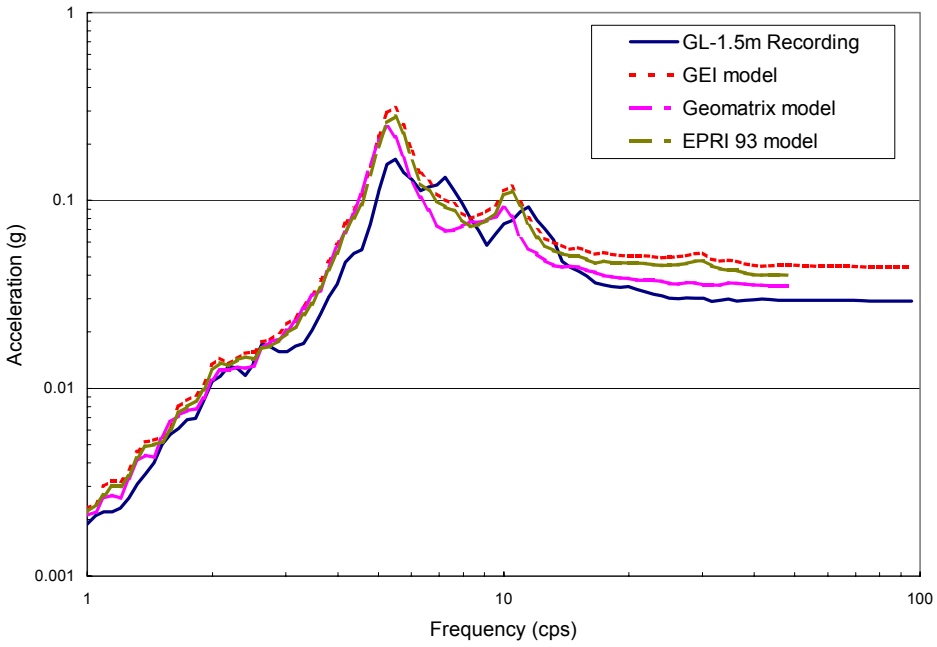

Figure 4-45. Comparison of the use of different degradation models for the Old Free-Field Point using Earthquake 157x.

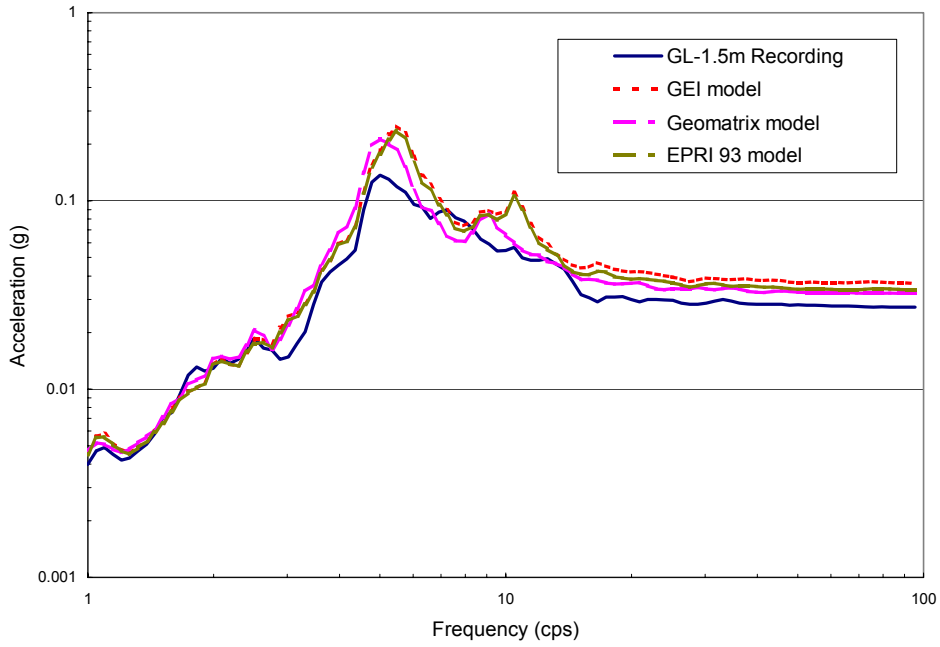

Figure 4-46. Comparison of the use of different degradation models for the Old Free-Field Point using Earthquake 157y.

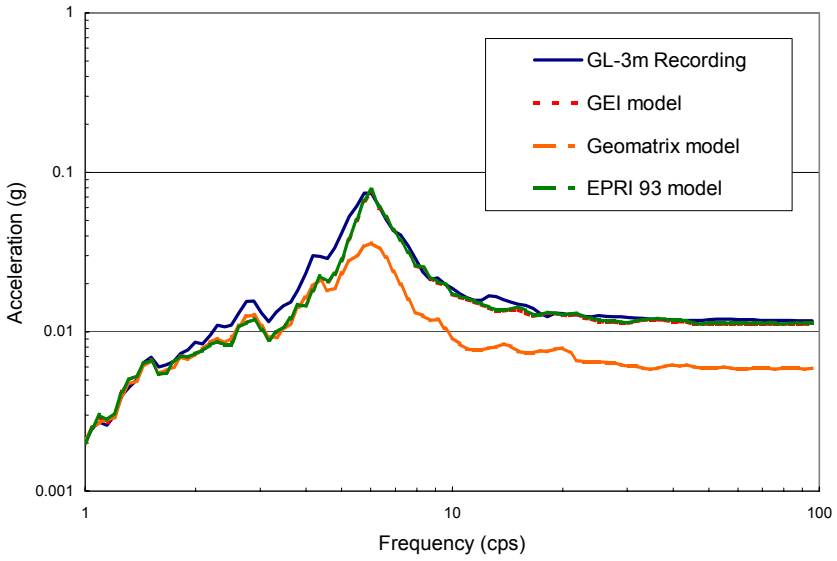

Figure 4-47. Comparison of the use of different degradation models for the New Free-Field Point using Earthquake 139x.

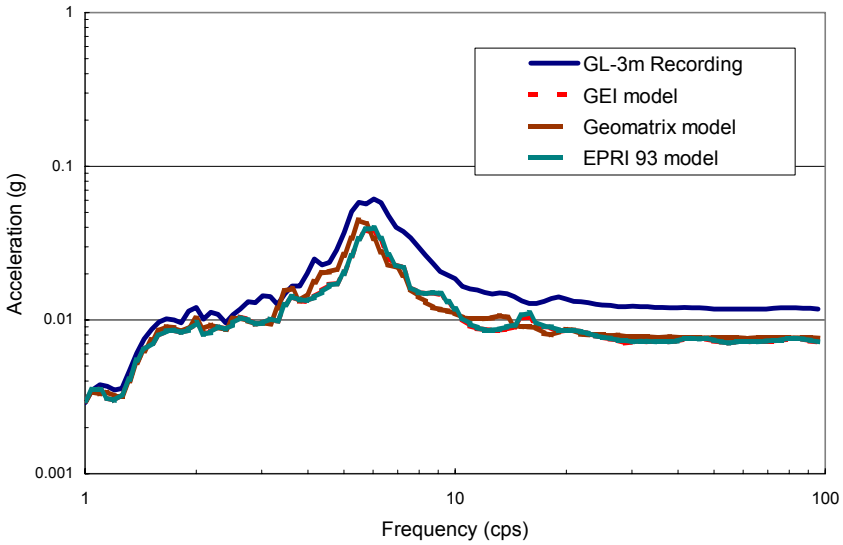

Figure 4-48. Comparison of the use of different degradation models for the New Free-Field Point using Earthquake 139y.

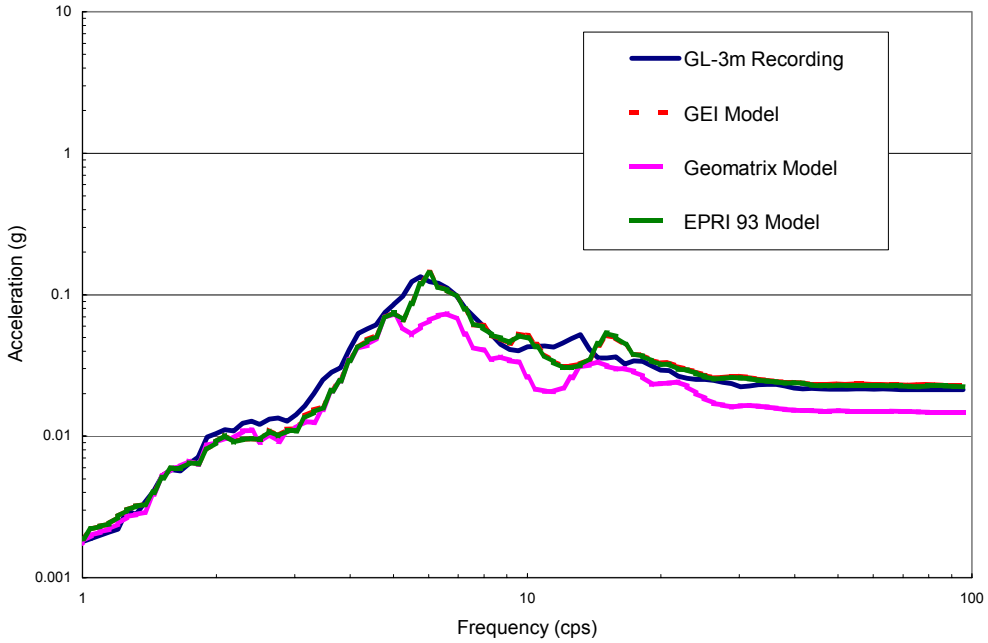

Figure 4-49. Comparison of the use of different degradation models for the New Free-Field Point using Earthquake 157x.

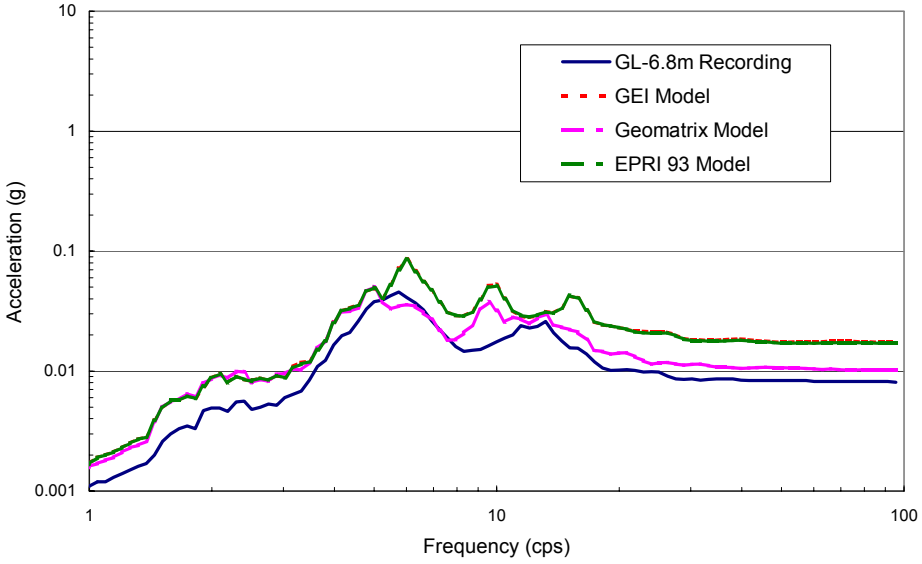

Figure 4-50. Comparison of the use of different degradation models for the New Free-Field Point using Earthquake 157x.

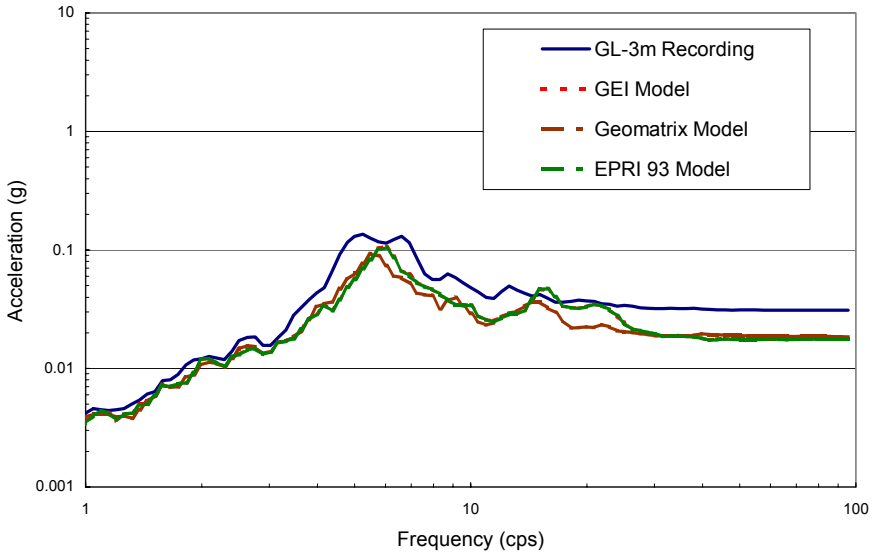

Figure 4-51. Comparison of the use of different degradation models for the New Free-Field Point using Earthquake 157y.

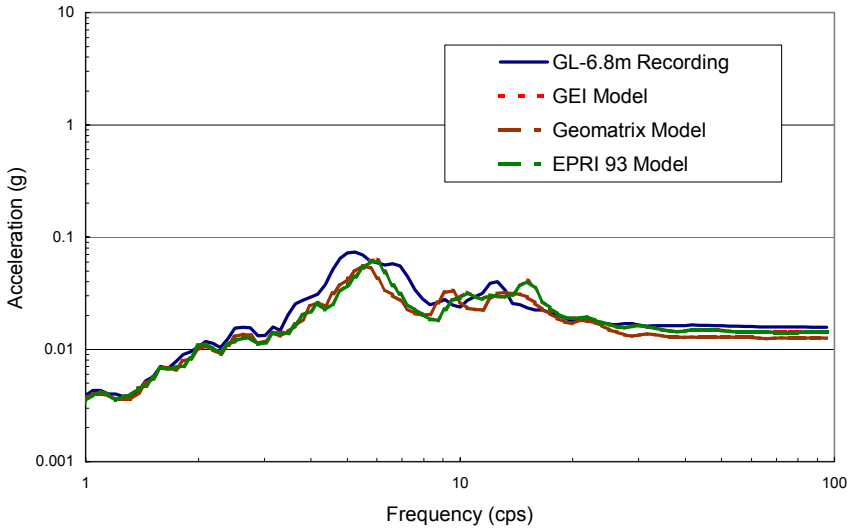

Figure 4-52. Comparison of the use of different degradation models for the New Free-Field Point using Earthquake 157y.

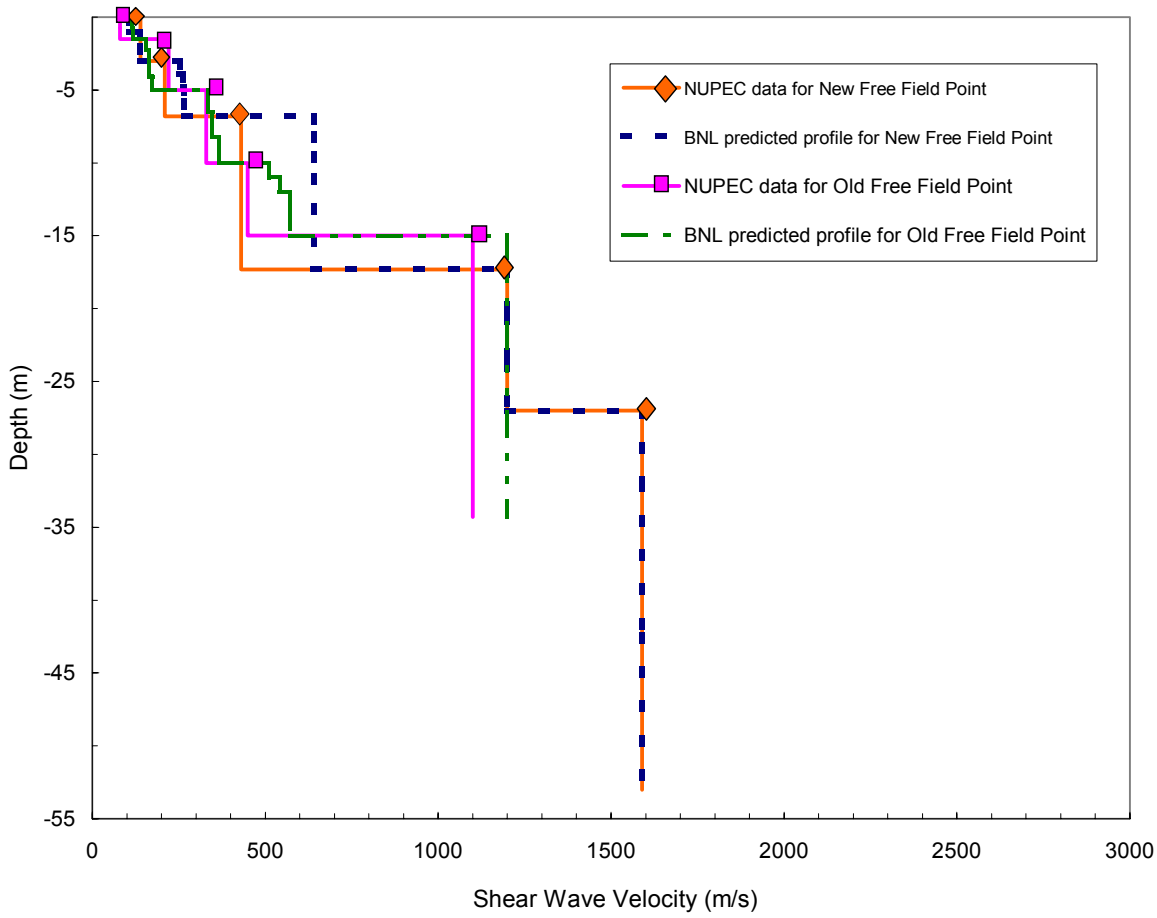

Figure 4-53. The BNL estimated low strain soil profiles for the old/new free-field points.

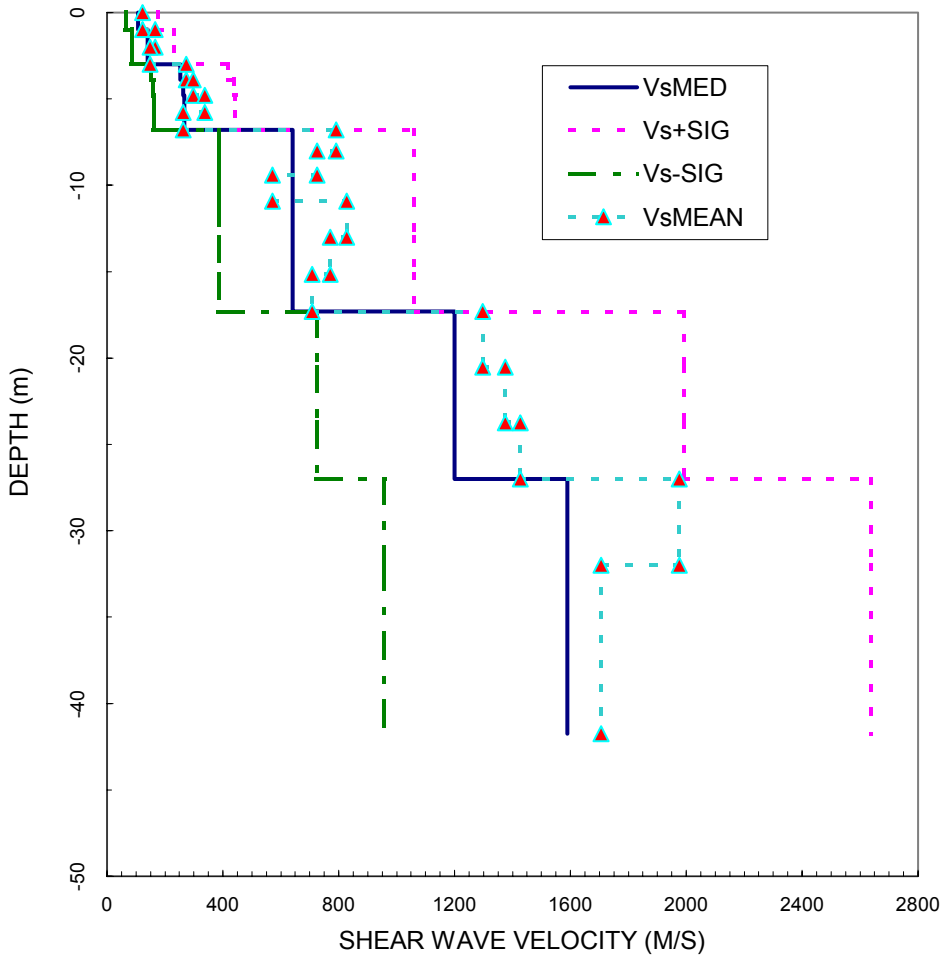

Figure 4-54. The ensemble distribution of the low strain soil profiles.

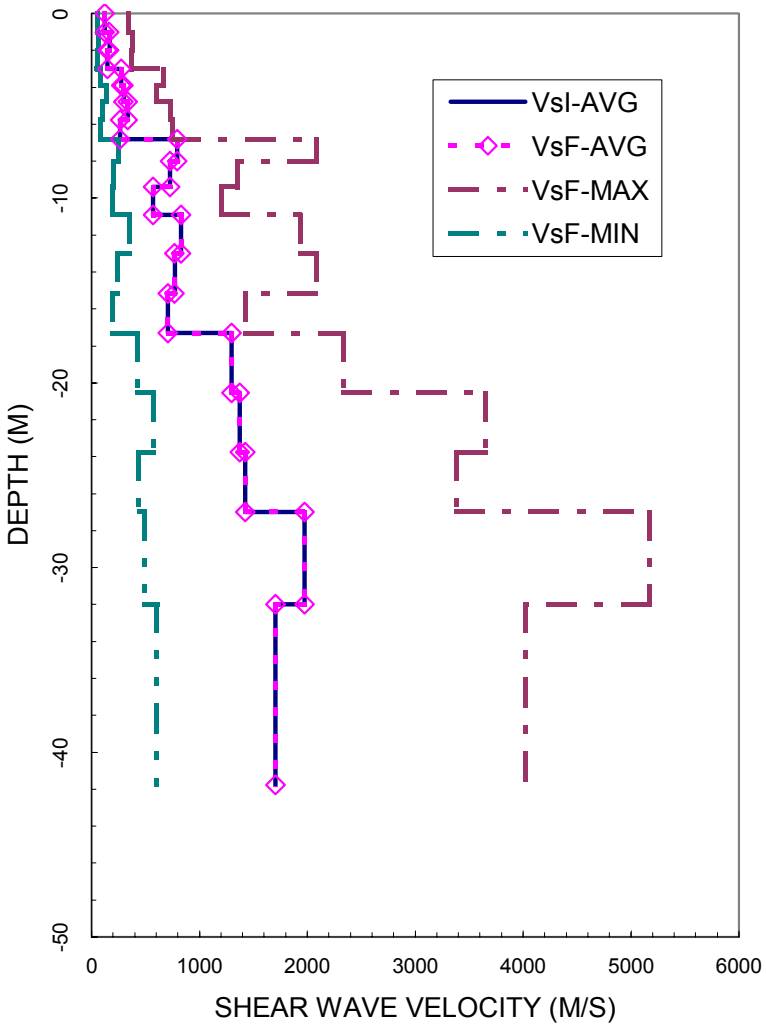

Figure 4-55. The computed distribution of the strain dependent soil profiles for Earthquake No 139x.

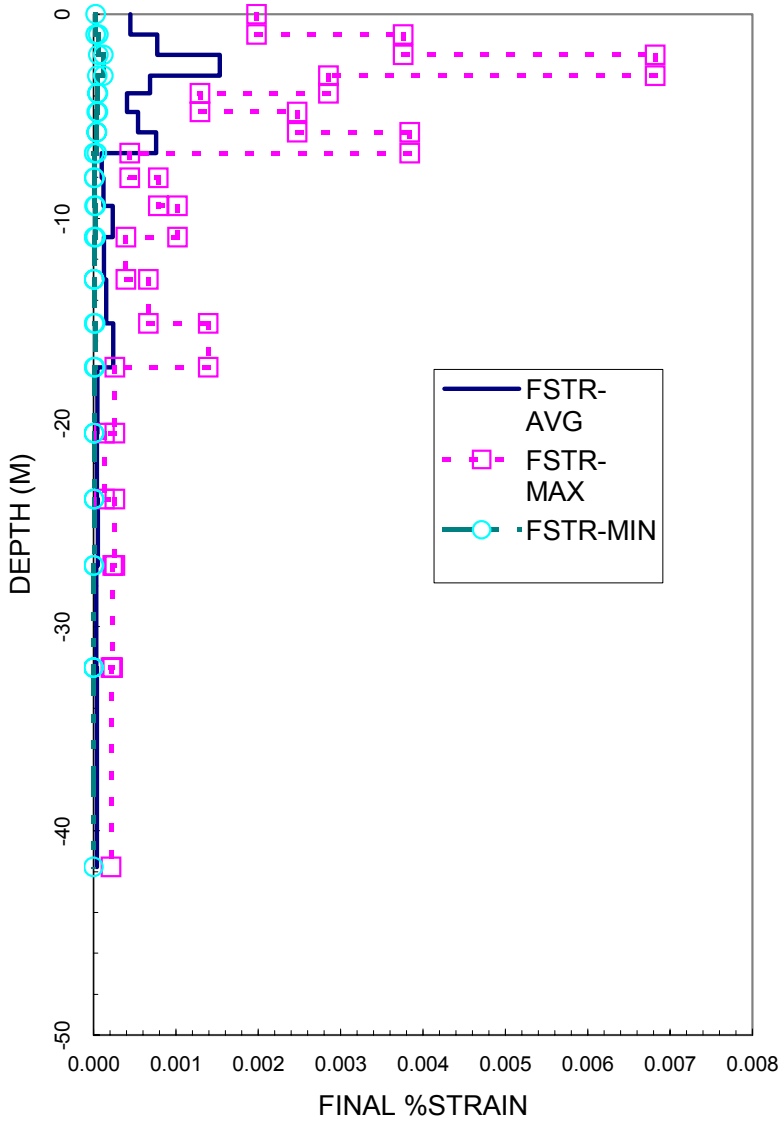

Figure 4-56. Range of iterated shear strains (%) for Earthquake No. 139x.

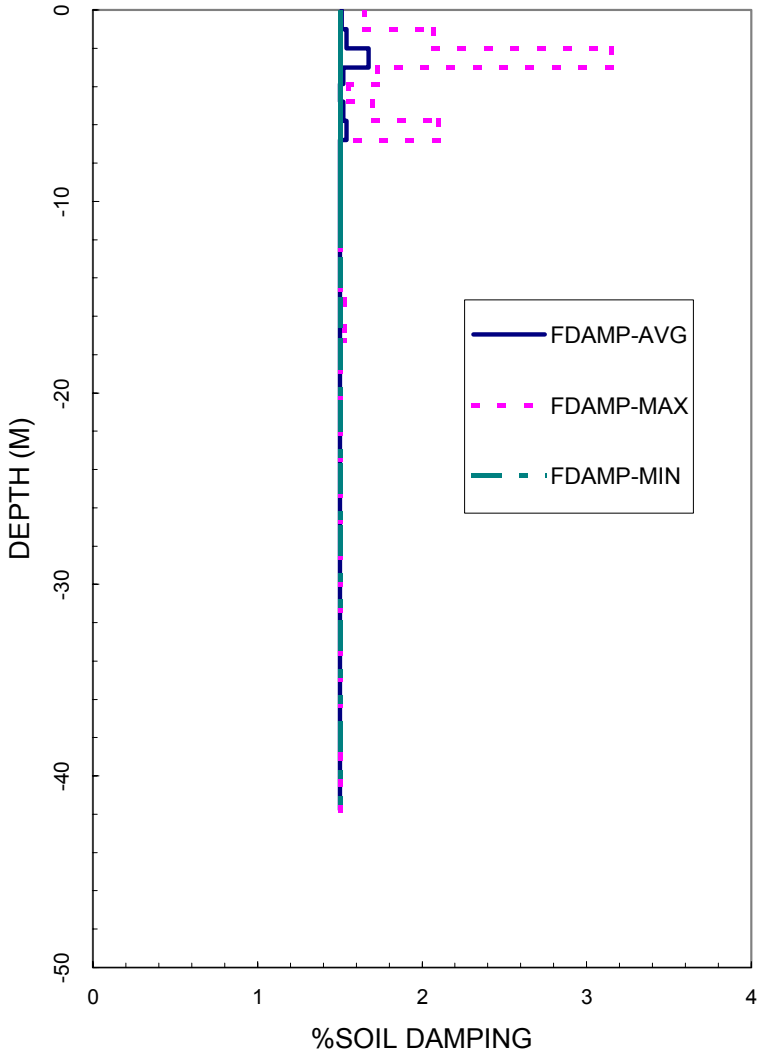

Figure 4-57. Range of iterated soil damping (%) for Earthquake No. 139x.

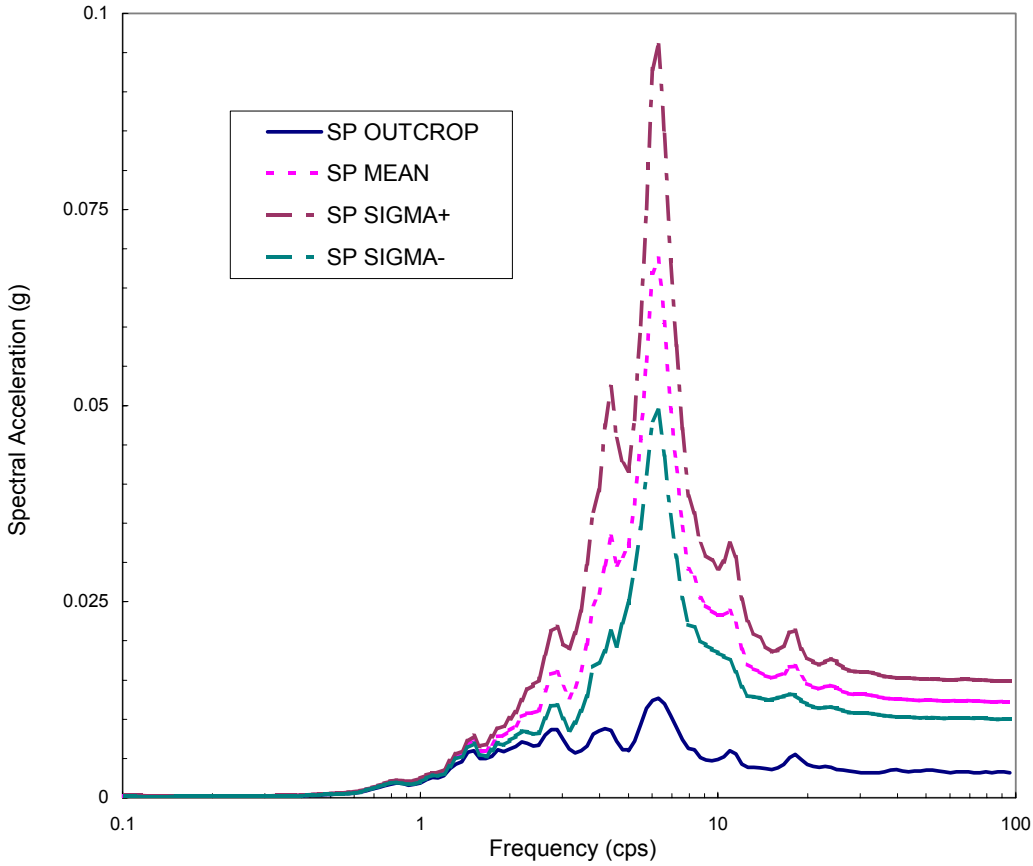

Figure 4-58. Computed ground surface response spectral distribution for Earthquake No. 139x.

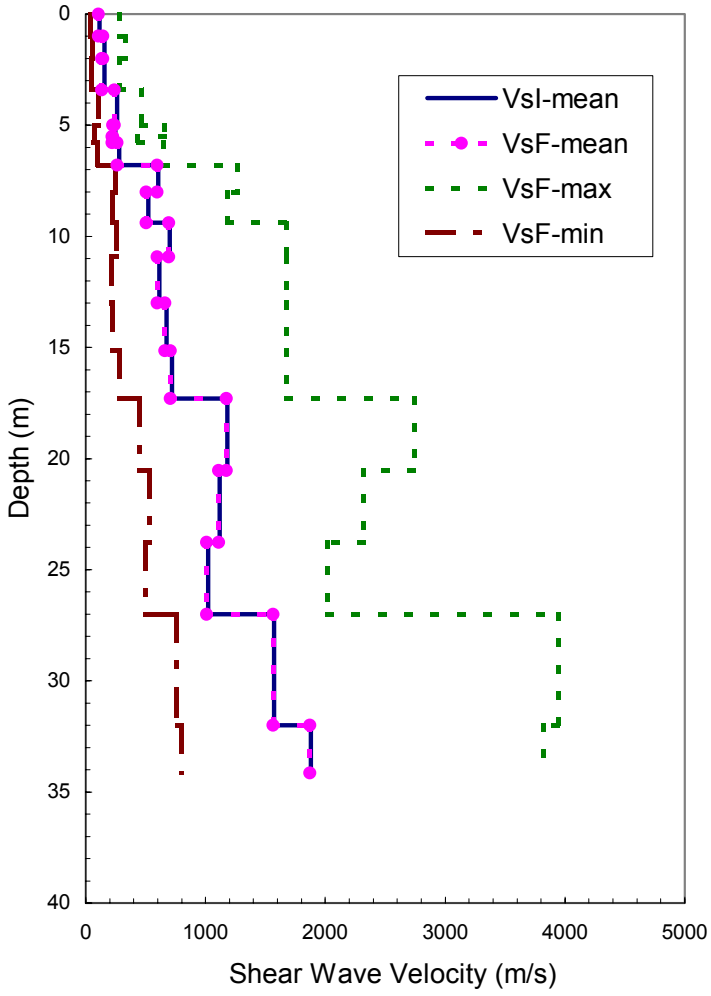

Figure 4-59. The computed distribution of the strain dependent soil profiles for Earthquake No 89x.

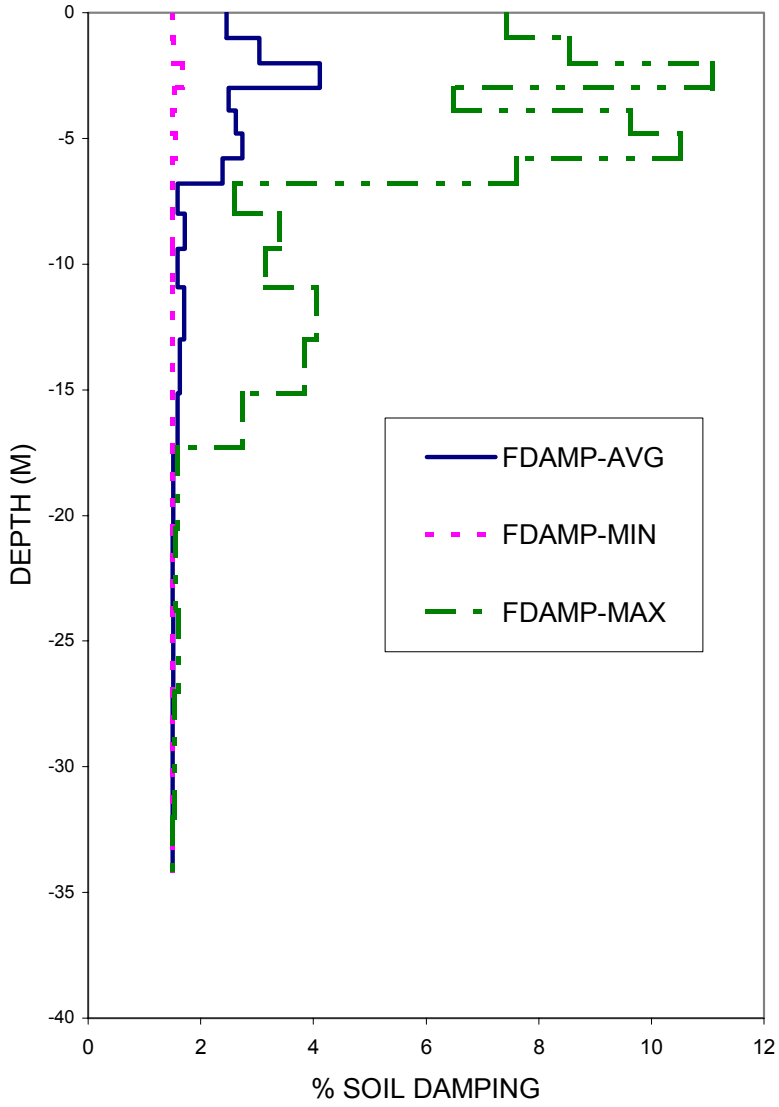

Figure 4-60. Range of iterated soil damping (%) for Earthquake No. 89x.

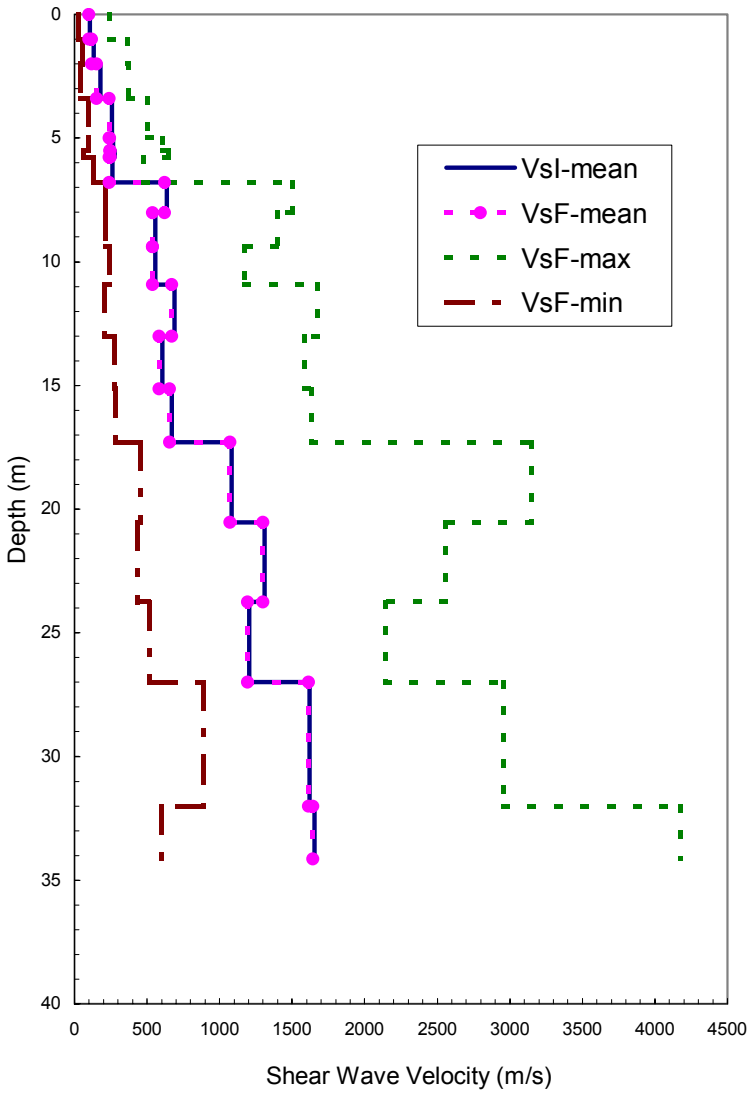

Figure 4-61. The computed distribution of the strain dependent soil profiles for Earthquake No 63x.

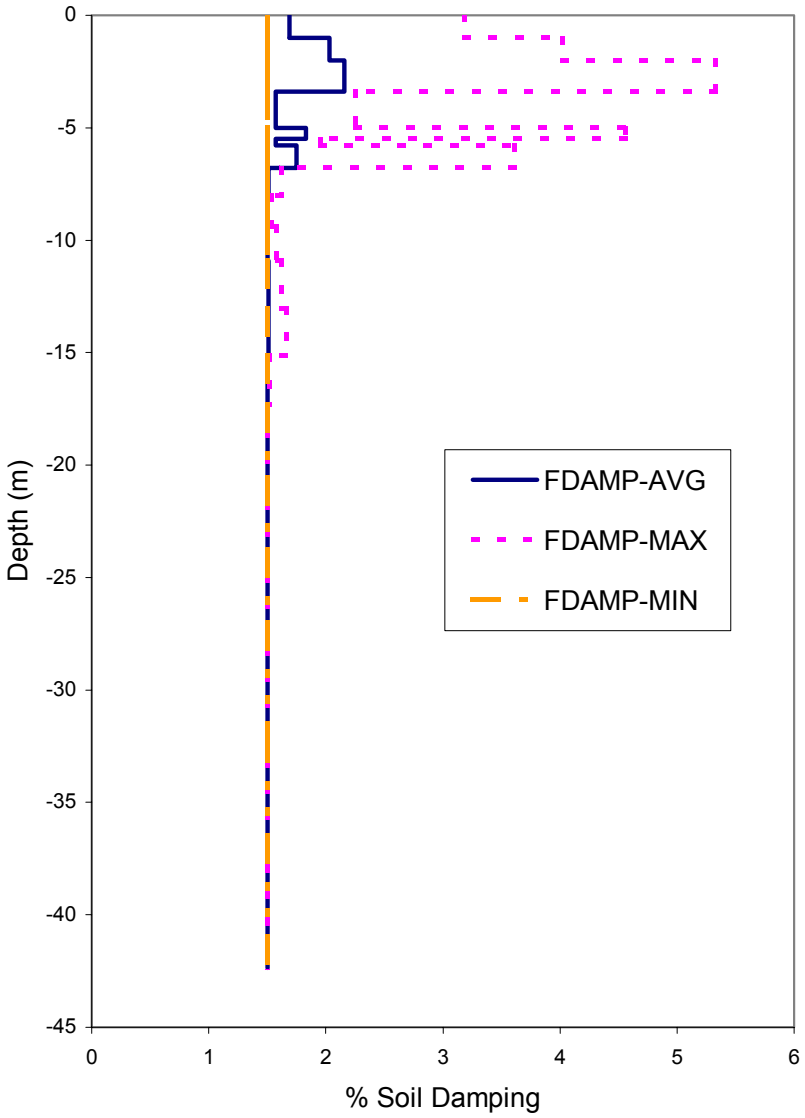

Figure 4-62. Range of iterated soil damping (%) for Earthquake No. 63x.

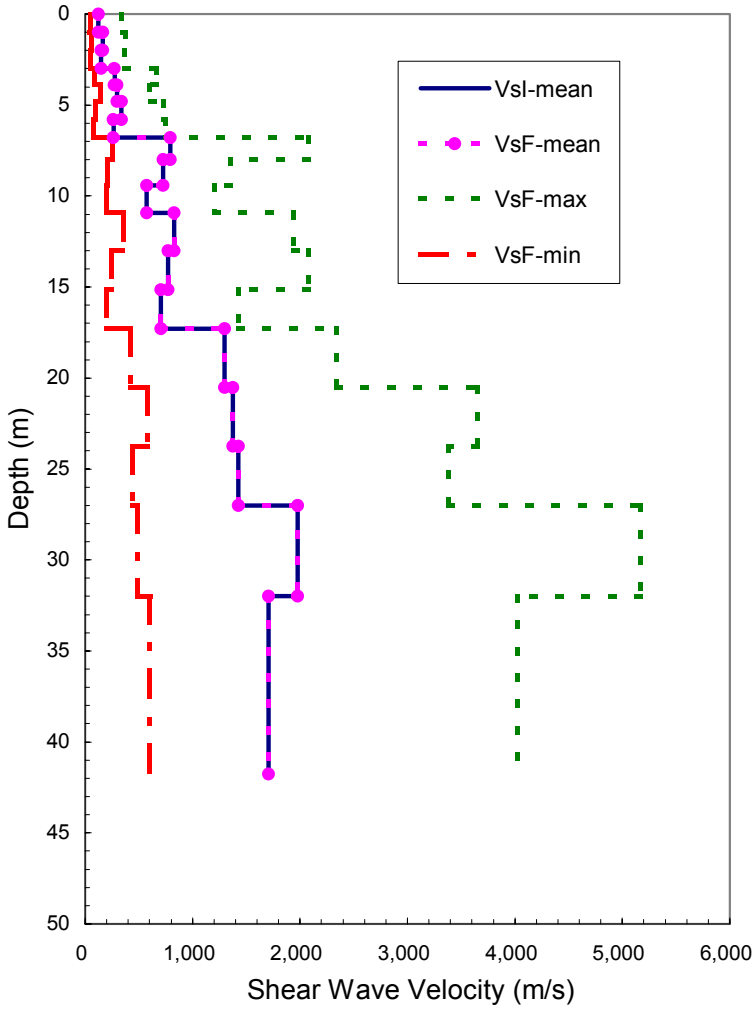

Figure 4-63. The computed distribution of the strain dependent soil profiles for Earthquake No 131x.

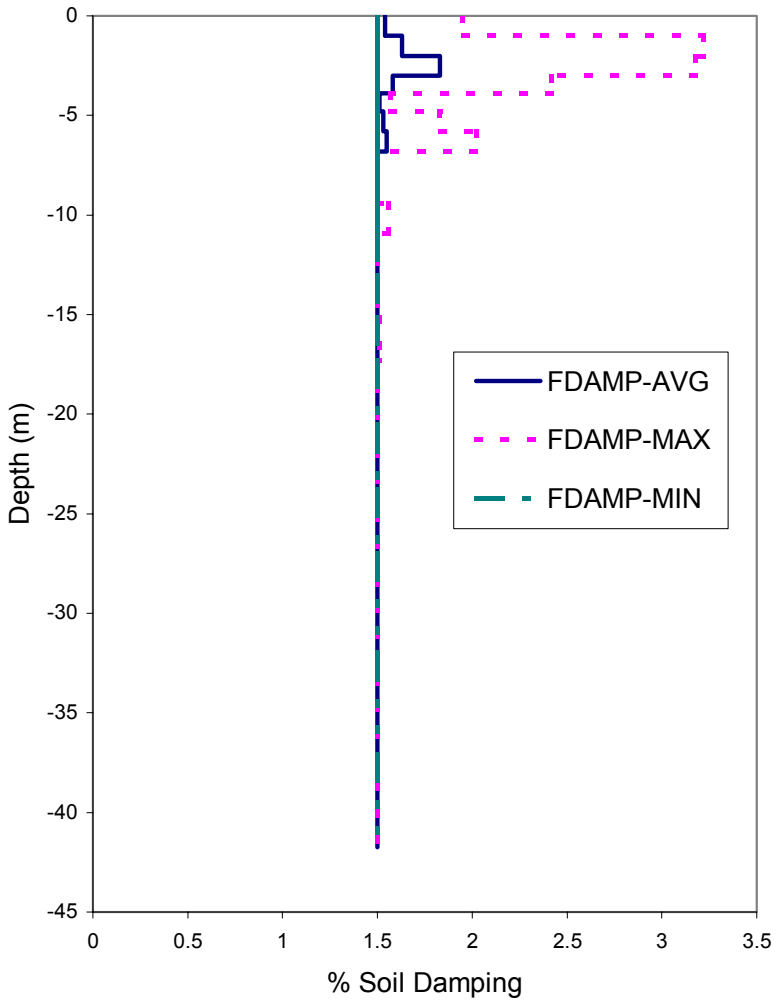

Figure 4-64. Range of iterated soil damping (%) for Earthquake No. 131x.

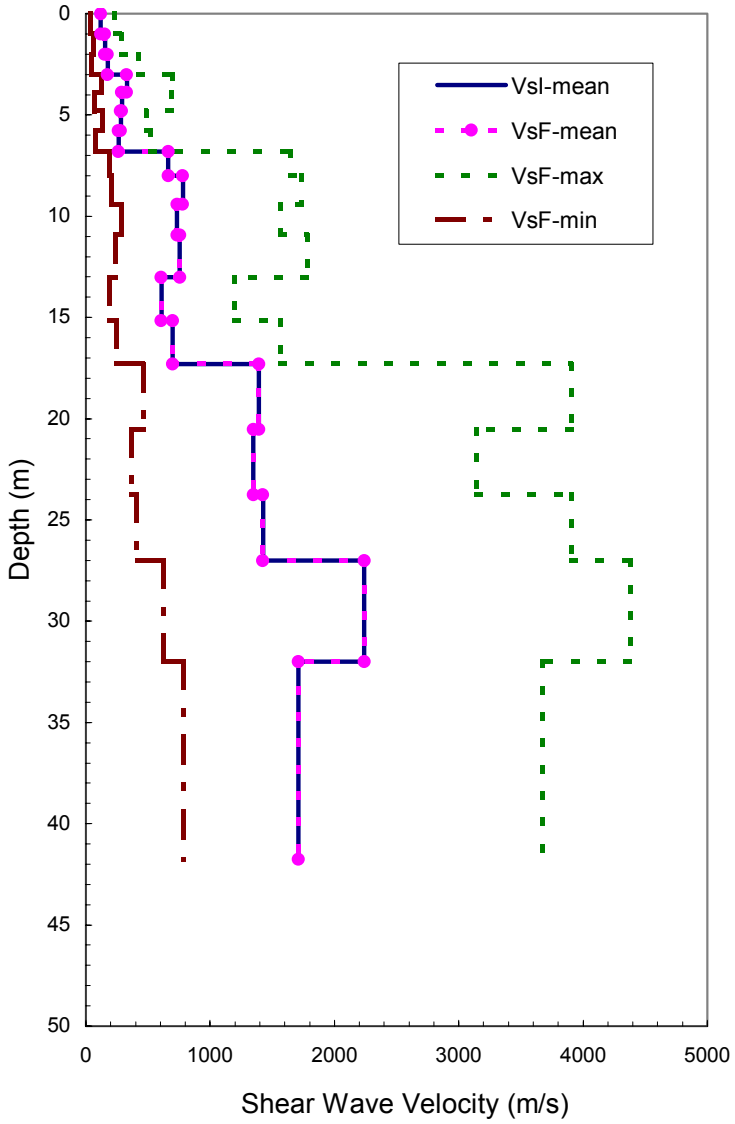

Figure 4-65. The computed distribution of the strain dependent soil profiles for Earthquake No 157x.

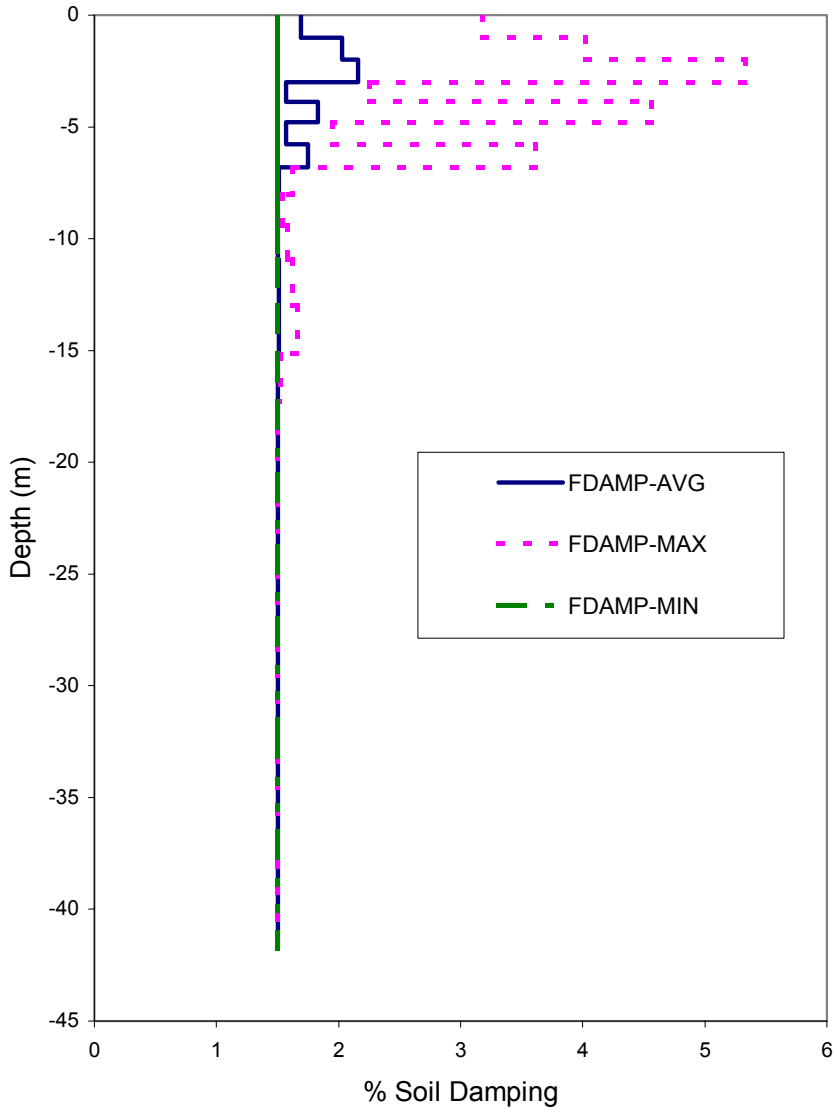

Figure 4-66. Range of iterated soil damping (%) for Earthquake No. 157x.

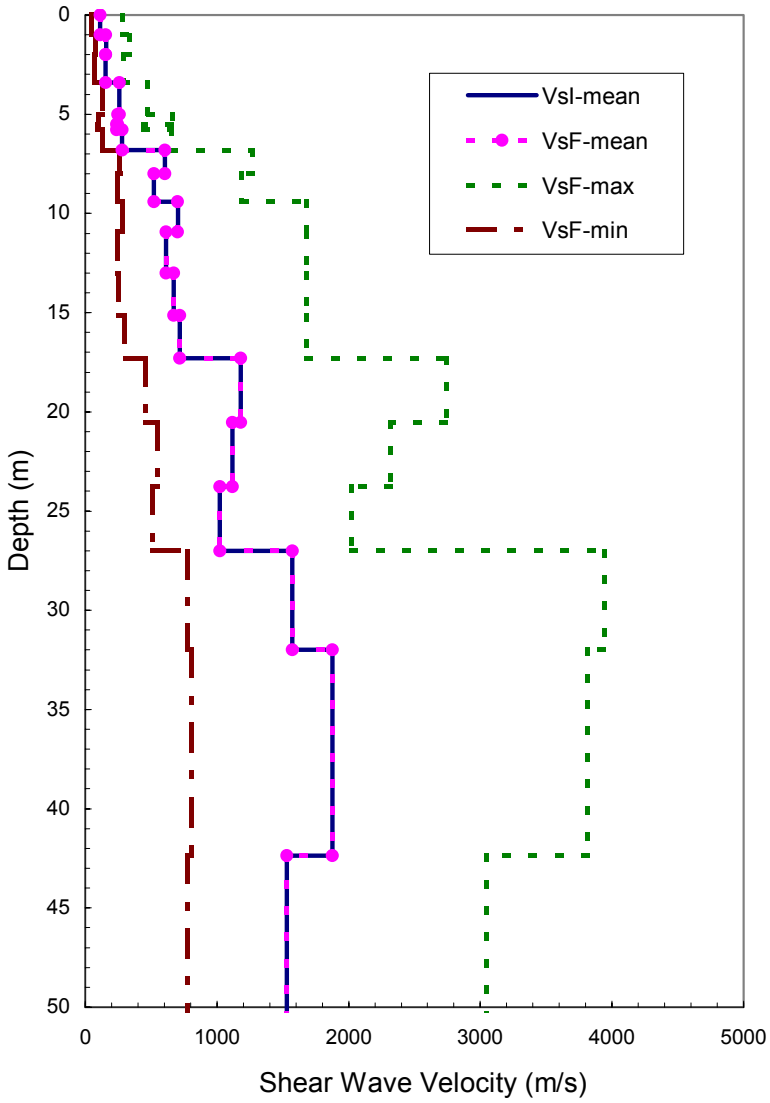

Figure 4-67. The computed distribution of the strain dependent soil profiles for Earthquake No 164x.

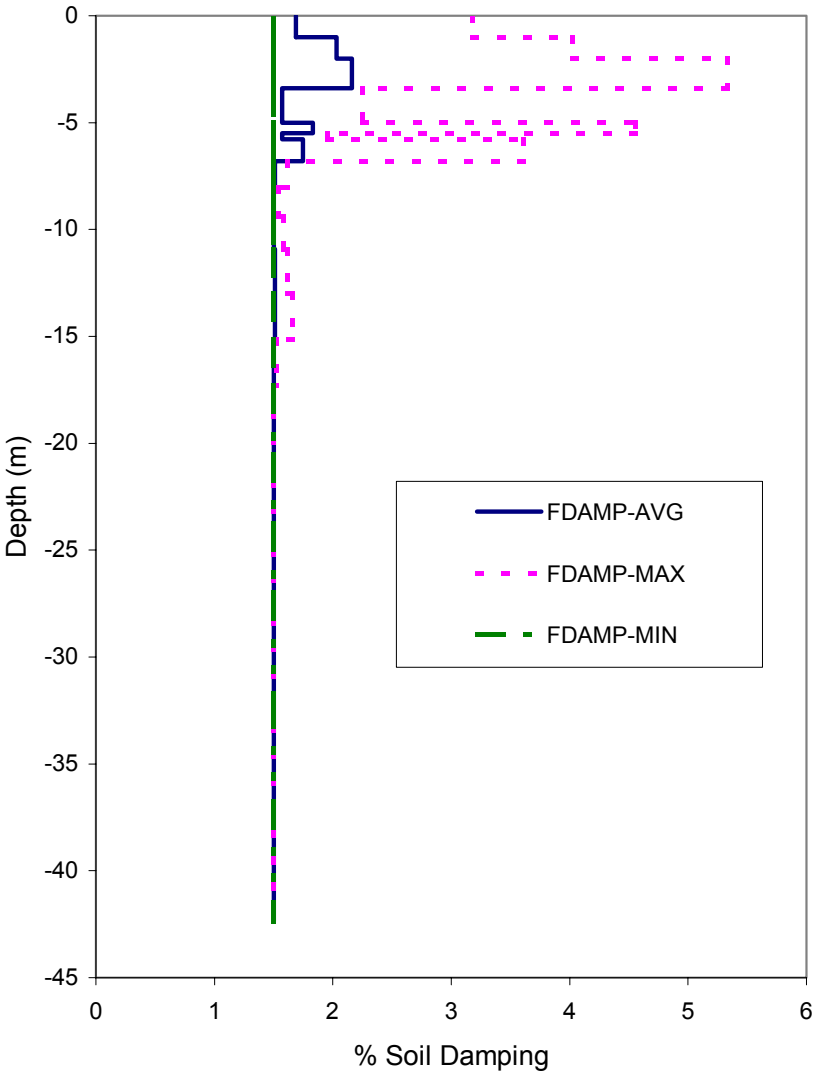

Figure 4-68. Range of iterated soil damping (%) for Earthquake No. 164x.

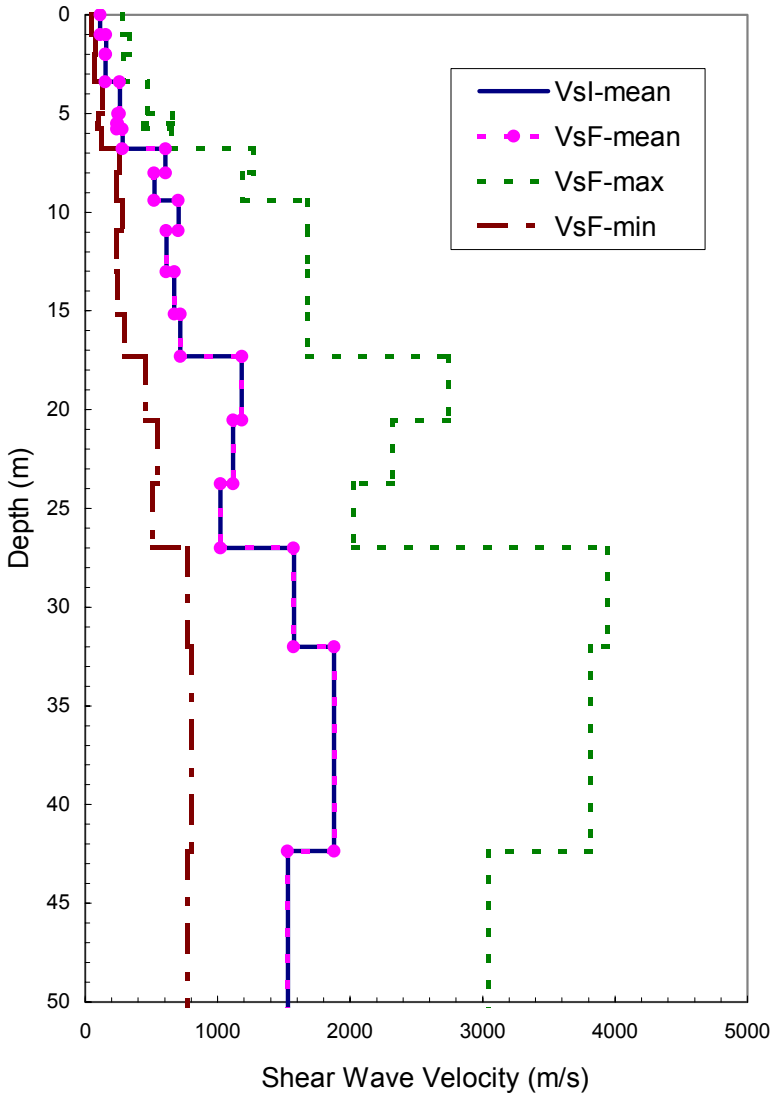

Figure 4-69. The computed distribution of the strain dependent soil profiles for Earthquake No 172x.

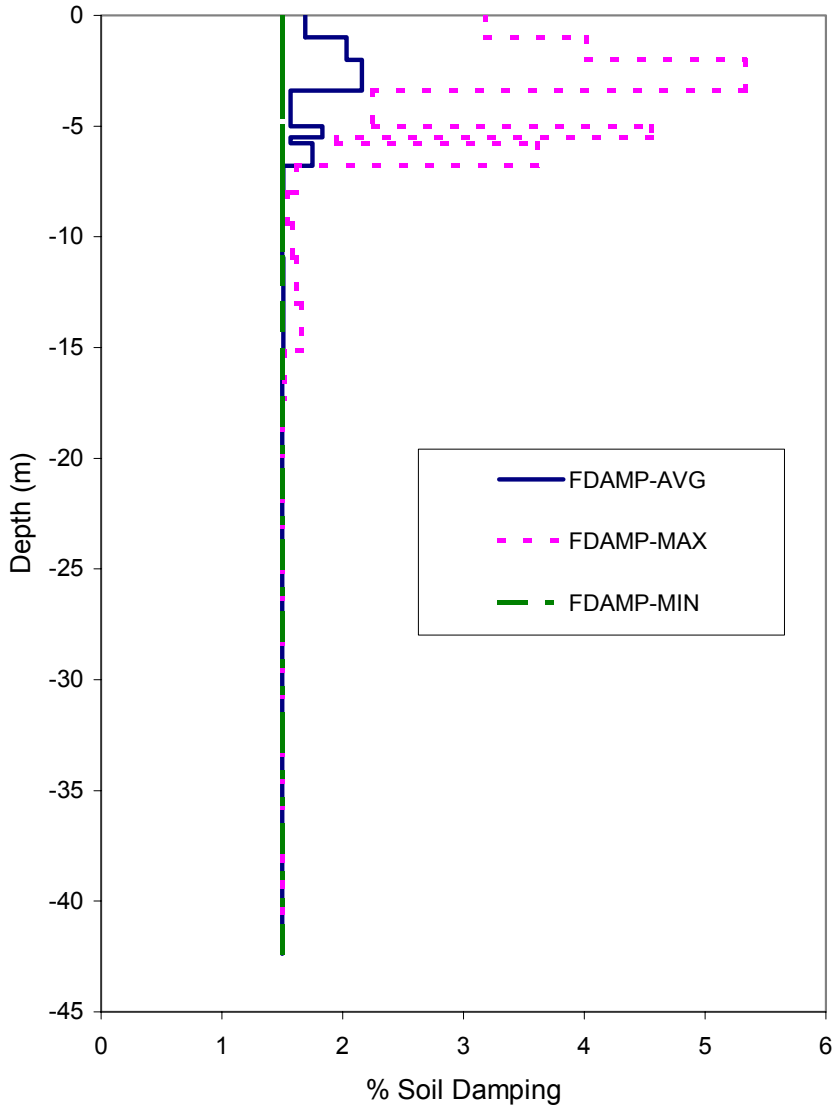

Figure 4-70. Range of iterated soil damping (%) for Earthquake No. 172x.

5.0 SSI ANALYSES OF NPP RESPONSES TO EARTHQUAKE MOTION

This section of the report presents and discusses the BNL analyses of the seismic responses of the model NPP structures including the SSI effect. The BNL SSI response analyses applied the current practice in the performance of the SSI analyses for the NUPEC model NPP structures with different configurations and embedment conditions and compared the seismic response predicted using the analytical models with the actual field measurements at the different locations within the structures. The examination of the comparisons between the analytical results and the recorded responses provides valuable insights into the capability of the current practice for the analytical treatments of the seismic responses of the NPP structures. Further, the comparisons are useful for examining the adequacy of current guidelines for incorporating the uncertainties of soil properties into the SSI analyses. Three structural configurations were analyzed by BNL including: 1) single reactor building; 2) two identical adjacent reactor buildings; and 3) adjacent reactor-turbine buildings. Earthquake responses were recorded for these three configurations in both the excavated and embedded conditions. The structural details and dimensions were described in Section 2. The plan and elevations of the model buildings are provided in Figures 2-3 to 2-5.

BNL's seismic analyses used the subtraction method as implemented in SASSI 2000 [Lysmer, 1999]. Sub-section 5.1 provides the descriptions of BNL's SASSI models of the three structural configurations with both excavated and embedded conditions; pertinent structural parameters employed for the structural models are also provided. The SASSI analyses for the excavated condition are presented in Sub-section 5.2, including the results in terms of the floor response spectra at the center of the top of the basemat and the roof, while the SASSI analyses of the embedded condition are provided and the results discussed in Sub-section 5.3. Sub-section 5.4 provides an evaluation of the dynamic cross interaction (DCI) effect.

5.1 Description of BNL SSI Models

The BNL models were developed based on the information provided by NUPEC. The details of the NUPEC models are described in Section 2. The metric units: kilo-Newton (KN), meters (M) and seconds (S) are employed in the numerical models and the SSI analyses. The models for the excavated condition are first discussed followed by the descriptions of the models for the embedded condition.

5.1.1 Excavated Models

The BNL study of the SSI response analyses employs the SASSI 2000 program. In the BNL models of the reactor and the turbine buildings, the portion of the structure below the ground surface is modeled with explicit finite elements (e.g., 3-D bricks and shells), while the portion above the ground surface is modeled with simple lumped masses and 3-D beams. Figure 5-1 shows the SASSI model of the single reactor building. The model consists of 808 nodes, 11 different element groups and 186 interaction nodes. Due to the symmetric configuration of the building, only half of the structure was modeled with the plane y=0 (east-west direction) as the symmetry plane. As seen in this figure, the basemat was modeled with brick elements and the sidewalls and internals were modeled with shell elements. The superstructure was modeled with lumped masses and beams. The base of the superstructure is connected to the sidewalls by rigid links to simulate the rigid diaphragm of the floor at grade level. Also as indicated in the figure, a thin layer of soil elements was added underneath the basemat to account for the softening effect induced by the excavation activities. In order to apply the subtraction method, the nodes at the boundary of the excavation need to be identified as the interaction nodes and the volume of the

excavated pit also needs to be modeled. In this case, due to the symmetry, only one-half of the volume needs to be modeled and it is done using brick elements in the SASSI model.

Since the twin reactor buildings were arranged in the north-south direction (x-axis), the adjacent building effect, or the DCI effect, is primarily amplified by the ground motion excited in the north-south direction. Therefore, to develop a model for the DCI effect, in addition to the symmetry condition used for the single reactor building, the SASSI model for the twin reactor building also introduces an anti-symmetry plane perpendicular to the x-axis located in-between the two reactors. Furthermore, due to symmetry and anti-symmetry planes introduced in the model for the twin reactor buildings, only one-quarter of the excavated volume is required to be modeled, instead of the one-half volume being modeled for the single reactor. The twin-reactor model consists of 628 nodes, 11 different element groups and 150 interaction nodes.

For the reactor-turbine buildings, which are arranged in the north-south direction (x-axis), only a symmetry condition (y=0) was introduced similar to the single reactor model. Figure 5-2 shows the SASSI model for the reactor-turbine buildings. Similar to the objective for the twin reactor building for developing a SASSI model for the DCI effect, the reactor-turbine buildings model was developed in which the gap between the two structures was explicitly modeled. Because the two structures are dissimilar, the size of the SASSI model also increased dramatically. The reactor-turbine buildings model consists of 1201 nodes, 22 different element groups and 298 interaction nodes, which is about twice the size for the twin reactor buildings model.

5.1.2 Embedded Models

As described in Section 2, the NUPEC structural models in the excavated condition were used to record the seismic responses to earthquake motions prior to 1998. As indicated in Figures 2-2 and 2-5, between 1998 and 2000, backfill soils were used to fill the excavated spaces surrounding the structural models such that these test models were fully embedded to grade level. However, it is not expected that the backfill soils would possess the same properties as the free-field soils in the same locations. Since the BNL SSI response analyses employ the sub-structuring method, the backfill soils possess the same properties as the free field at the same locations. This unavoidably introduces uncertainties in the SSI analyses. As will be discussed later in this report, an attempt was made to account for the uncertainties in the soil properties by performing a variability study of the SSI responses.

As for the structural models in the embedded condition, the building models are the same as those for the excavated condition. The excavation for an embedded case is the embedment of the structure. Therefore, the volume of the excavation for the embedded cases is substantially less than the volume for the excavated models. The modeling effort is also substantially reduced compared with the excavated case modeling. The SASSI model for the embedded single reactor building consists of only 283 nodes (compared to the excavated case which is 808 nodes), 111 interaction nodes (vs. 186 interaction nodes for the excavated case) and 11 element groups (the same as the excavated case). The SASSI model for the embedded cases are significantly smaller.

The SASSI model of the embedded twin reactor buildings, is shown in Figure 5-3. The embedded twin-reactor model consists of 327 nodes (compared to 628 nodes for the excavated case), 11 different element groups (the same as the excavated model), and 107 interaction nodes (compared to 150 interaction nodes for excavated case).

For the reactor-turbine buildings, the embedded model is depicted in Figure 5-4. The embedded reactor-turbine buildings model consists of 708 nodes, 28 different element groups and 223 interaction nodes, which is much smaller than the size for the excavated model.

5.2 Analyses Results for Excavated Structures

BNL performed the SSI response analyses using the SASSI 2000 program for the models described in the previous section and the earthquake data provided by NUPEC, as listed in Table 2-1. The BNL analyses results were compared to the recorded responses at the basemat center and the roof center. The comparisons of the results were presented in terms of the response spectra at 5% damping. All comparisons were made for the earthquake motion components excited in the north-south direction.

As discussed before, there are certain uncertainties in soil properties (such as the backfill soils) that may not be adequately accounted for in the BNL SSI modeling process. The BNL analyses, however, attempted to address these uncertainties by performing the variability analyses for the SSI responses with the lognormal standard deviation of sigma = 0.2 for the shear wave velocity of the free-field soils. The thin layer of soil of about 0.5m under the basemat also appears softer than the free field, as explained by NUPEC as caused by the excavation activities. Based on the data provided by NUPEC, the BNL analyses assumed the following low strain soil properties: V_s=150m/s and Poisson ratio = 0.12 for the thin soil layer. The BNL analyses also assumed that the thin layer extends laterally throughout the free field. This assumption would not impact the input motion to the SSI response analyses, since the control point for the BNL SSI analyses is placed at the ground surface and the corresponding earthquake input motions were developed by the BNL probabilistic analyses using the free-field properties.

In the following sub-sections, the SSI response analysis and the results comparisons with recorded responses for the single reactor building are discussed first, followed by the discussion of the results comparisons for the twin reactor buildings. Finally, the BNL analysis results for the reactor-turbine buildings and their comparisons with the recorded responses are presented.

5.2.1 Single Reactor

Prior to performing the SSI response analyses, BNL used the single excavated reactor SSI model to compare measured and calculated frequency dependent impedance functions. Measured impedance functions were provided by NUPEC for the forced vibration (shaker) tests performed with exciters located on the roof of the single reactor model. Local structural flexibility effects were not removed from these measured data. Calculated impedance functions were determined by applying frequency dependent unit displacements to the mass-less rigid models of the single reactor structure. The real part of the impedance represents the dynamic stiffness of the soils supporting the structure and the imaginary part is associated with the radiation damping effect of the soils. The impedance for the model was calculated by inverting the compliance matrices obtained from the SASSI analysis. The structural part of the SSI model was first made rigid by increasing the material stiffness of the structure by several orders of magnitude and mass-less by assigning zero mass density to the structural elements. The compliance was then computed by applying a unit force to the basemat of the SSI model and calculating the corresponding displacement.

Three sets of soil profiles were utilized in the impedance calculation and subsequent SSI response analyses. These profiles are the mean, mean plus sigma and mean minus sigma low strain soil profiles. The profiles were developed by the BNL probabilistic free-field analyses as discussed in

Section 4. The mean plus sigma and mean minus sigma profiles were calculated by a simple linear scaling of the mean profile using the standard deviation (sigma). Figures 5-5 and 5-6 show the comparisons of the calculated horizontal real and imaginary impedance functions with the corresponding field test data, while the comparisons for the rocking impedance are provided in Figures 5-7 and 5-8. As can be seen, the measured impedance functions are either bounded by or close to the calculated impedance values generated from the mean, mean plus sigma and mean minus sigma soil profiles recommended by the standard analysis procedures. The sharp peaks noted in the measured data are attributed to the effects of local flexibilities in the actual structure not captured in the structural model.

Applying the mean surface input motion and utilizing the mean, the mean minus sigma and the mean plus sigma profiles developed for each earthquake record, BNL performed the SASSI analyses for the three sets of profiles to generate the structural SSI responses, which are correspondingly referred to as the mean response, sigma- and sigma + responses, respectively. These SSI responses were expressed in terms of 5% damped response spectra, which were then compared with the response spectra calculated from recorded motions. Figures 5-9 and 5-10 present the response spectral comparisons between the BNL analysis and the recorded data for Earthquake No. 63. Figure 5-9 plotted the response comparison for the location at the center of the top of the basemat, while Figure 5-10 depicted the response comparison for the location at the roof center. As exhibited in these figures, although a one-to-one comparison may not be achieved between the recorded response and the computed response (mean or mean minus sigma or mean plus sigma), the calculated response with all three sets of soil profiles very conservatively enveloped the recorded response. These comparisons further reinforced the observation that the current practice accounting for the uncertainties of the soil properties in the SSI analyses of the NPP structures is not only adequate but possibly over conservative.

To demonstrate the sensitivity of the effect of the disturbed soil in close proximity to the foundation, the SSI response to Earthquake No. 89 was analyzed for a variation of the soil property of the 0.5m thin soil layer underneath the basemat. Two sets of the SSI response calculations were performed, one for the thin soil layer using the nominal value of V_s=150m/s, based on the data provided by NUPEC, and the other for the soil layer assuming a reduced value of V_s=110m/s. Figures 5-11 to 5-12 show the SSI responses for the soil property of the thin soil layer with V_s=150m/s, while Figures 5-13 and 5-14 depict the SSI responses for the soil property of the thin layer with V_s=110m/s. Figures 5-11 and 12 show that the computed mean, sigma- and sigma+ responses exhibit either lower response or a frequency shift, while the Figures 5-13 and 5-14 show excellent comparisons between the computed response and recorded data when the thin soil layer assumes a reduced V_s=110m/s. A similar phenomenon was also observed in the Hualien (Taiwan) field tests. The effect of local disturbance due to the softening by excavation activities may become more pronounced when the media are stiffer.

The mean, mean minus sigma and mean plus sigma SSI responses were also computed for Earthquake Nos. 131, 139 and 157. Figures 5-15 and 5-16 show the SSI response comparisons for Earthquake No. 131, Figures 5-17 and 5-18 depict the SSI response comparisons for Earthquake No. 139 and the response comparisons for Earthquake No. 157 are plotted in Figures 5-19 and 5-20. These figures all exhibited that the calculated SSI response in terms of the mean, mean minus sigma and mean plus sigma conservatively enveloped the corresponding recorded responses.

5.2.2 Twin Adjacent Reactors

The purpose of having two structures built near to each other is to study the adjacent building interaction or the DCI effect. For the twin reactors, the gap between the two structures is 0.6m and the seismic motion analyzed for the SSI response is the north-south component, which is the direction in which the two reactors are aligned. As discussed in Sub-section 5.1, the BNL SSI model is a quarter representation of the twin reactors configuration, taking advantage of a symmetry condition and an anti-symmetry condition. BNL performed SASSI analyses for three earthquakes, and this sub-section presents and discusses the BNL results and their comparisons with the field test data.

Figures 5-21 and 5-22 show the response comparisons for Earthquake No. 131 for the basemat and the roof locations. The comparisons indicated the calculated SSI response conservatively enveloped the recorded data. Similar observation can also be made for the response comparisons for Earthquake Nos. 139 and No. 157, which are shown in Figures 5-23 through 5-26. These comparisons also indicate that the conventional SSI analysis techniques, such as the sub-structuring method employed for this study, are capable of predicting the seismic response of a structure as long as the practice of accounting for the soil uncertainties is properly exercised.

5.2.3 Adjacent Reactor-Turbine Structures

In a typical nuclear power plant, the reactor building is usually situated adjacent to other structures such as the auxiliary building or turbine building. Therefore, the DCI effect of adjacent buildings with different structural characteristics was also of interest in the collaboration study. This sub-section discusses the BNL SSI response results for the adjacent reactor-turbine configuration and the resulting comparisons with the test data. Later in Sub-section 5.4, the SSI responses considering the DCI effect will be discussed in light of the comparisons with the SSI response of the single structure.

As discussed in Sub-section 5.1, the BNL SSI model for the reactor-turbine buildings represents a half structural configuration with one symmetry condition. The gap between the reactor and the turbine building is 0.1m. Only one earthquake (No. 157) was analyzed for the DCI effect for the reactor-turbine buildings. Figures 5-27 to 5-30 show the resulting comparisons between the BNL analysis and the recorded responses. The comparisons for the reactor showed that the BNL predictions captured the overall characteristics of the SSI response for the reactor-turbine configuration and generally over predicted the response amplitudes, as indicated in Figures 5-27 and 5-28. As depicted in Figures 5-29 and 5-30 for the turbine building, the BNL results generally enveloped the recorded response at the basemat and over predicted the first peak at the roof; however, the BNL calculation under-predicted slightly the response at the second peak. Nonetheless, the minor under-prediction at the second peak would be remedied by the standard design practices such as peak widening.

5.3 Analyses Results for Embedded Structures

After a number of earthquake motions were recorded both in the free field and on the excavated model structures, the excavations surrounding the model structures were filled with backfill soils to grade level to establish the embedded model structures. As the information provided by NUPEC indicates, there are some differences between the properties for the backfill soil and the free-field properties at the same locations. The BNL numerical analyses for the SSI responses utilized the free-field properties for the embedment. Although the BNL analysis models did not

directly address the effect of the backfill soil differing from the free field, the variation analyses in terms of the mean, the mean minus sigma and mean plus sigma responses should sufficiently encompass the uncertainty effect on the SSI responses.

BNL performed the SSI response analyses for the embedded model structures as described in Sub-section 5.1. This sub-section presents the BNL SASSI analysis results and discusses the comparisons between the BNL analysis results and the recorded response for Earthquake Nos. 63, 89, 164, and 172. Sub-section 5.3.1 provides the BNL analysis results of the SSI responses and their comparisons with the recorded data for the embedded single reactor building. The analysis results for the embedded twin reactor buildings and their comparisons with recorded responses are given in Sub-section 5.3.2. Finally, the BNL analysis results for the reactor-turbine buildings are presented in Sub-section 5.3.3. Comparisons among both the recorded data and the BNL SASSI analyses for the embedded reactor in the configurations of the single, twin and reactor-turbine arrangements were also made to examine the DCI effects, as discussed in Subsection 5.4.

5.3.1 Single Reactor

The SSI response analyses were performed for the single embedded reactor building subjected to Earthquake Nos. 63, 89, 164 and 172 (as discussed previously, only the x-component in the north south direction was analyzed). The description of these earthquakes was provided in Table 2-1. As seen in this table, Earthquake Nos. 63 and 89 are moderate earthquakes, which may induce to a certain extent some strain effect, and Earthquake Nos. 164 and 172 are rather small magnitude motions, which are expected to exhibit no noticeable strain effect. Figures 5-31 and 5-32 show the SSI response comparisons between the BNL analysis and the recorded responses for Earthquake No. 63. As exhibited in these figures, the BNL analysis mostly over-predicted the response compared with the recorded data, except for the frequencies lower than 2.5Hz, where the BNL SSI response was lower than the recorded data at the basemat.

Figures 5-33 and 5-34 depict the SSI response comparisons between the BNL analysis and the recorded data for Earthquake No. 89. The BNL SSI analysis for Earthquake No. 89 was performed using the soil profile and the ground surface input motion generated by performing the probabilistic free-field analysis with the recorded downhole data at GL-13m below the ground surface, since the recorded downhole data at GL-34m were proven deficient as established by the Arias intensity analysis presented in Section 4. As exhibited in Figures 5-33 and 5-34, the BNL SSI analysis both captured the frequency characteristics and predicted the peak responses compared with the recorded responses.

Finally, the BNL SSI results were also compared with the recorded data for Earthquakes No. 164 and 172, as shown in Figures 5-35 to 5-38. Even for such small earthquake motions, the response comparisons showed that the BNL analysis results generally envelop the recorded data, reconfirming the fact that the current procedure for the SSI analyses of the NPP structures is conservative.

5.3.2 Adjacent Twin Reactors

The SSI response analyses for the twin embedded reactor buildings were analyzed for Earthquake Nos. 164 and 172. Figures 5-39 and 5-40 show the response comparisons between the BNL analysis and the recorded data for Earthquake No. 164, while Figures 5-41 and 5-42 depict the similar comparisons for Earthquake No. 172. For both comparisons, the BNL SSI responses enveloped the recorded data and the BNL analysis showed much higher peak response than the recorded data.

5.3.3 Adjacent Reactor-Turbine Structures

The SSI response analyses for the embedded reactor-turbine buildings were also analyzed for Earthquake Nos. 164 and 172. Figures 5-43 to 5-46 present the SSI response comparisons between the recorded data and the BNL analysis for Earthquake No. 164. The comparisons were made at the locations in both the reactor and the turbine building. As indicated in these figures, the BNL analysis results enveloped the recorded data at all locations for both buildings. Figures 5-47 to 5-50 provide the response comparisons for Earthquake No. 172. Once again, as indicated in these figures, the BNL analysis results enveloped the recorded data at all locations for both buildings.

5.4 Evaluation of Dynamic Cross Interaction (DCI) Effect

As stated in the introduction, a primary objective of this study is to 1) assess the significance of potential DCI effect on seismic response, 2) evaluate the adequacy of the industry practice for capturing the DCI phenomenon, and 3) assess the DCI effect on the overall methodology and regulatory guidelines for performing the SSI analysis. This section provides a discussion on the DCI effect based on comparisons using both recorded data and the SASSI analysis results. In order to isolate the DCI effect, both recorded and the analysis responses for the twin reactor and reactor-turbine cases were compared with those from the single reactor cases for both the embedded and excavated site conditions.

Figures 5-51 through 5-54 present comparisons at the basemat and roof for the twin and single reactor excavated cases for Earthquake No. 131. As may be noted, the recorded spectra from the twin reactor condition are significantly lower than those for the single reactor case. Some small upward shift in frequency at the spectral peaks may be noted at about 6 hz. The corresponding comparison of computed spectra shows a similar characteristic at the fundamental frequency, but with no shift in the spectral peak.

Figures 5-55 to 5-58 present the results from Earthquake No. 139, for the excavated site condition. In this case, as opposed to Earthquake No. 131, the recorded spectra from the twin reactor case are somewhat greater than those from the single reactor case. There is still some apparent small shift upward in frequency at the spectral peaks, although not as pronounced as those from Earthquake No. 131. The comparisons of the computed responses are similar to those from Earthquake No. 131. This would be expected since the method of analysis is the same and the SSI frequencies for these two earthquakes are approximately the same with little difference in degradation noted from the free-field response analysis.

Figures 5-59 to 5-62 present results from Earthquake No. 157 for the excavated site condition. Again, the recorded responses from the twin reactor condition exceed those from the single reactor condition with an upward shift in frequency at the peak. The calculated responses in this case from the twin reactor condition exceed those from the single reactor condition, which is the opposite of the comparisons of the calculated responses for Earthquake Nos. 131 and 139. This is apparently due to the shift in the fundamental SSI frequency associated with the degraded site soil conditions from this larger event.

Before further discussing the results from Earthquake No. 157, it needs to be pointed out that, due to the different elevations to which the reactor and turbine structures were situated in the reactor-turbine (R-T) configuration, the basemat of the reactor building was embedded one meter into

soil (see Figure 2-5). The reactor buildings in the single and the twin configurations did not include such embedment.

As depicted in Figure 5-59 for the basemat response, the peak recorded response from the R-T condition also exceeds that from the single reactor condition. As noticed in the previous comparisons, an upward shift in frequency at the peak was also observed for the R-T reactor relative to the single reactor response. The slightly larger frequency shift seen in the R-T reactor response may be influenced by the 1 m embedment for the R-T reactor. The embedment for the R-T reactor may also contribute to its reduced peak response compared to the twin reactor response. Nonetheless, the DCI effect in this case appears to result in an increase in the peak response. The comparison of the recorded responses at the roof as provided in Figure 5-60 shows that the peak response of the R-T reactor was noticeably reduced compared to the single reactor building. Again, since the embedment would provide a restraint to the structure from rocking, the roof response which is largely influenced by the rocking motion could therefore be reduced by this effect.

As illustrated in Figures 5-61 and 5-62, the computed responses for the R-T reactor building showed a consistent reduction of the peak response compared to the single reactor. The reduced calculated response for the R-T reactor could be influenced by the uncertainty in calculated properties for soils in the vicinity of the embedment that has resulted in stiffer soil in the analytical model than the in-situ case. Therefore, this may amplify the reduction effect for the R-T reactor response.

The spectral ratios of twin or reactor-turbine reactor response to the response of the single reactor were also developed for recorded data to draw insights into the relative importance of the DCI effect. The spectral ratios from the recorded responses for these three events for the excavated site condition are shown in Figure 5-63 and 5-64. For the ratio of the twin to the single reactor configuration, the exceedance reaches values of about 2.0 in the frequency range between 6.0 and 8.0 hz for Earthquake Nos. 139 and 157. For Earthquake No. 131, the exceedances reach a value of only about 1.2. Figures 5-65 and 5-66 indicate exceedances of about 2.0 for the case of the reactor-turbine configuration to the single turbine configuration.

For the fully embedded configuration, Figures 5-67 through 5-70 present comparisons of both recorded and computed responses for the reactor-turbine, twin reactor and single reactor cases for Earthquake No. 164. Figures 5-71 through 5-74 present similar results for Earthquake No. 172. A comparison of the spectral ratios from the recorded responses for the fully embedded configuration is shown in Figures 5-75 and 5-76. Figures 5-77 and 5-78 show similar behavior for the ratios of the reactor-turbine response to the single reactor response.

A general trend observed from these comparisons of recorded responses is that, for the same earthquake input, the magnitudes of the differences in spectra between the single reactor and the other two configurations with adjacent structures tend to be larger for the excavated structural condition as compared to the fully embedded condition. Further, the DCI effect may not always lead to reduction of the response, in fact, as noted in many of the comparisons discussed above, significant amplifications were observed due to the DCI effect.

Figures 5-79 through 5-94 present comparisons of the recorded spectral ratios with the corresponding results obtained from the computed responses. The results from the computed responses include those generated for the best estimate, upper bound and lower bound soil cases. The purpose of the comparison is to determine if the common procedure to perform a range of SSI analyses to cover a range of uncertainty in the computations leads to a reasonable

conservatism to capture the DCI effect as well. As may be noted from these comparisons, some exceedances in the recorded ratios occur even for the relatively wide range of soil properties used in the SSI calculations. The cause of these exceedances may be attributed to the small data set of earthquakes used in these comparisons. It is not clear, however, if some significant influence of DCI in the SSI calculation is being overlooked. For example, when treating two identical adjacent structures, the analysis may not capture higher mode relative responses between the two structures. Some small uncertainty in configuration (mass, cg location, etc.) may need to be introduced into the analysis to determine if such higher motion response is significant.

When comparing the mean computed responses for the three structural conditions (single reactor, twin reactor and reactor-turbine), the differences in the spectral ratios (DCI effect) are not as great as observed in the recorded data. However, by considering the upper and lower bound soil properties, the computed spectral ratios are generally equal to or greater than recorded values.

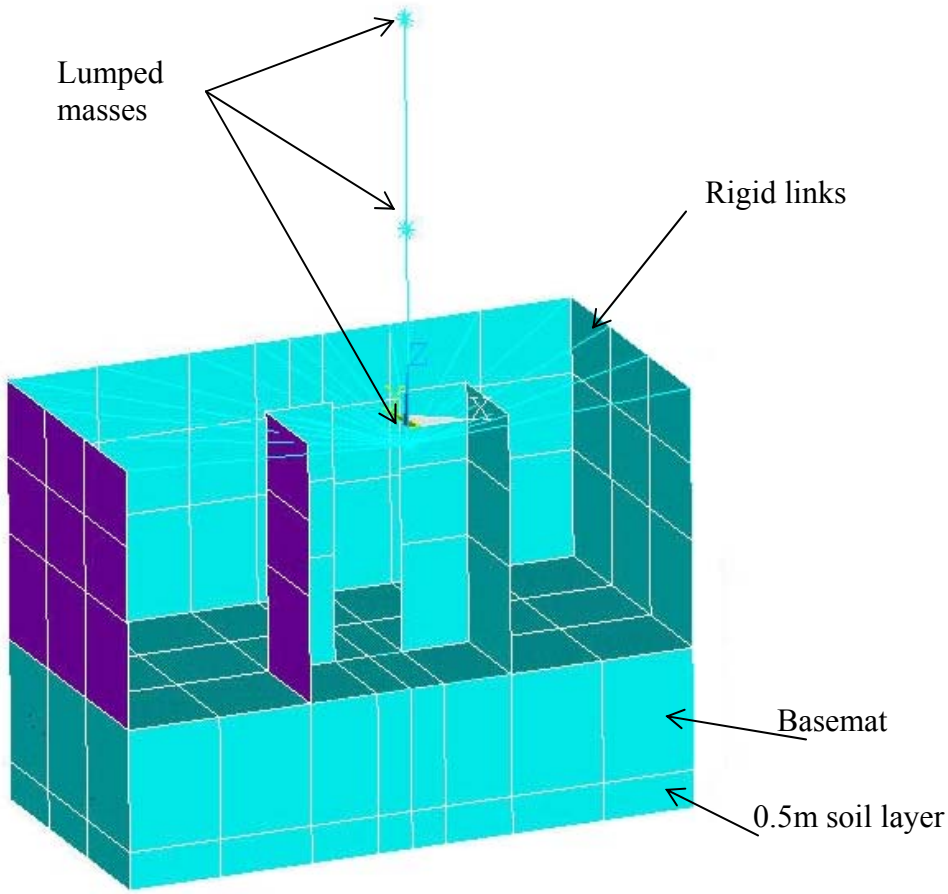

Figure 5-1. BNL SASSI model of the excavated single reactor building.

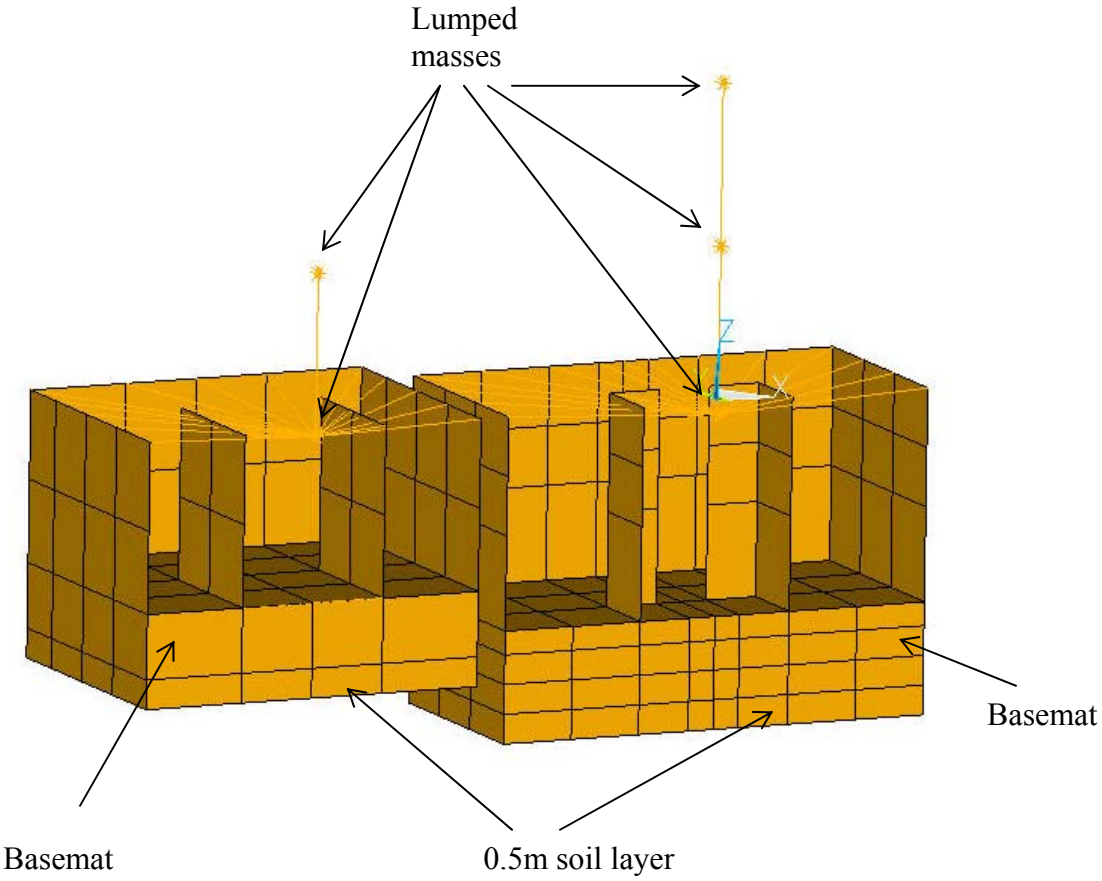

Figure 5-2. BNL SASSI model of the excavated reactor-turbine buildings.

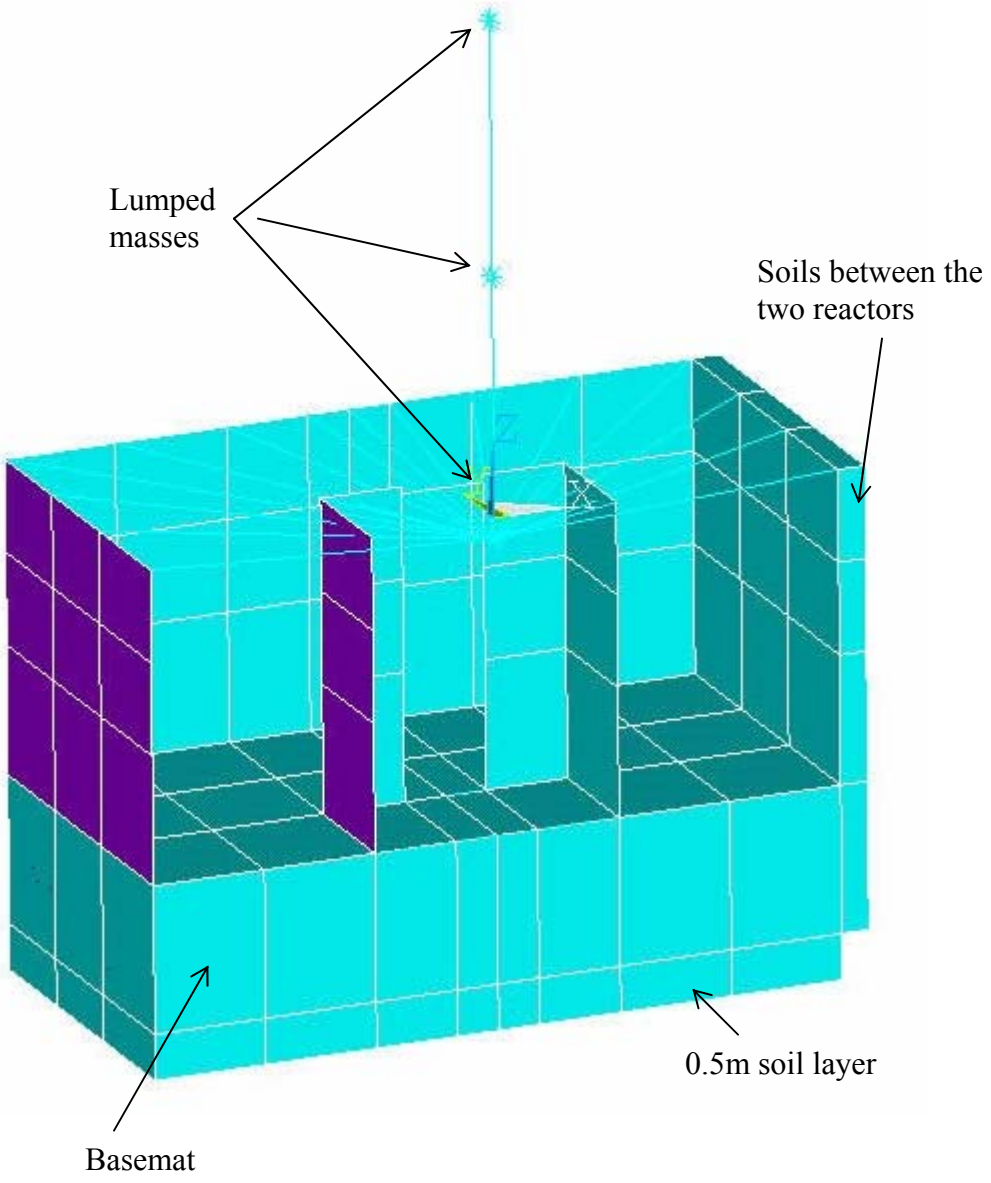

Figure 5-3. BNL SASSI model of the embedded twin-reactor buildings.

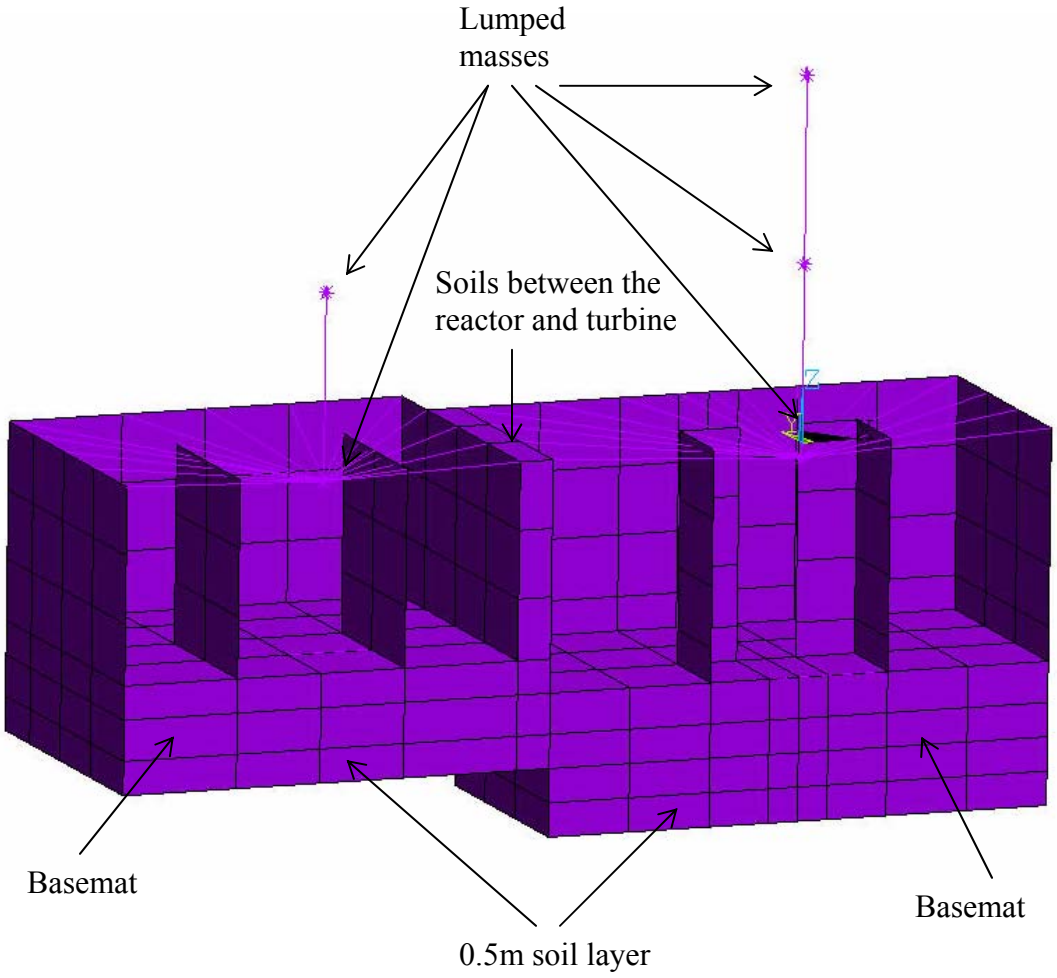

Figure 5-4. BNL SASSI model of the embedded reactor-turbine buildings.

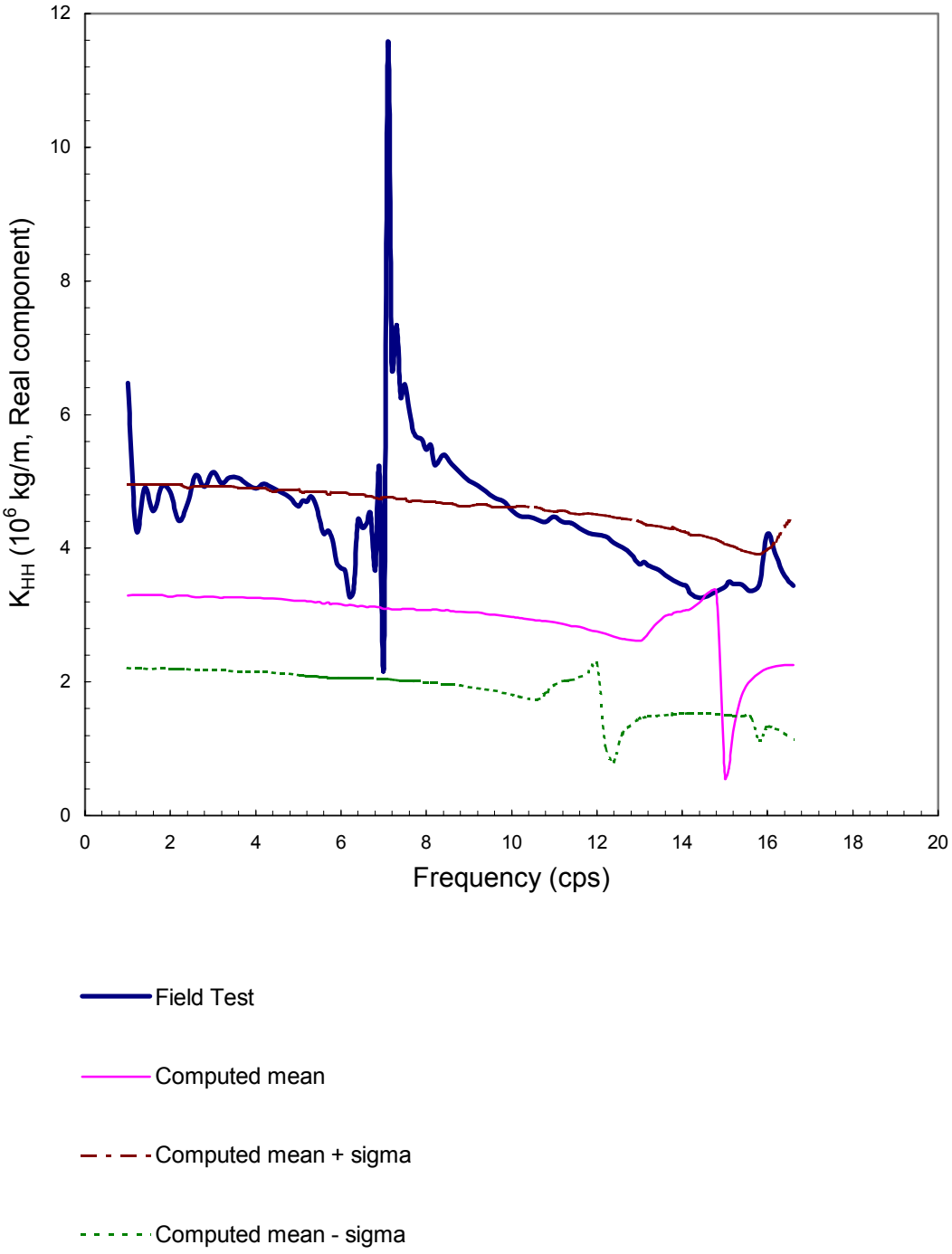

Figure 5-5. Comparison of horizontal impedance for single excavated structure (real component).

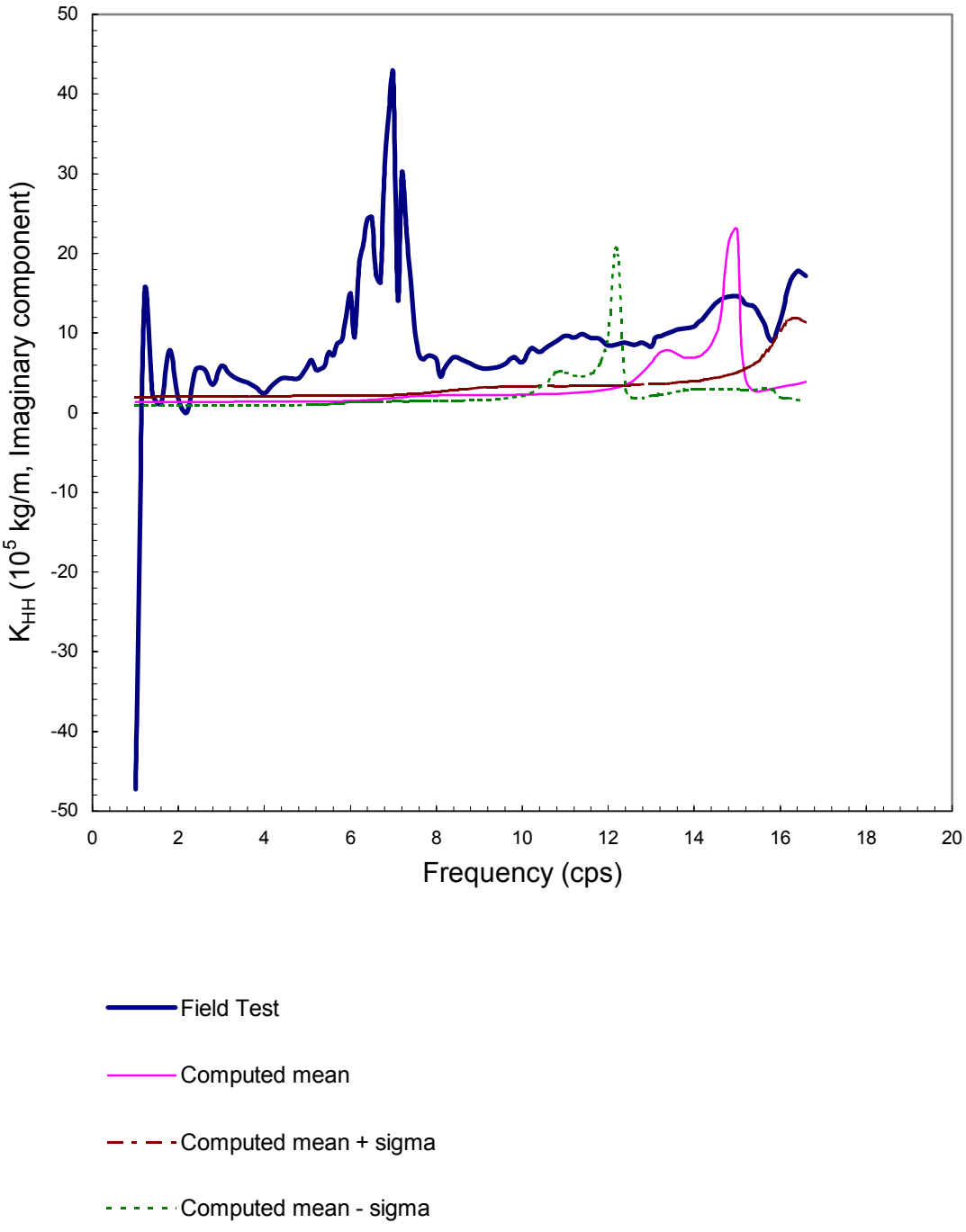

Figure 5-6. Comparison of horizontal impedance for single excavated structure (imaginary component).

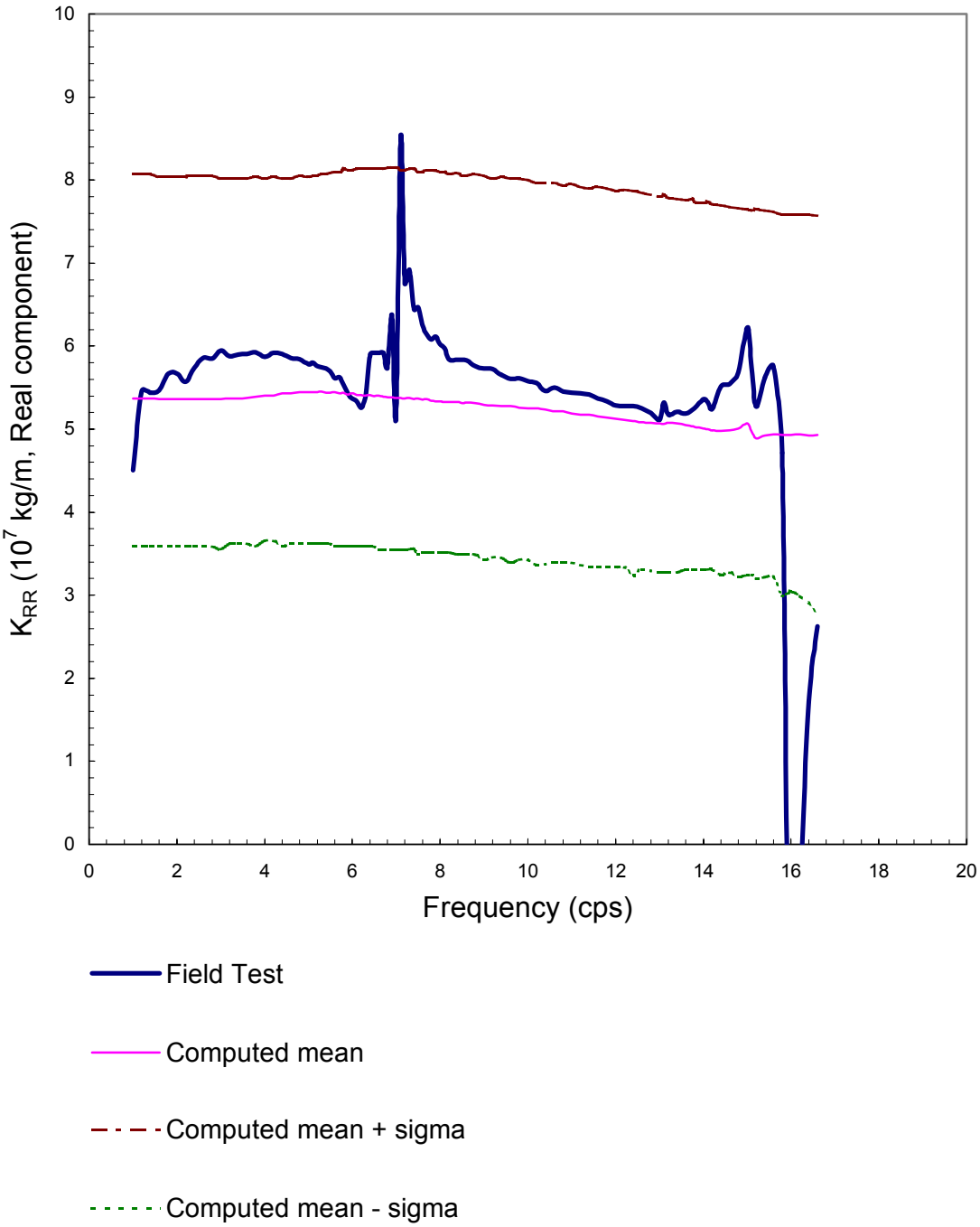

Figure 5-7. Comparison of rocking impedance for single excavated structure (real component).

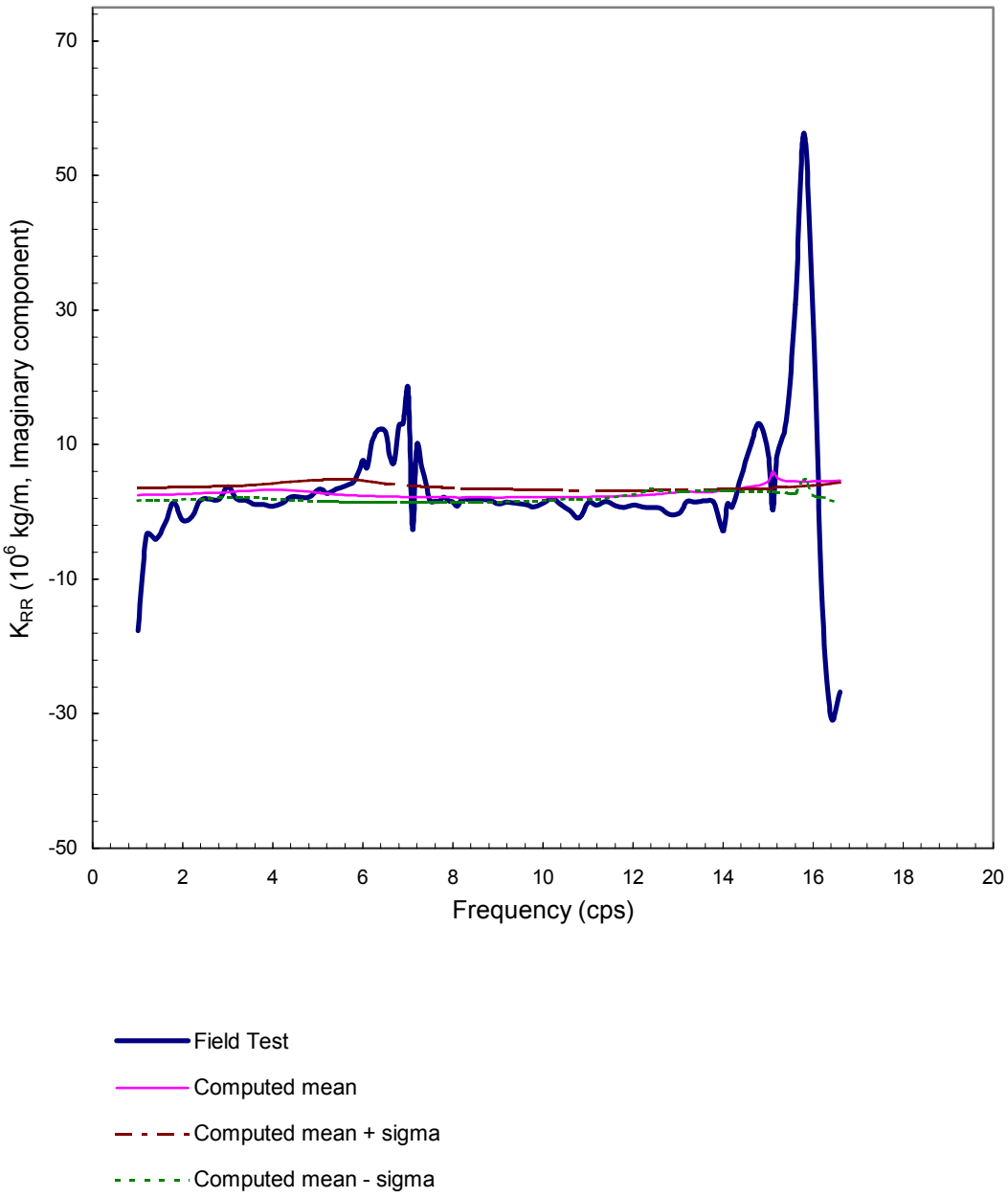

Figure 5-8. Comparison of rocking impedance for single excavated structure (imaginary component).

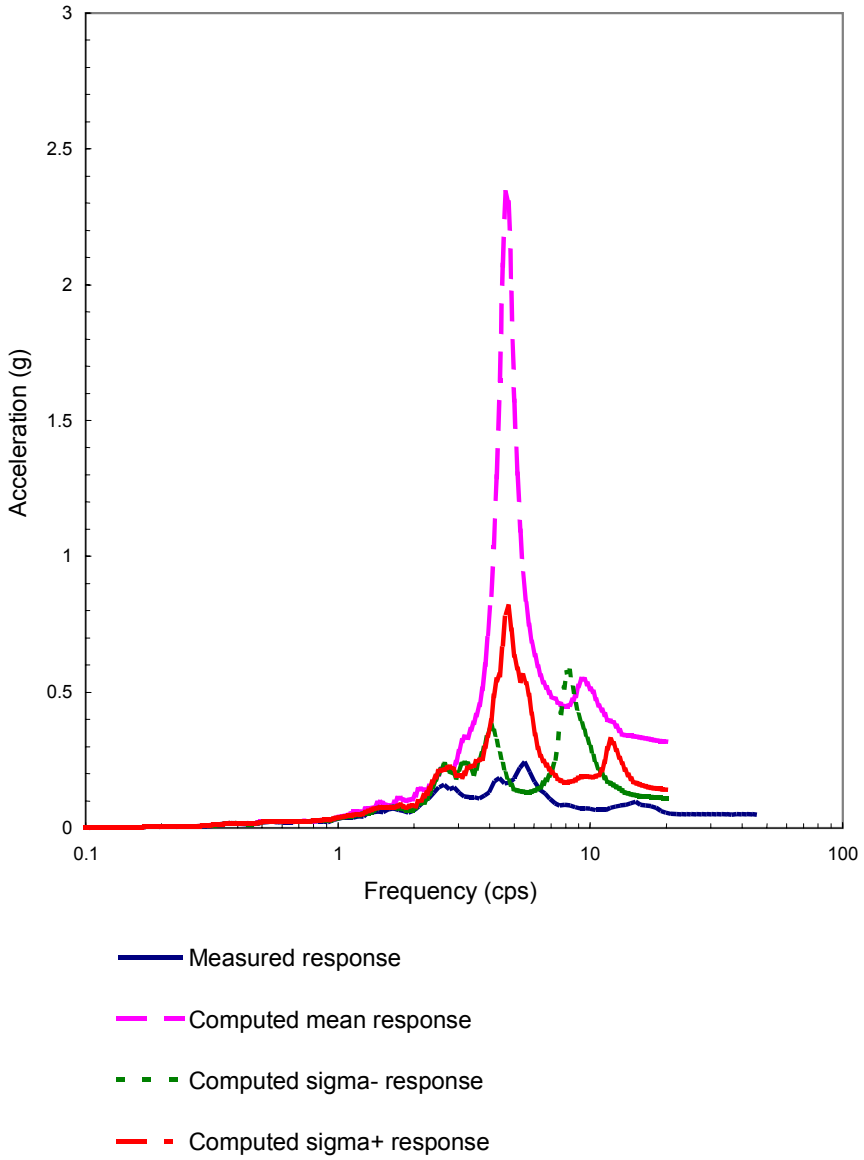

Figure 5-9. Comparison of response spectra at the basemat center of the excavated single reactor building in NS direction (No.63).

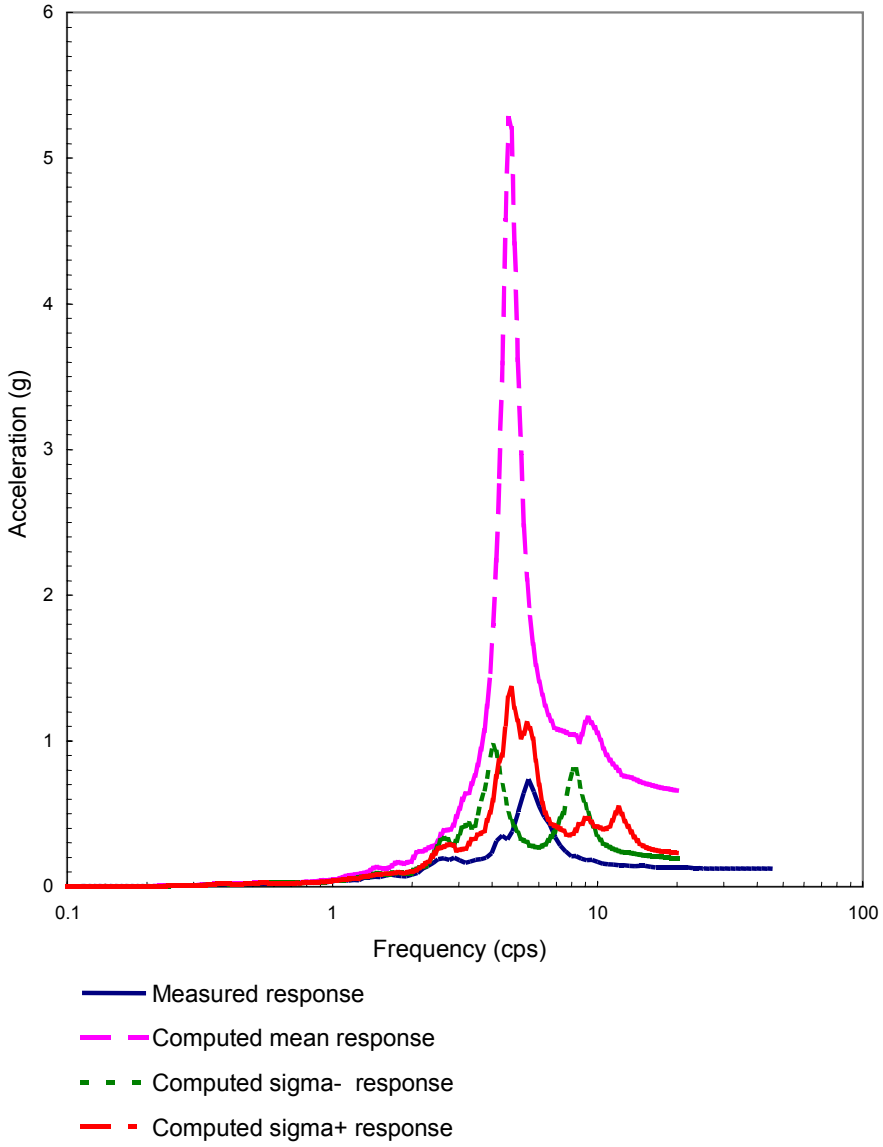

Figure 5-10. Comparison of response spectra at the roof center of the excavated single reactor building in NS direction (No.63).

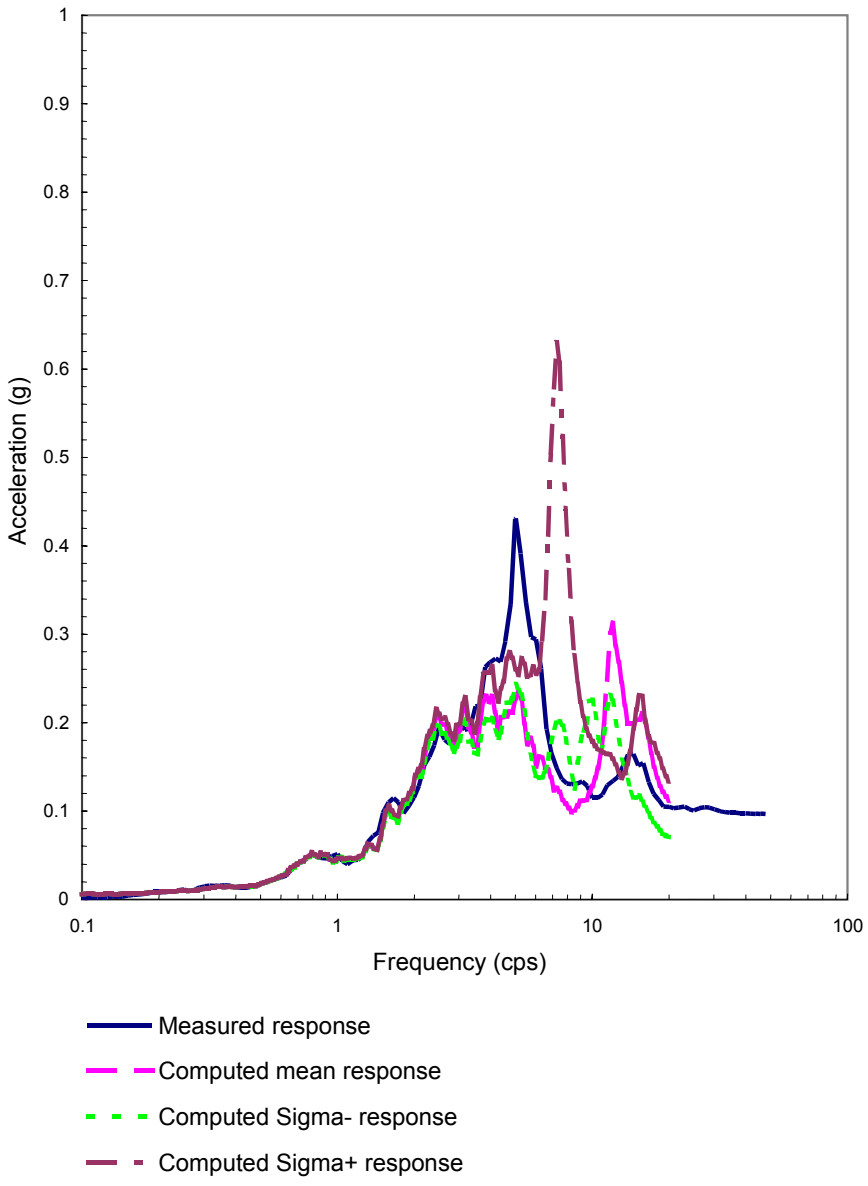

Figure 5-11. Comparison of response spectra at the basemat center of the excavated single reactor building in NS direction (No.89), V_s=150m/s for the 0.5m thin layer under the basemat.

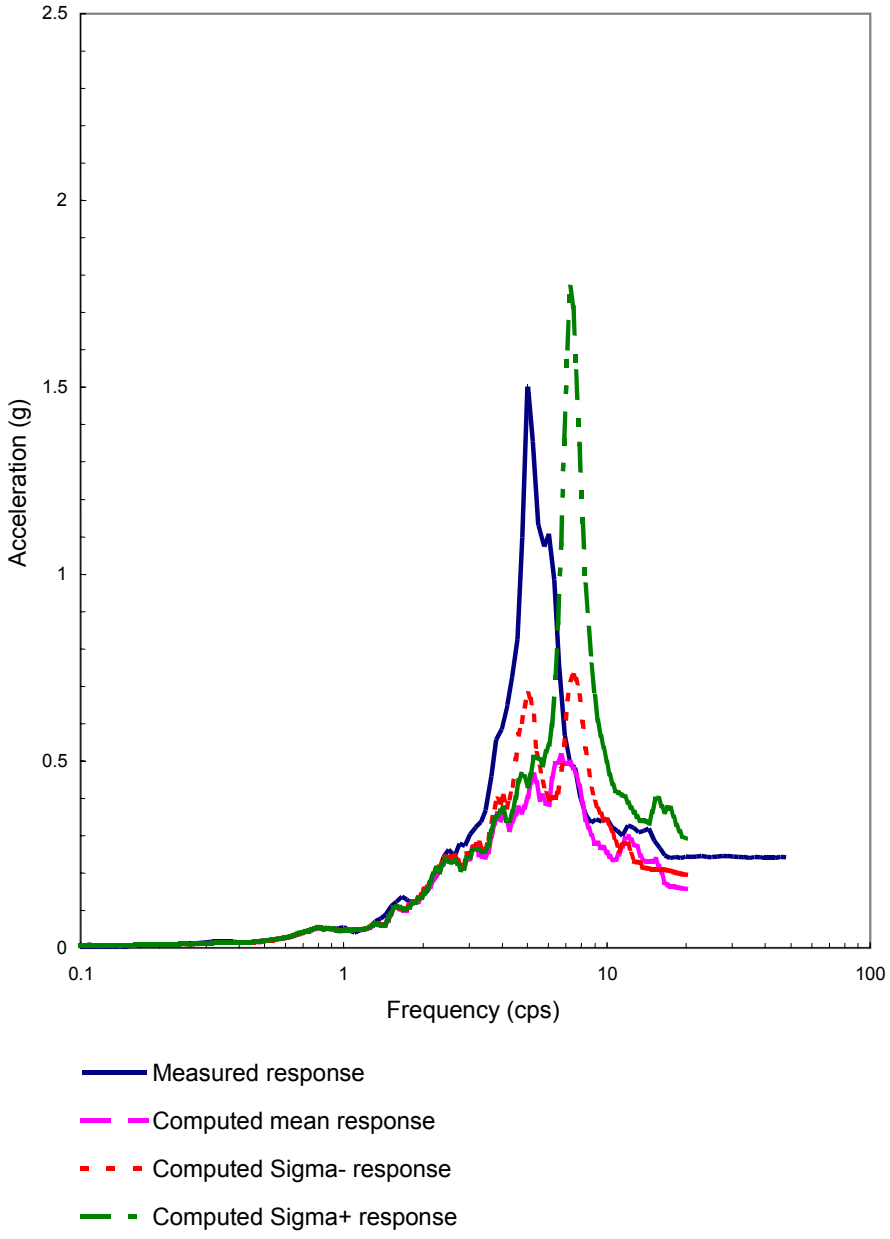

Figure 5-12. Comparison of response spectra at the roof center of the excavated single reactor building in NS direction (No.89), V_s=150m/s for the 0.5m thin layer under the basemat.

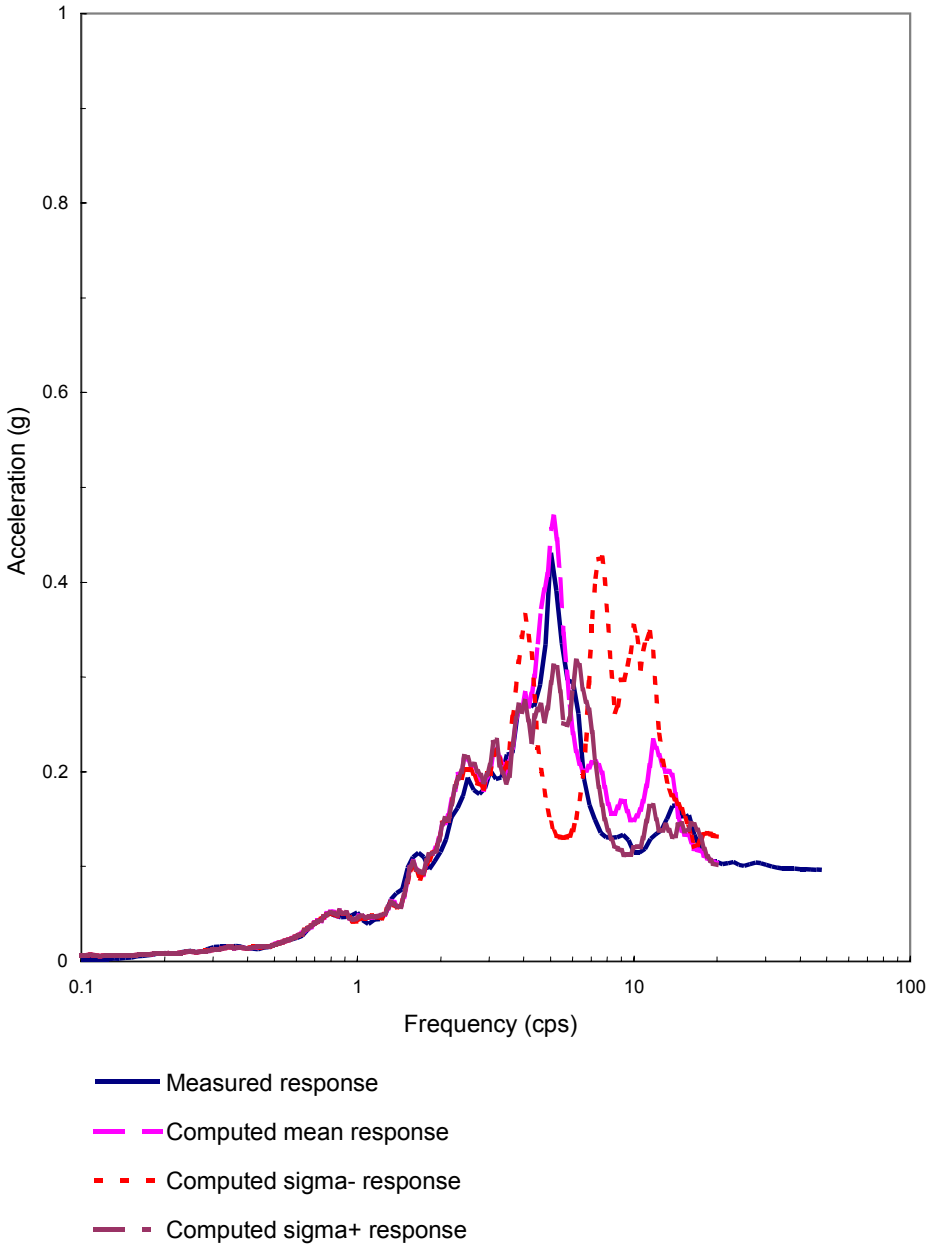

Figure 5-13. Comparison of response spectra at the basemat center of the excavated single reactor building in NS direction (No.89), V_s=110m/s for the 0.5m thin layer under the basemat.

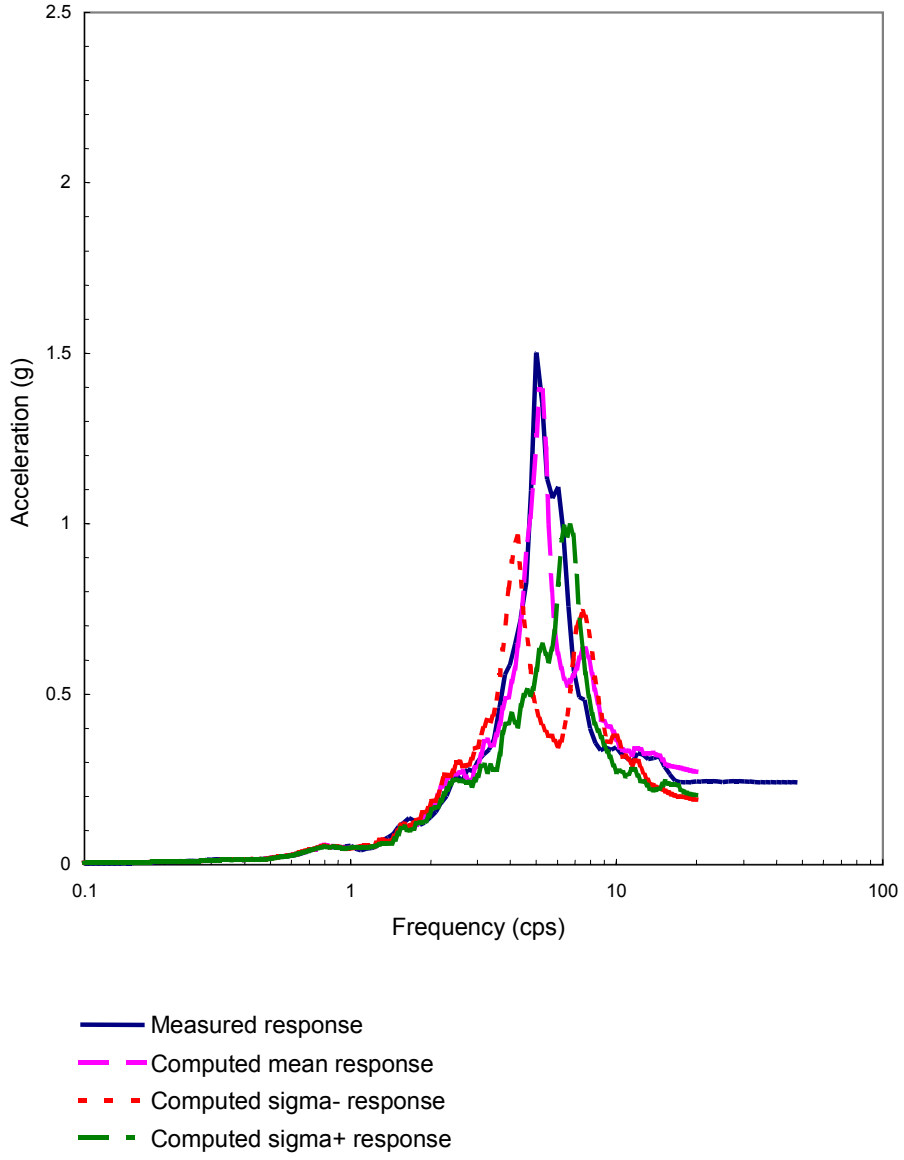

Figure 5-14. Comparison of response spectra at the roof center of the excavated single reactor building in NS direction (No.89), V_s=110m/s for the 0.5m thin layer under the basemat.

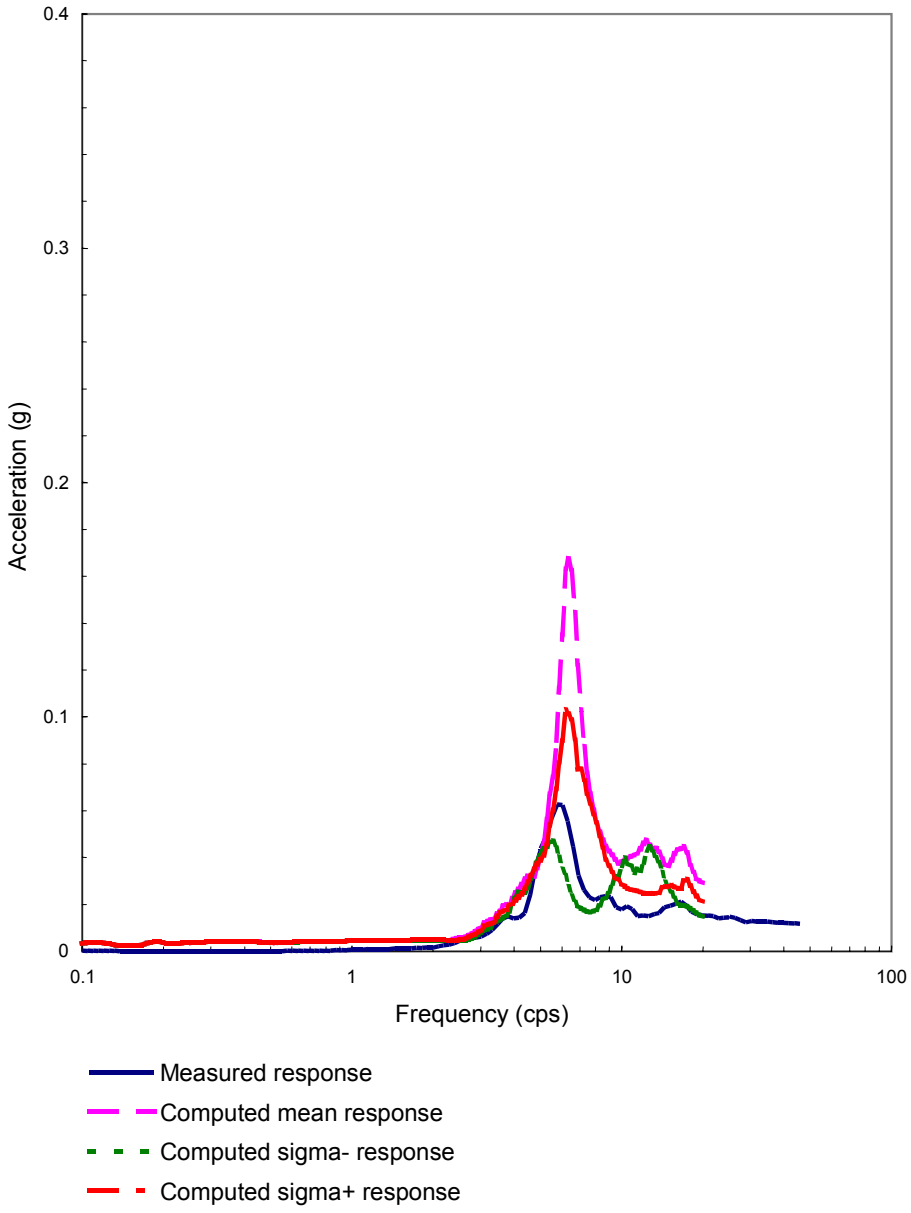

Figure 5-15. Comparison of response spectra at the basemat center of the excavated single reactor building in NS direction (No.131).

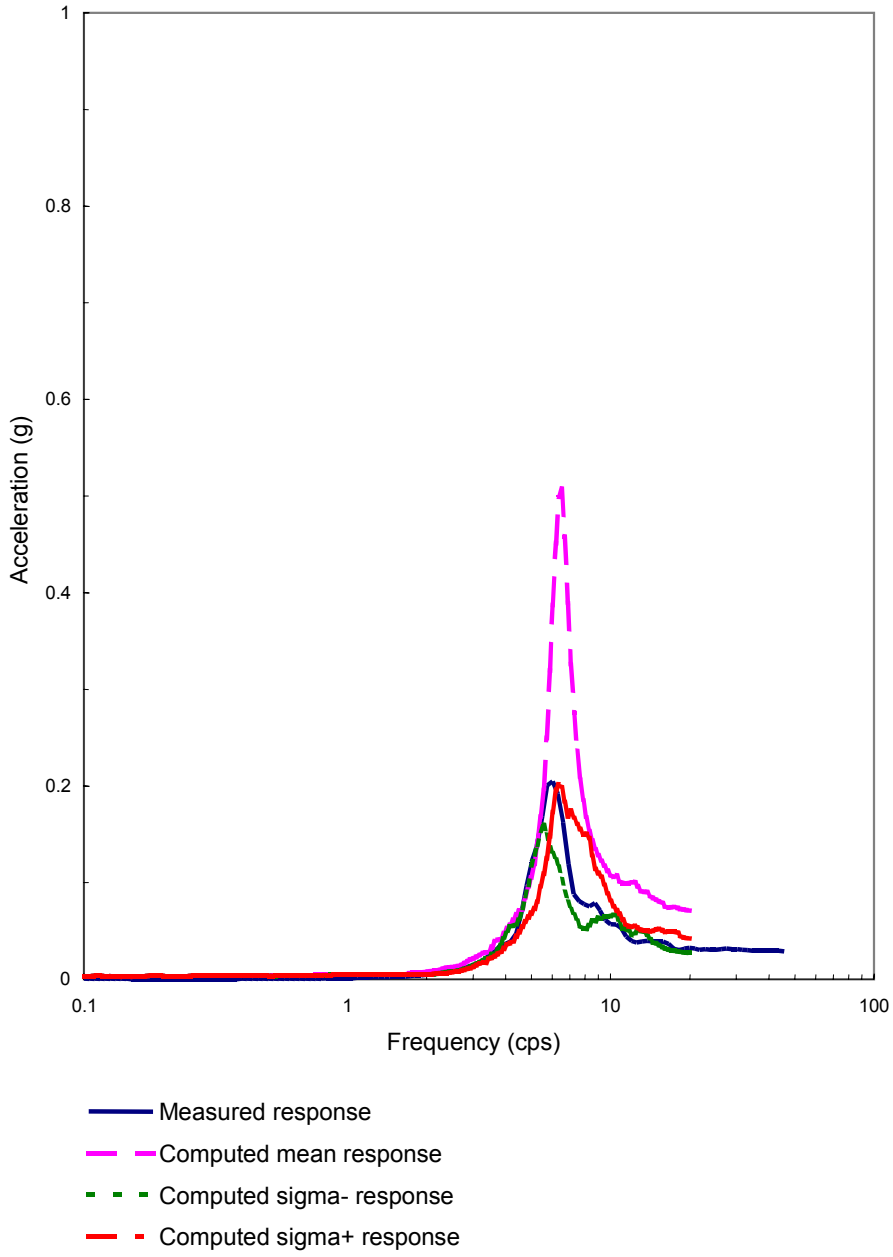

Figure 5-16. Comparison of response spectra at the roof center of the excavated single reactor building in NS direction (No.131).

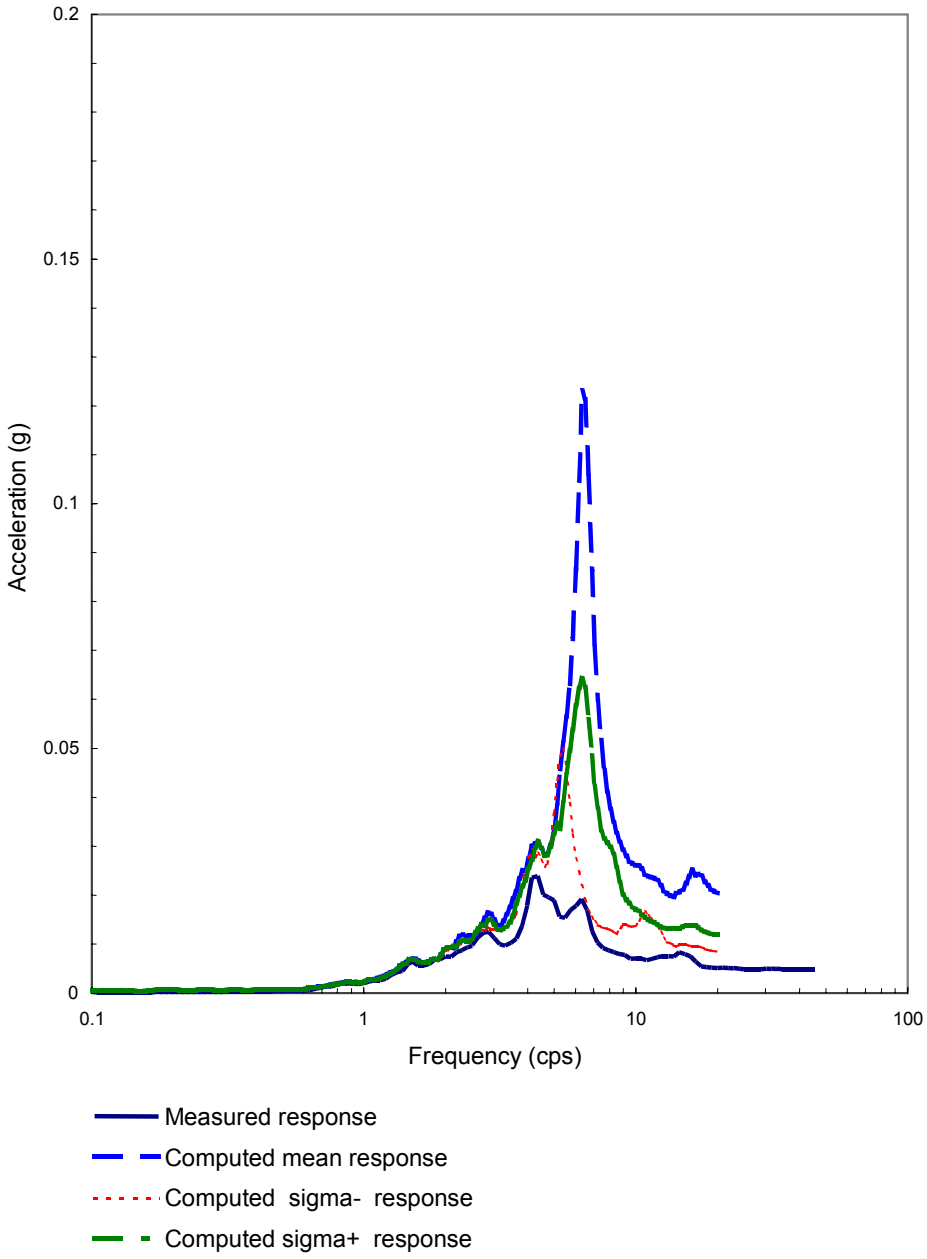

Figure 5-17. Comparison of response spectra at the basemat center of the excavated single reactor building in NS direction (No.139).

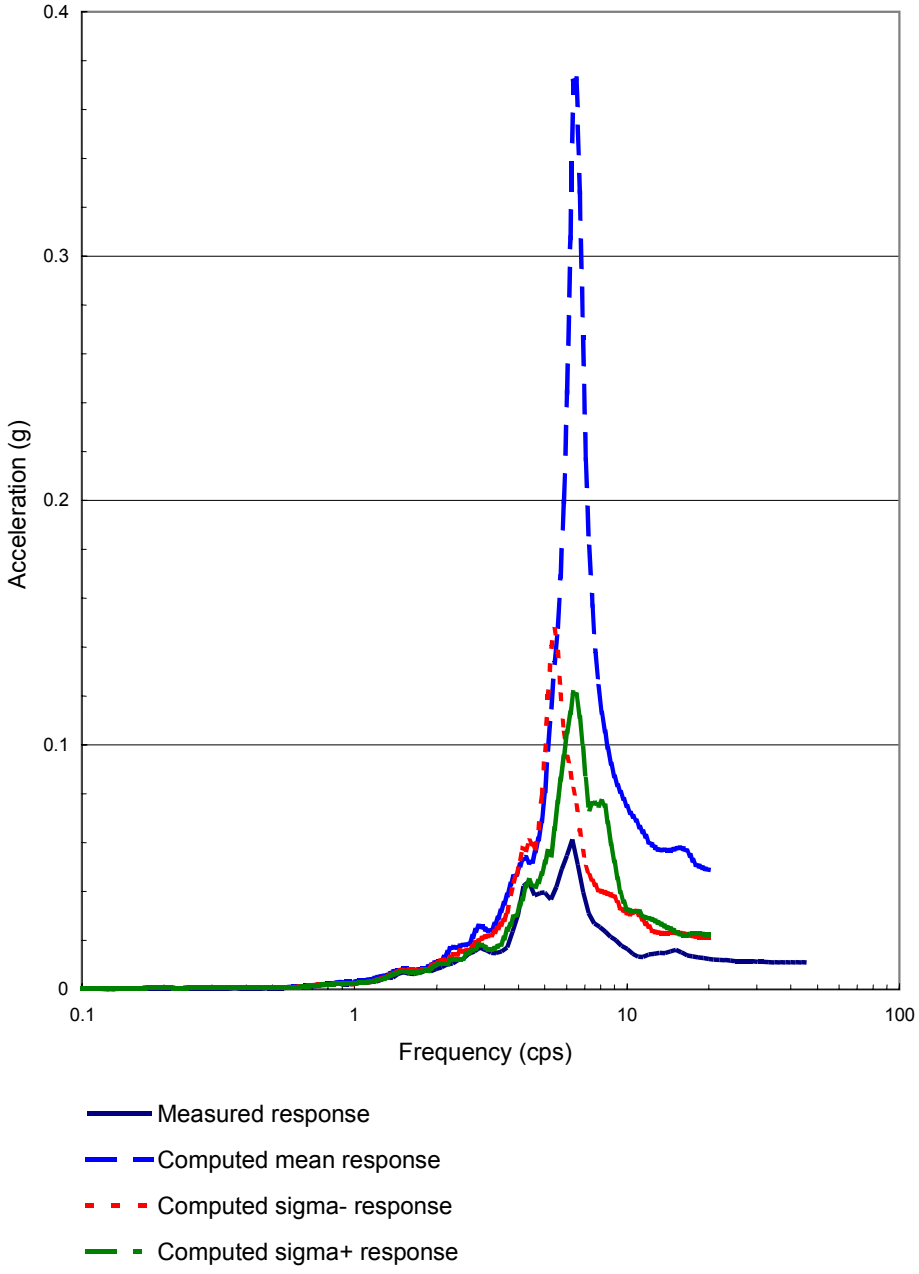

Figure 5-18. Comparison of response spectra at the roof center of the excavated single reactor building in NS direction (No.139).

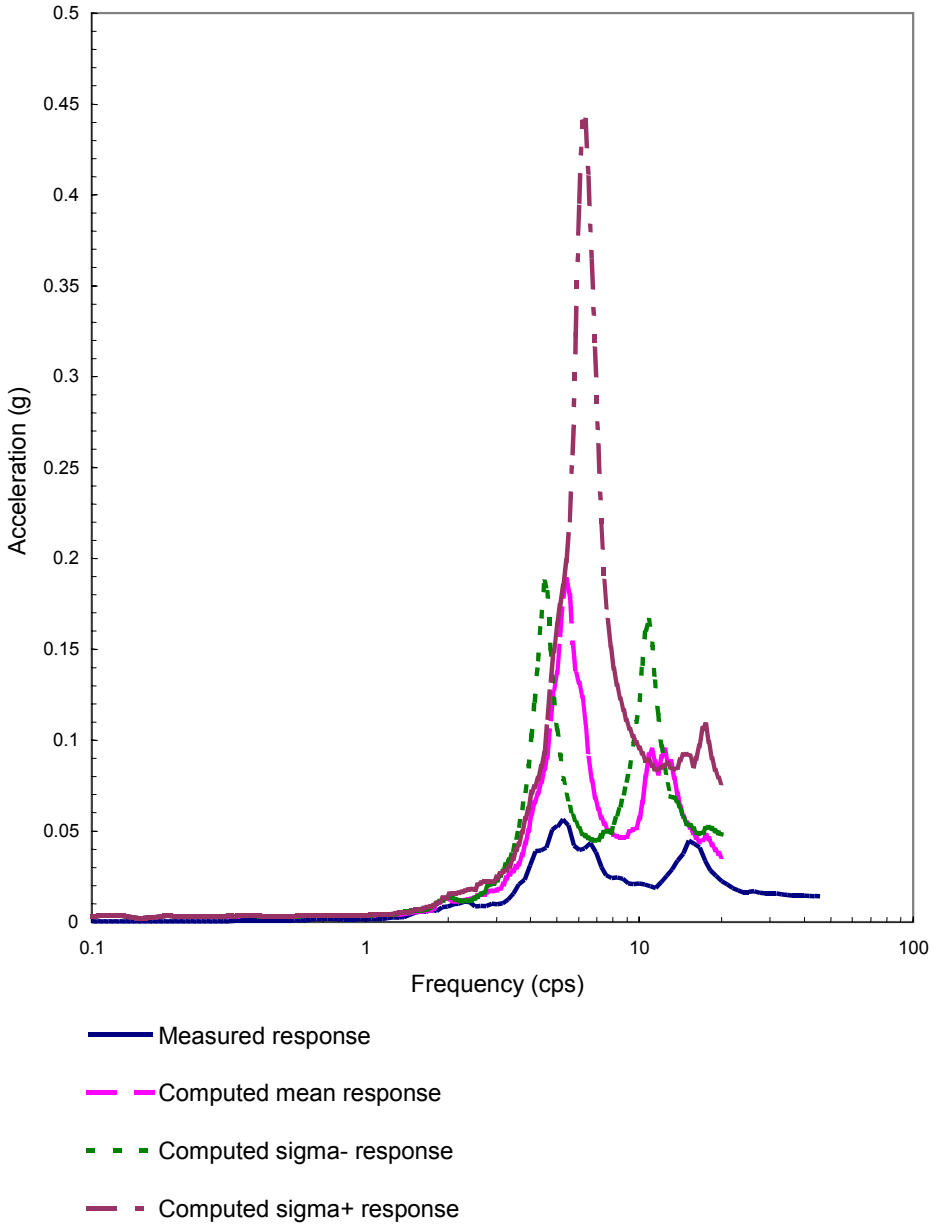

Figure 5-19. Comparison of response spectra at the basemat center of the excavated single reactor building in NS direction (No.157).

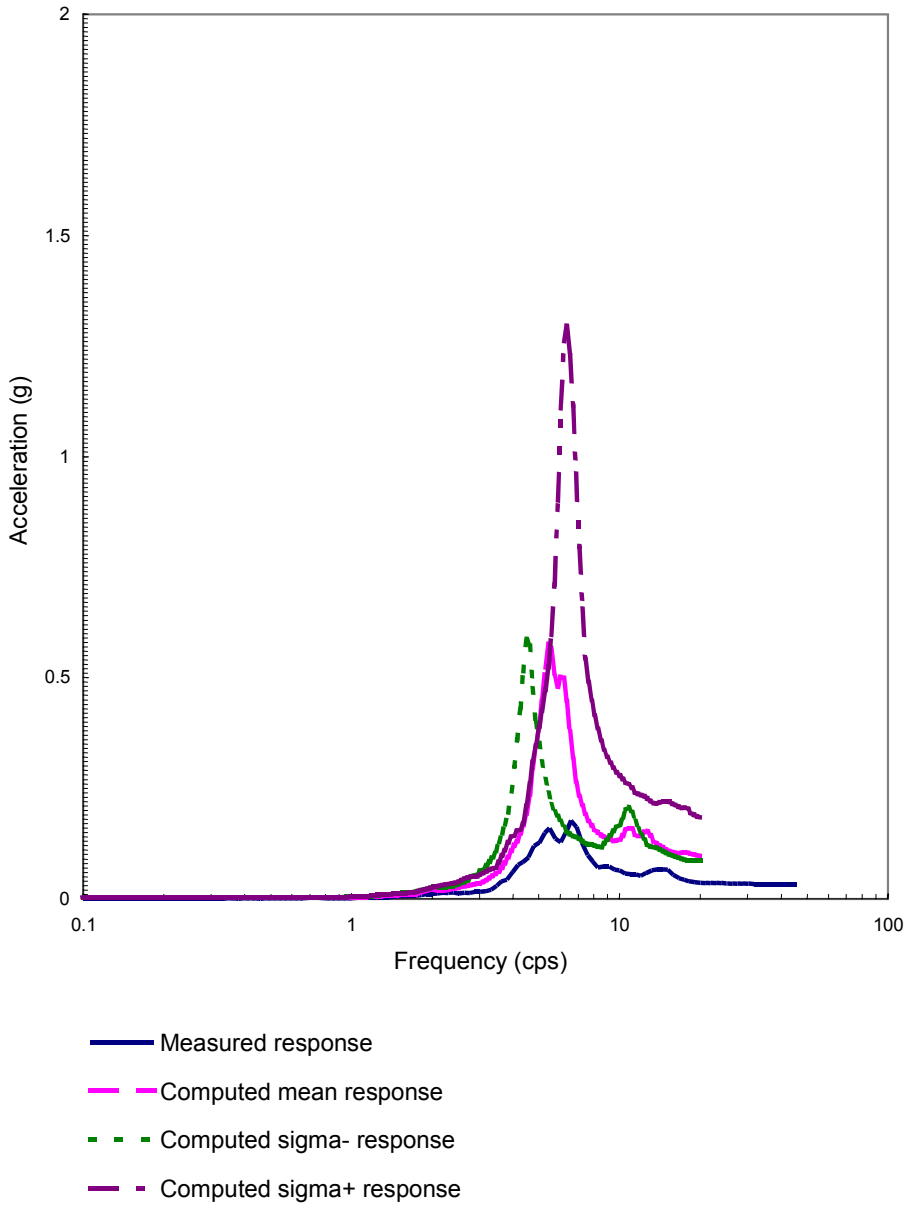

Figure 5-20. Comparison of response spectra at the roof center of the excavated single reactor building in NS direction (No.157).

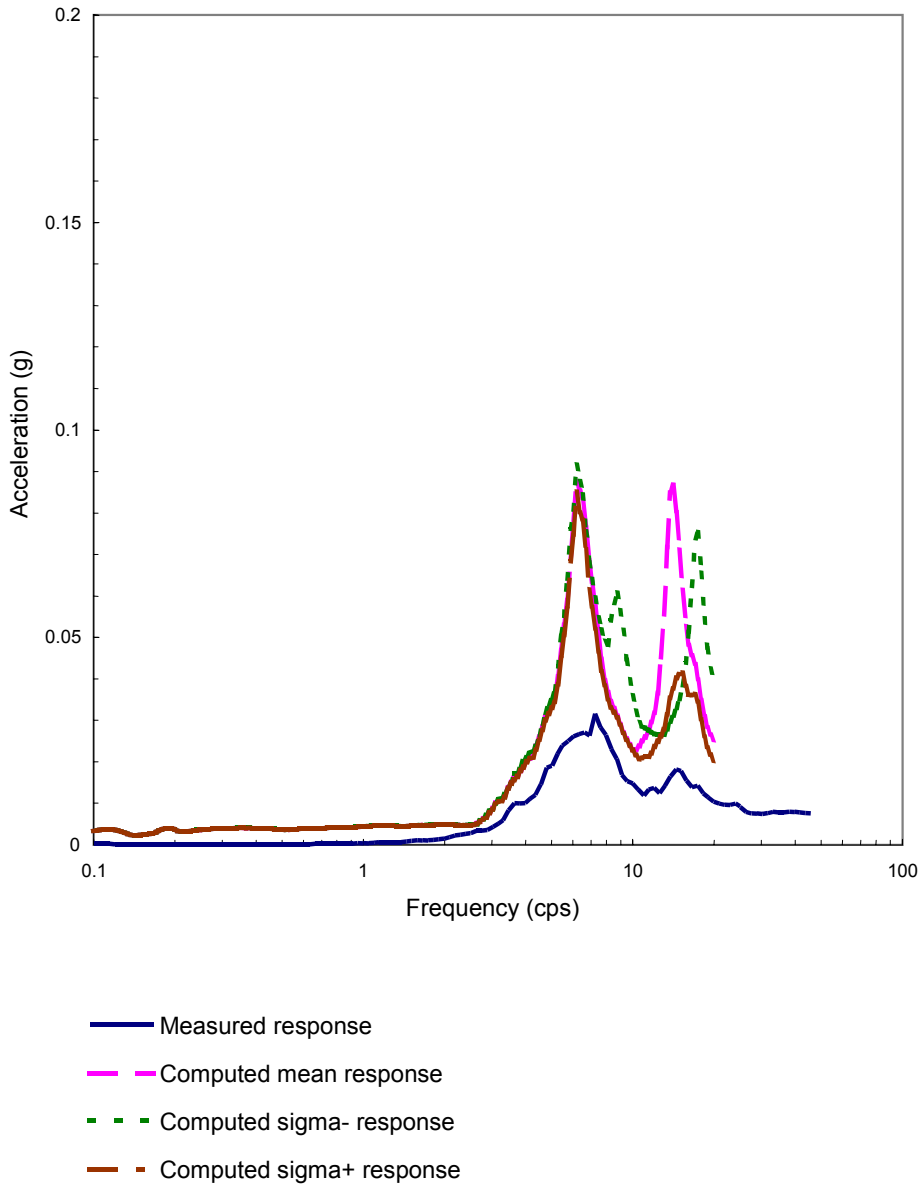

Figure 5-21. Comparison of response spectra at the basemat center of the excavated twin reactor buildings (BAS) in NS direction (No.131).

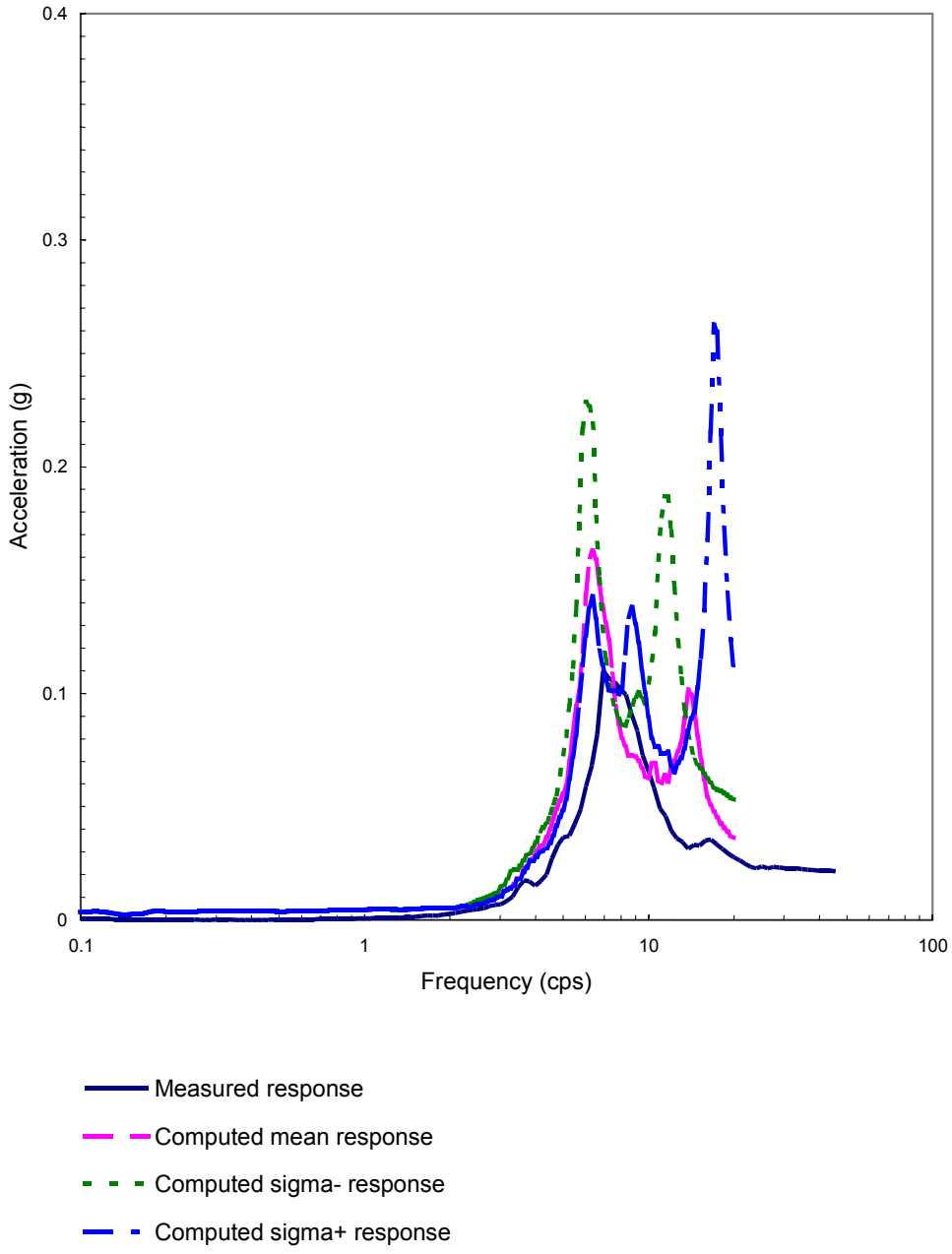

Figure 5-22. Comparison of response spectra at the roof center of the excavated twin reactor buildings (BAS) in NS direction (No.131).

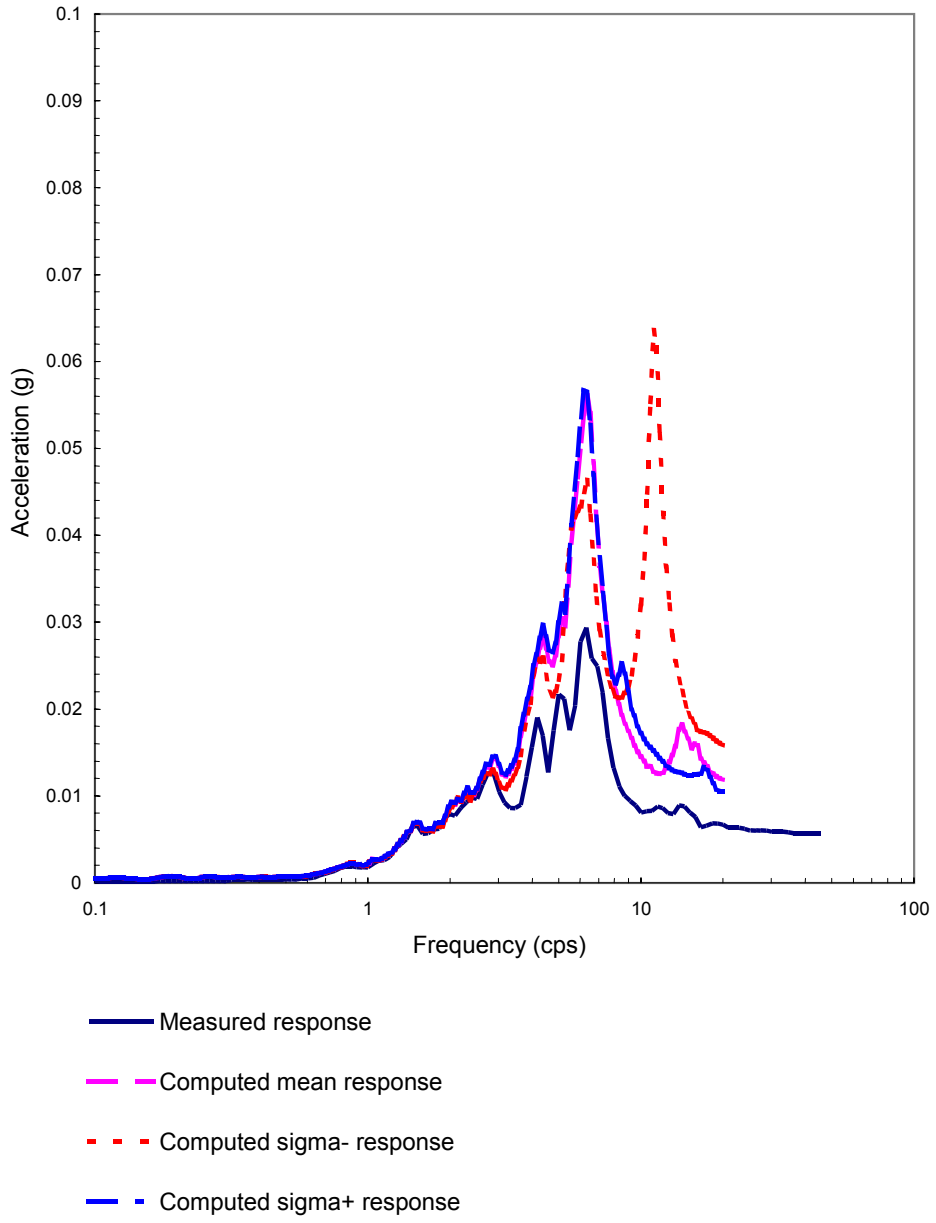

Figure 5-23. Comparison of response spectra at the basemat center of the excavated twin reactor buildings (BAS) in NS direction (No.139).

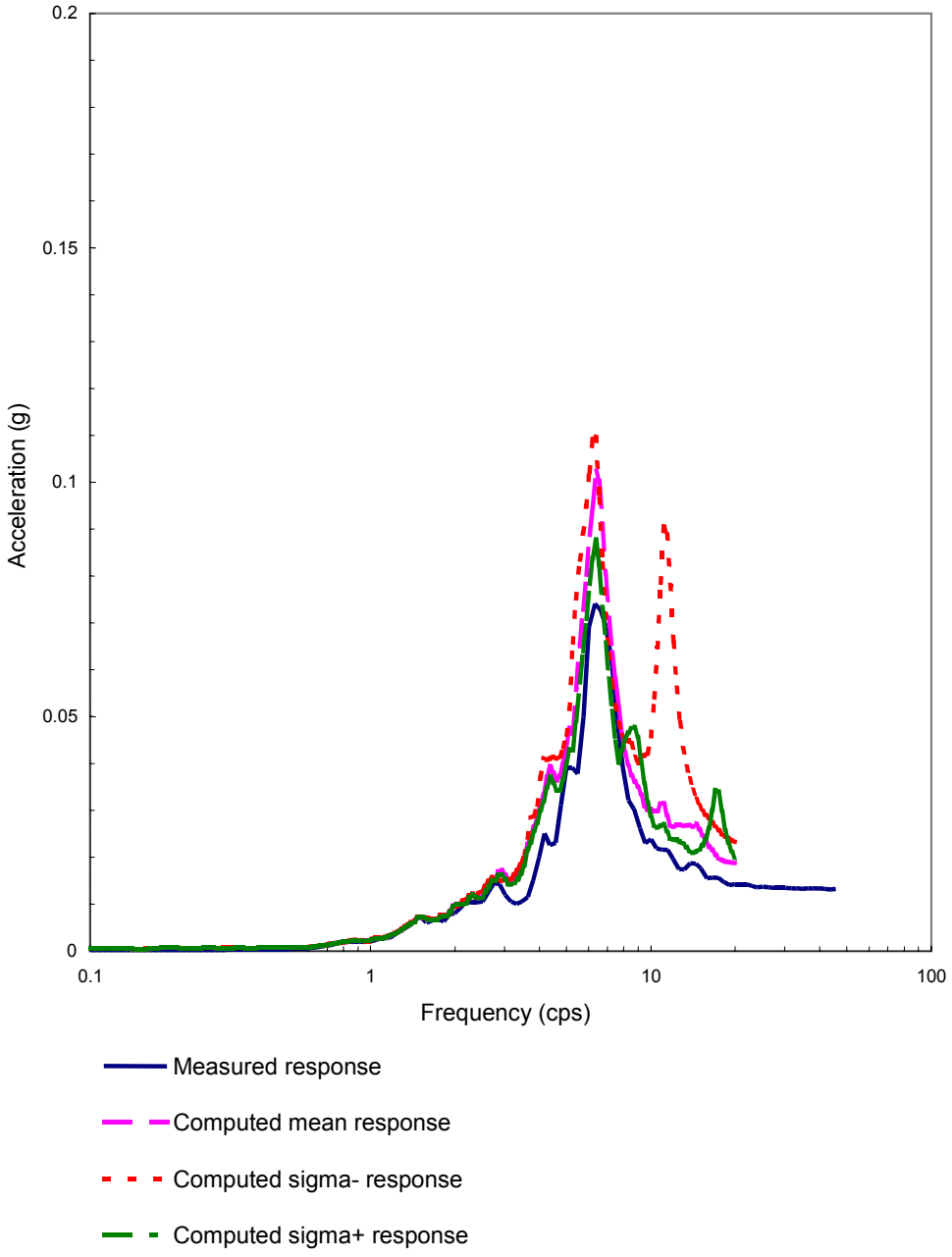

Figure 5-24. Comparison of response spectra at the roof center of the excavated twin reactor buildings (BAS) in NS direction (No.139).

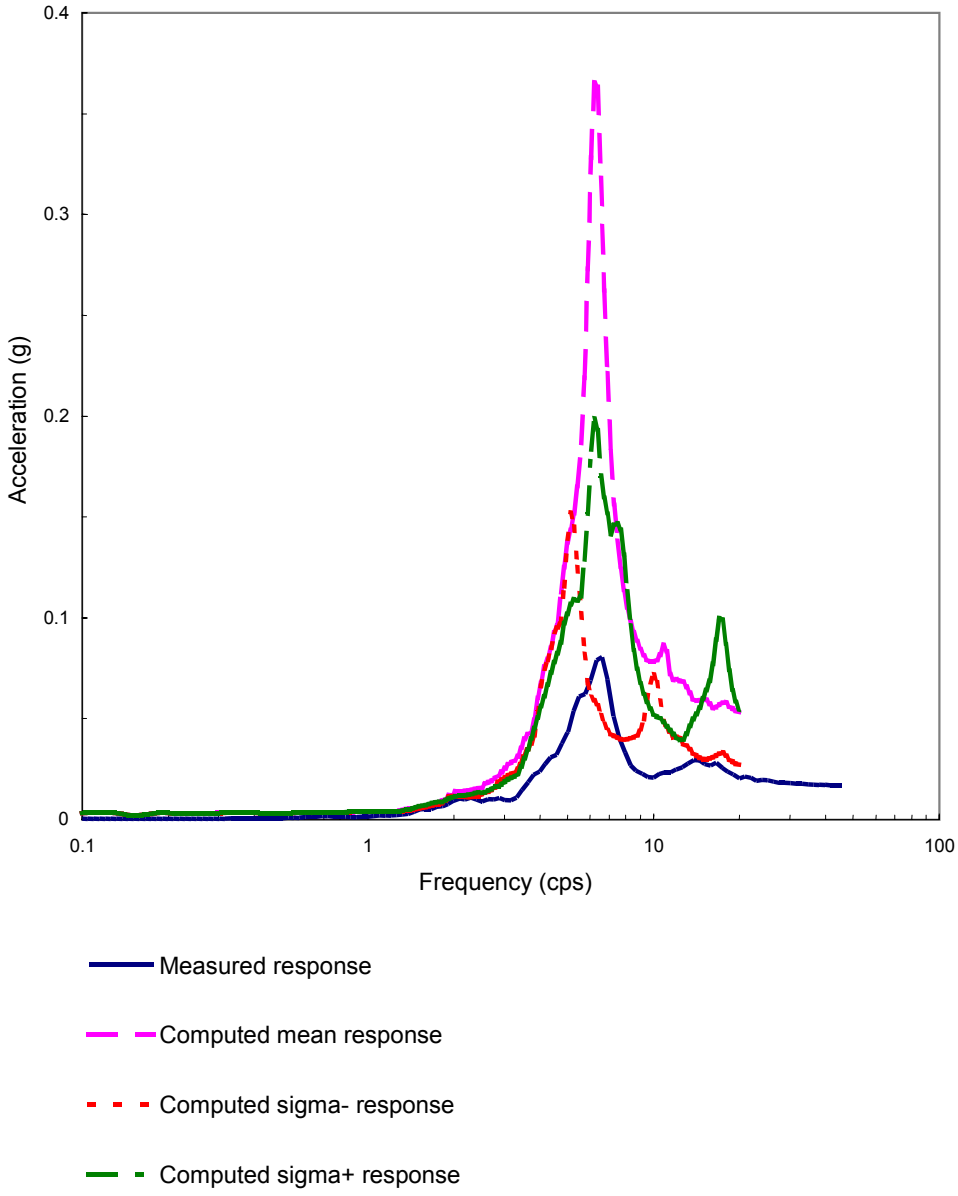

Figure 5-25. Comparison of response spectra at the basemat center of the excavated twin reactor buildings (BAS) in NS direction (No.157).

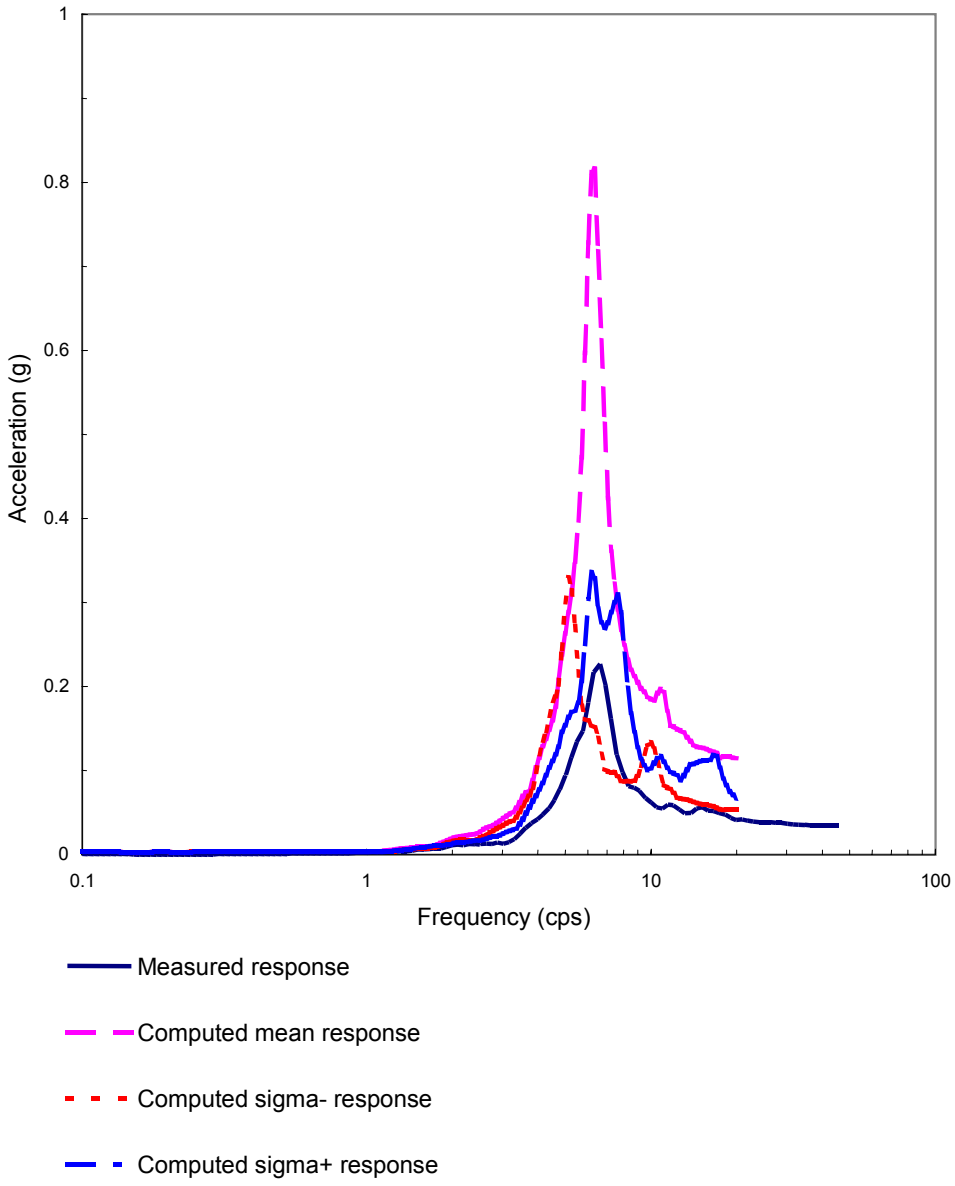

Figure 5-26. Comparison of response spectra at the roof center of the excavated twin reactor buildings (BAS) in NS direction (No.157).

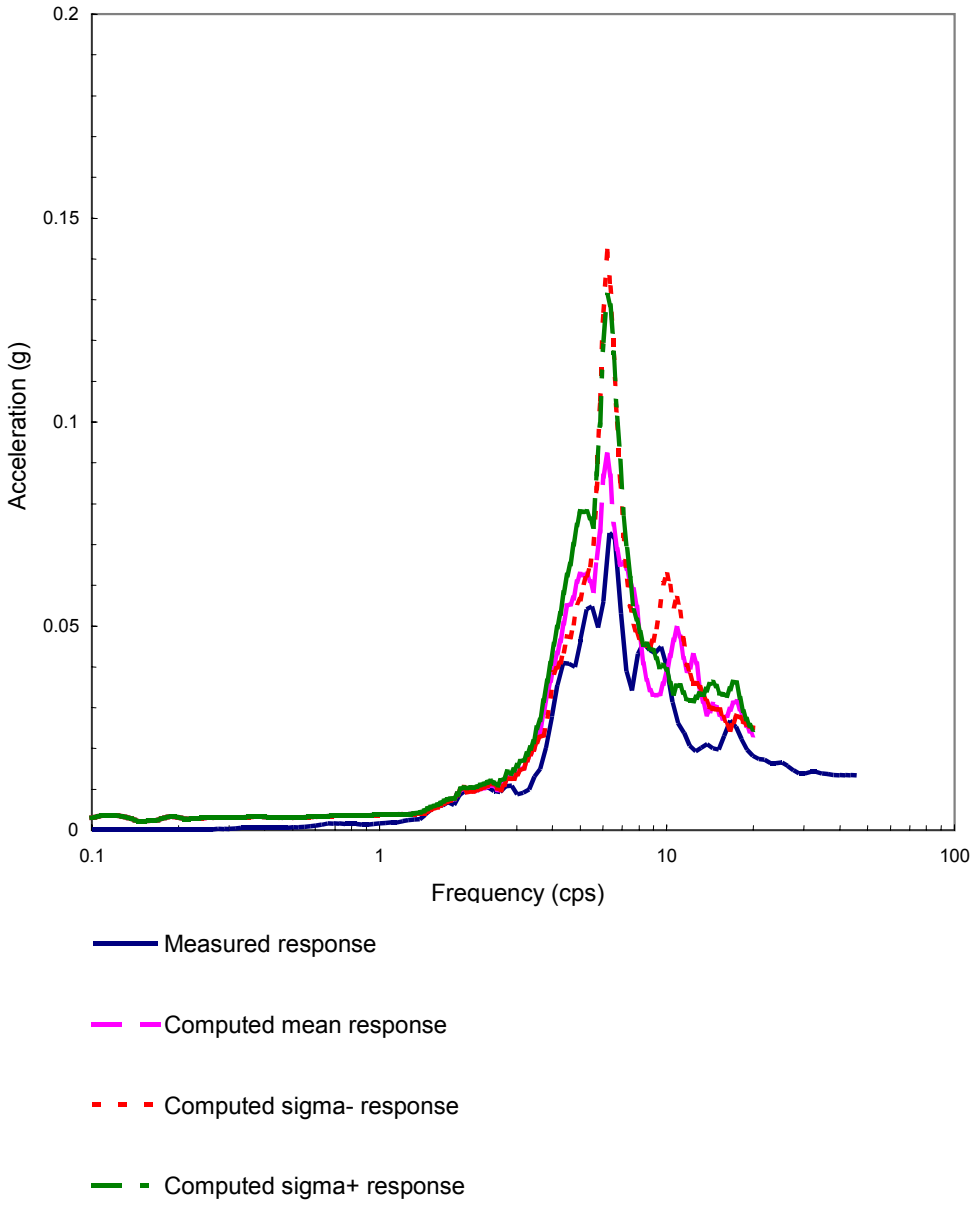

Figure 5-27. Comparison of response spectra at the basemat center of DA of the excavated reactor-turbine buildings in NS direction (No.157).

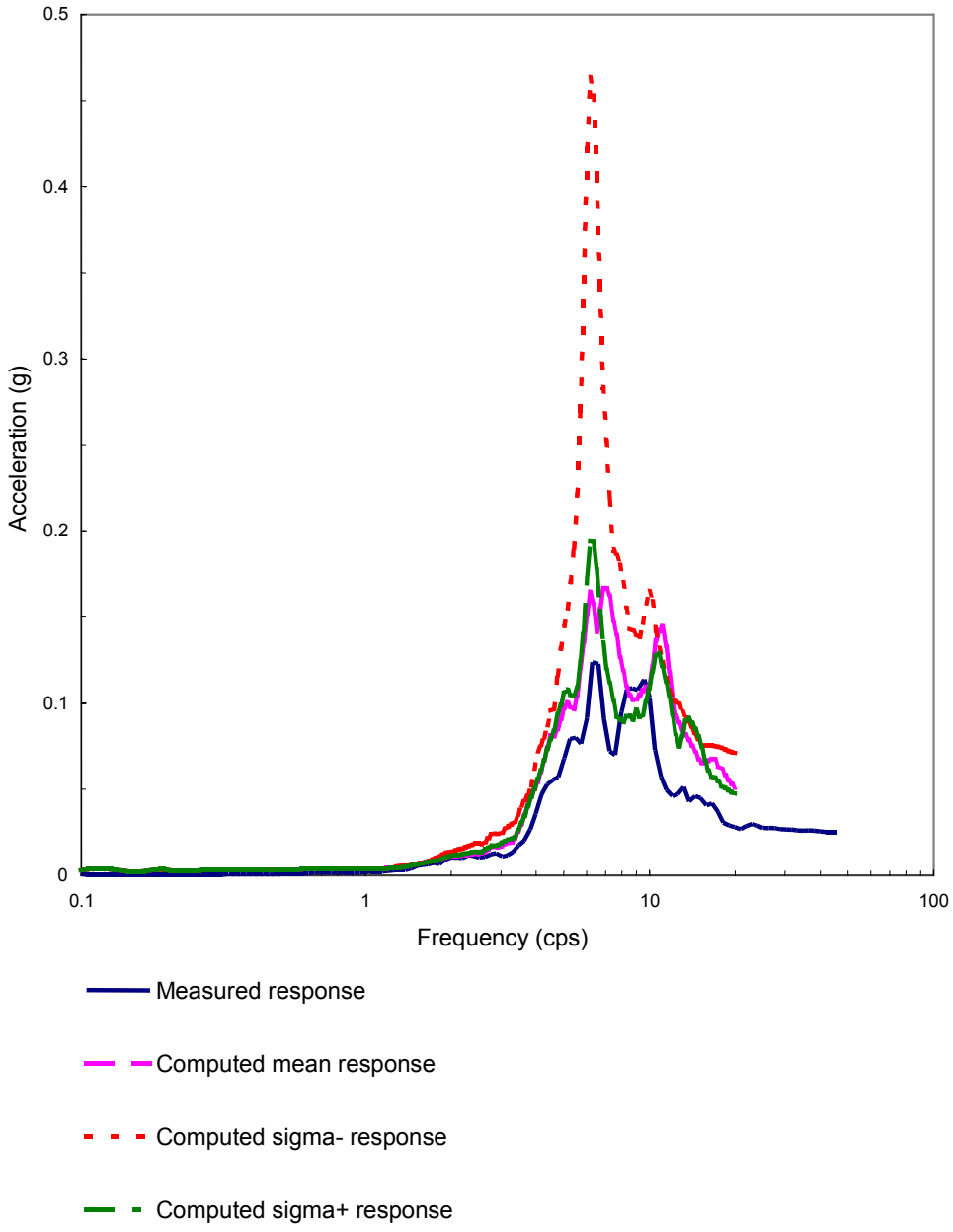

Figure 5-28. Comparison of response spectra at the roof center of DA of the excavated reactor-turbine buildings in NS direction (No.157).

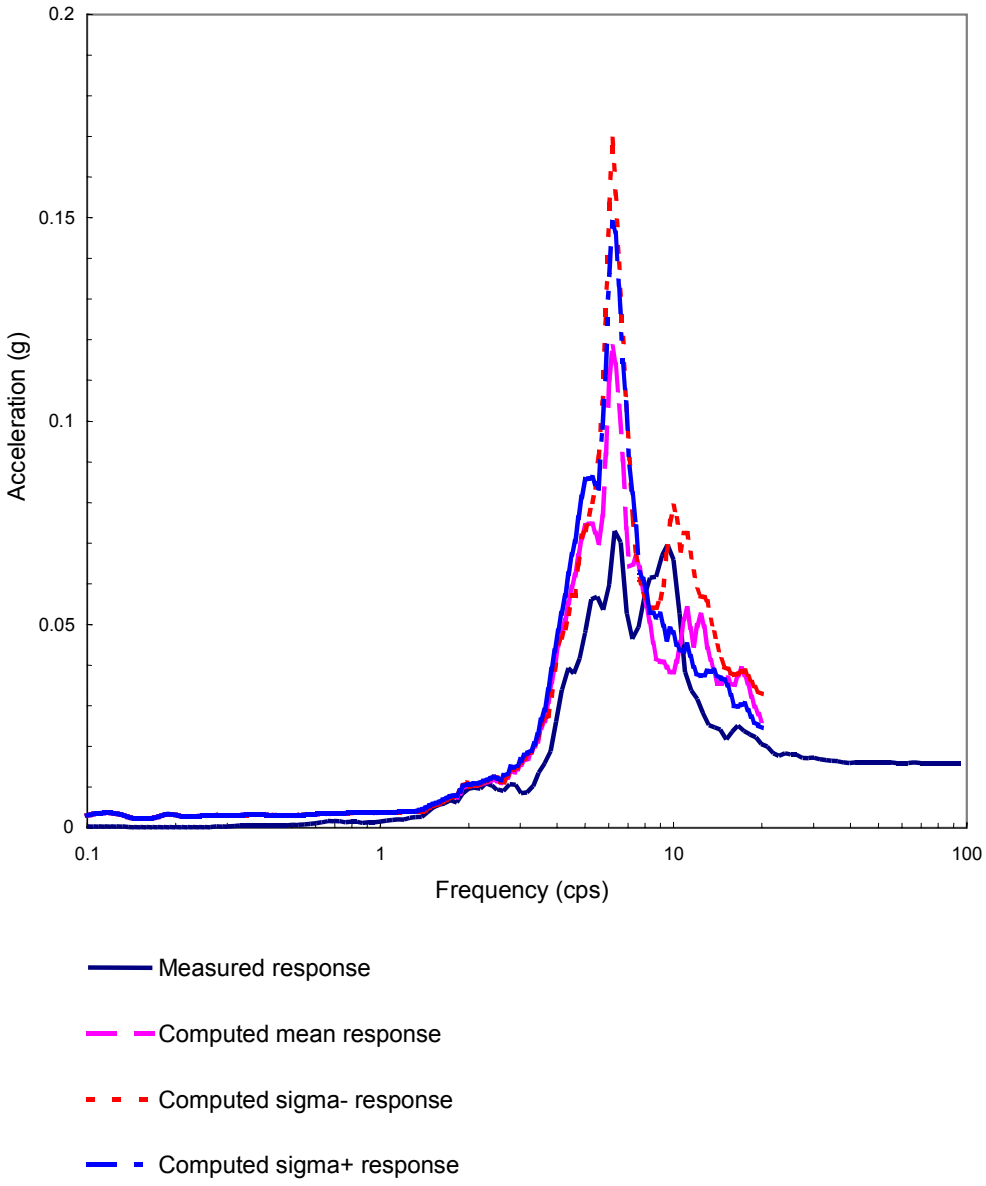

Figure 5-29. Comparison of response spectra at the basemat of DF of the excavated reactor-turbine buildings in NS direction (No.157).

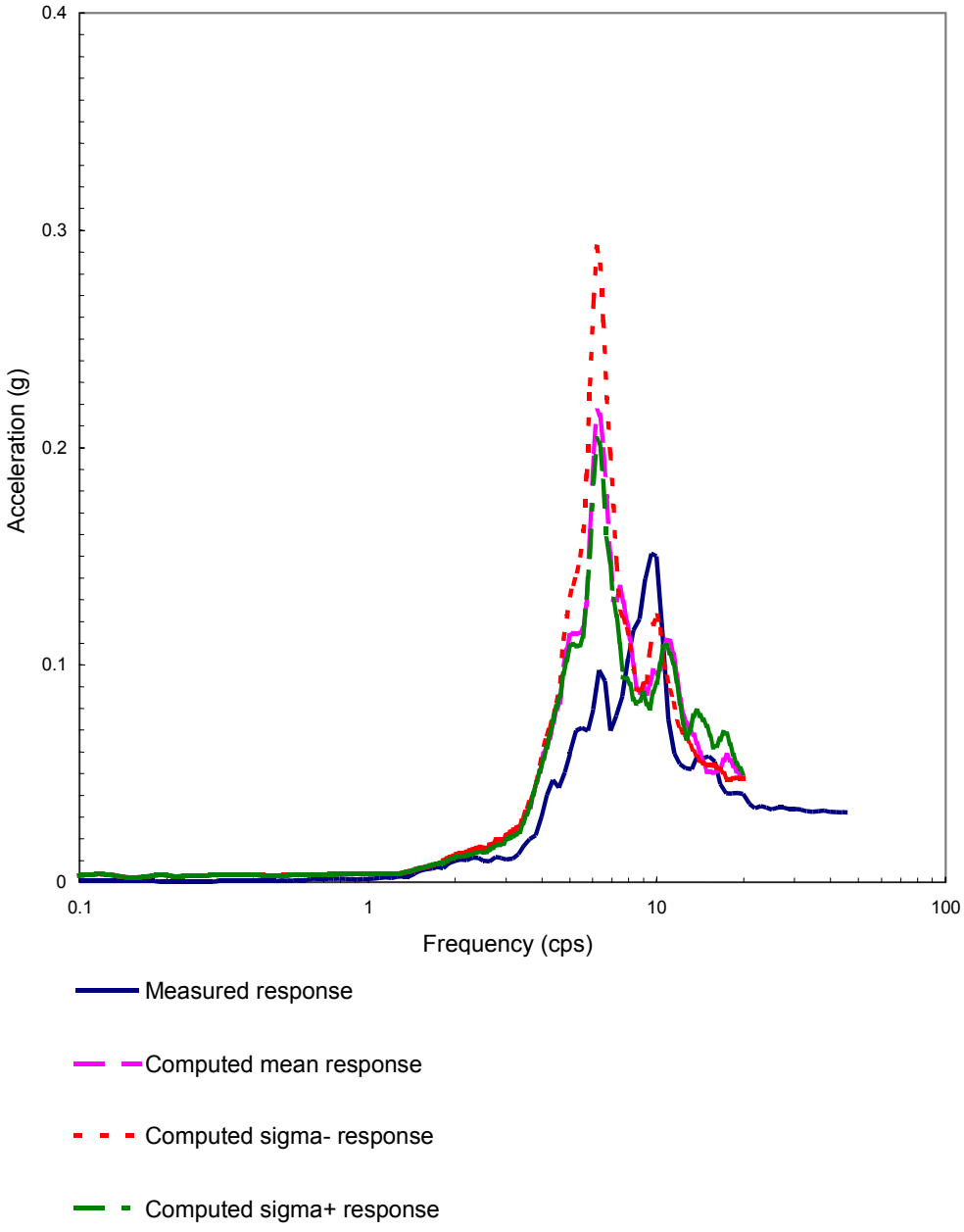

Figure 5-30. Comparison of response spectra at the roof center of DF of the excavated reactor-turbine buildings in NS direction (No.157).

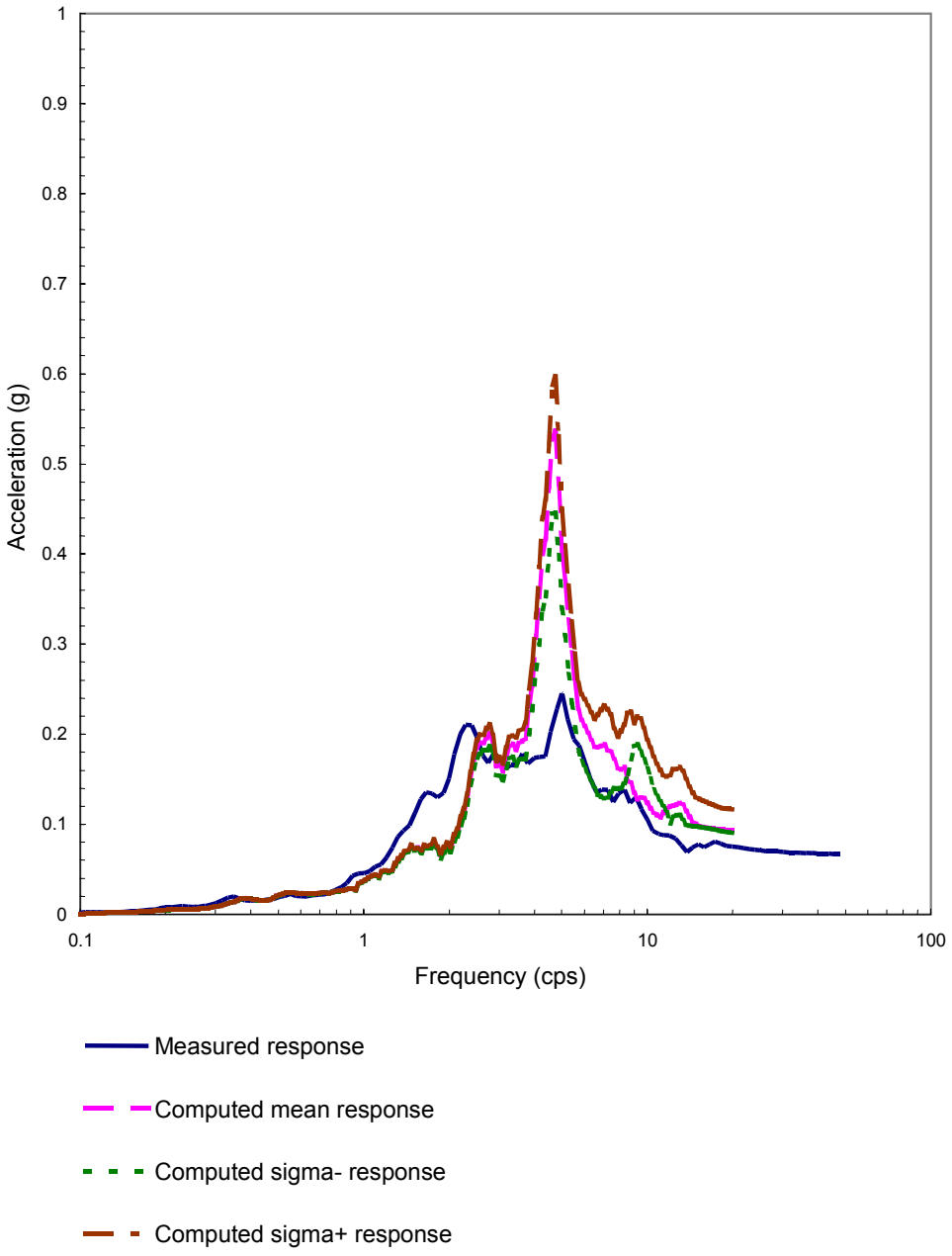

Figure 5-31. Comparison of response spectra at the basemat center of the embedded single reactor building in NS direction (No.63).

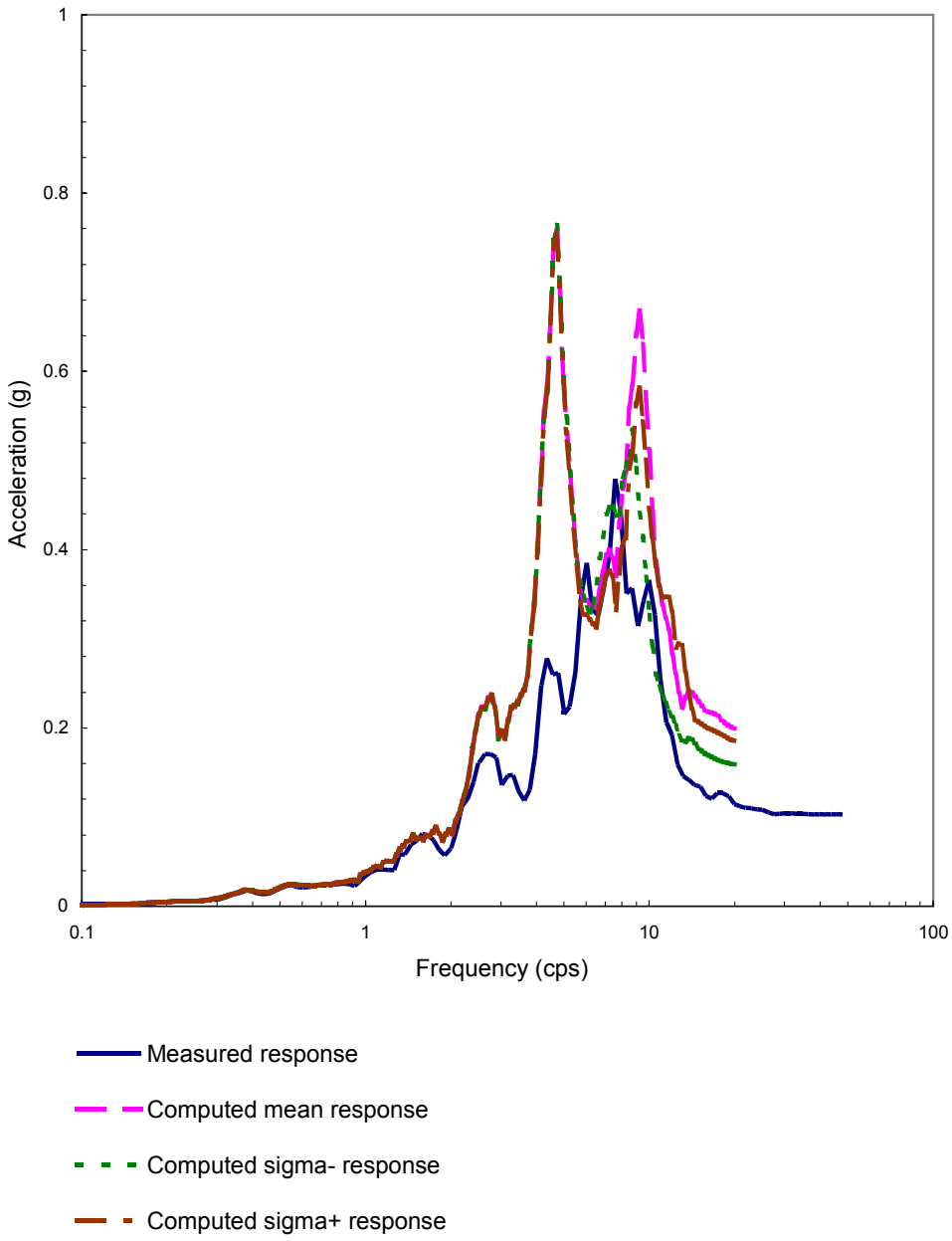

Figure 5-32. Comparison of response spectra at the roof center of the embedded single reactor building in NS direction (No.63).

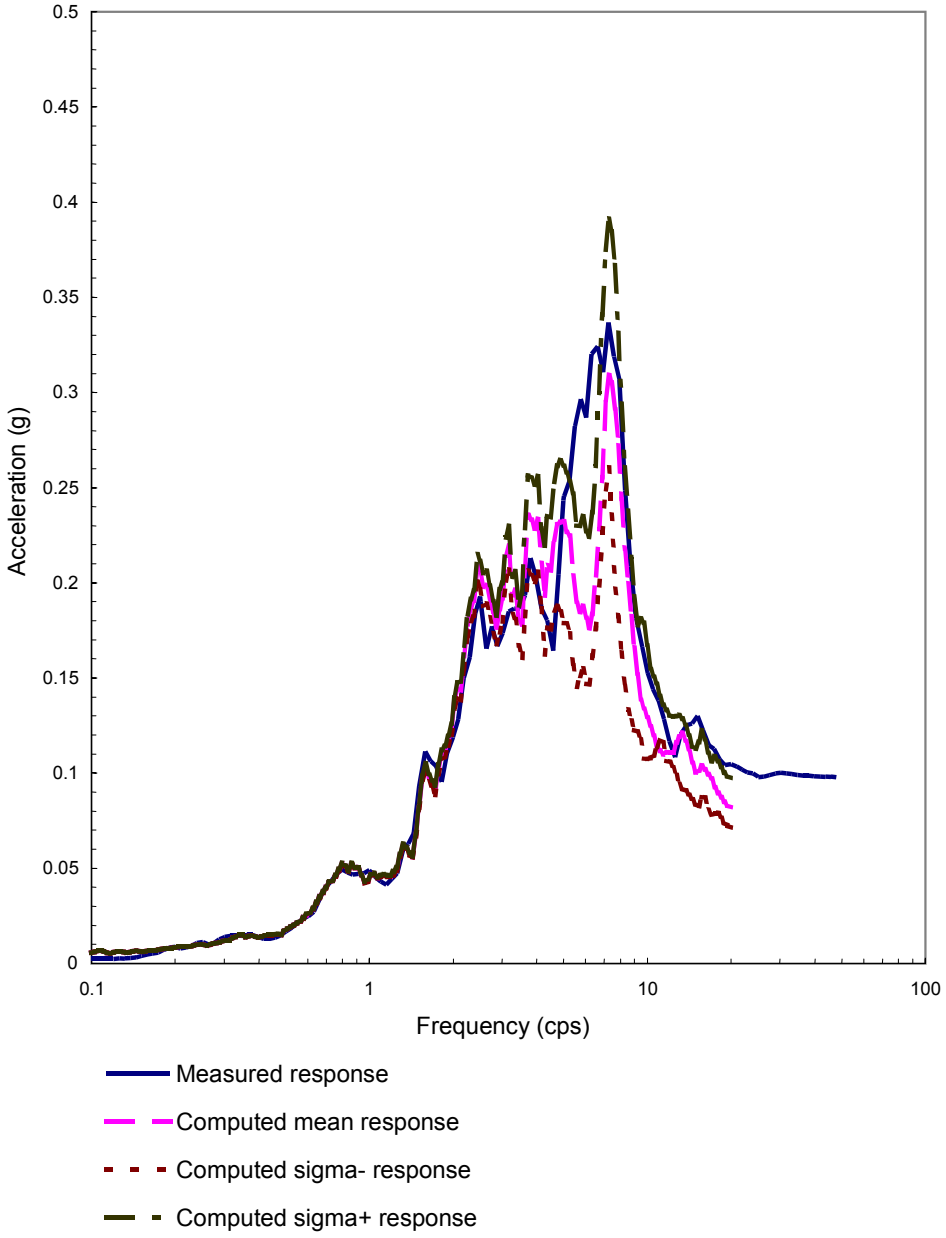

Figure 5-33. Comparison of response spectra at the basemat center of the embedded single reactor building in NS direction (No.89).

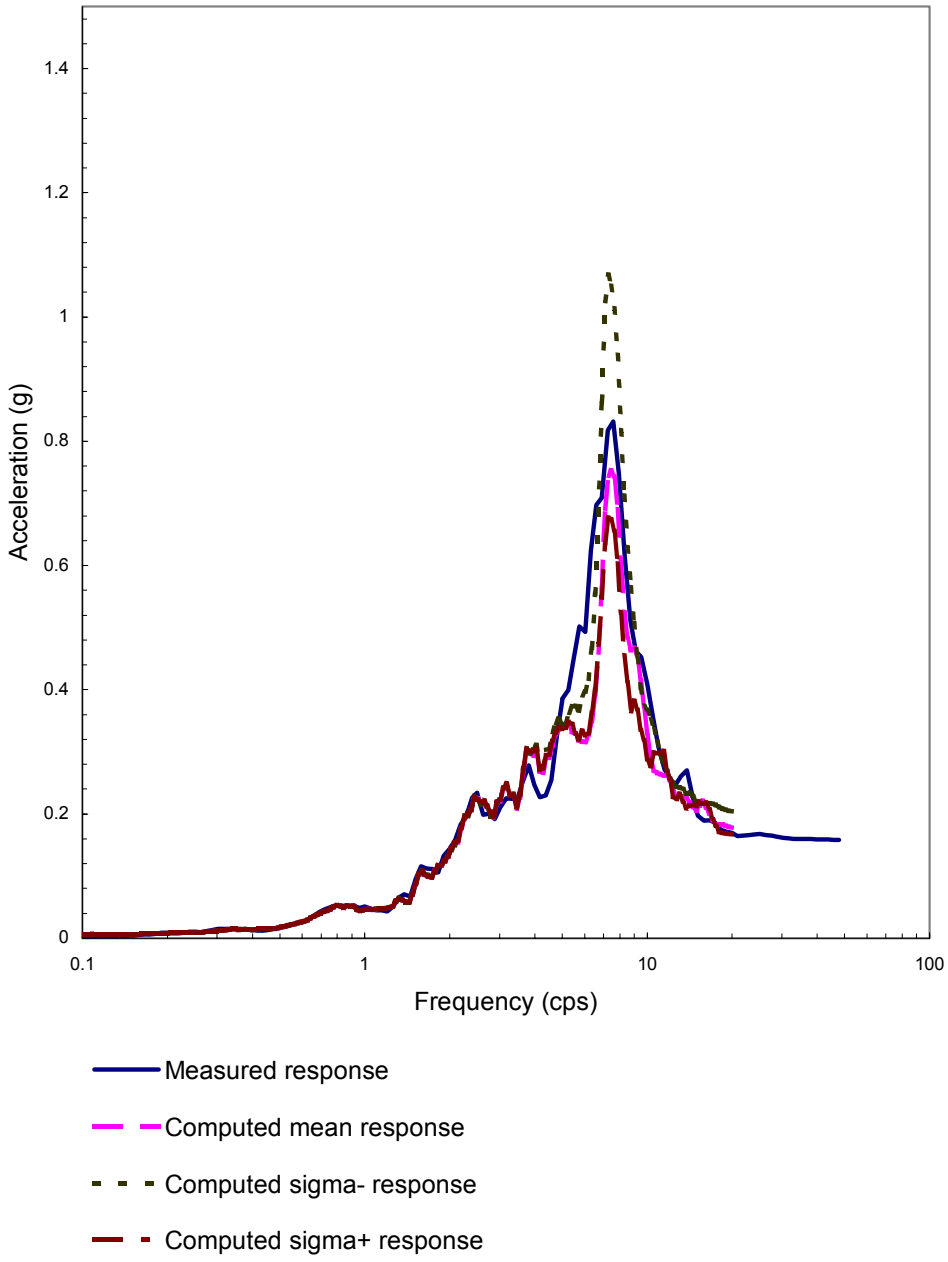

Figure 5-34. Comparison of response spectra at the roof center of the embedded single reactor building in NS direction (No.89).

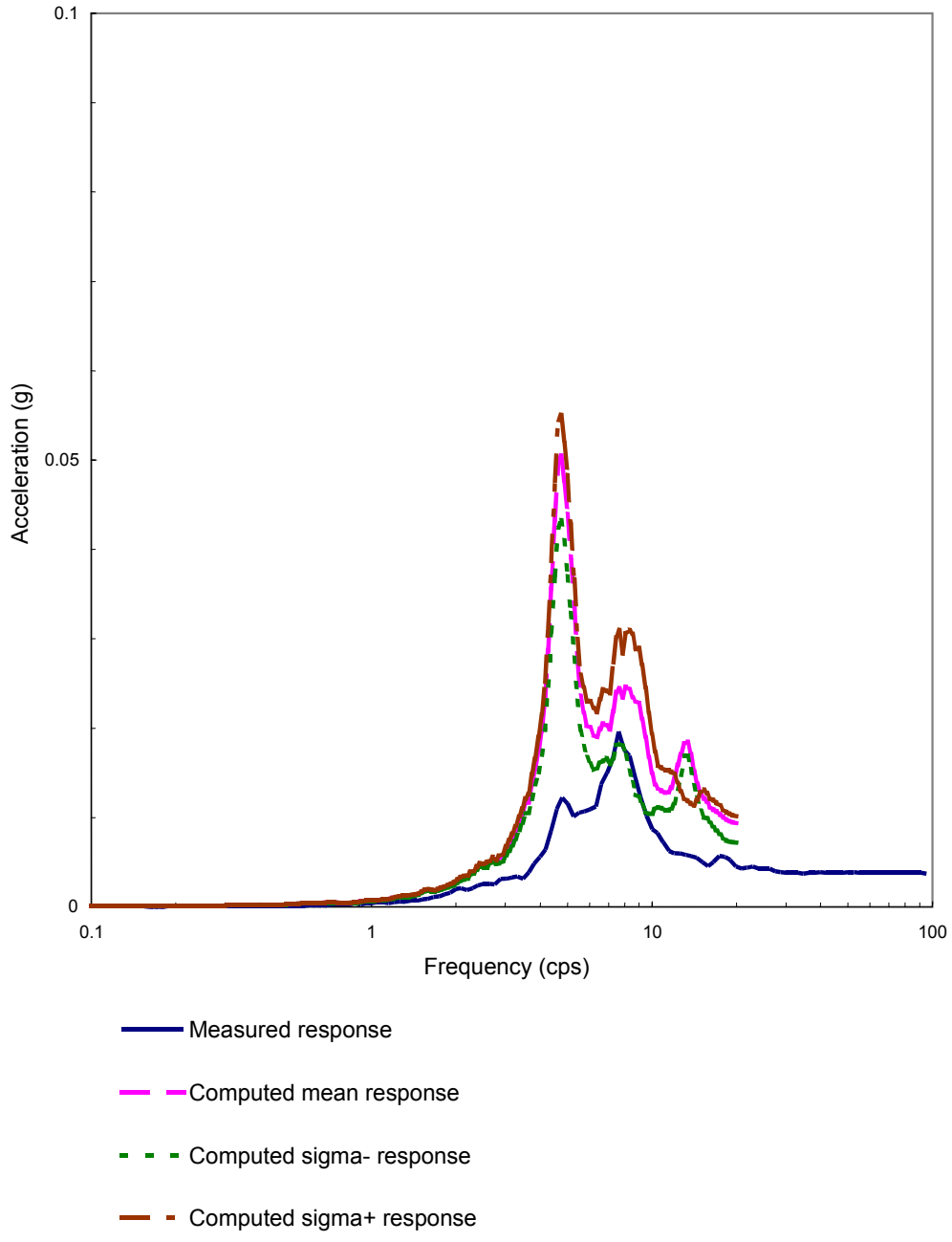

Figure 5-35. Comparison of response spectra at the basemat center of the embedded single reactor building in NS direction (No.164).

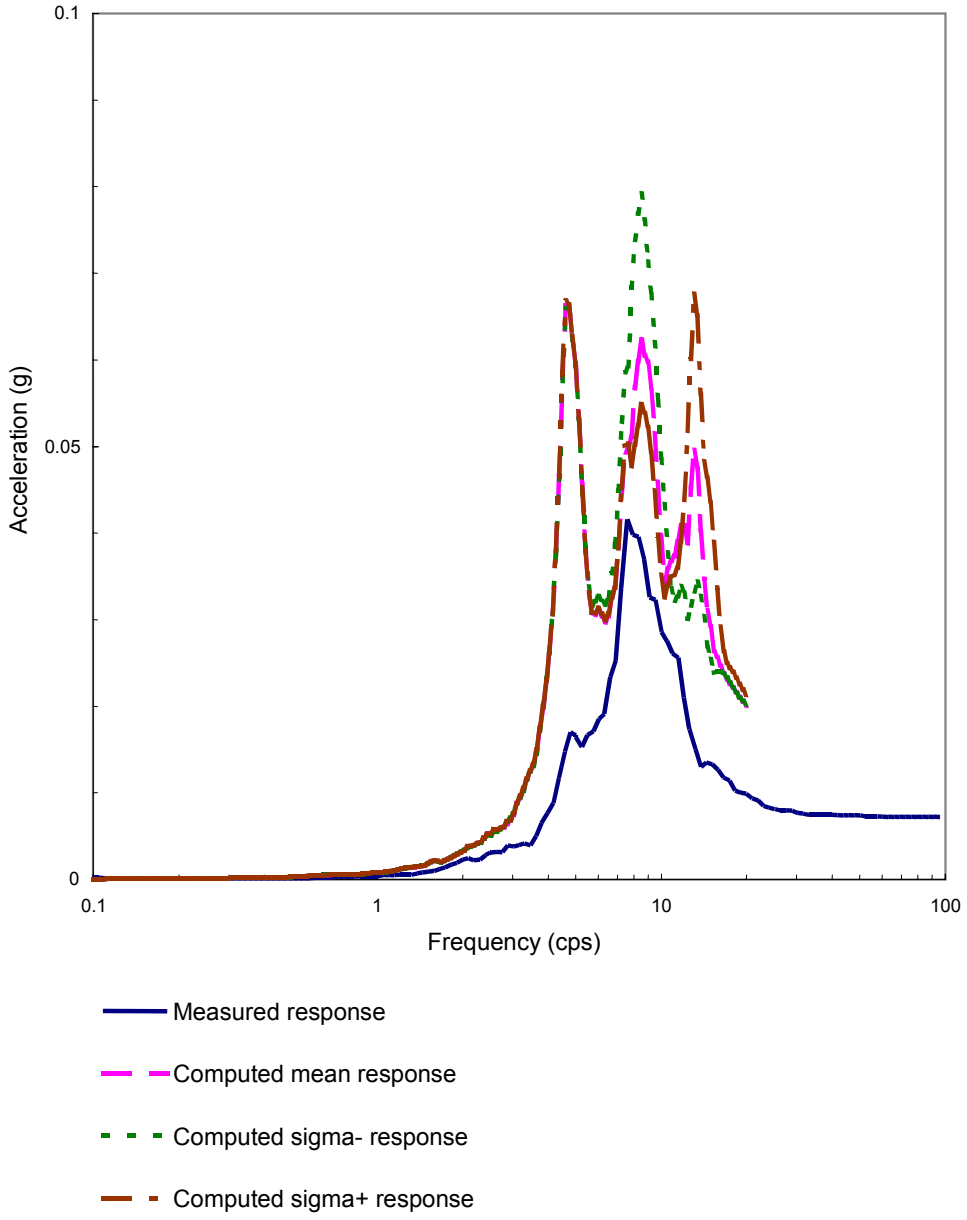

Figure 5-36. Comparison of response spectra at the roof center of the embedded single reactor building in NS direction (No.164).

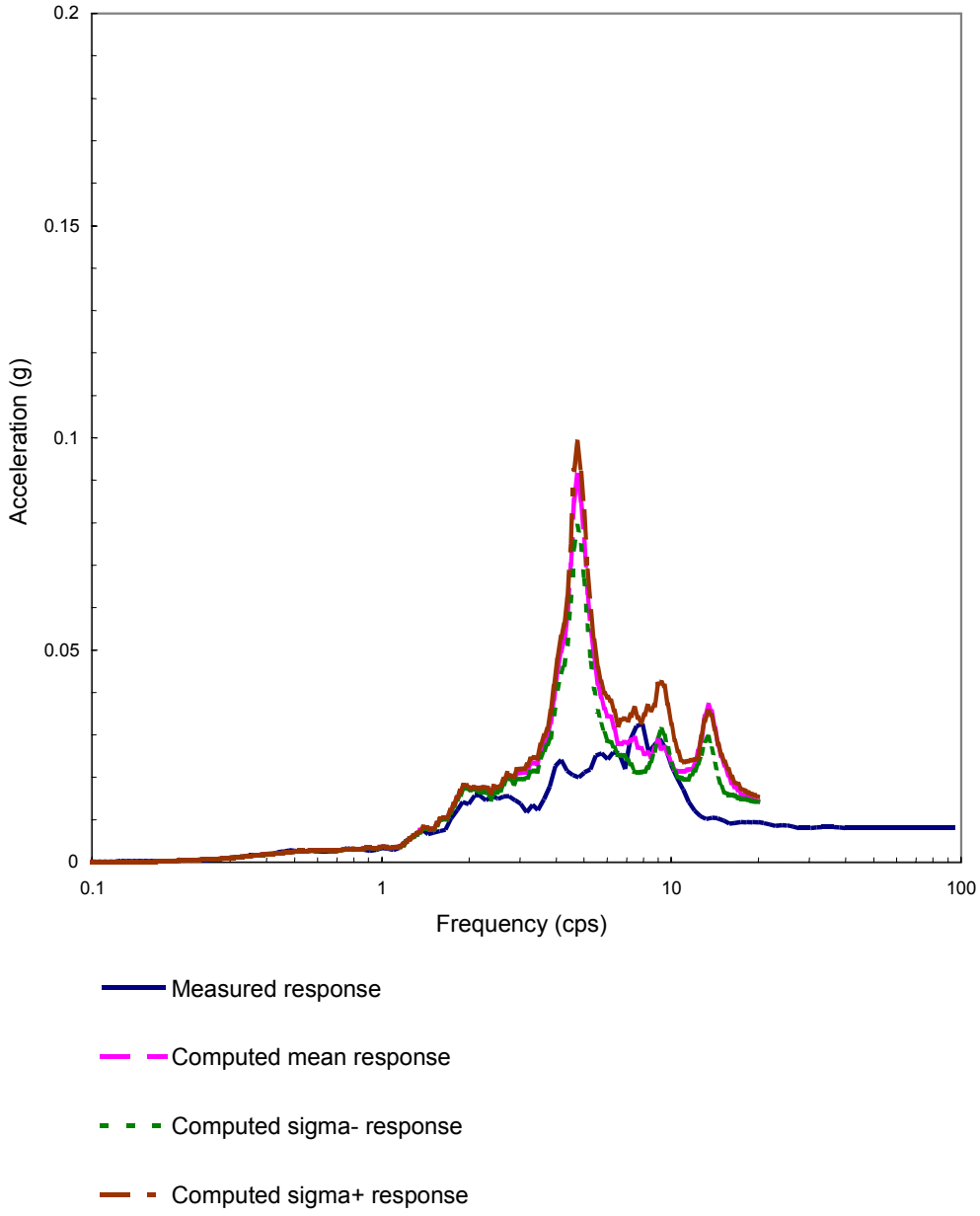

Figure 5-37. Comparison of response spectra at the basemat center of the embedded single reactor building in NS direction (No.172).

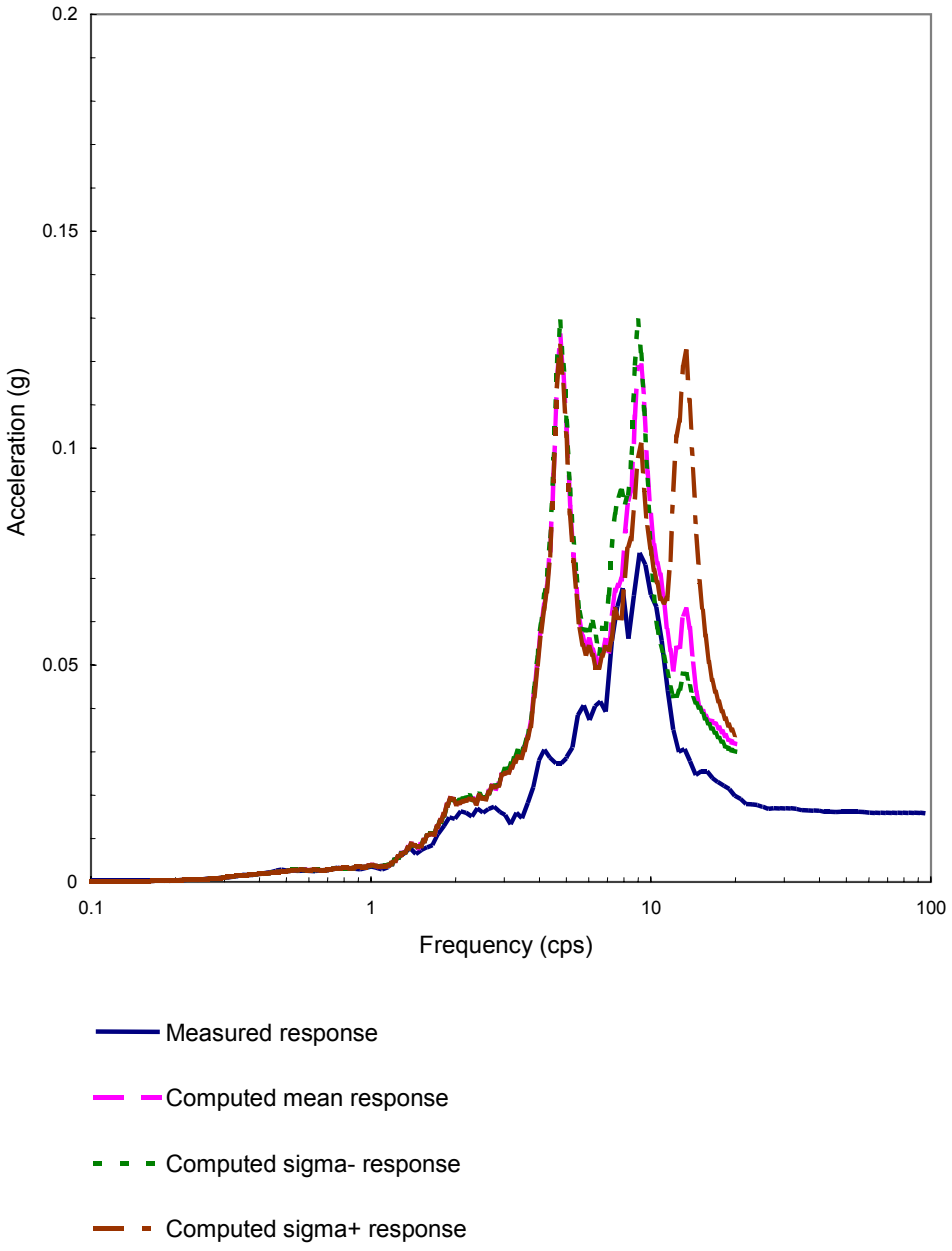

Figure 5-38. Comparison of response spectra at the roof center of the embedded single reactor building in NS direction (No.172).

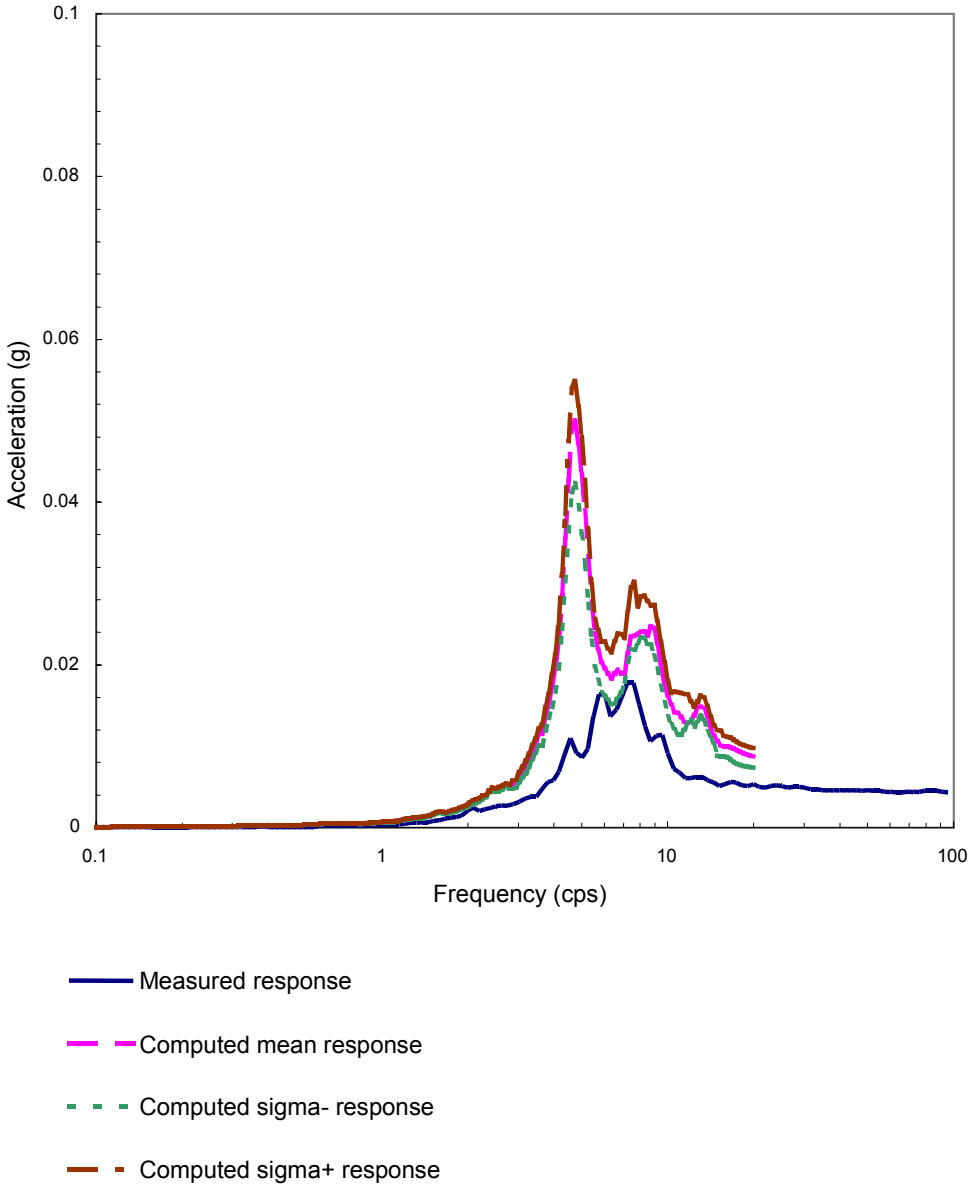

Figure 5-39. Comparison of response spectra at the basemat center of the embedded twin reactor buildings (BAS) in NS direction (No.164).

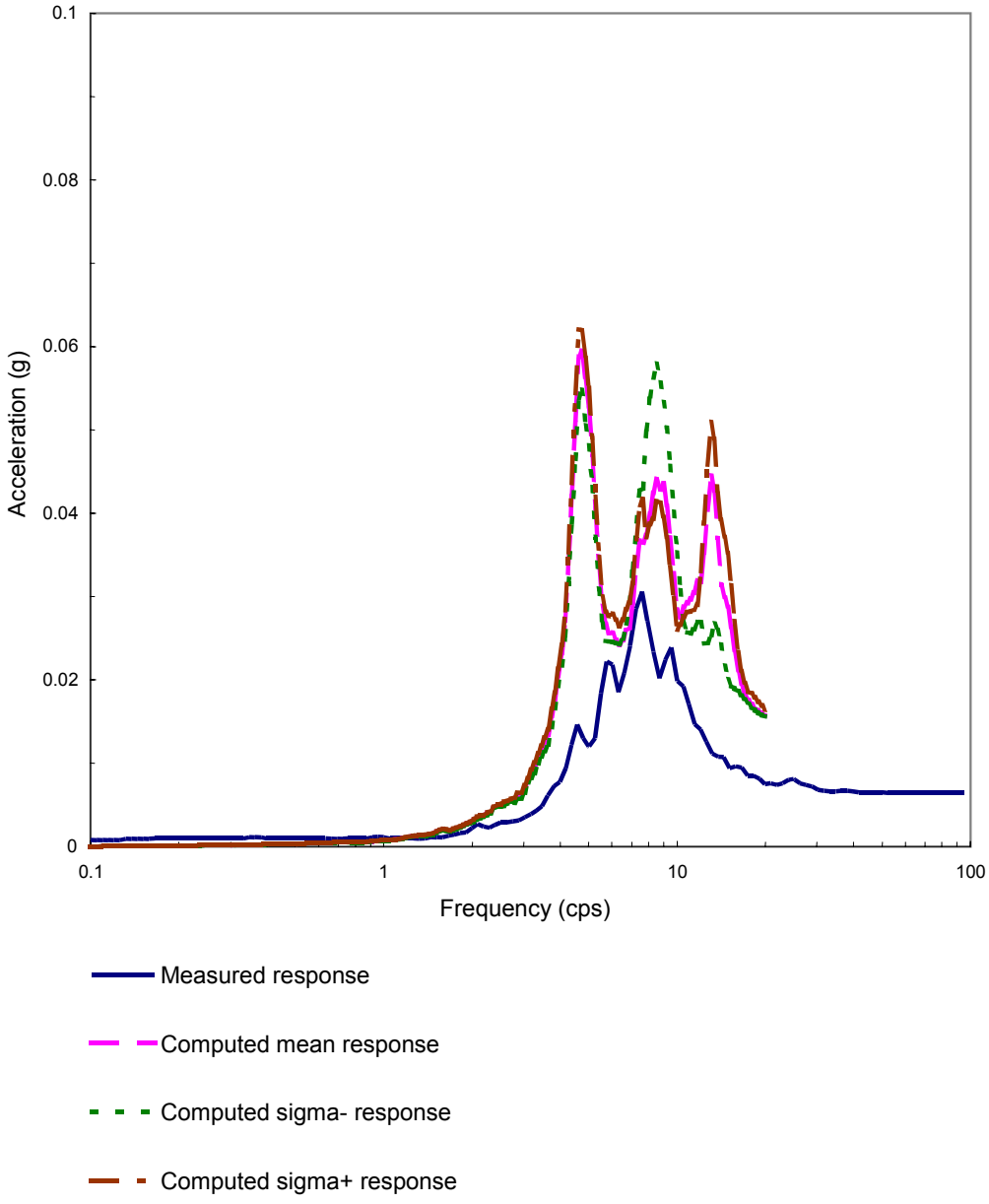

Figure 5-40. Comparison of response spectra at the roof center of the embedded twin reactor buildings (BAS) in NS direction (No.164).

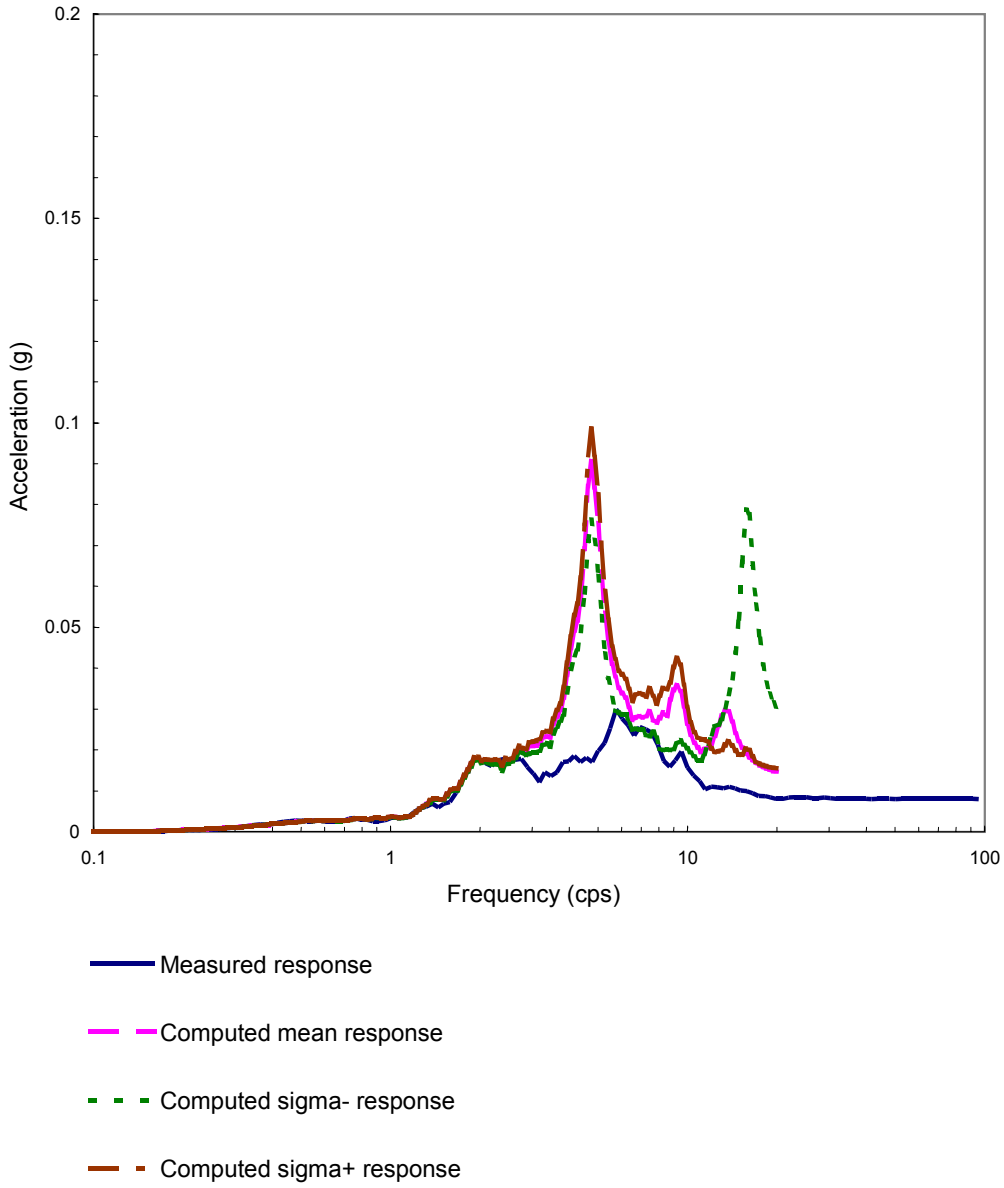

Figure 5-41. Comparison of response spectra at the basemat center of the embedded twin reactor buildings (BAS) in NS direction (No.172).

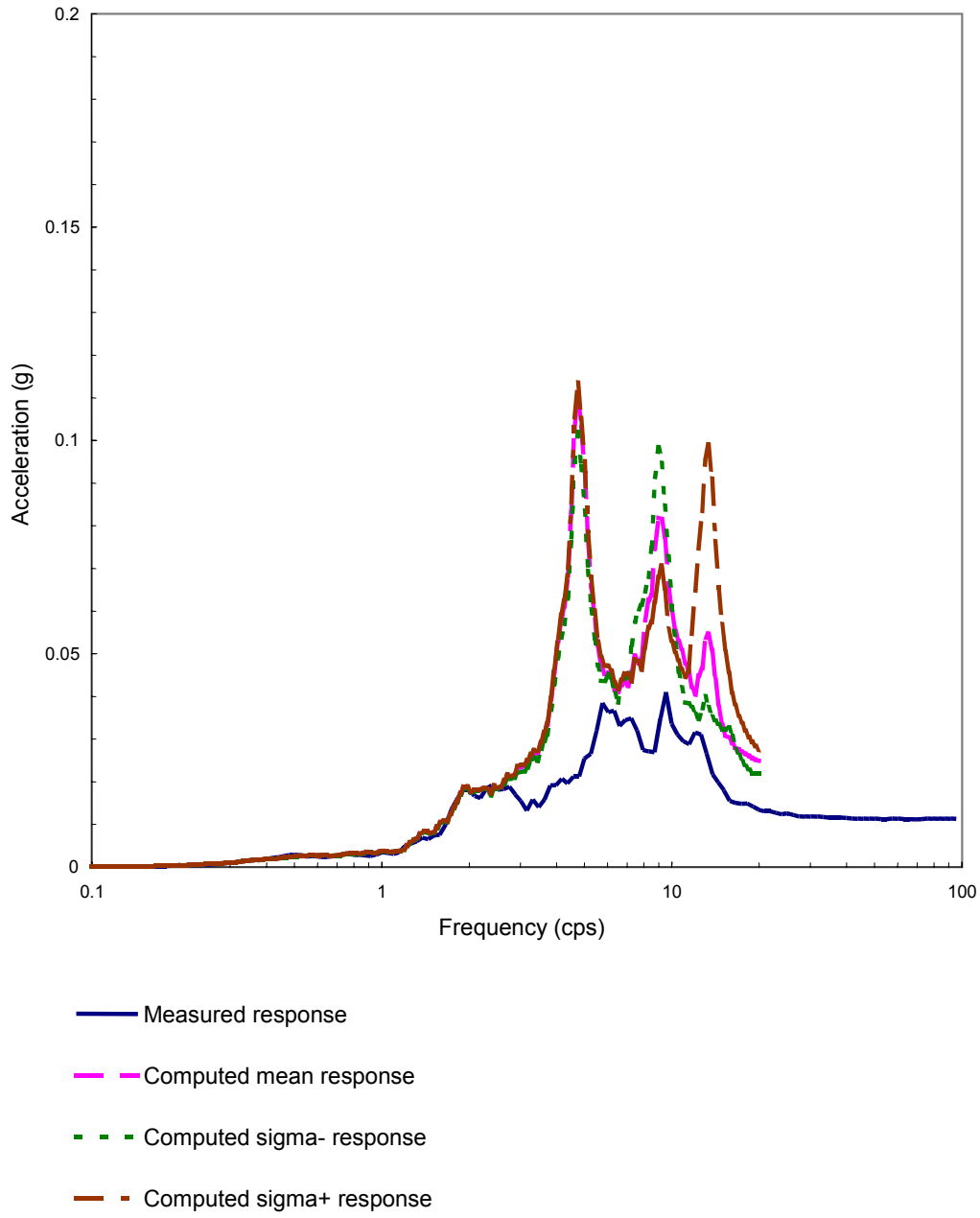

Figure 5-42. Comparison of response spectra at the roof center of the embedded twin reactor buildings (BAS) in NS direction (No.172).

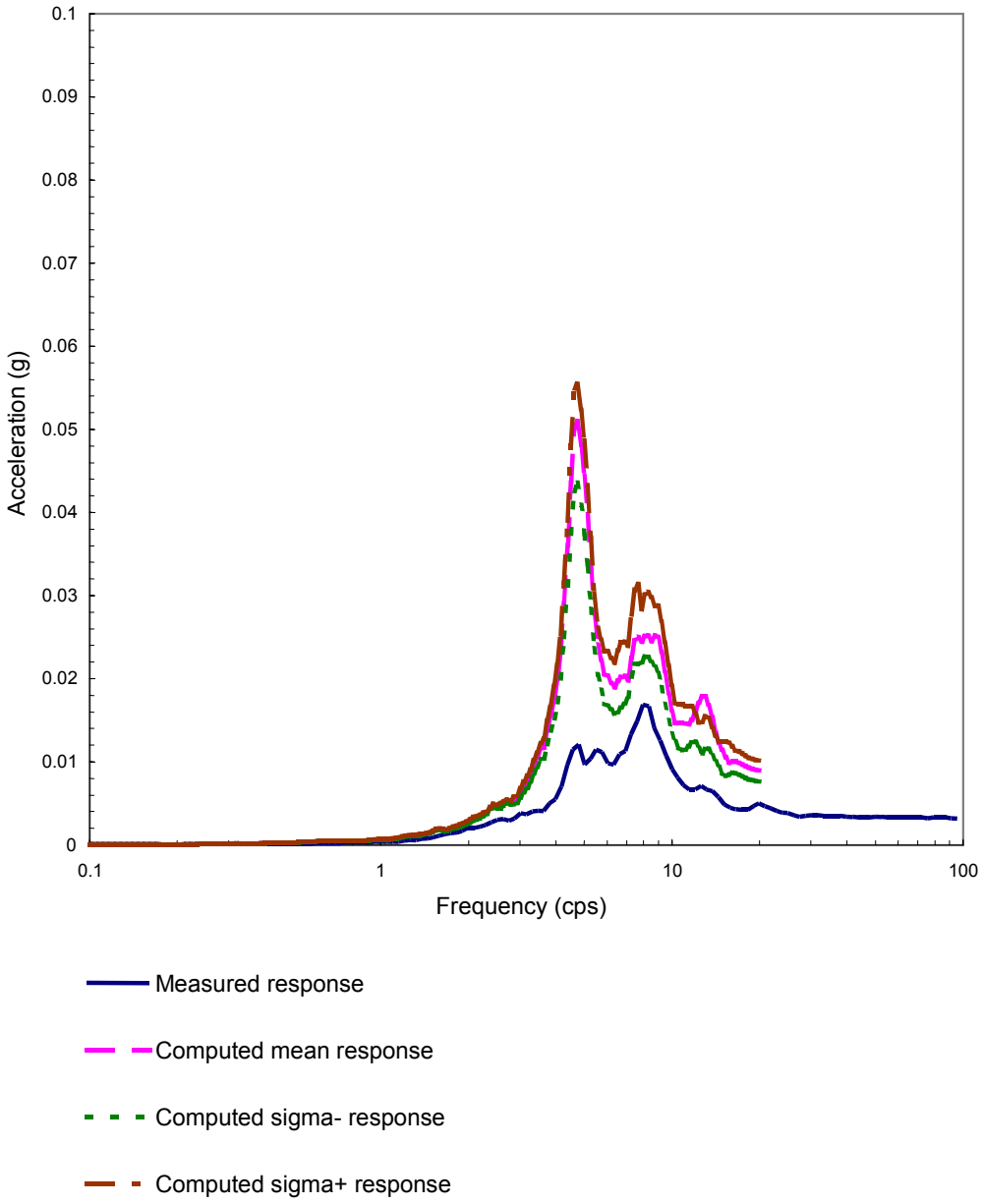

Figure 5-43. Comparison of response spectra at the basemat of DA of the embedded reactor-turbine buildings in NS direction (No.164).

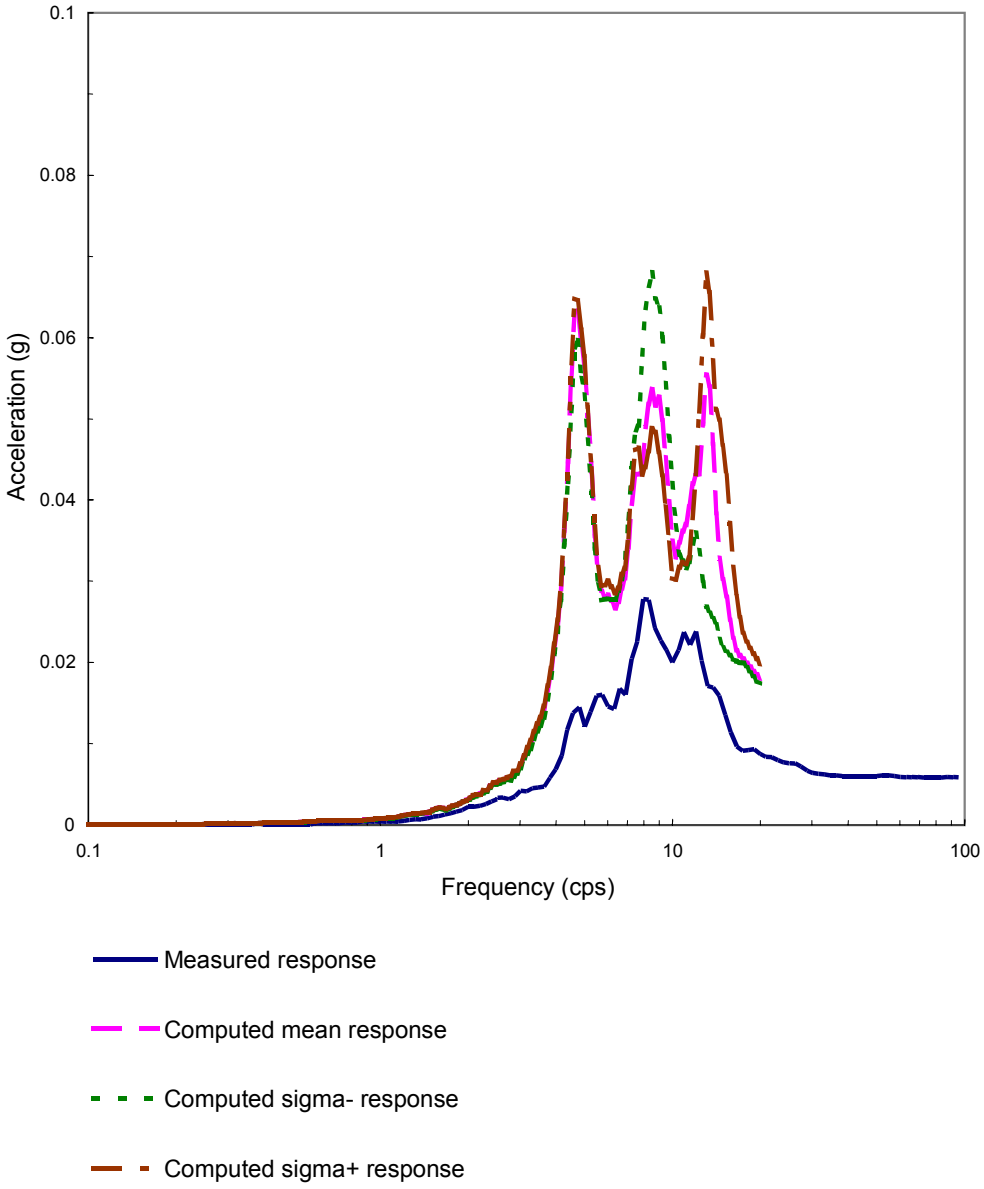

Figure 5-44. Comparison of response spectra at the roof center of DA of the embedded reactor-turbine buildings in NS direction (No.164).

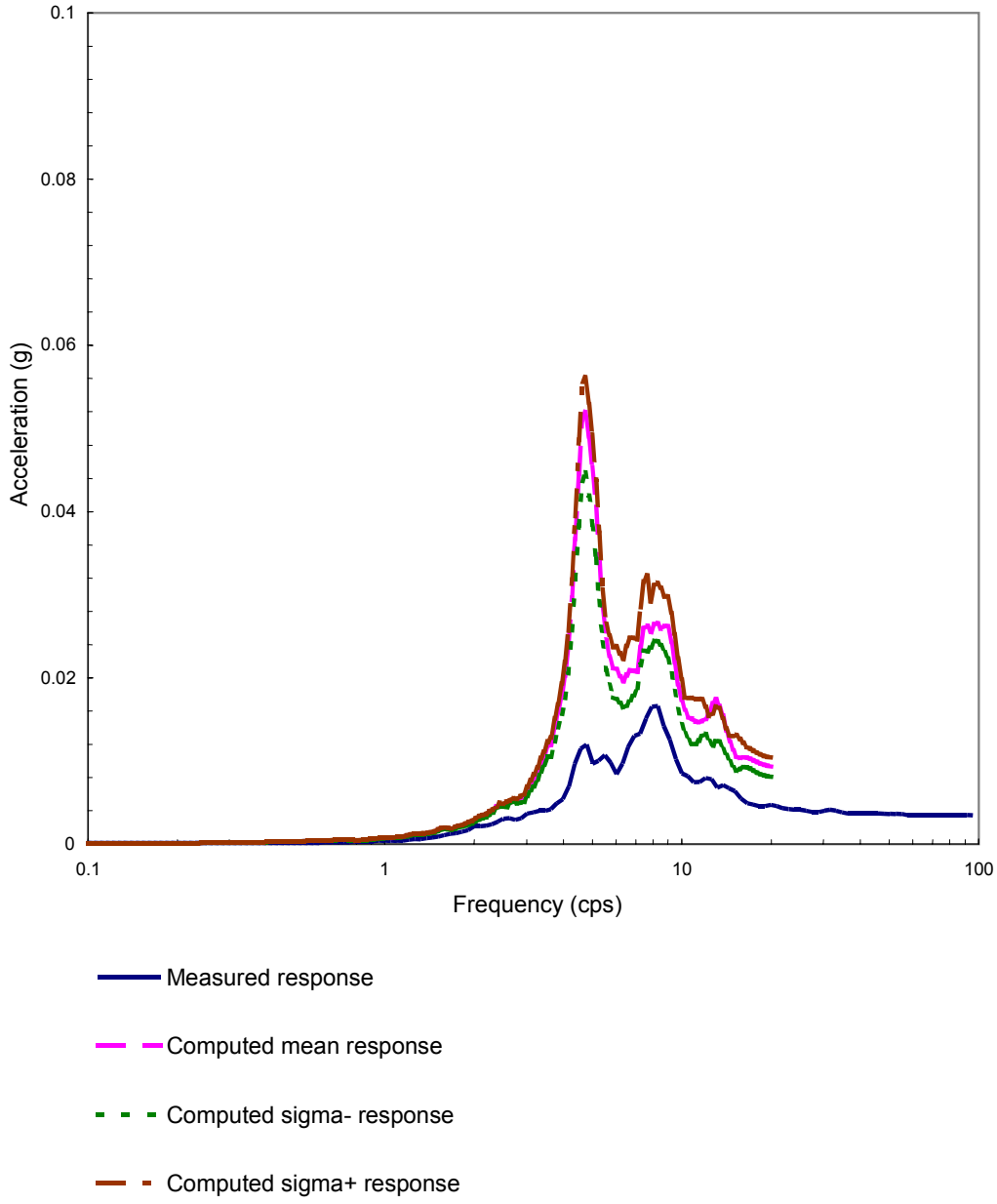

Figure 5-45. Comparison of response spectra at the basemat of DF of the embedded reactor-turbine buildings in NS direction (No.164).

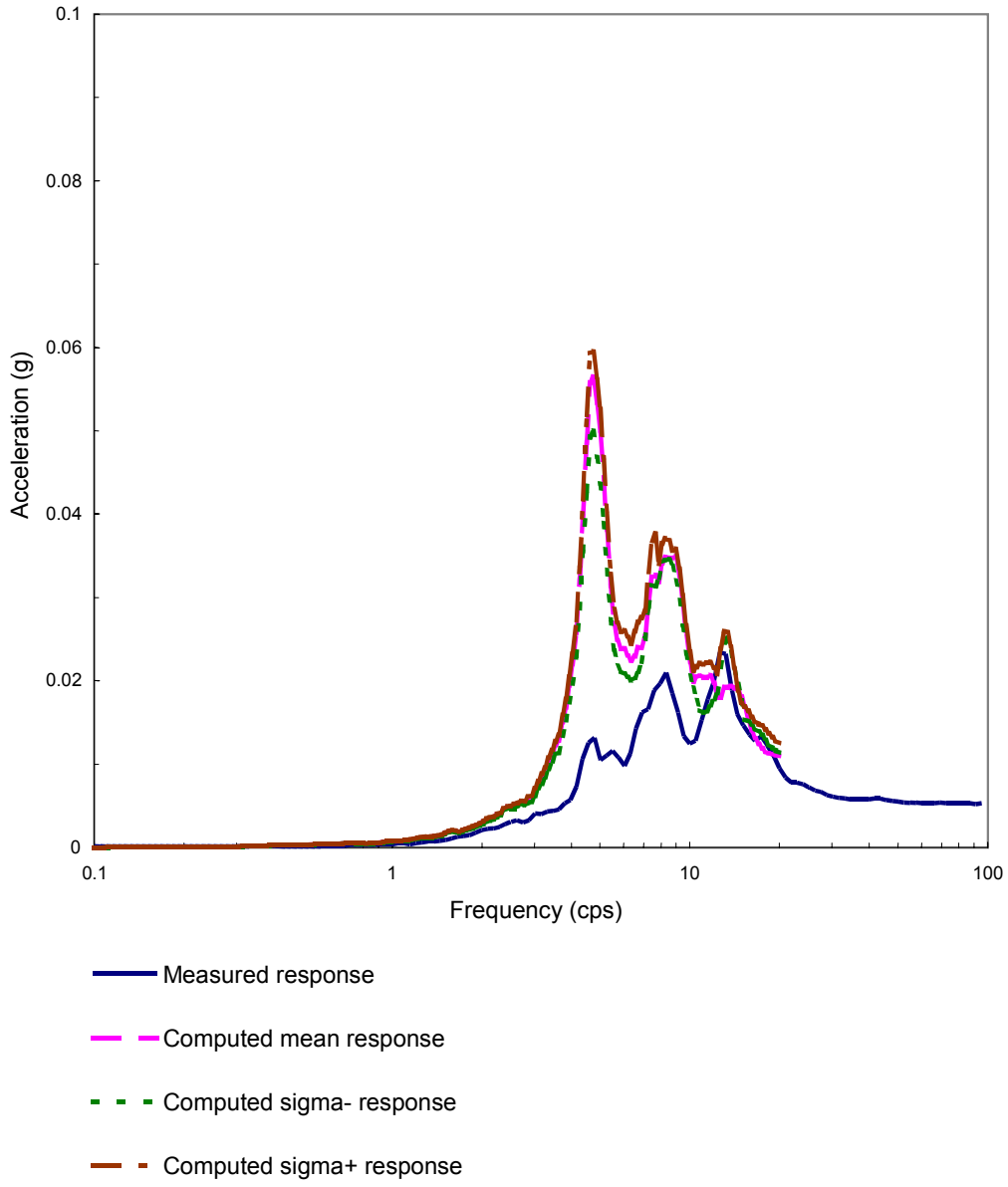

Figure 5-46. Comparison of response spectra at the roof center of DF of the embedded reactor-turbine buildings in NS direction (No.164).

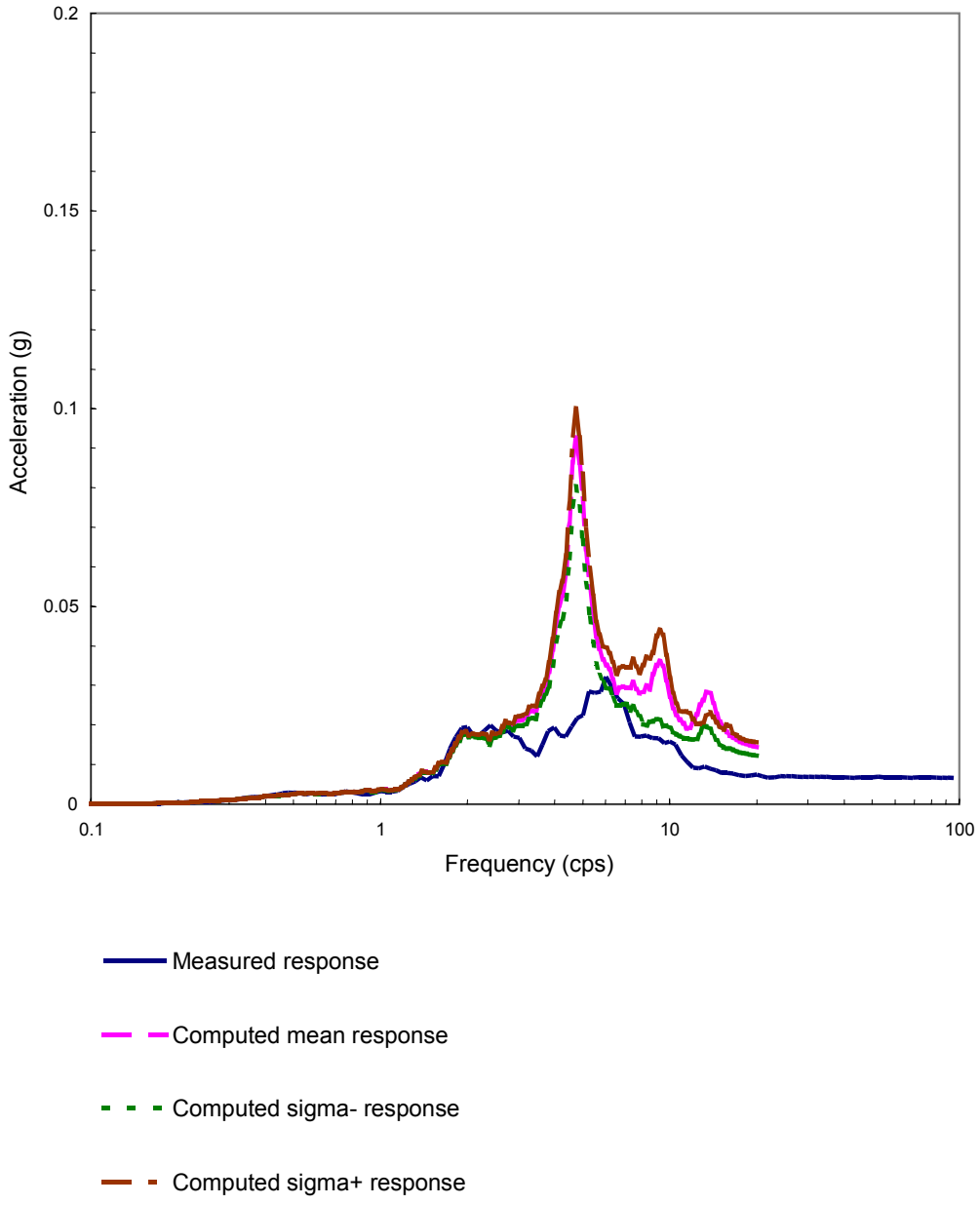

Figure 5-47. Comparison of response spectra at the basemat of DA of the embedded reactor-turbine buildings in NS direction (No.172).

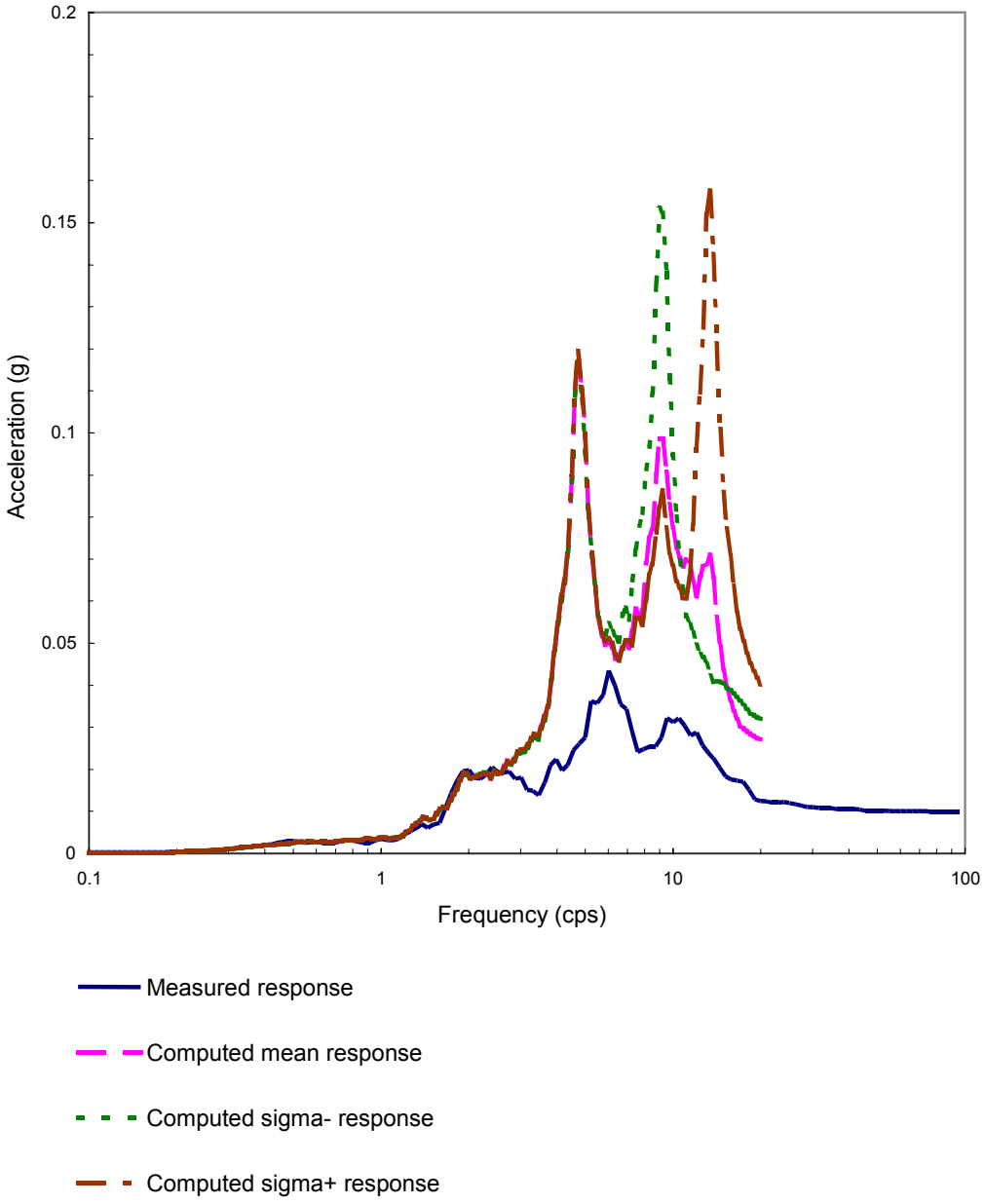

Figure 5-48. Comparison of response spectra at the roof center of DA of the embedded reactor-turbine buildings in NS direction (No.172).

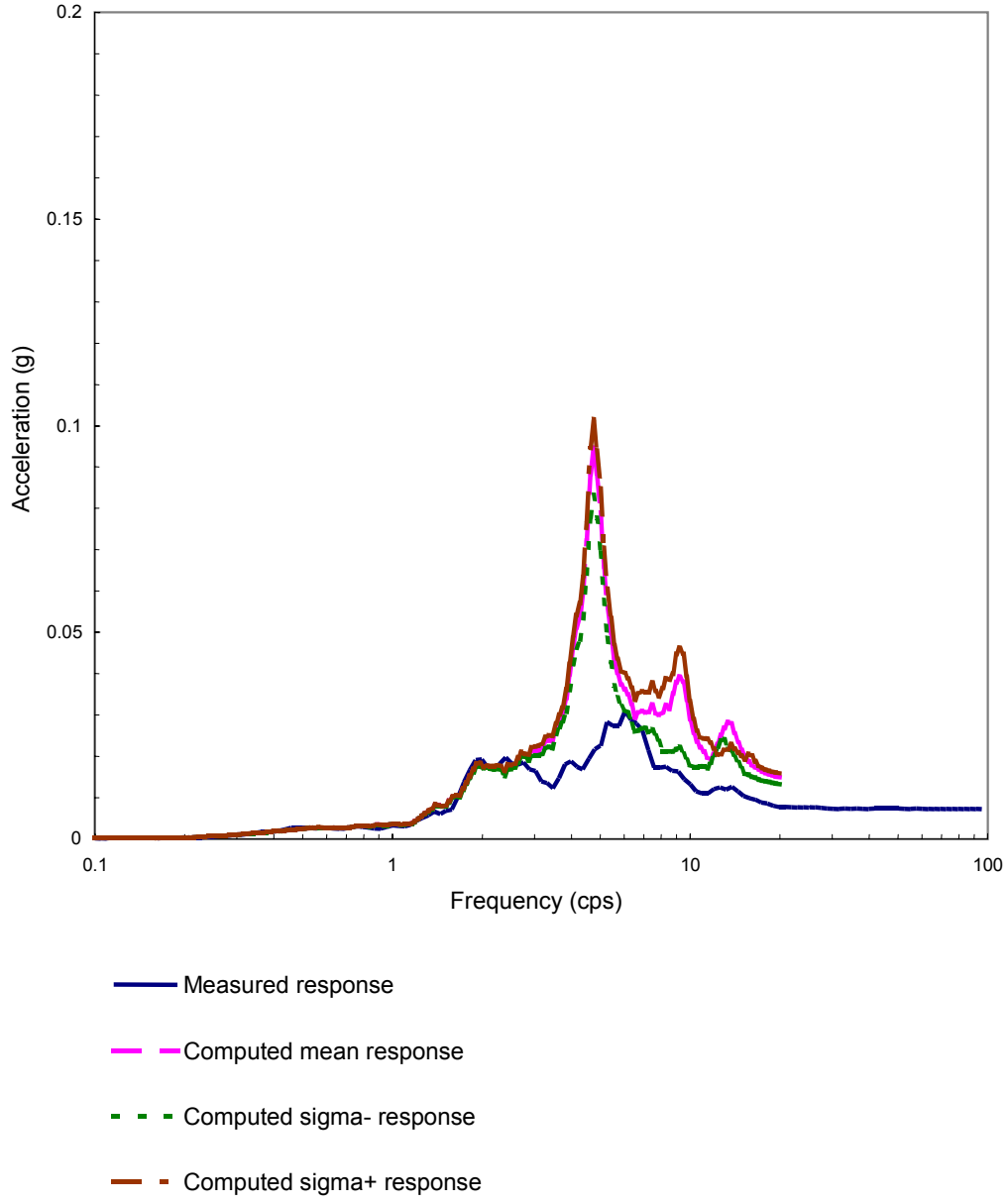

Figure 5-49. Comparison of response spectra at the basemat of DF of the embedded reactor-turbine buildings in NS direction (No.172).

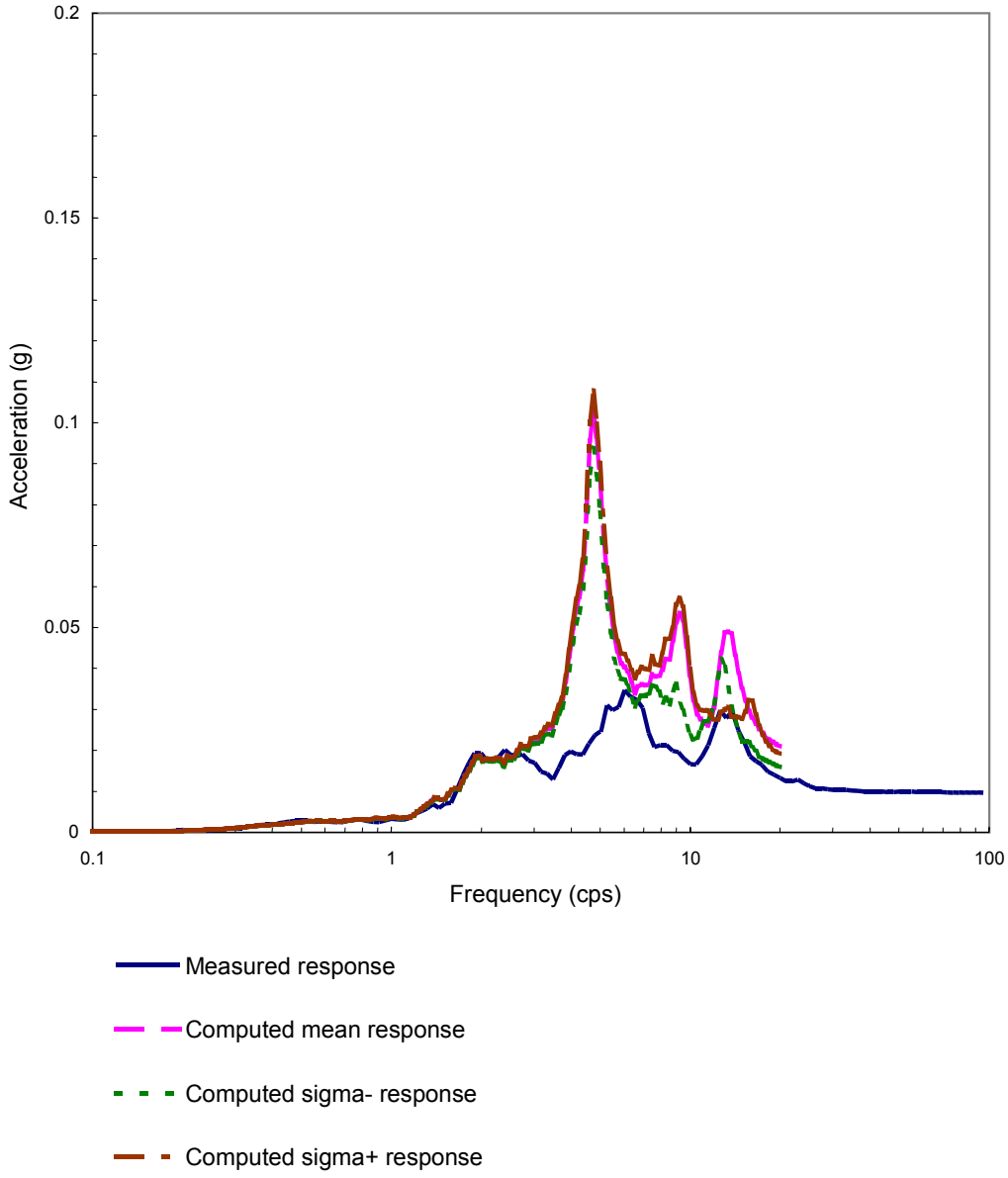

Figure 5-50. Comparison of response spectra at the roof center of DF of the embedded reactor-turbine buildings in NS direction (No.172).

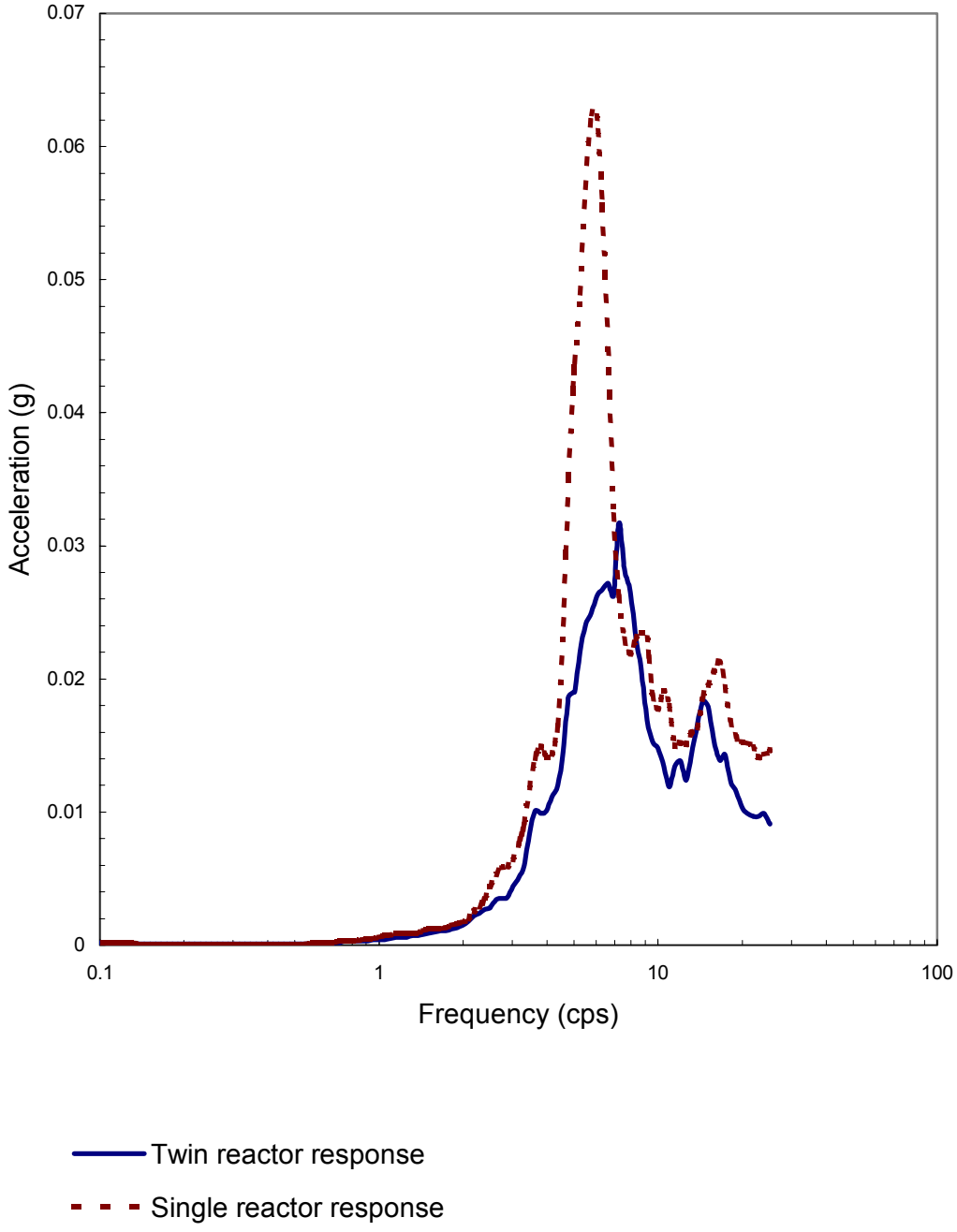

Figure. 5-51 Comparison of the recorded response spectra at the basemat of excavated reactor buildings in NS direction (No.131).

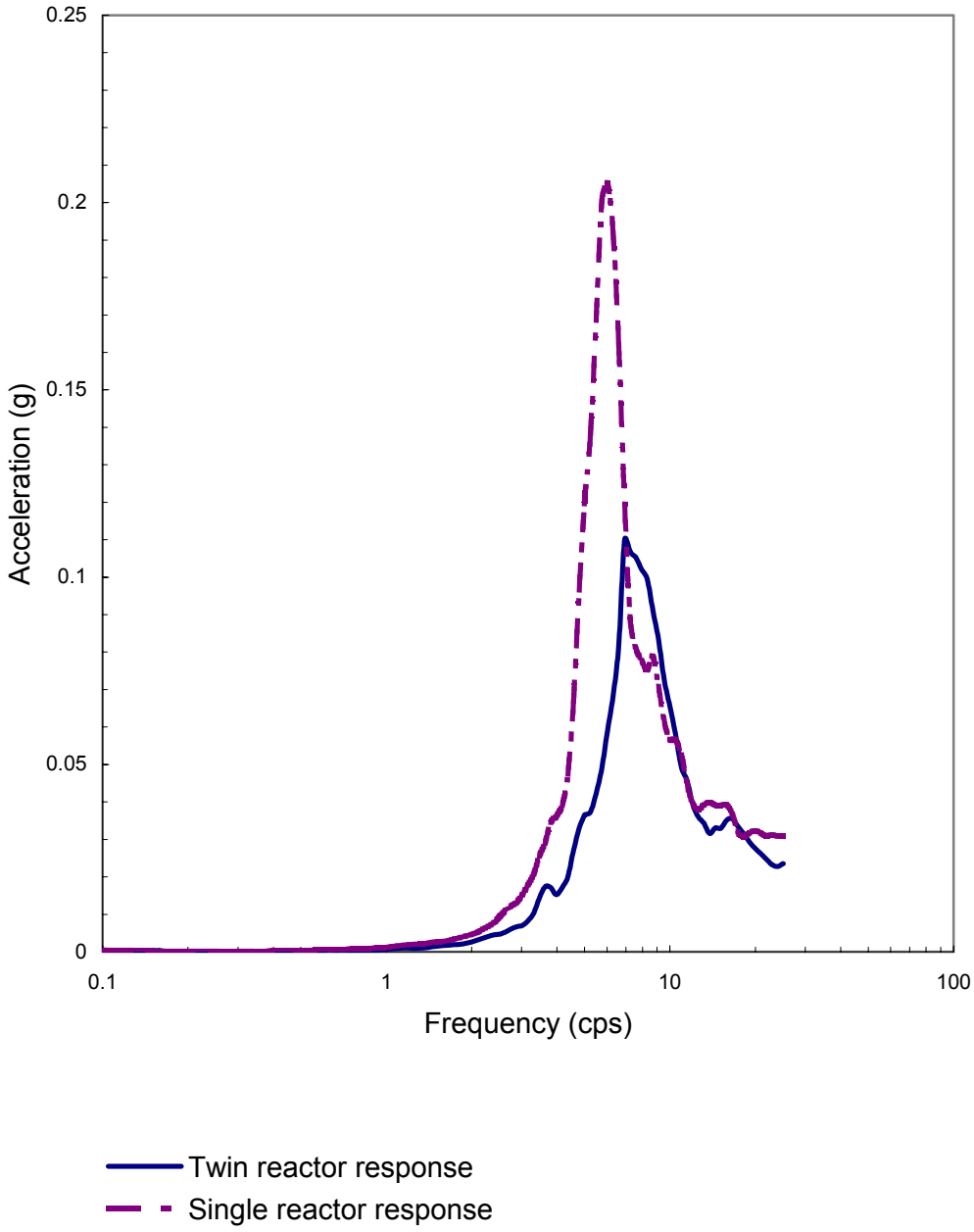

Figure. 5-52 Comparison of the recorded response spectra at the roof of excavated reactor buildings in NS direction (No.131).

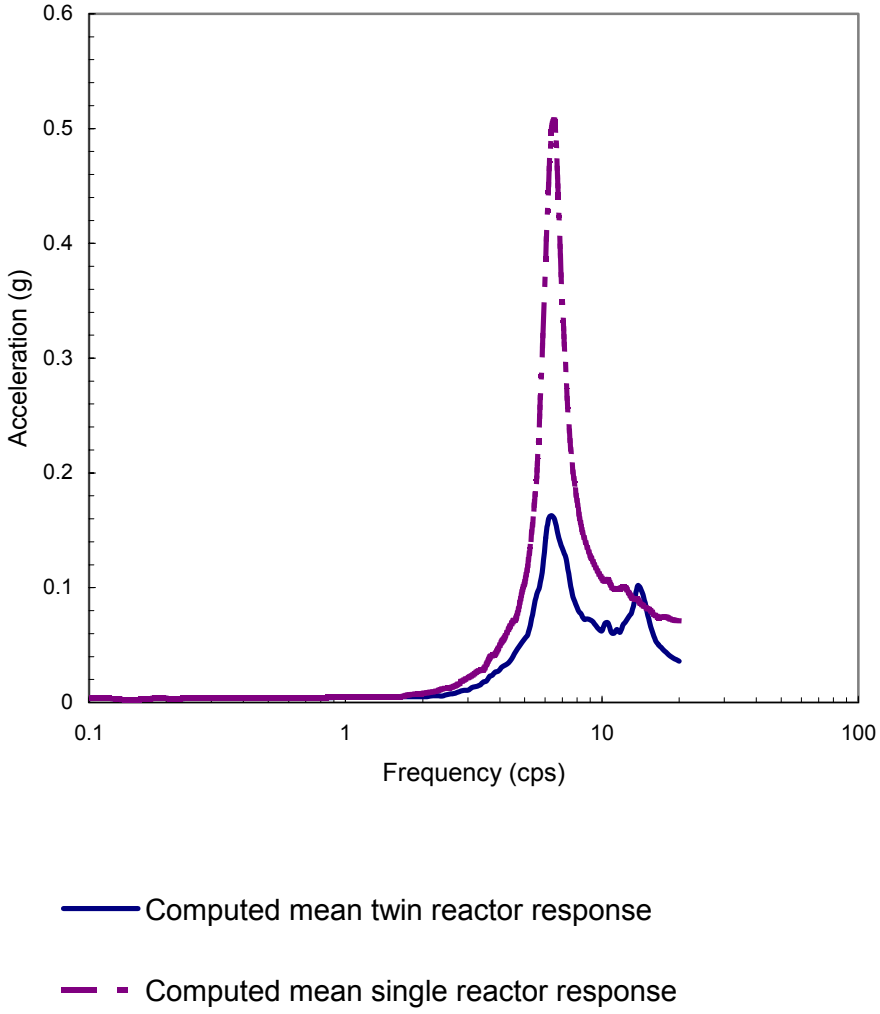

Figure. 5-53 Comparison of the predicted response spectra at the basemat of excavated reactor buildings in NS direction (No.131).

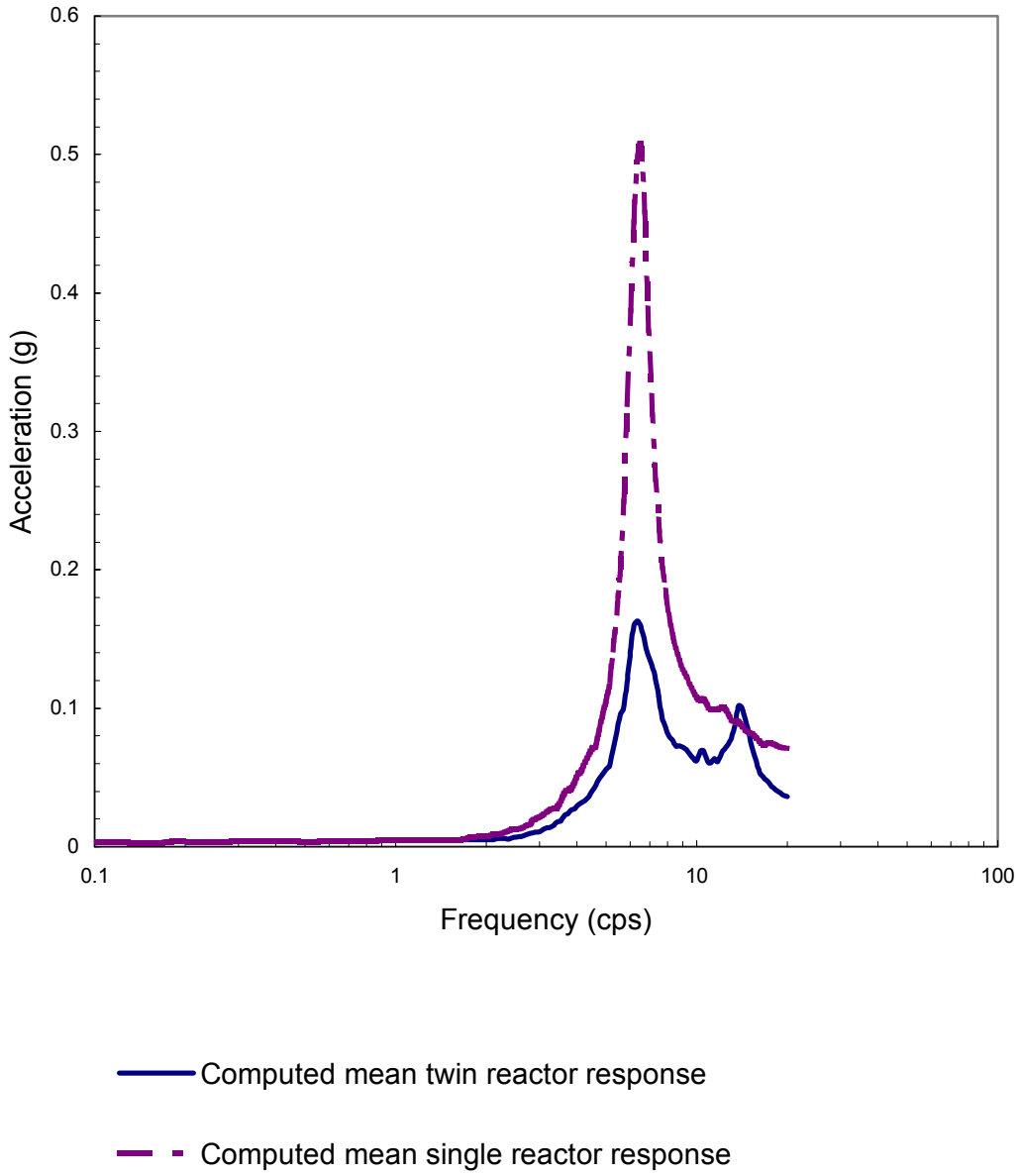

Figure. 5-54 Comparison of the predicted response spectra at the roof of excavated reactor buildings in NS direction (No.131).

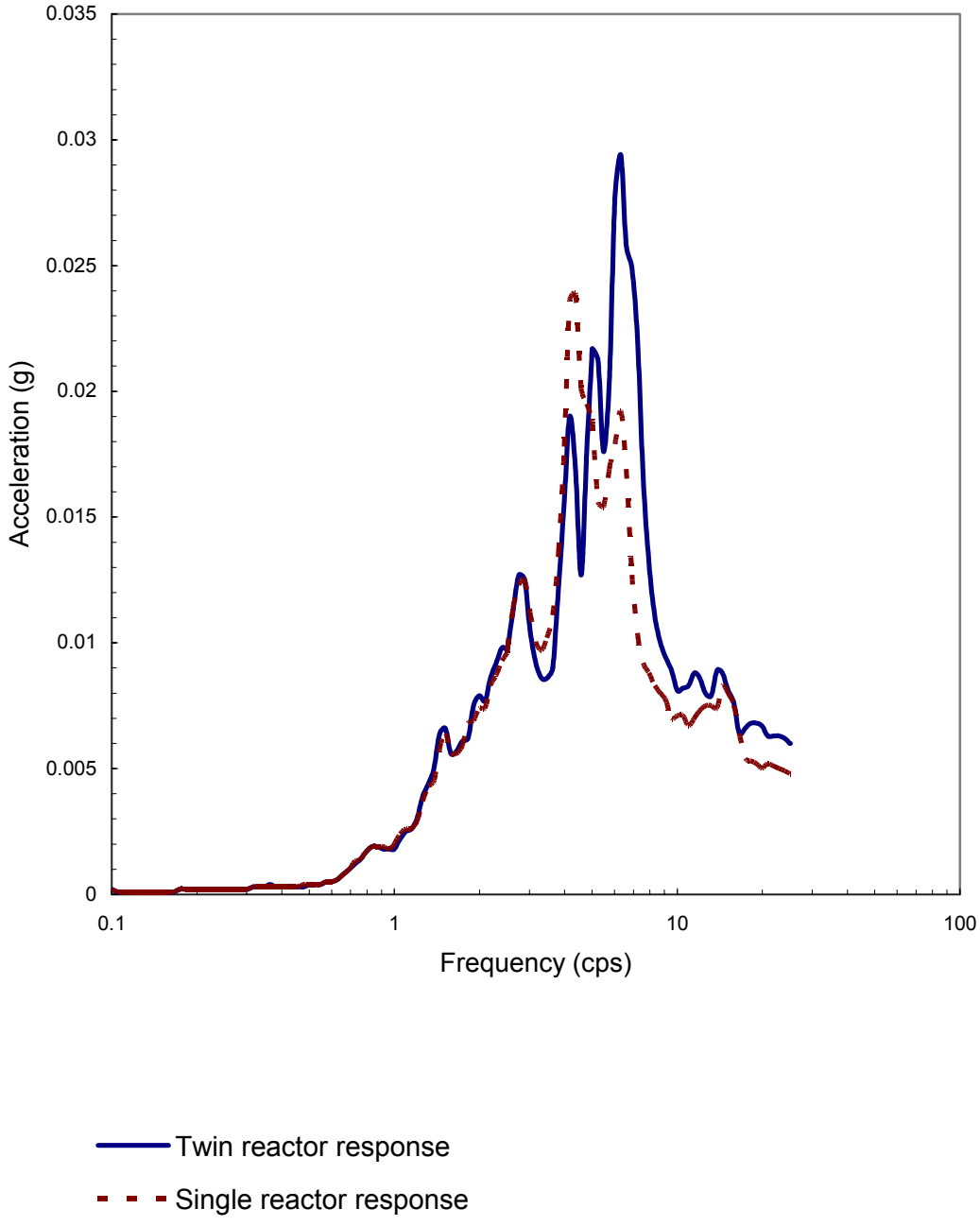

Figure. 5-55 Comparison of the recorded response spectra at the basemat of excavated reactor buildings in NS direction (No.139).

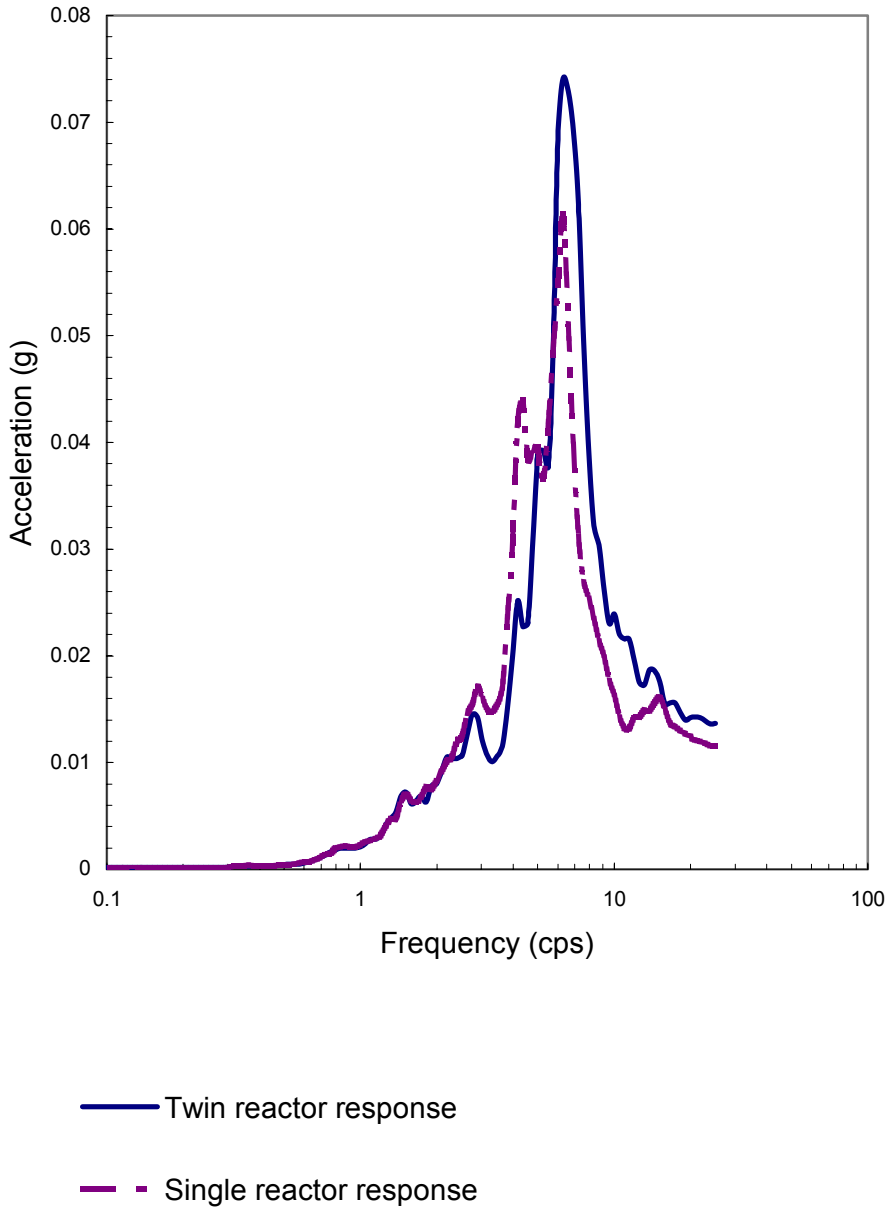

Figure. 5-56 Comparison of the recorded response spectra at the roof of excavated reactor buildings in NS direction (No.139).

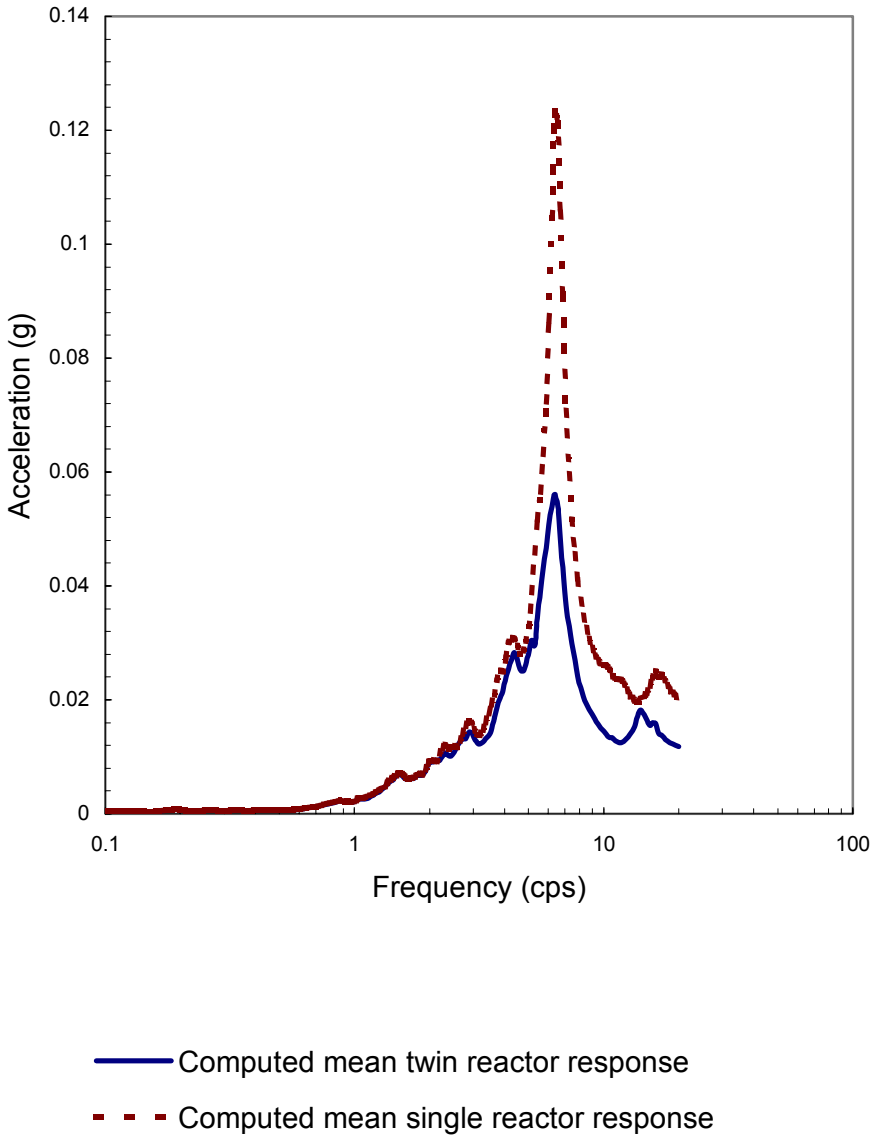

Figure. 5-57 Comparison of the predicted response spectra at the basemat of excavated reactor buildings in NS direction (No.139).

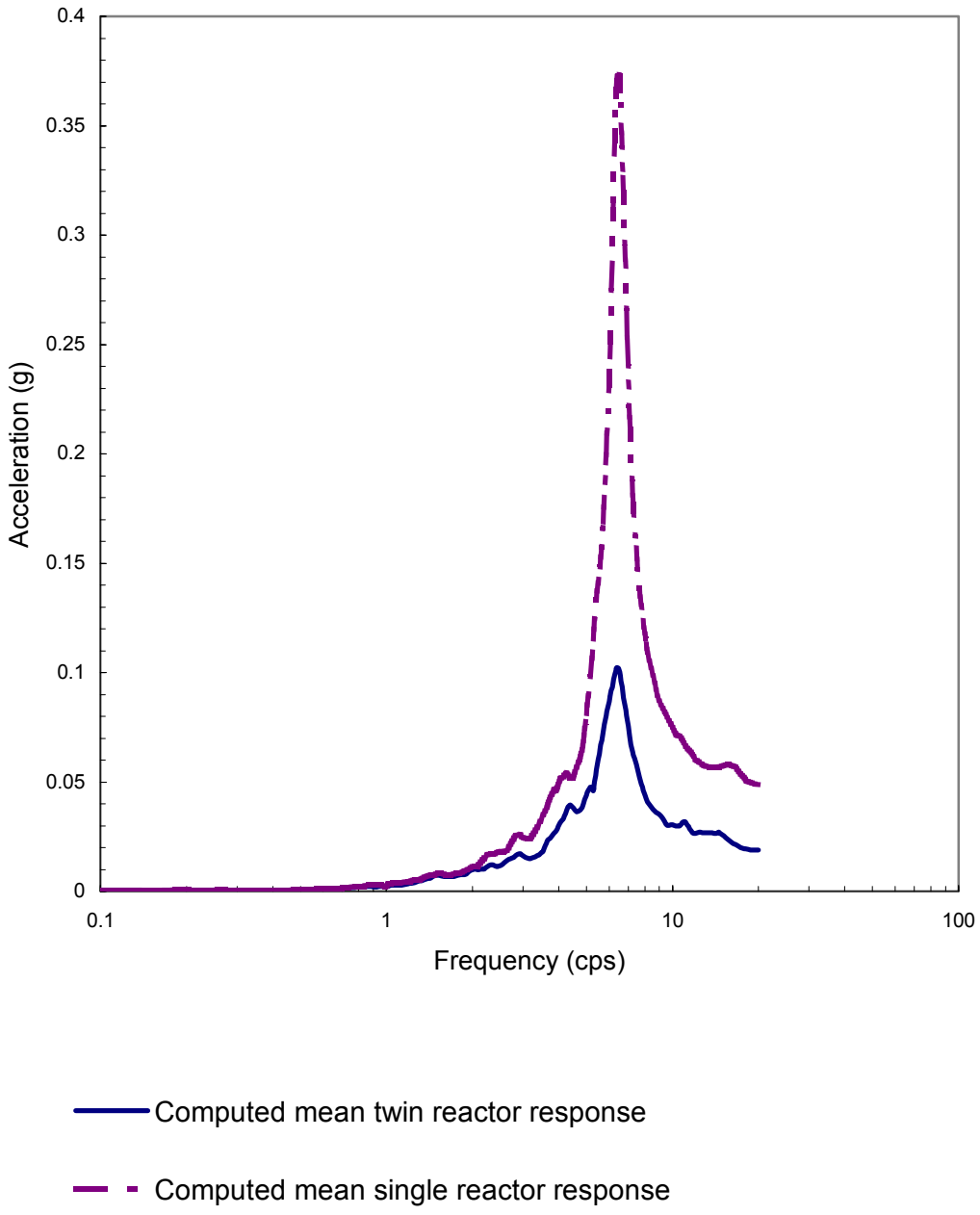

Figure. 5-58 Comparison of the predicted response spectra at the roof of excavated reactor buildings in NS direction (No.139).

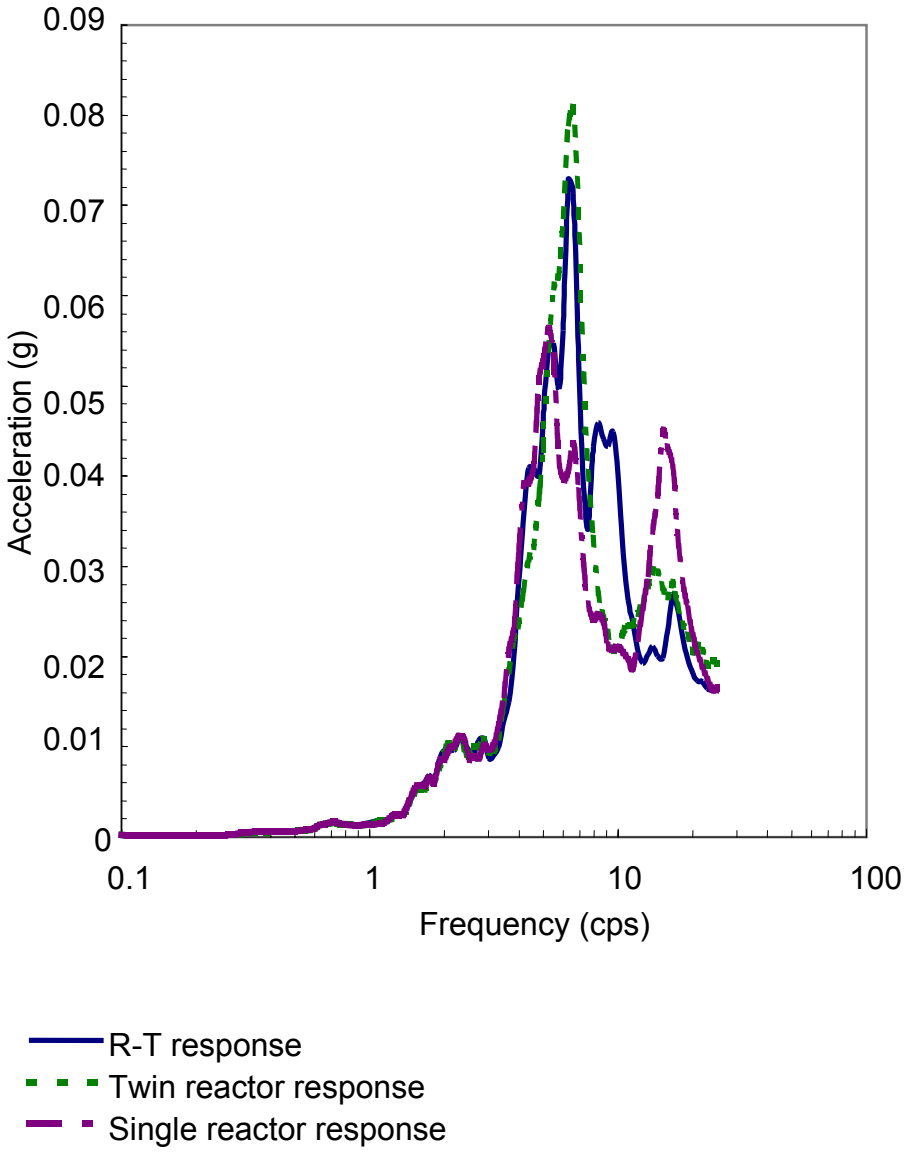

Figure. 5-59 Comparison of the recorded response spectra at the basemat of excavated reactor buildings in NS direction (No.157).

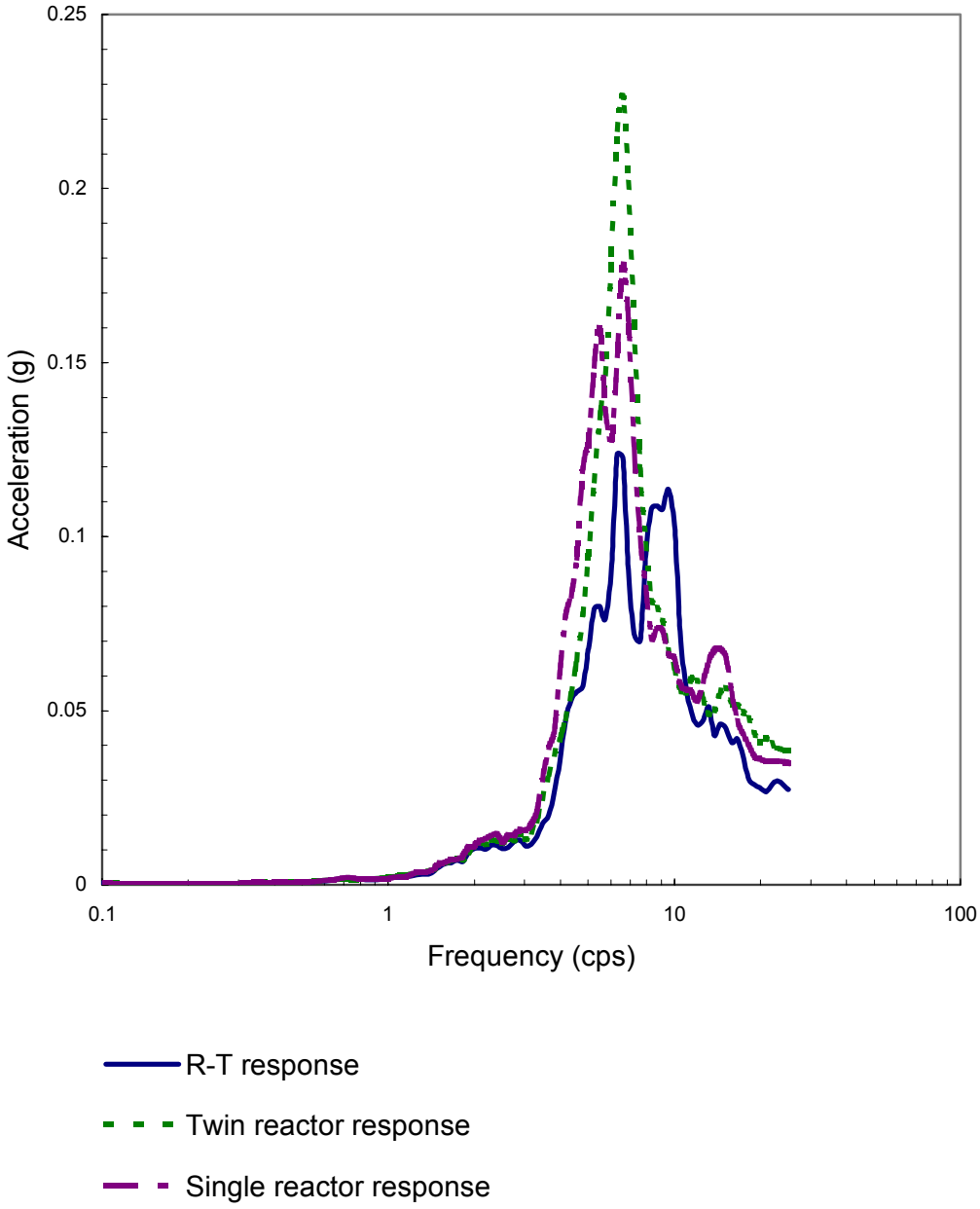

Figure. 5-60 Comparison of the recorded response spectra at the roof of excavated reactor buildings in NS direction (No.157).

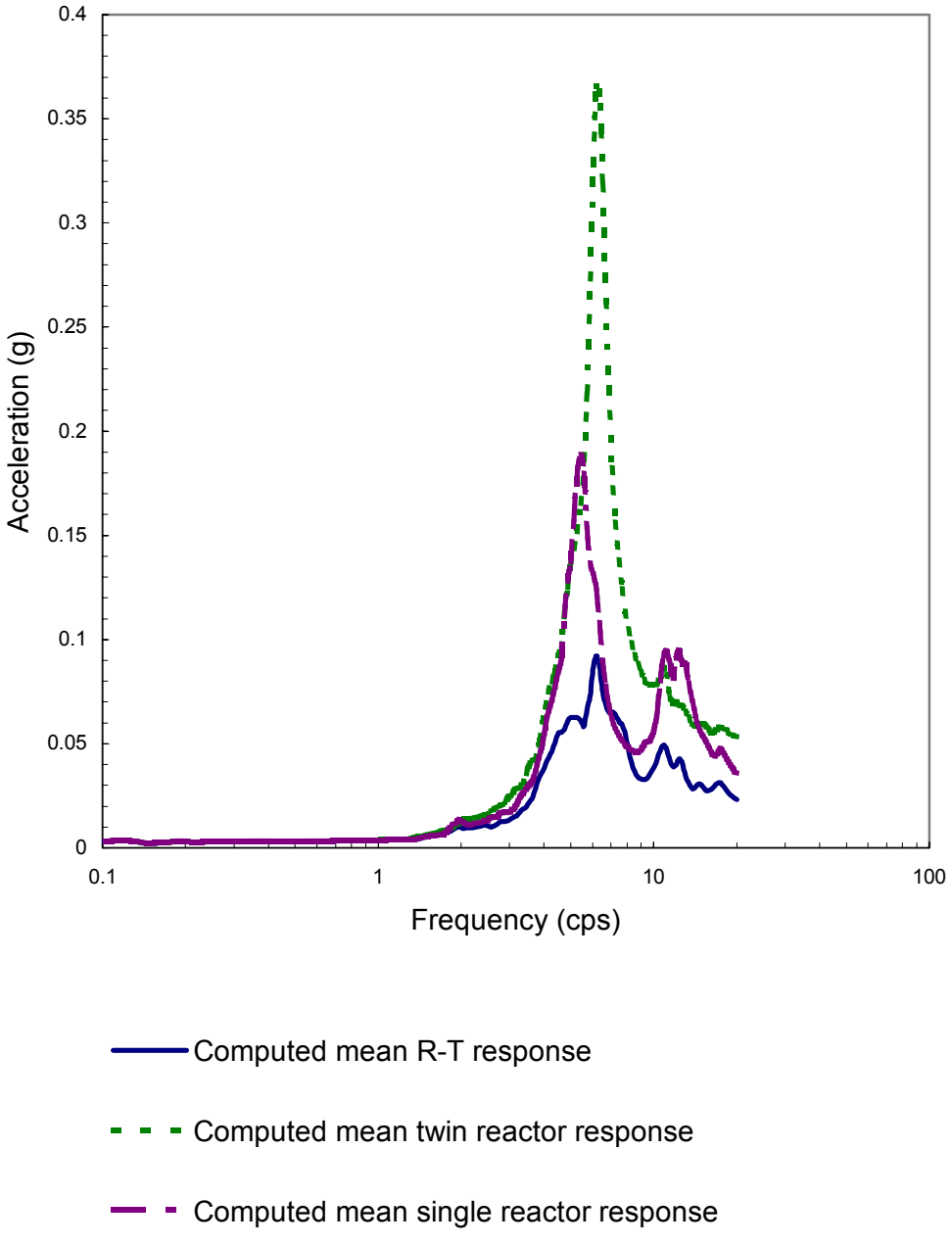

Figure. 5-61 Comparison of the predicted response spectra at the basemat of excavated reactor buildings in NS direction (No.157).

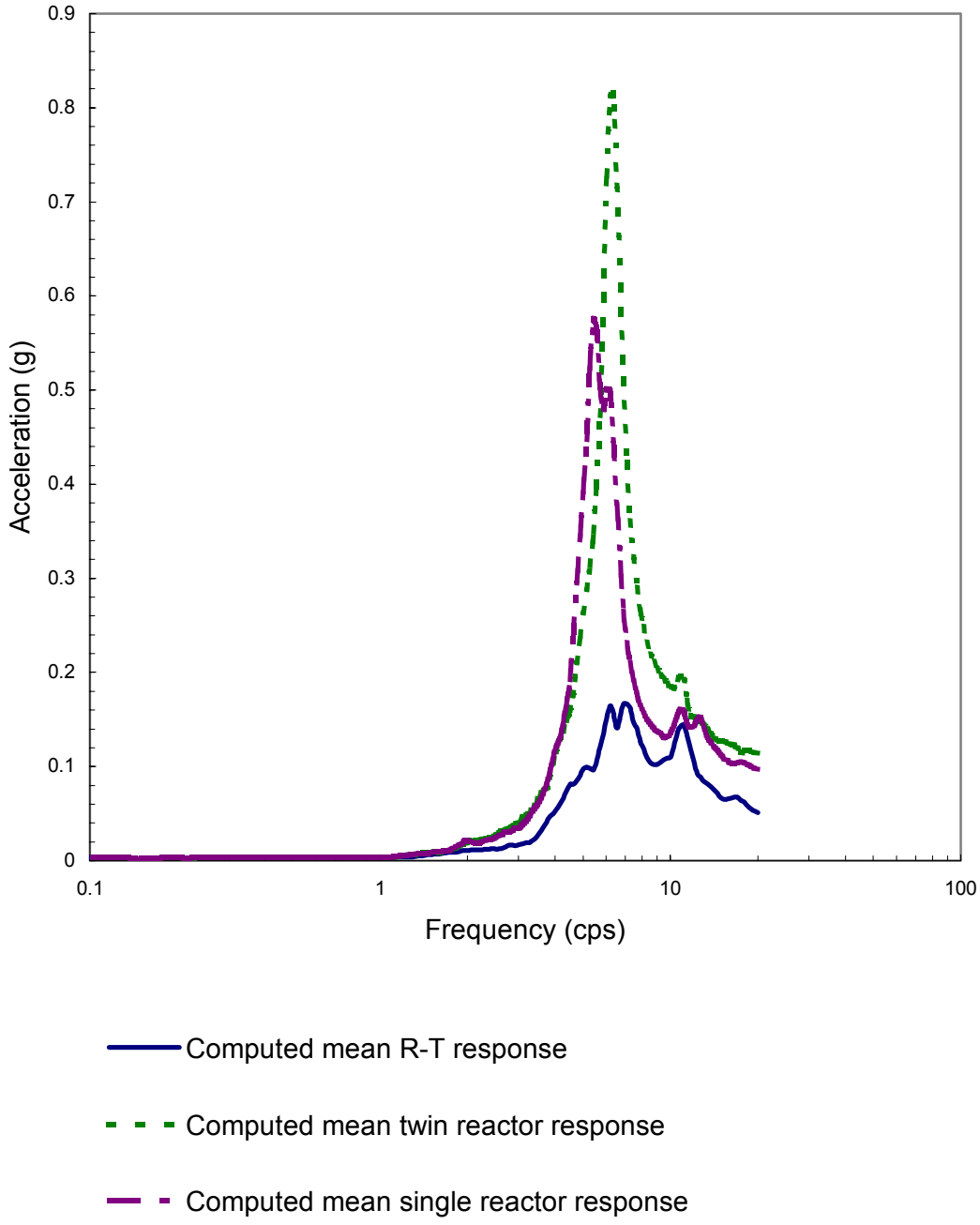

Figure. 5-62 Comparison of the predicted response spectra at the roof of excavated reactor buildings in NS direction (No.157).

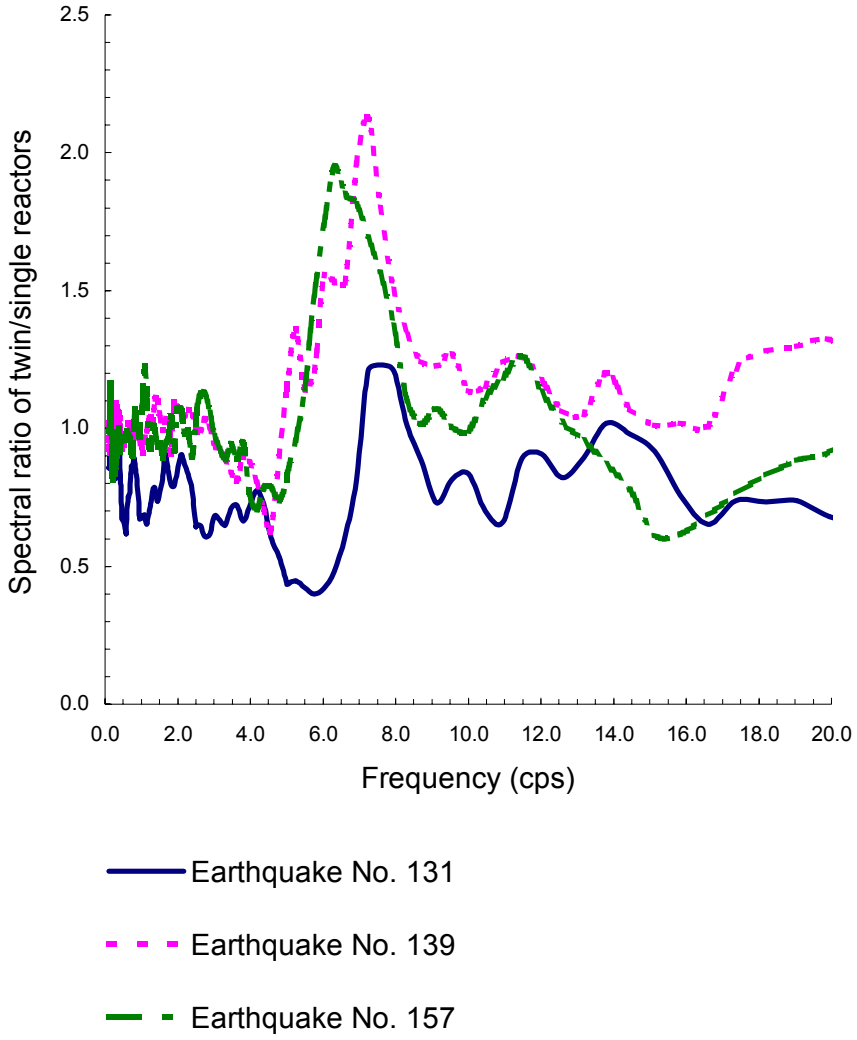

Figure. 5-63 Comparison of recorded DCI effect at basemat of excavated Twin Reactor

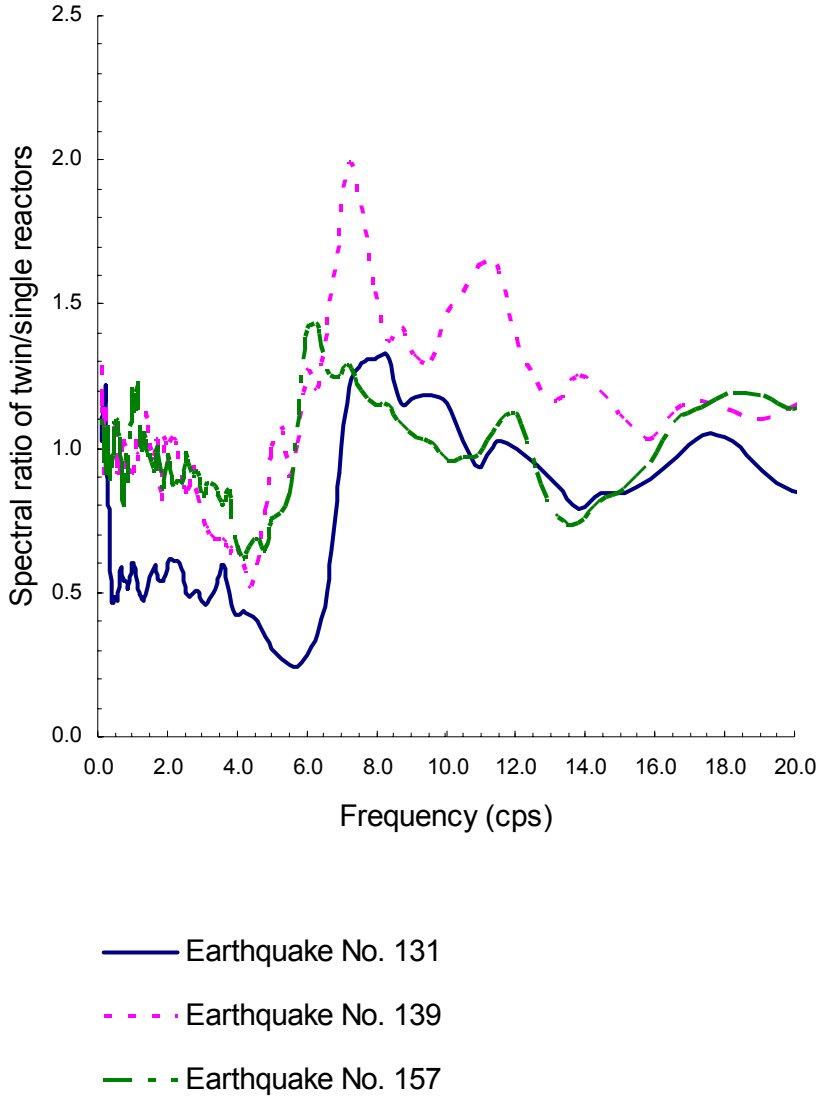

Figure. 5-64 Comparison of recorded DCI effect at roof of excavated Twin Reactor

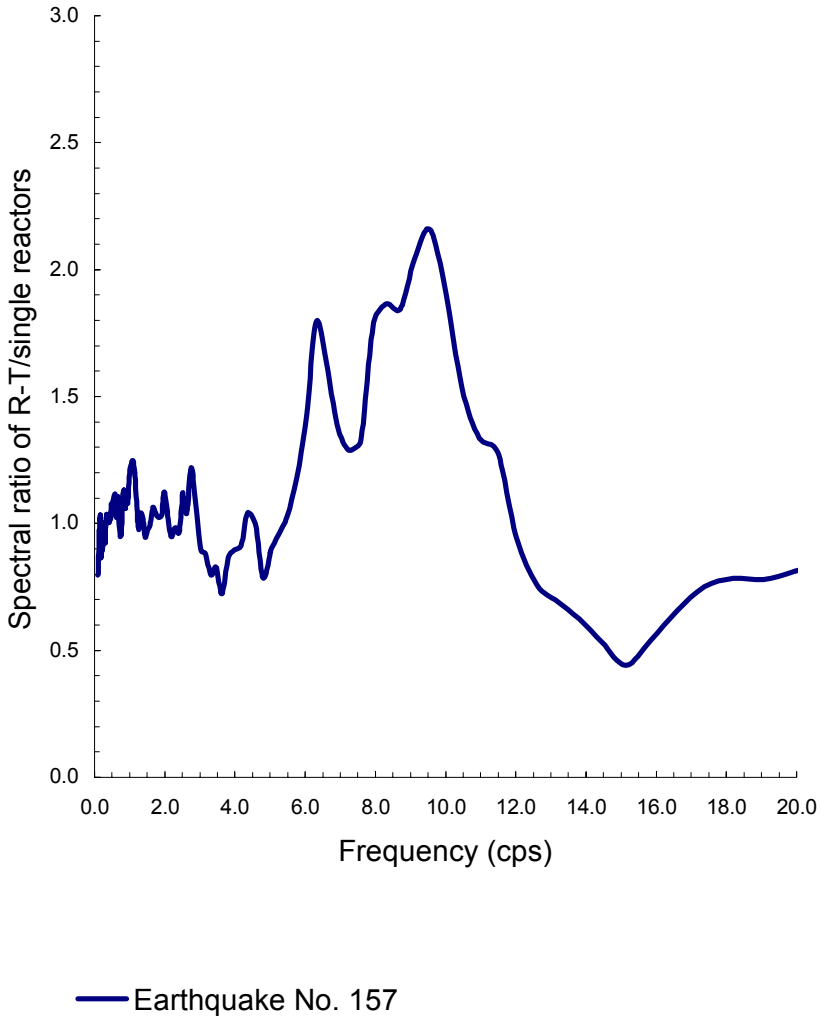

Figure. 5-65 Comparison of recorded DCI effect at basemat of excavated R-T Reactor

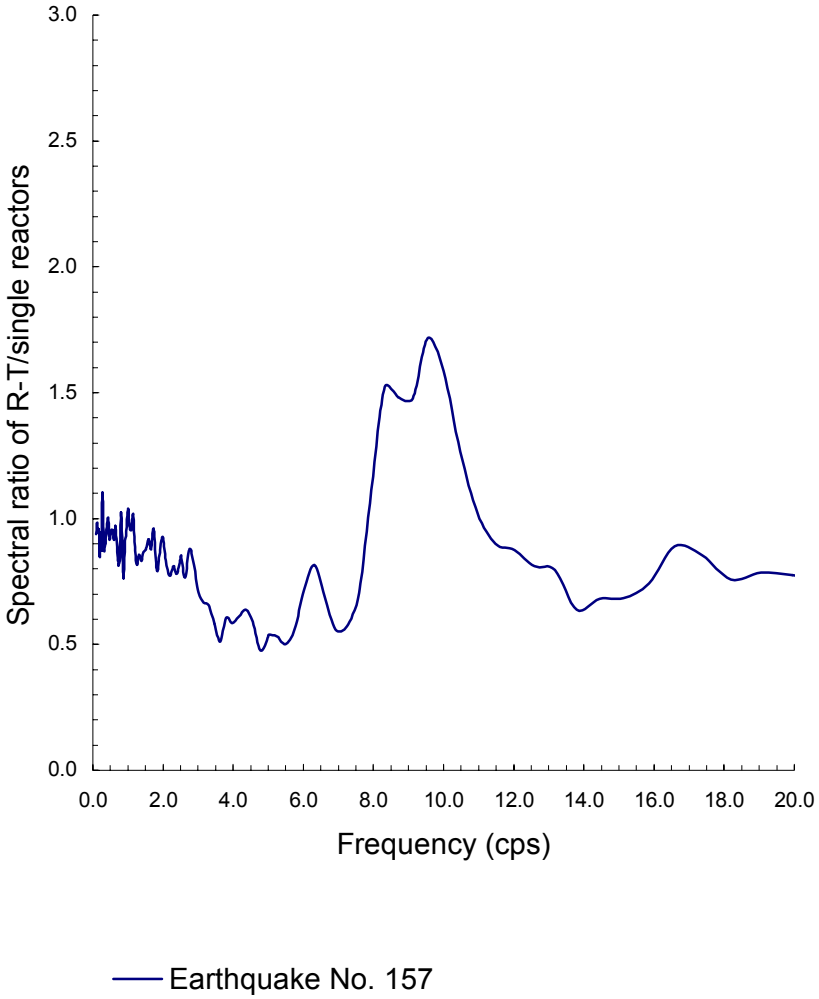

Figure. 5-66 Comparison of recorded DCI effect at roof of excavated R-T Reactor

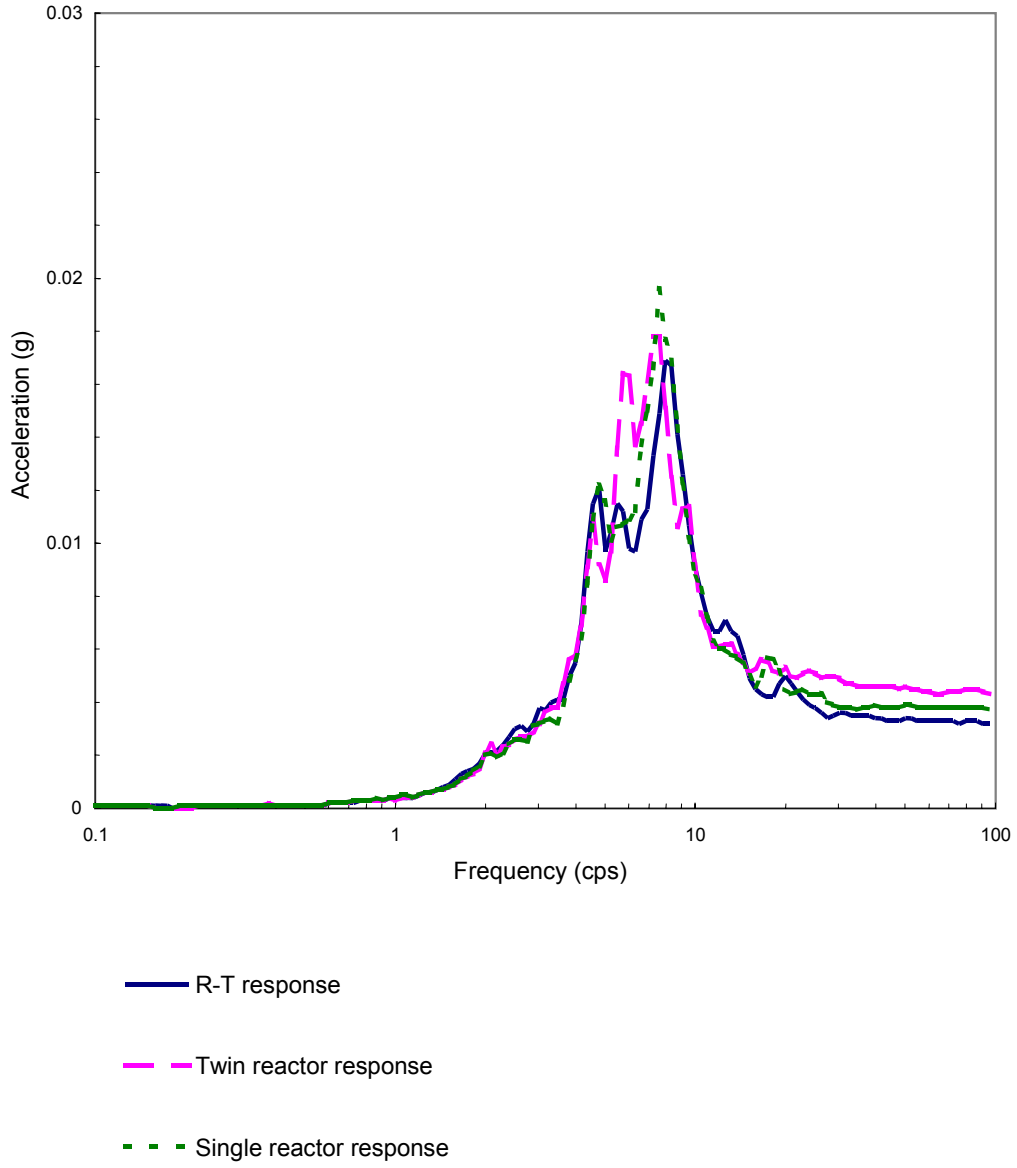

Figure 5-67. Comparison of the recorded response spectra at the basemat center of the embedded reactor building in NS direction (No.164).

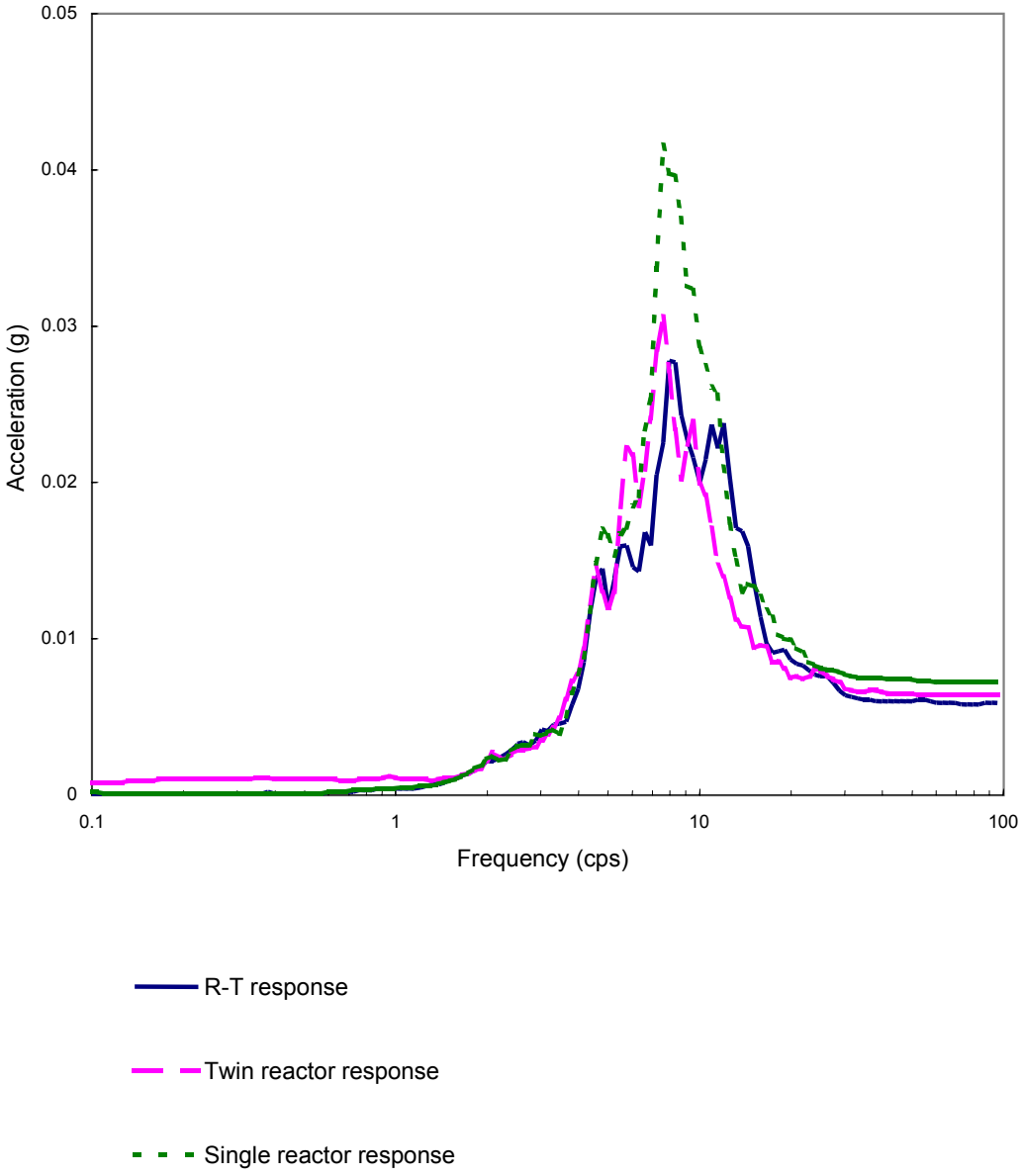

Figure 5-68. Comparison of the recorded response spectra at the roof center of the embedded reactor building in NS direction (No.164).

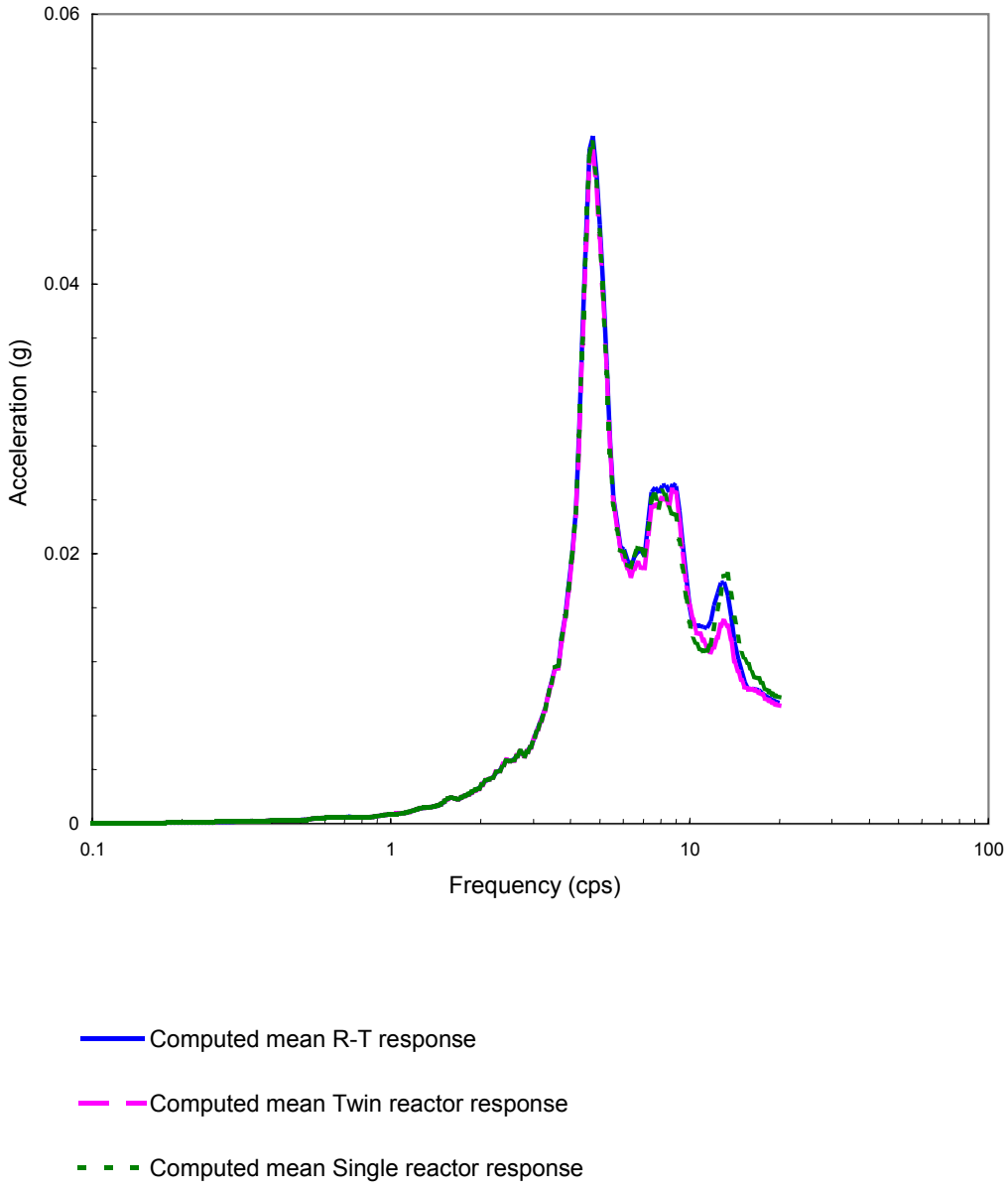

Figure 5-69. Comparison of the predicted response spectra at the basemat center of the embedded reactor building in NS direction (No.164).

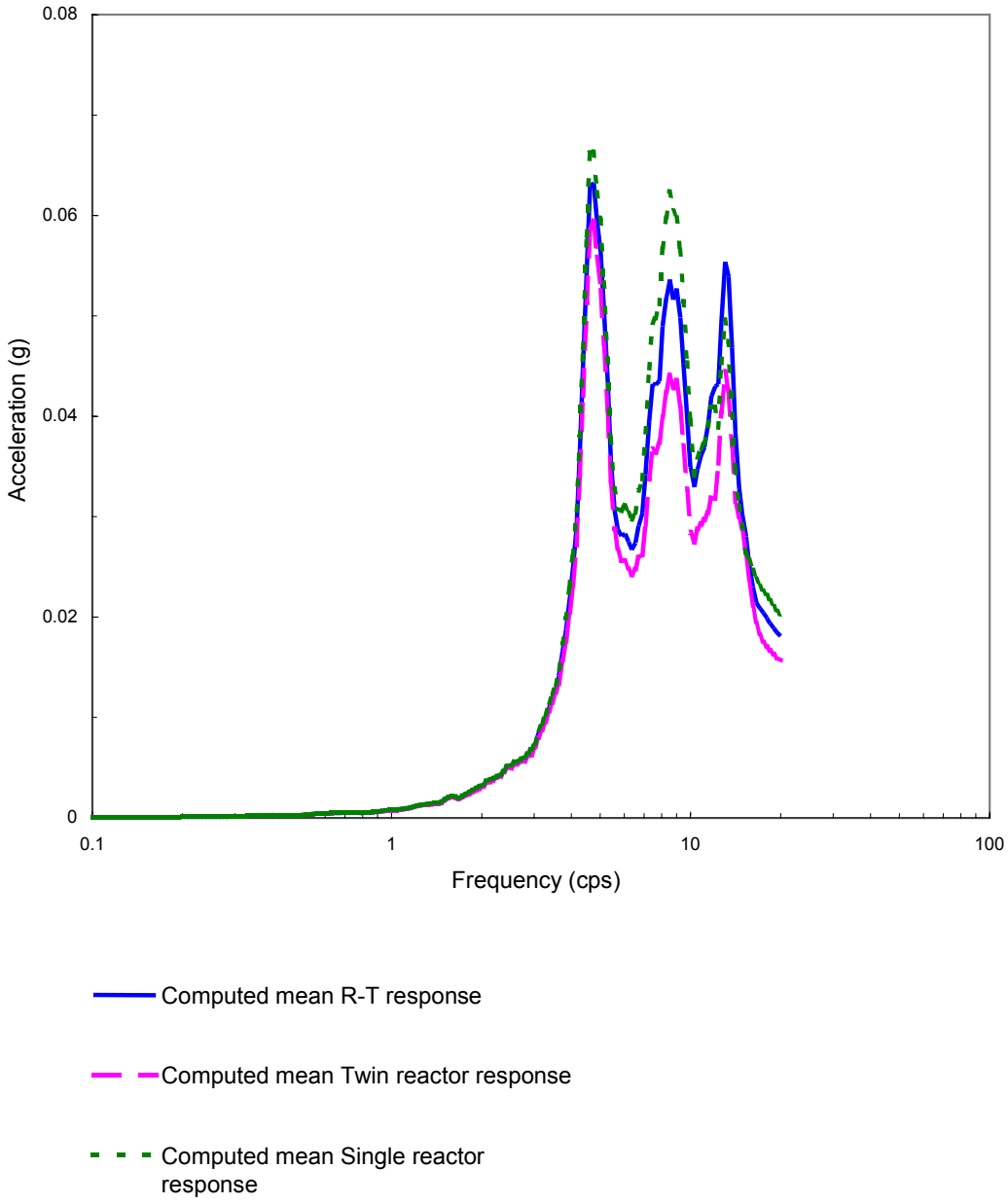

Figure 5-70. Comparison of the predicted response spectra at the roof center of the embedded reactor building in NS direction (No.164).

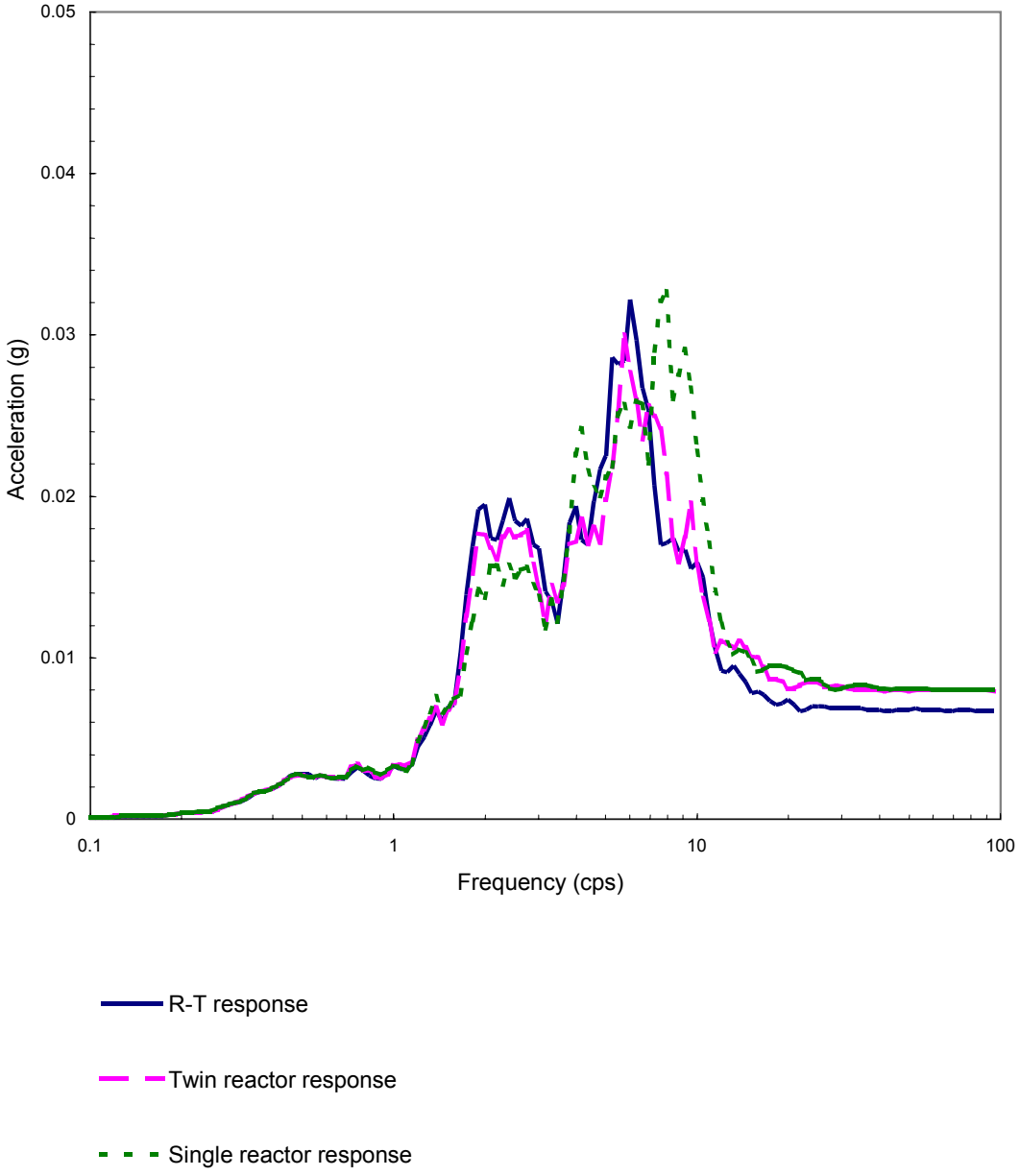

Figure 5-71. Comparison of the recorded response spectra at the basemat center of the embedded reactor building in NS direction (No.172).

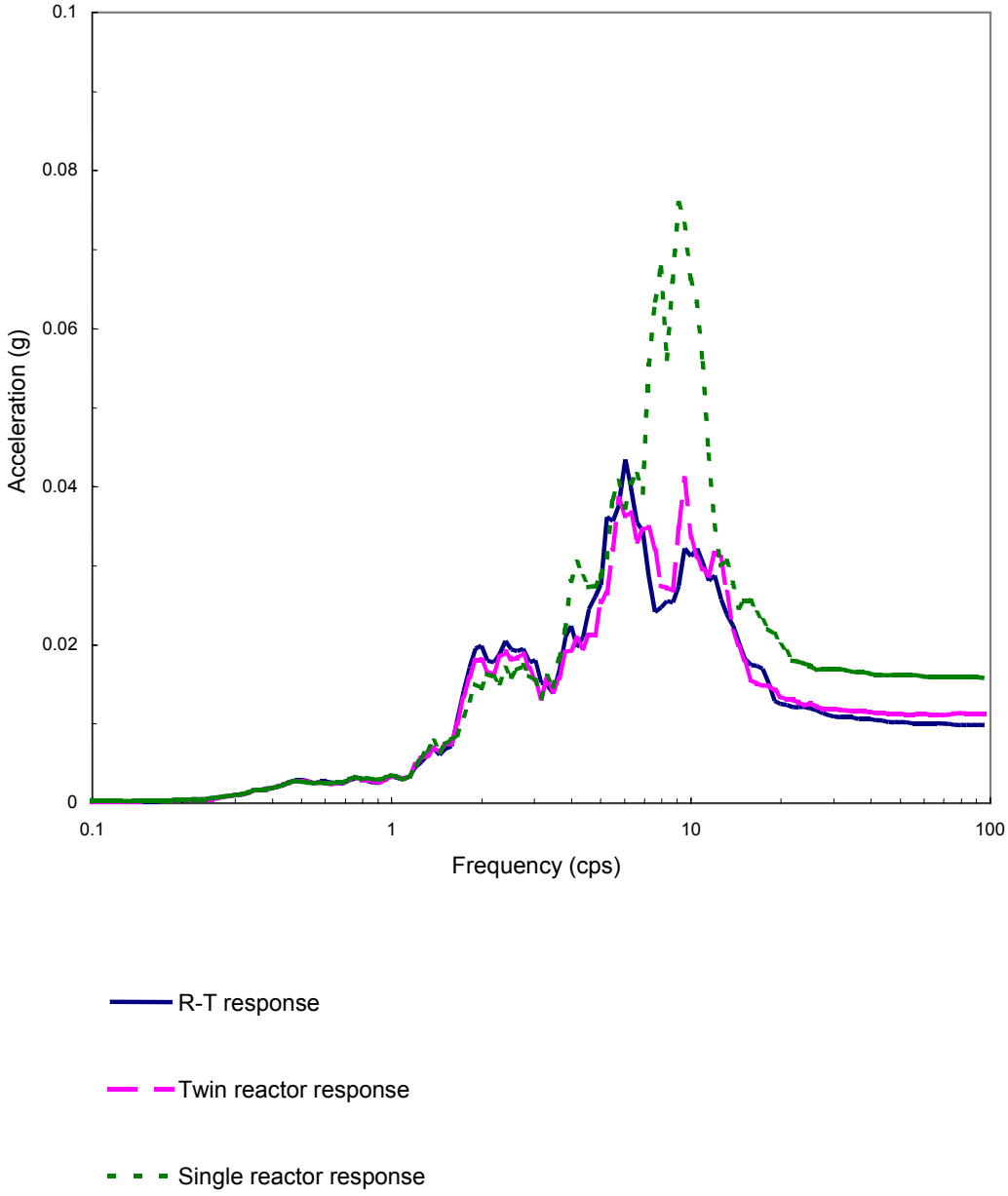

Figure 5-72. Comparison of the recorded response spectra at the roof center of the embedded reactor building in NS direction (No.172).

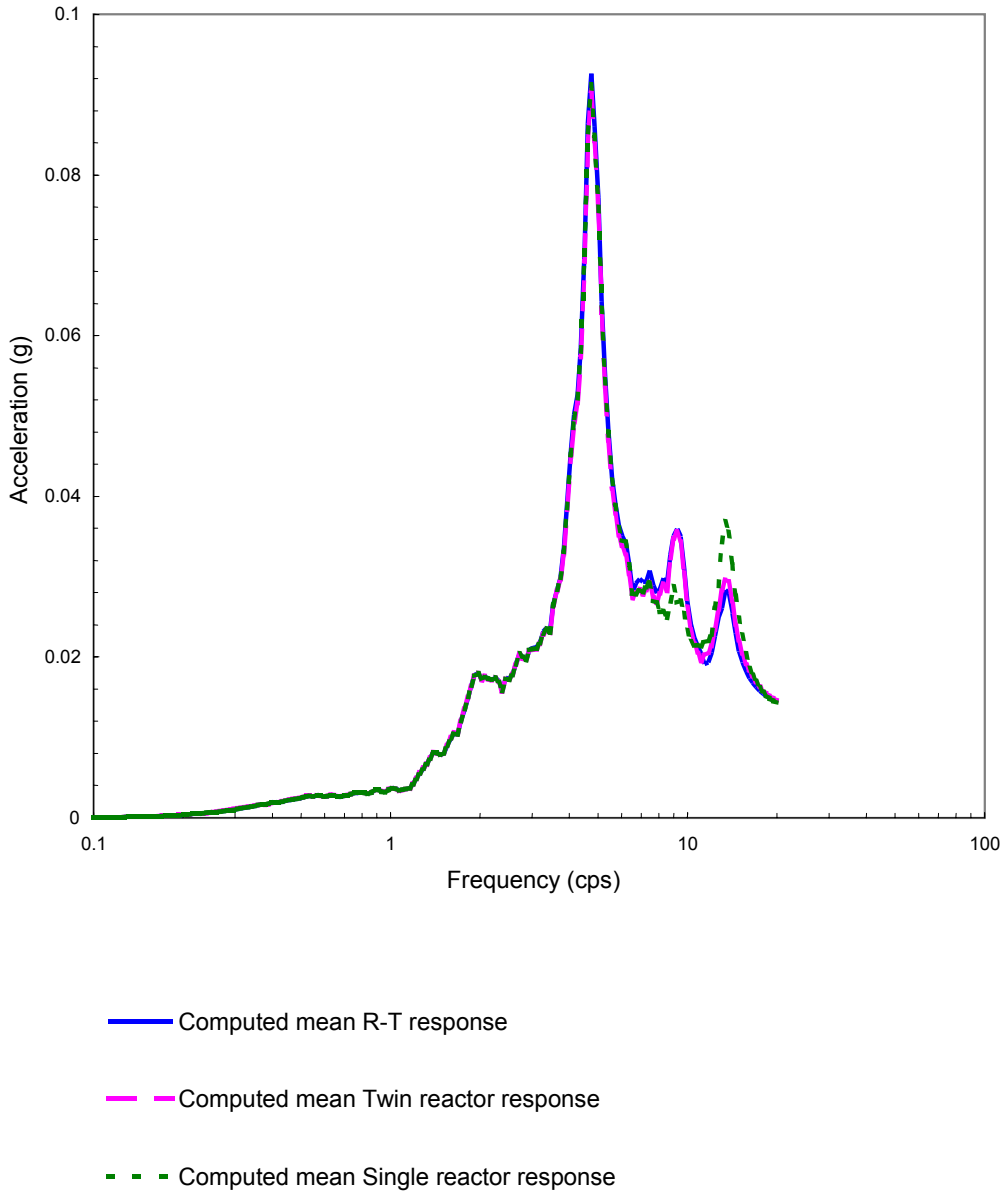

Figure 5-73. Comparison of the predicted response spectra at the basemat center of the embedded reactor building in NS direction (No.172).

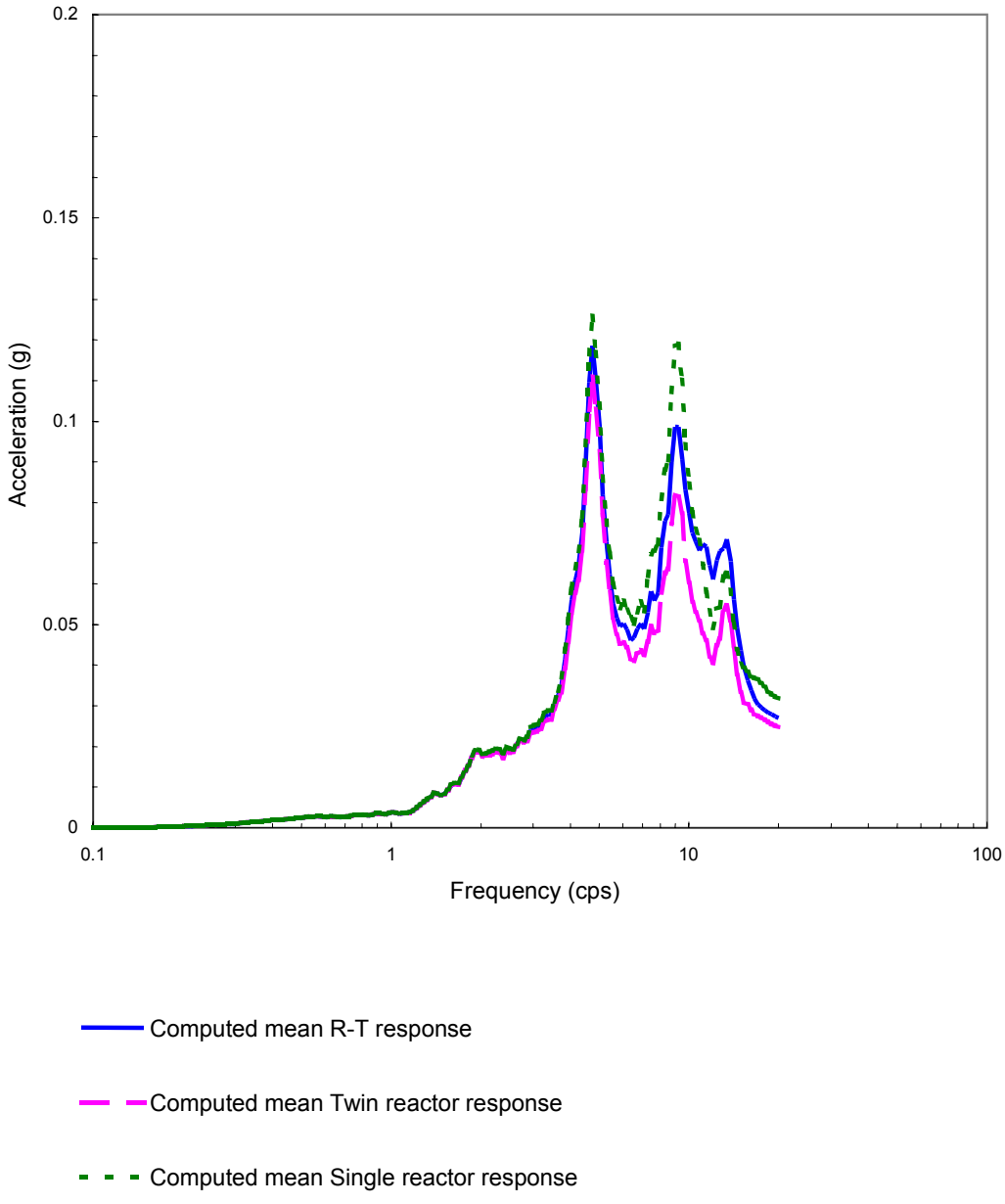

Figure 5-74. Comparison of the predicted response spectra at the roof center of the embedded reactor building in NS direction (No.172).

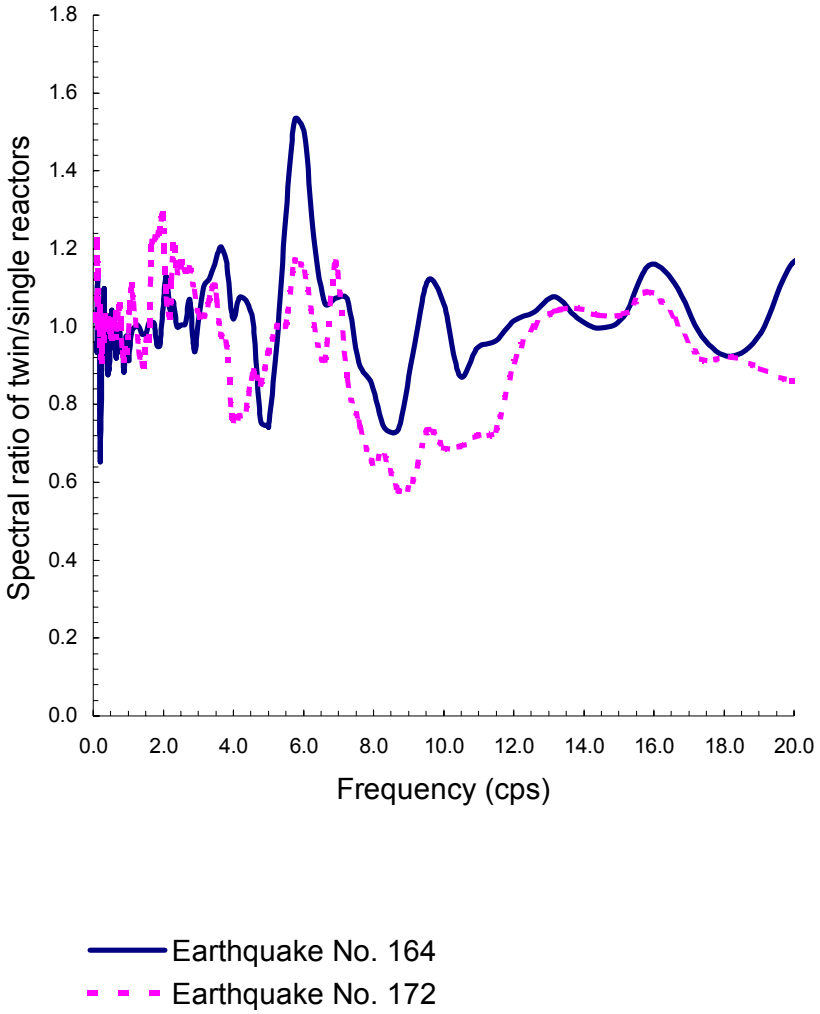

Figure 5-75. Comparison of recorded DCI effect at basemat of embedded Twin Reactor.

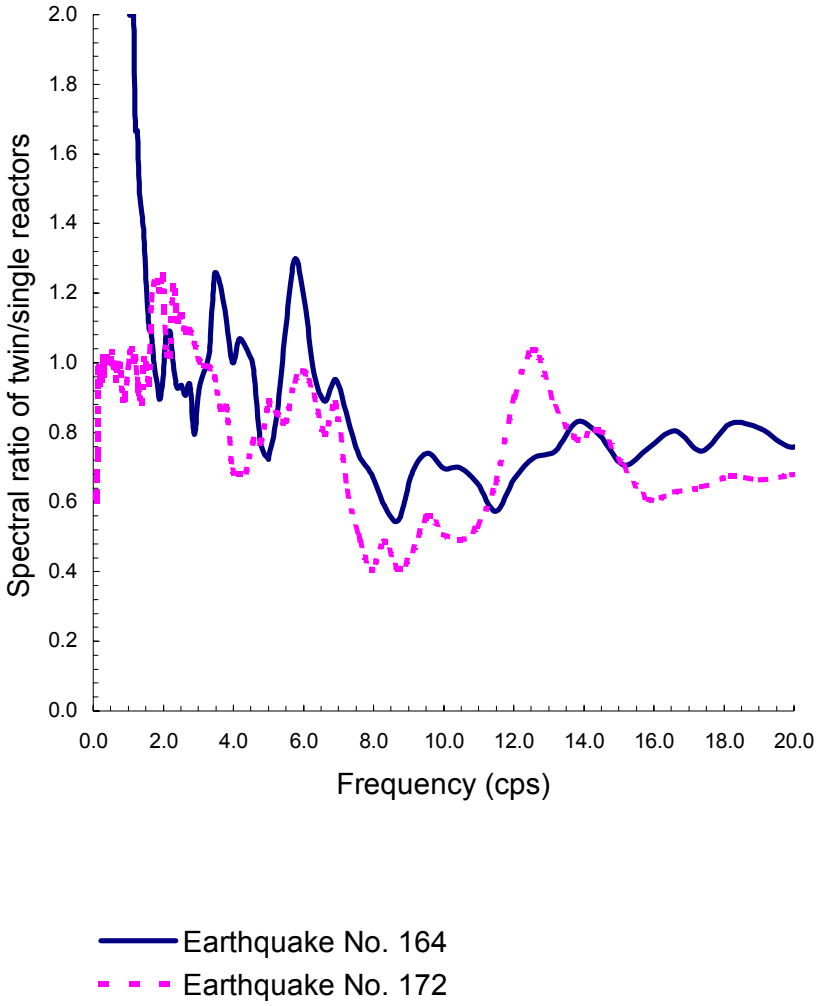

Figure 5-76. Comparison of recorded DCI effect at roof of embedded Twin Reactor.

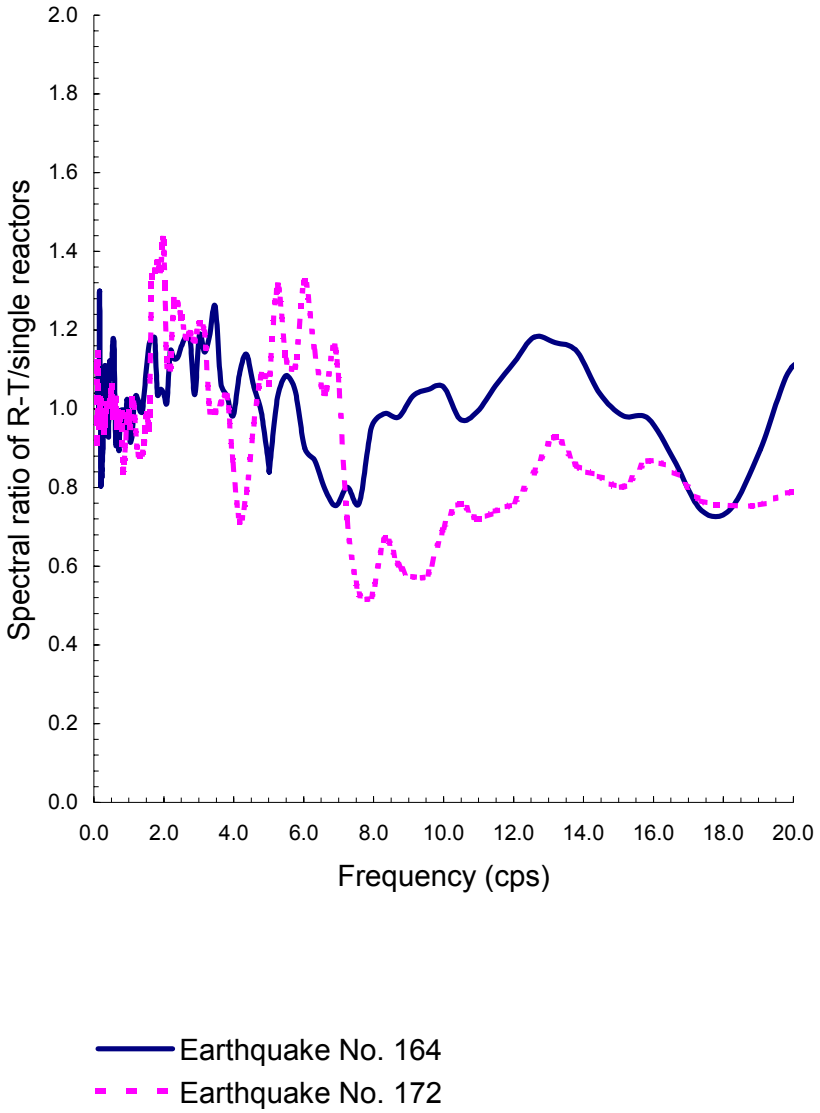

Figure 5-77. Comparison of recorded DCI effect at basemat of embedded R-T Reactor.

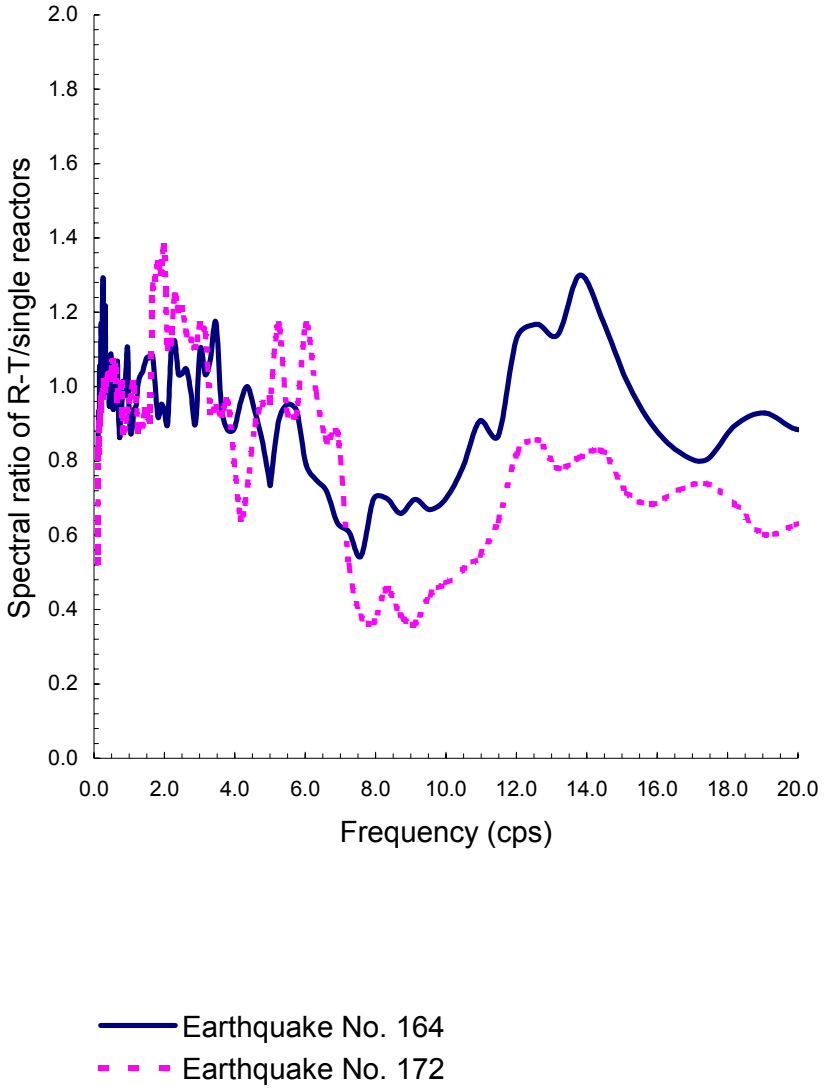

Figure 5-78. Comparison of recorded DCI effect roof of embedded R-T Reactor.

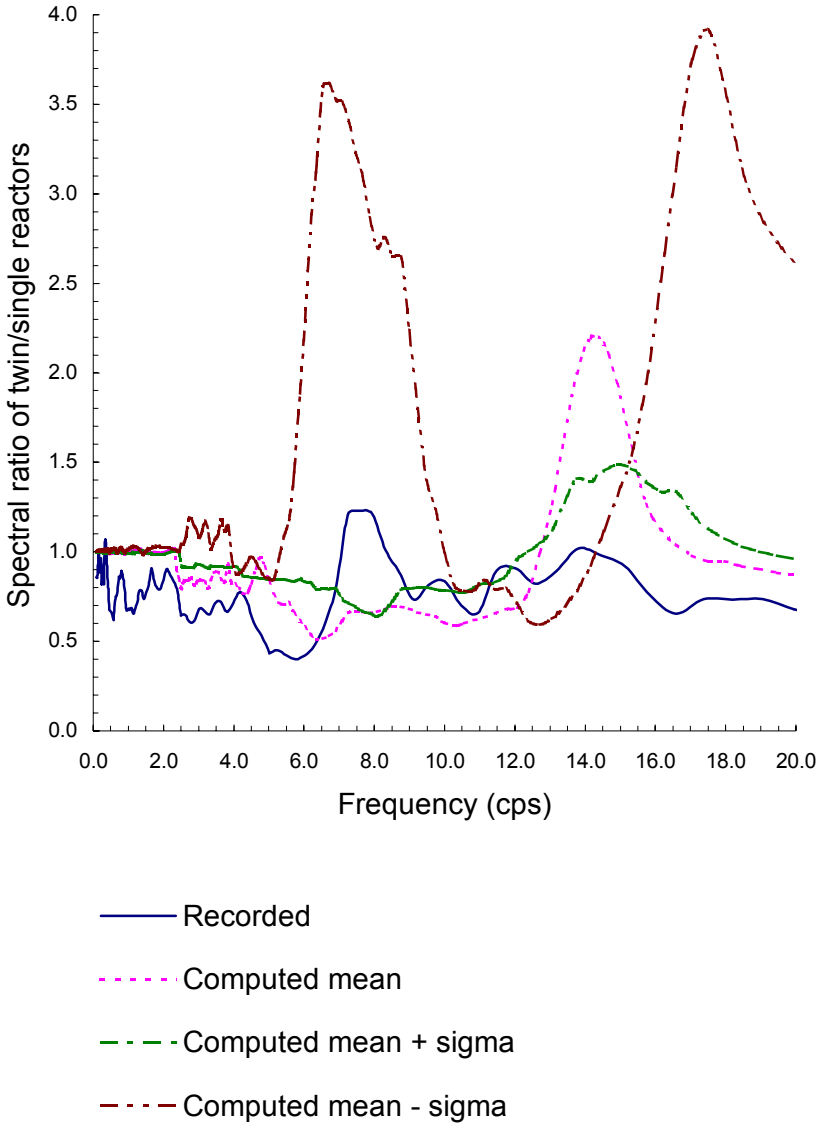

Figure 5-79. Comparison of DCI effect at basemat of excavated Twin Reactor for Earthquake 131x.

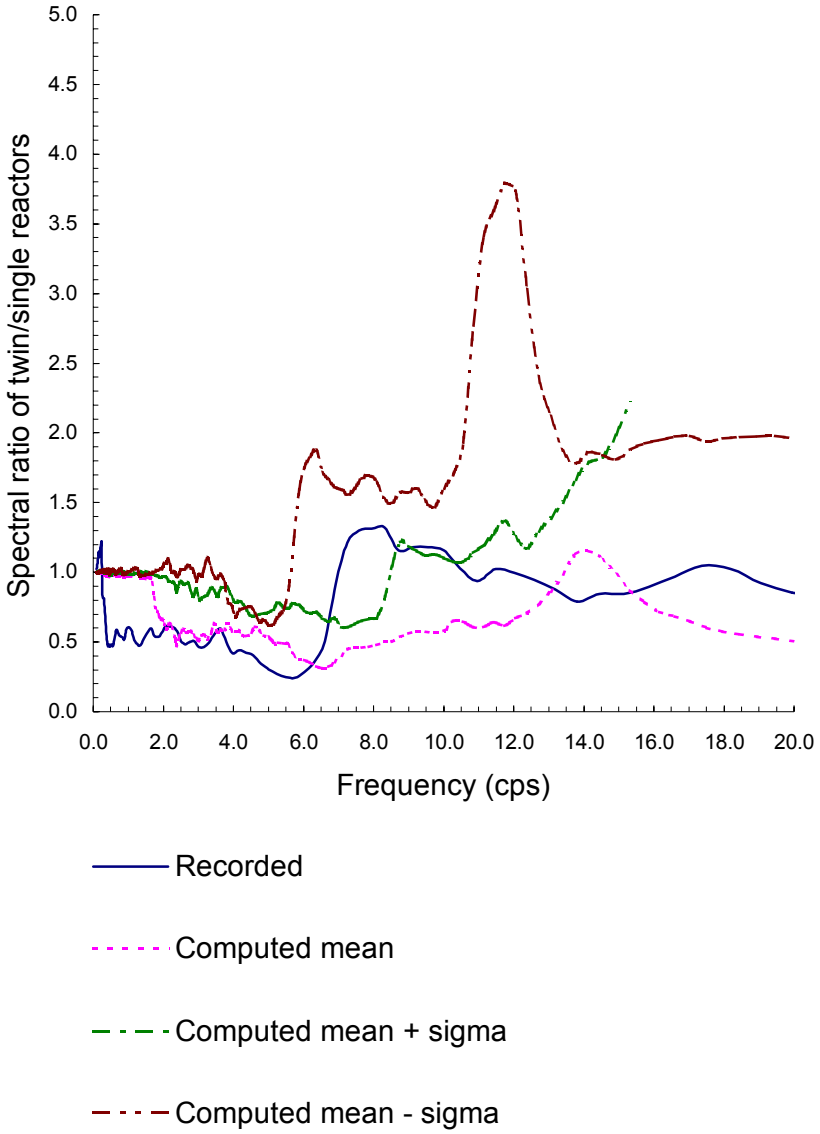

Figure 5-80. Comparison of DCI effect at roof of excavated Twin Reactor for Earthquake 131x.

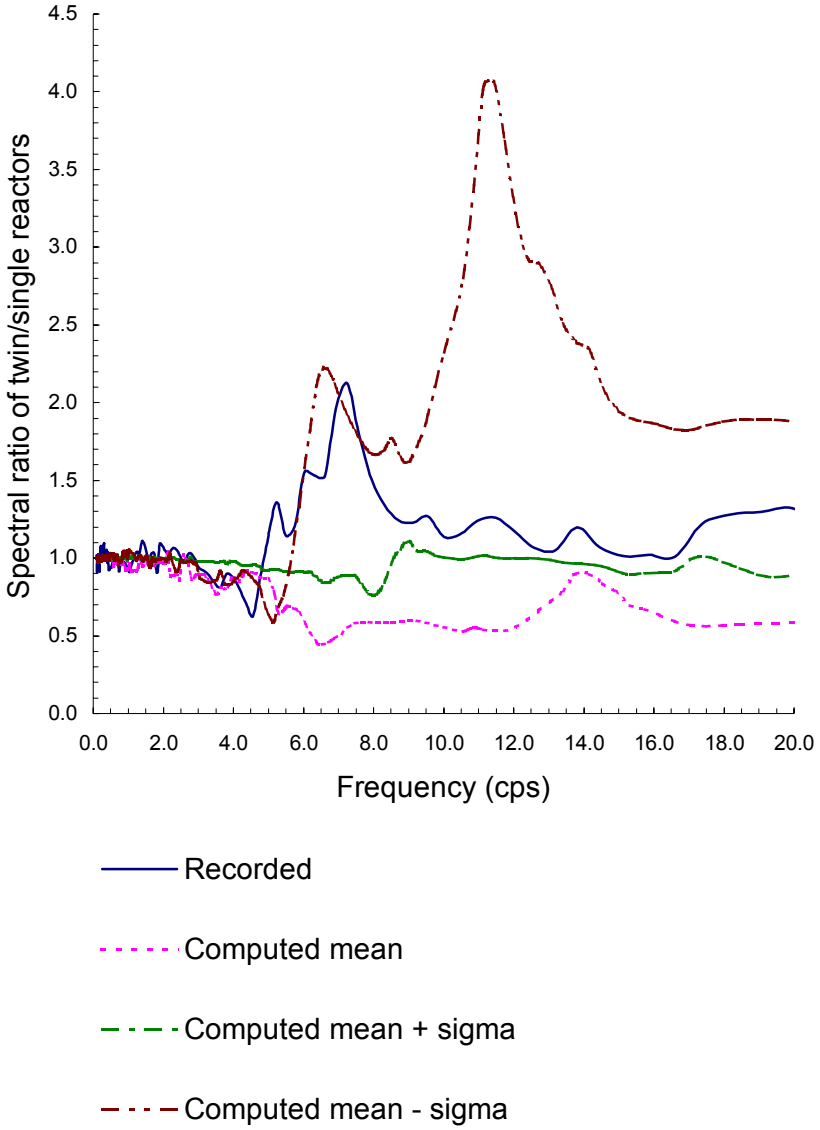

Figure 5-81. Comparison of DCI effect at basemat of excavated Twin Reactor for Earthquake 139x.

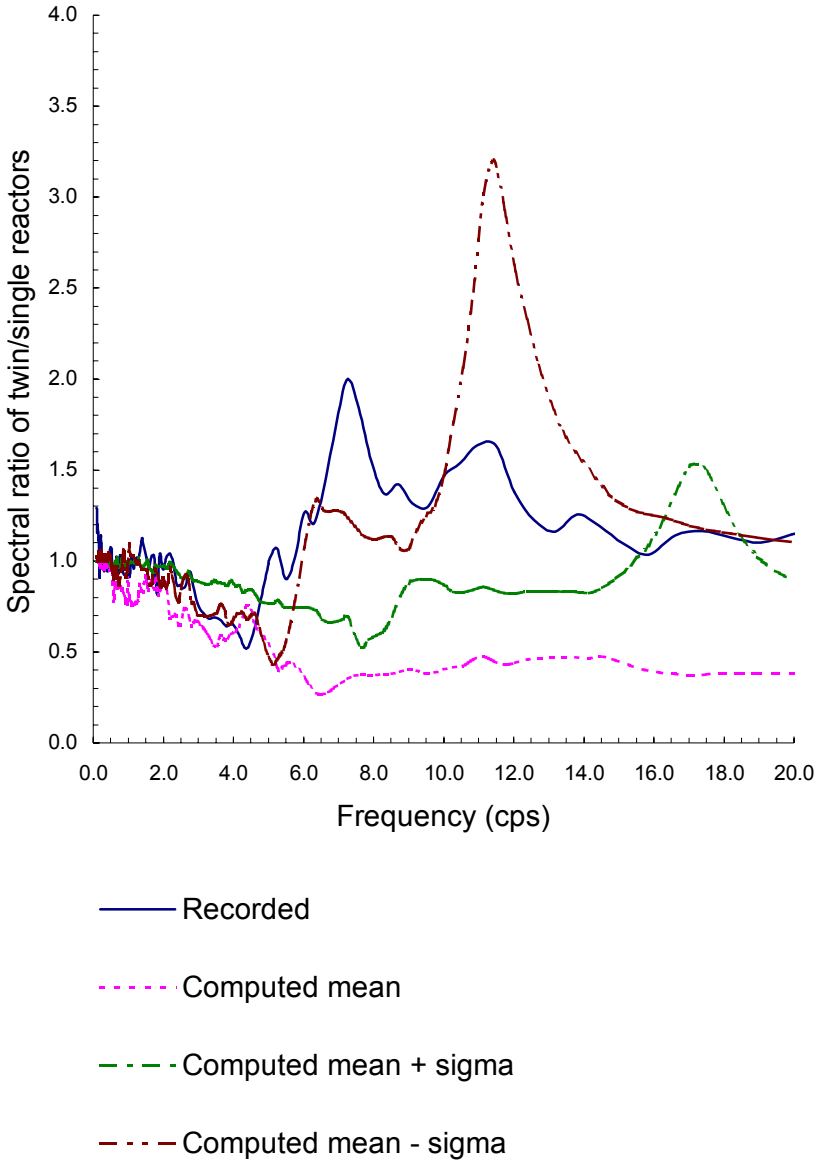

Figure 5-82. Comparison of DCI effect at roof of excavated Twin Reactor for Earthquake 139x.

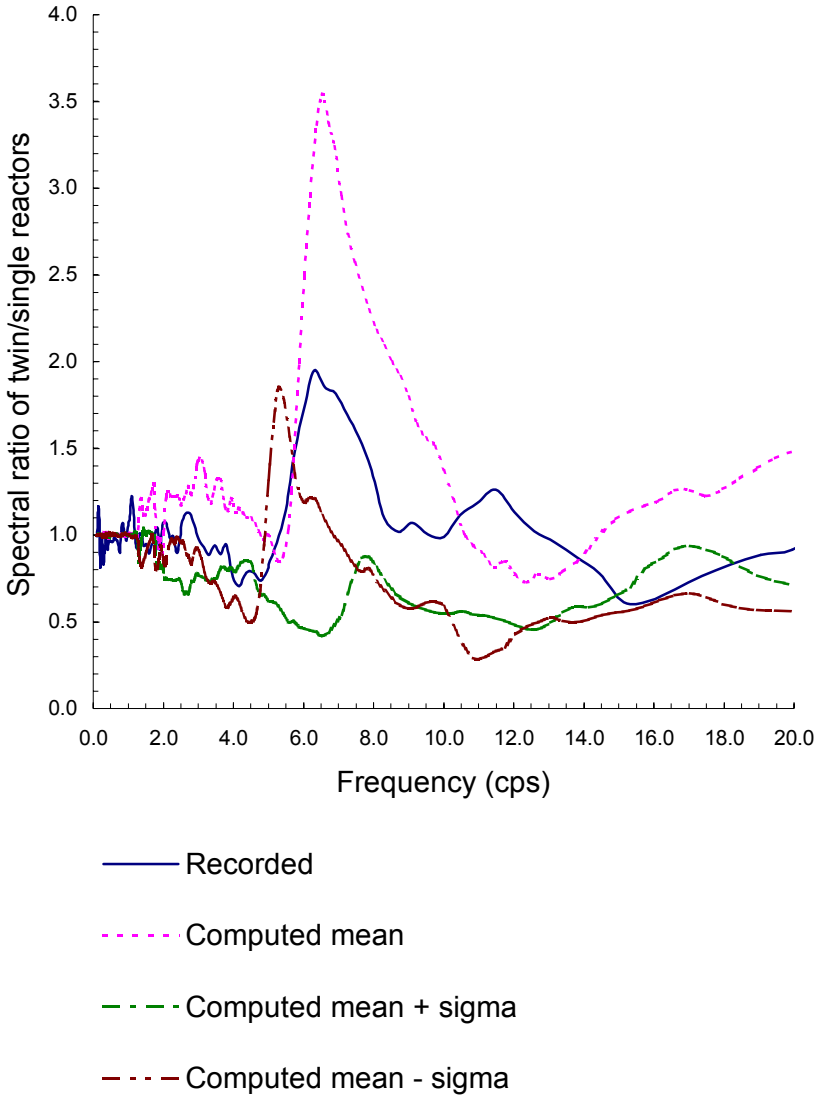

Figure 5-83. Comparison of DCI effect at basemat of excavated Twin Reactor for Earthquake 157x.

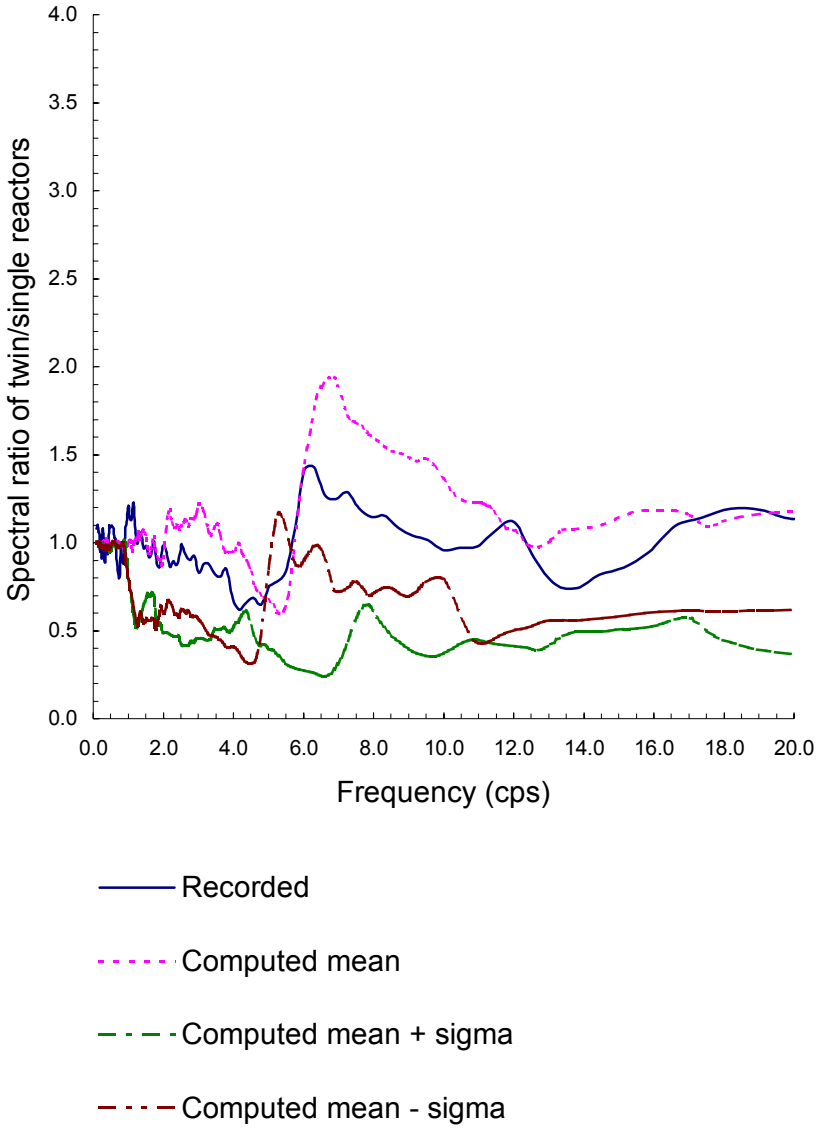

Figure 5-84. Comparison of DCI effect at roof of excavated Twin Reactor for Earthquake 157x.

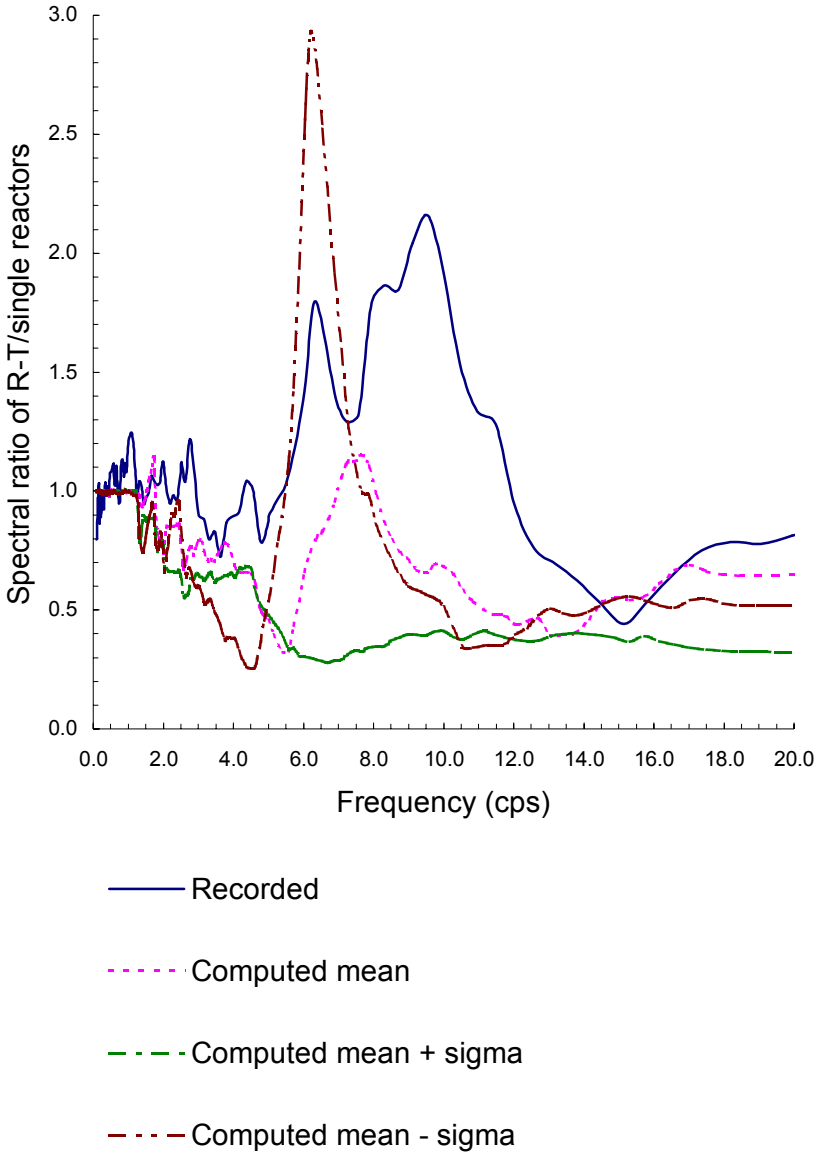

Figure 5-85. Comparison of DCI effect at basemat of excavated R-T Reactor for Earthquake 157x.

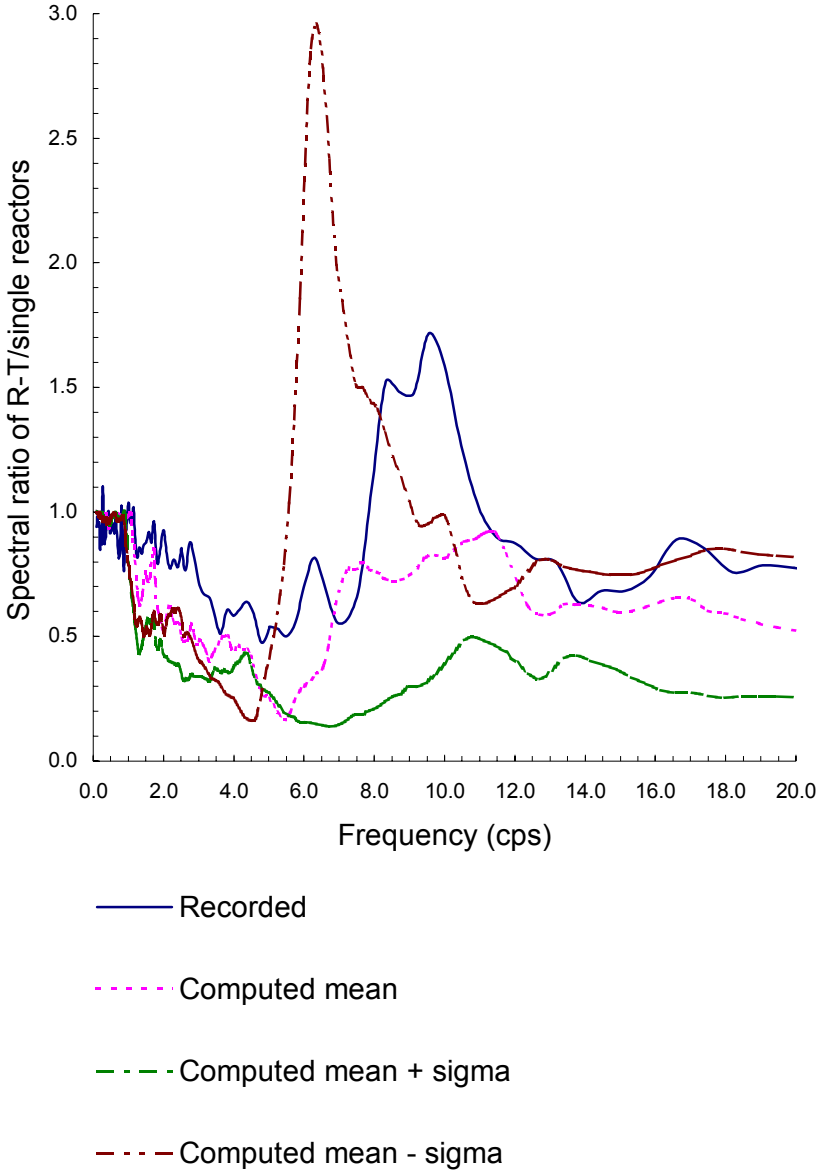

Figure 5-86. Comparison of DCI effect at roof of excavated R-T Reactor for Earthquake 157x.

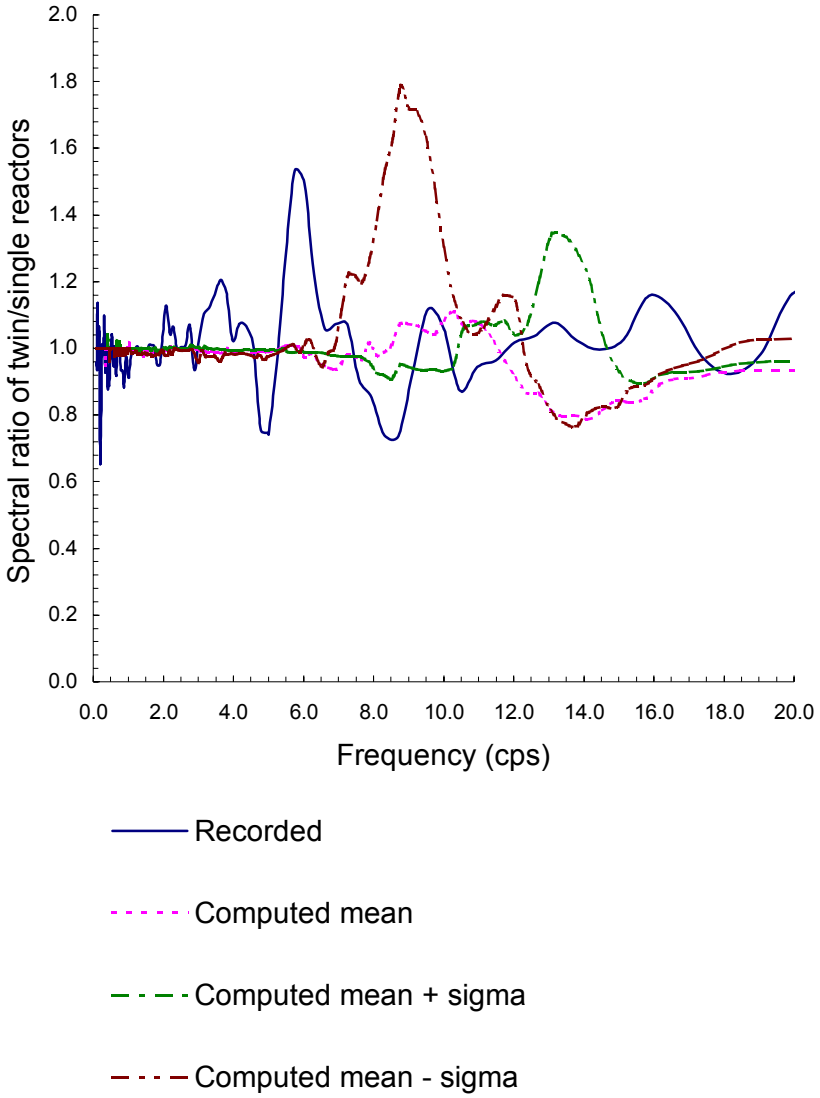

Figure 5-87. Comparison of DCI effect at basemat of embedded Twin Reactor for Earthquake 164x.

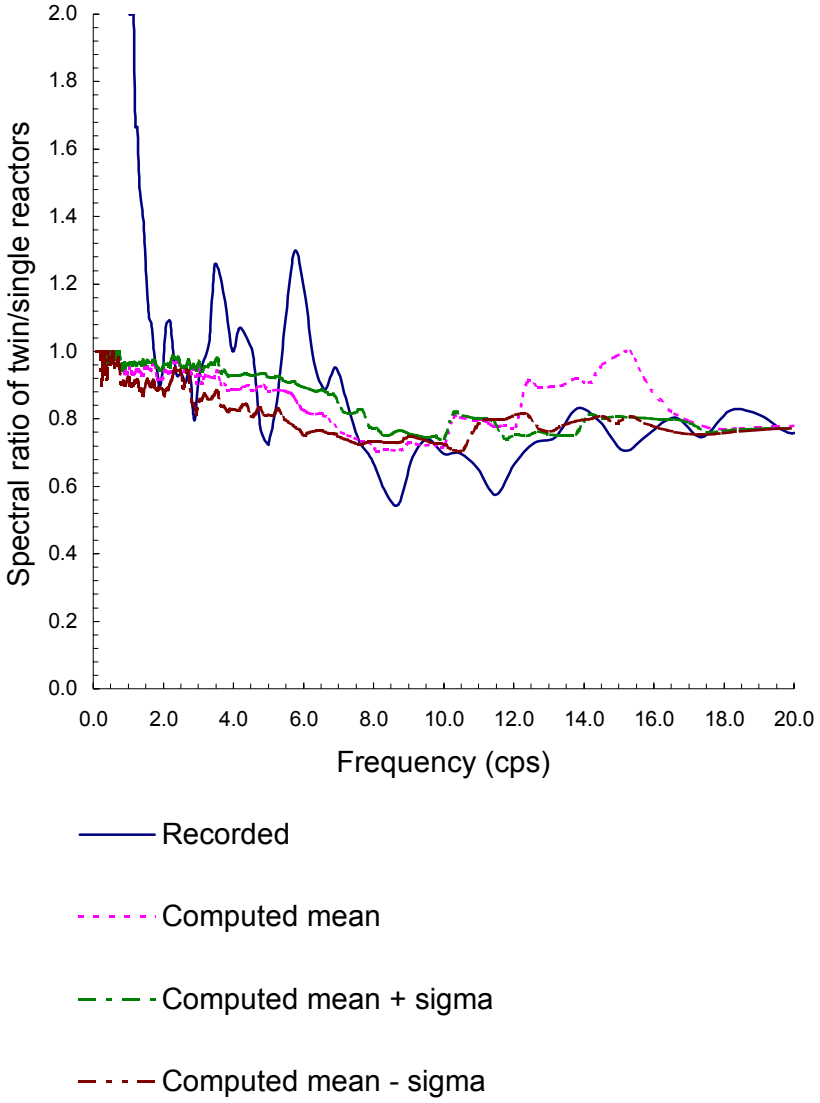

Figure 5-88. Comparison of DCI effect at roof of embedded Twin Reactor for Earthquake 164x.

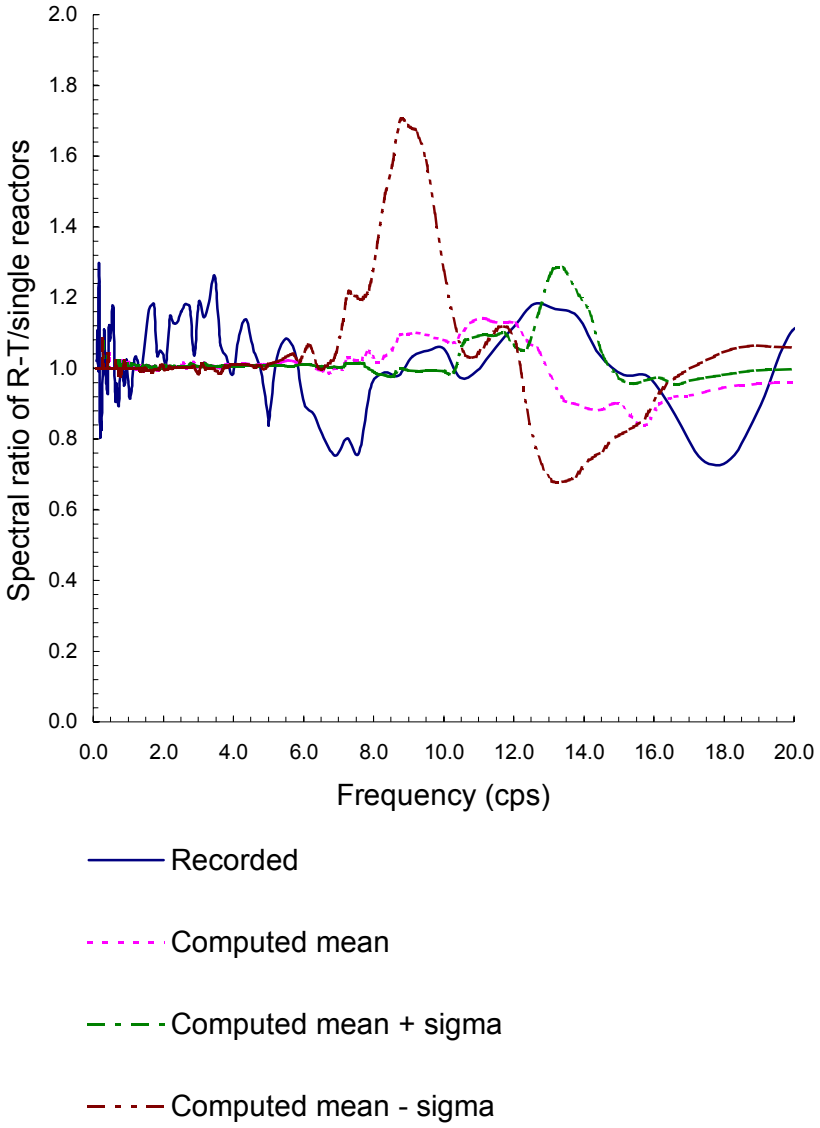

Figure 5-89. Comparison of DCI effect at basemat of embedded R-T Reactor for Earthquake 164x.

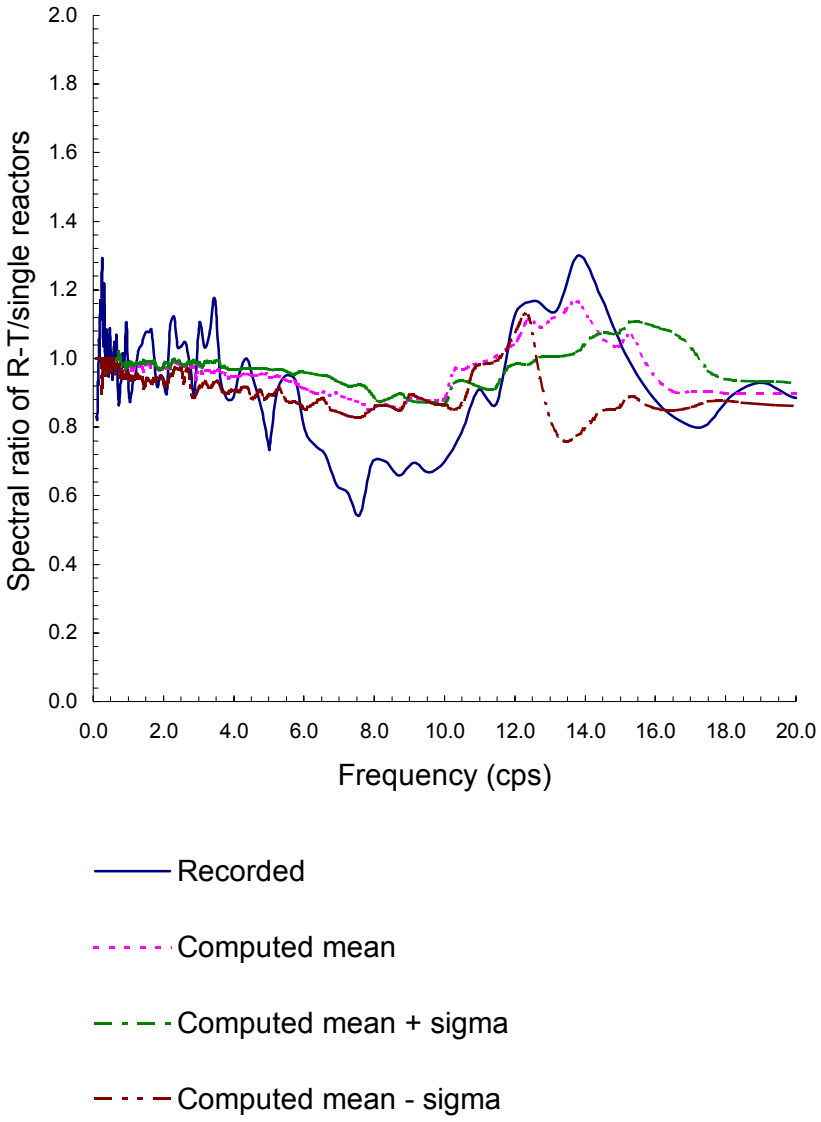

Figure 5-90. Comparison of DCI effect at roof of embedded R-T Reactor for Earthquake 164x.

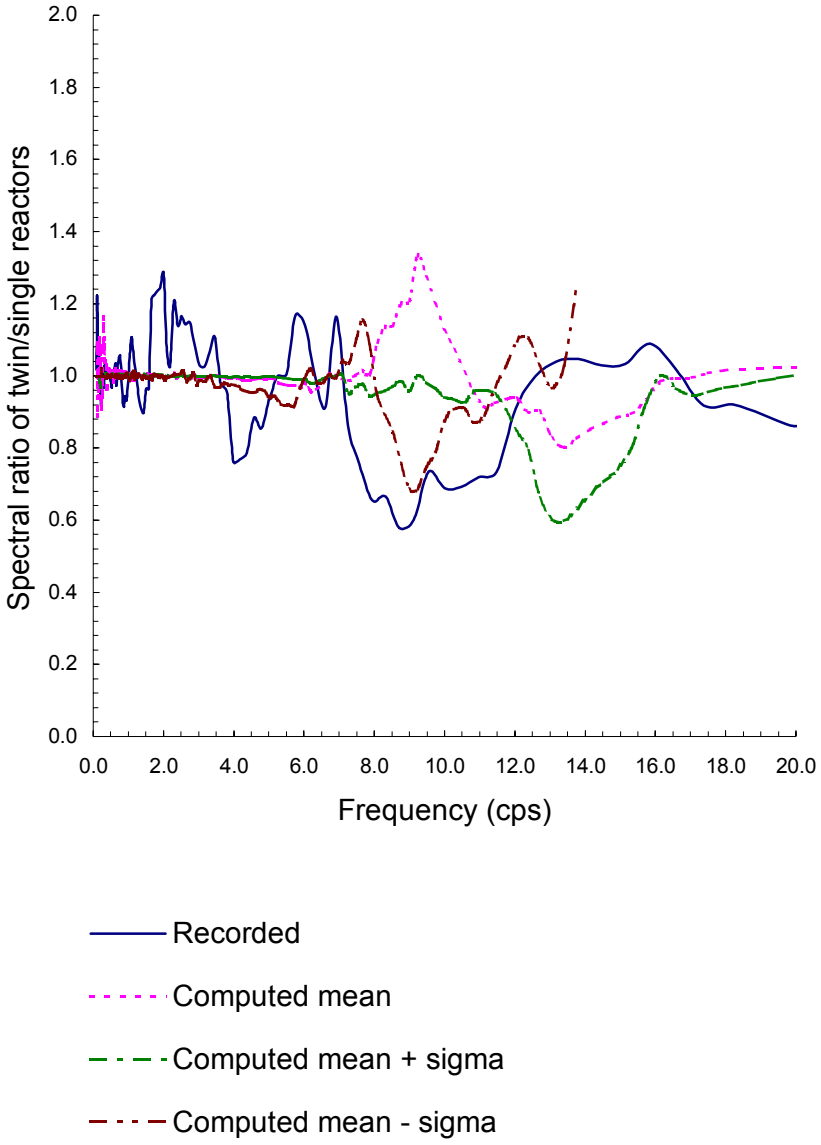

Figure 5-91. Comparison of DCI effect at basemat of embedded Twin Reactor for Earthquake 172x.

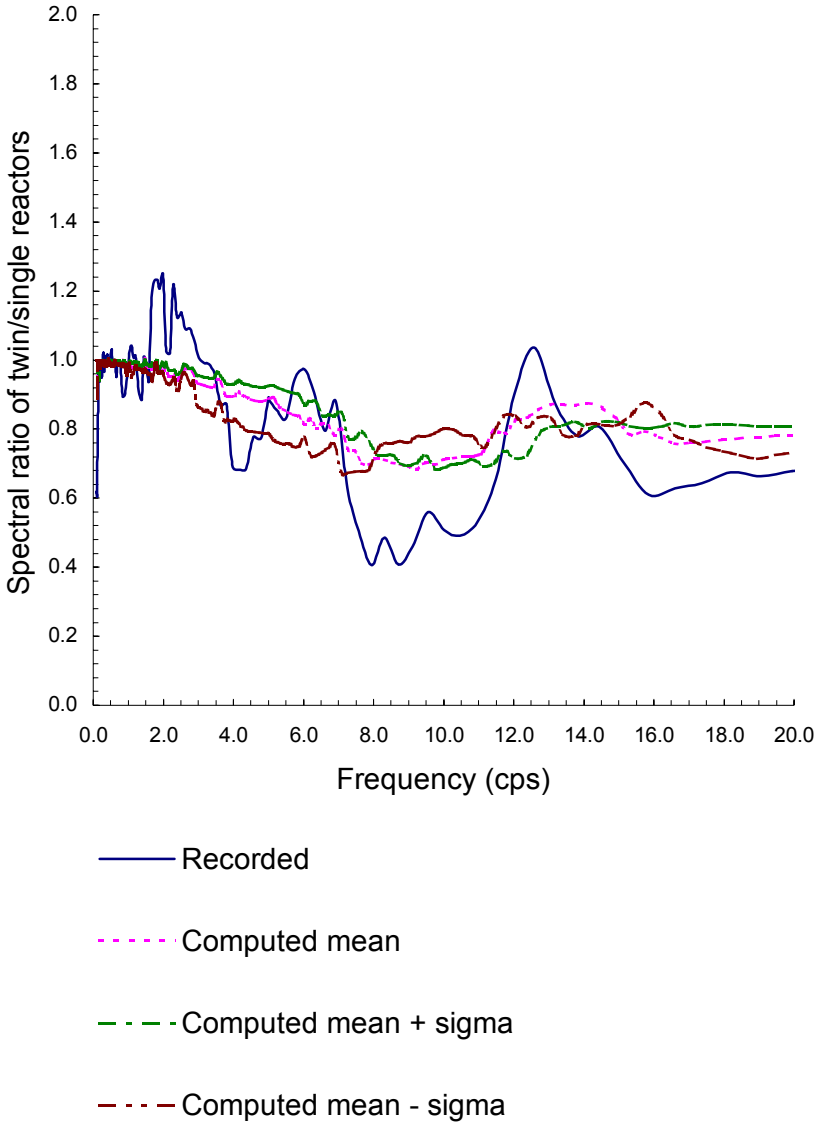

Figure 5-92. Comparison of DCI effect at roof of embedded Twin Reactor for Earthquake 172x.

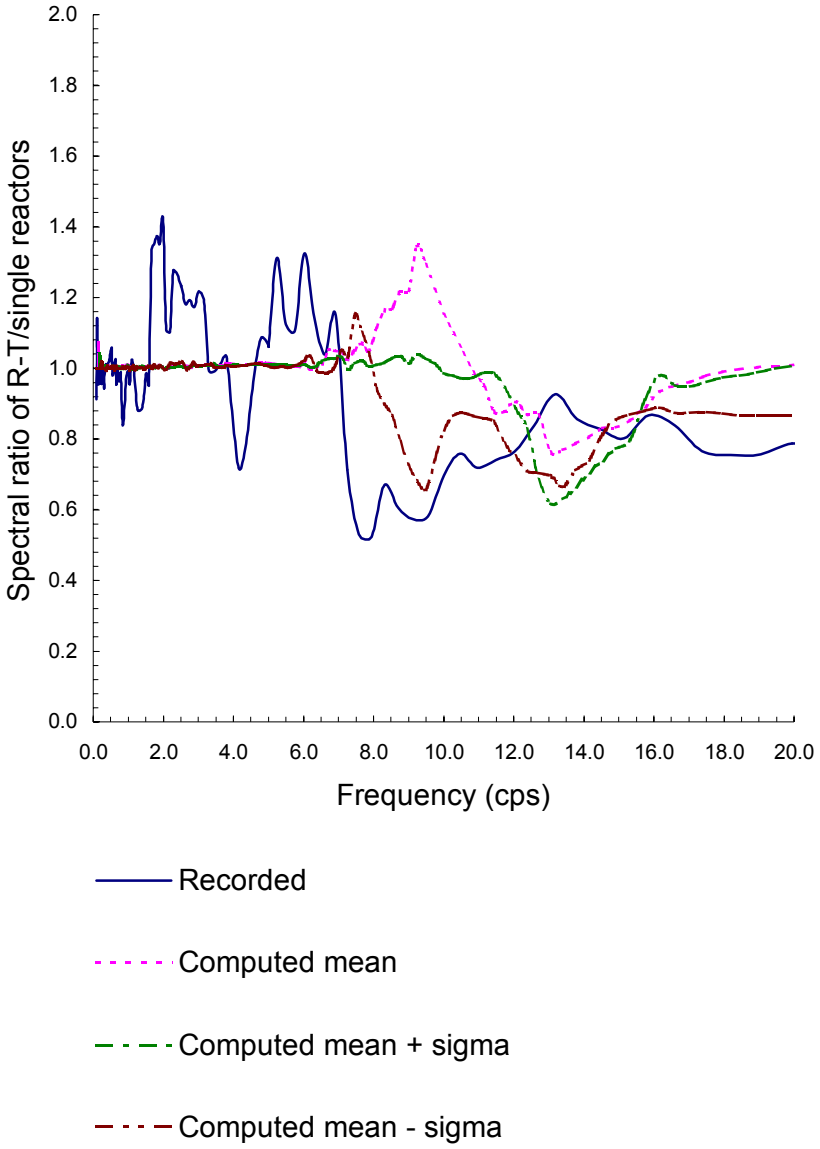

Figure 5-93. Comparison of DCI effect at basemat of embedded R-T Reactor for Earthquake 172x.

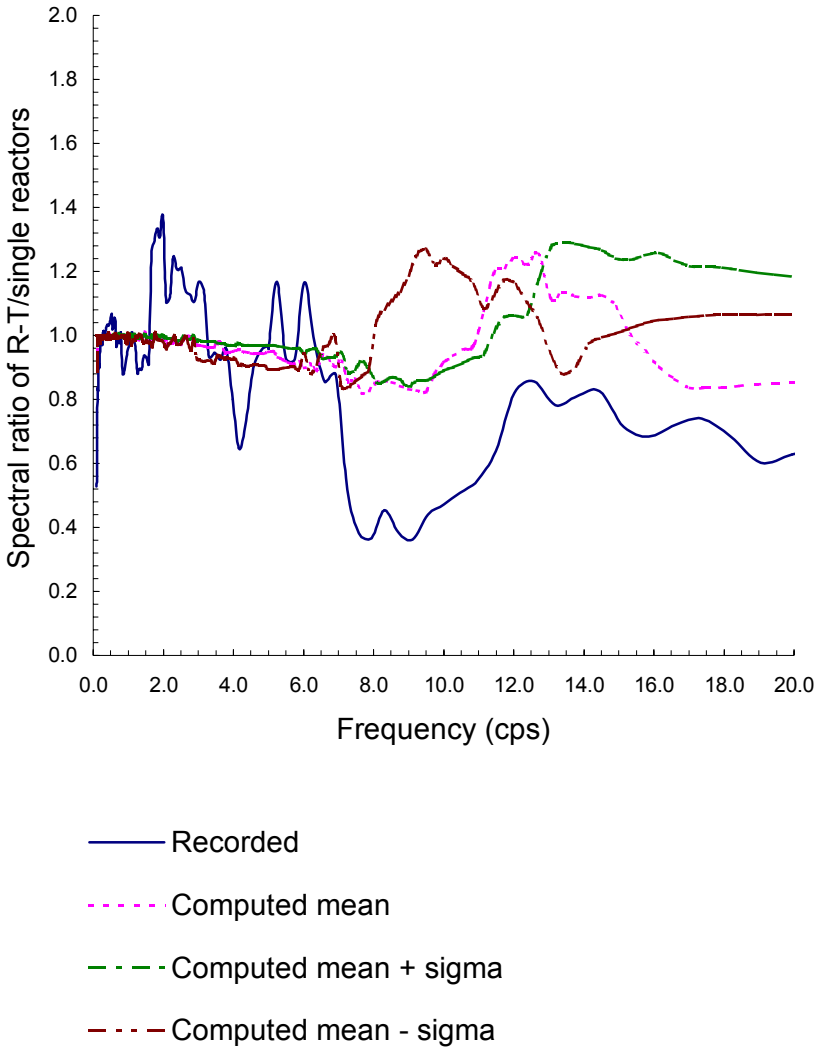

Figure 5-94. Comparison of DCI effect at roof of embedded R-T Reactor for Earthquake 172x.

6.0 CONCLUSIONS AND RECOMMENDATIONS

The Nuclear Power Engineering Corporation (NUPEC) conducted a multi-year test program for the Ministry of Economy, Trade and Industry (METI) of Japan to investigate different aspects of the soil-structure interaction (SSI) effect. The program, consisting of both field and laboratory tests, was developed to address various SSI aspects, including the dynamic cross interaction (DCI) effect on the seismic response of NPP structures built in close proximity to each other. The program also was performed to verify the adequacy of the available analytical tools for predicting the SSI effect. As part of collaborative efforts between the United States and Japan on seismic issues, the US Nuclear Regulatory Commission (NRC) and Brookhaven National Laboratory (BNL) participated in a program to apply the industry practice to predict the structural response to recorded earthquake events, including the DCI effect, and to interpret the observed data. The overall objectives of the US-Japan collaboration on the DCI issue were, through the exchange of mutual knowledge and useful information on the DCI test data, to gain valuable insights into understanding the complex phenomena and dynamic response mechanism of DCI effects under earthquake ground motions. Another objective was to validate, confirm, and capture the limitations of analytical methods or computer codes, which may lead to improvements of the existing analysis methods, and remove unnecessary conservatism in seismic design. BNL has completed its study of the field test data as provided by NUPEC. This report summarizes the BNL study and the insights drawn from the comparisons of the BNL analysis results and the NUPEC field recorded earthquake responses.

The BNL study consisted of two parts: 1) free-field analyses, and 2) SSI response analyses. Four elements were included in the free-field analyses including: 1) Arias intensity analysis, 2) low-strain best estimate soil profile analysis, 3) selection of the appropriate strain degradation model, and 4) probabilistic site identification analysis to determine the strain dependent soil profiles and the surface input motions for the SSI response analyses. BNL has applied the current practice for performing free-field analyses and correlated the analytical results with the recorded data provided by NUPEC. The analyses documented in this report have generally demonstrated the conservatism of the current practice.

The SSI response analyses performed in this study covered three structural configurations, which include the single reactor building, twin reactor buildings and reactor-turbine buildings. BNL analyzed these configurations for both the excavated and embedded conditions. By applying the current approach for the SSI analyses of the NPP structures, BNL performed the seismic response calculations in terms of the mean, mean minus sigma and mean plus sigma values to account for uncertainties in the soil properties (sigma represents the lognormal standard deviation of the soil profile in terms of shear modulus, G_s). As described in this report, the BNL SSI response results either closely matched or exceeded the recorded responses, which further substantiated the conservatism in the analytical procedures as many have suggested. Based on the BNL analyses and comparisons between the analysis results and the recorded earthquake responses, the following conclusions were drawn:

1. The BNL analyses have demonstrated the application of the current approach for addressing uncertainties for SSI analyses. The consideration of soil uncertainties in the SSI analyses is necessary to assure conservatism in the computed structural response.

2. Most of the earthquake data used in this study involved recorded earthquake motions in the range of 0.01g-0.03g and for these earthquakes, the BNL analyses generally enveloped the in-structure response spectra generated from the test data for all configurations.

3. Two (2) moderate size earthquakes: No. 63 (0.1g) and No. 89 (0.13g) were analyzed for both the excavated and embedded single-reactor model (field test data for other configurations were not available). For the embedded case, the analysis enveloped the in-structure response spectra generated from the test data for both No. 63 and No. 89. For the excavated case, the analysis enveloped the in-structure response spectra generated from the test data for No. 63, but did not envelop No. 89. However, by adjusting the soil property for the 0.5m thin layer under the basemat, the analysis was able to match closely No. 89. The effect of the disturbed soil in close proximity to the foundation was found to be an important aspect in the SSI analysis for the excavated cases.

4. Based on the comparison of recorded spectral data, Dynamic Cross Interaction (DCI) effects were observed to be important. For the earthquake data studied, some show that the DCI effects cause amplification in response with respect to the single reactor configuration, while some suggested a reduction of response when compared with the single reactor configuration. The analytic results generally showed conservative estimates of the DCI effect when considering soil uncertainty in the calculations.

5. An increase in frequency at the spectra peak was also observed from the recorded motions with the DCI effect. No similar shift in frequency was noted in the computations.

6. The exceedances caused by the DCI effect were lower for the fully embedded configuration as compared to the excavated configuration.

7. It is not clear that current approaches to SSI response analysis adequately capture potential DCI effects. Additional studies may be required to investigate the impact of this effect on peak structural response.

Based on the BNL analyses, the evaluation of the NUPEC recorded data and the conclusions described above, the following recommendations are made:

1. In light of the smaller earthquake data investigated in this study, the issues related to the DCI effect need to be confirmed for larger magnitude earthquakes comparable to the SSE level for typical NPP safety related structures, systems, and components. The U.S.-Japan collaboration effort should be continued to investigate the availability of other relevant SSI data from strong earthquakes and simulation experiments such as shaking table tests, as well as the possibility of data from future blast tests at a strip mine.

2. The investigation performed in this study indicated the importance of the DCI effect on seismic response, especially the findings concerning the amplifications induced by the DCI effect as compared with situations without the DCI effect. It is recommended that the implication of the findings of this study regarding the DCI effect be assessed with respect to the industry practice and the regulatory guidelines for performing SSI analyses.

3. As the results of this study indicated, some significant influences of the DCI effect on the SSI calculations may be associated with inherent uncertainties in structural properties which may not be adequately captured by the analytical models; e.g, the frequency shift in the twin reactor response. It is recommended that further study be performed to investigate the modeling aspects of SSI analysis for treating adjacent structural effects. As discussed in Section 5.4, the higher mode relative responses between the two identical

adjacent structures may be responsible for the frequency shift as seen in the recorded data. Small uncertainty in the analytical modeling parameters (mass, cg location, etc.) may need to be introduced into the analysis to determine if such higher mode response is significant.

7.0 REFERENCES

Arias, A., 1970, "A Measure of Earthquake Intensity," Seismic Design for Nuclear Power Plants, edited by R. Hansen, The MIT Press.

ASCE 4-98, 1998, "ASCE Standard – Seismic Analysis of Safety Related Nuclear Structures and Commentary on Standard for Seismic Analysis of Safety Related Nuclear Structures," American Society of Civil Engineers.

Chin, M.M., et al., 1998, "Site Response Analysis of Vertical Excitation," ASCE, Geotechnical Earthquake Engineering and Soil Dynamics III, Vol. 1.

Costantino, C.J., Miller, C.A., Heymsfield, E., Yang, A., September, 1999, "CARES: Computer Analysis for Rapid Evaluation of Structures," Version 1.2, Costantino, Miller & Associates for U.S. Nuclear Regulatory Commission.

Costantino, C.J., Silva, W.J., January, 2001, "Considerations in the Evaluation of Site Characteristics on Seismic Response," OECD/NEA Workshop on the Engineering Characterization of Seismic Input, Brookhaven National Laboratory, NEA/CSNI/R(2000)2/Volume 2.

Department of Energy Standard, September, 1995, "Natural Phenomena Hazards Assessment Criteria," DOE-STD-1023-95.

EPRI, 1993, "Guidelines for Determining Design Ground Motions," EPRI TR-102293.

Fletcher R., 1971, "A Modified Marquadt Subroutine for Nonlinear Least Square Records," Harwell Report, AERE-R, 6799.

Fukuoka, A., 1995, "Dynamic Soil-Structure Interaction of Embedded Structure," Trans. 13th SMiRT, Vol. III, Port Alegre.

Geomatrix Consultants Inc., 1991, "Ground Motion Following Selection of SRS Design Basis Earthquake and Associated Deterministic Approach," WSRC Report AA20210s, Prepared for Westinghouse Savannah River Site.

Geotechnical Engineers Inc. (GEI), 1983, "Evaluation of Dynamic Soil Properties for F-Area Sand Filter Structures," Report Prepared for E.I. Dupont de Nemours &Co.

Harp, E.L., et al., 1994, "Shaking Intensity Thresholds for Rock Fall and Slides: Evidence from 1987 Whitter Narrows and Superstition Hill Earthquake Strong-Motion Records," Bulletin of Seismological Society of America, Vol. 85.

Hirotani, T., et al., 2001, "Model Test on Dynamic Cross Interaction of Adjacent Buildings in Nuclear Power Plants – Laboratory Test." Trans. 16th SMiRT, Washington DC.

Idriss, I.M., 1991, "Earthquake Ground Motions at Soft Soil Sites," Proceedings: 2nd Int'l Conf. on Recent Adv. In Geotech. Earthquake Engin. and Soil Dyn., St. Louis, Missouri, Invited Paper LP01, 2265-2272.

Iguchi, M., et al., 1987, “Model Tests on Interaction of Reactor Building and Soil,” Trans. 9th SMiRT, Vol. K1, pp. 317-322, Lausanne, Switzerland.

Joyner, W.B., et al., 1976, “Analysis of Seismograms from a Downhole Array in Sediments near San Francisco Bay,” Bull. Seism. Soc. Am., 66:937-958.

Joyner, W.B., et al., 1981, "The Effect of Quaternary Alluvium of Strong Ground Motion in the Coyote Lake, California Earthquake of 1979," Bull. Seism. Soc. Am., 71(4): 1333-1349.

Kitada, Y., et al., 2001, “Model Test on Dynamic Cross Interaction of Adjacent Buildings in Nuclear Power Plants – Overview and Outline of Earthquake Observation in the Field Test,” Trans. 16th SMiRT, Session K10/5, Washington DC.

Kitada, Y., et al., 1999, “Model Test on Dynamic Structure-Structure Interaction of Nuclear Power Plant Buildings,” Nuclear Engineering and Design (192), 205-216.

Kurita, T., 1997, “Dynamic Characteristics of Soil Deposits Identified from Seismic Records,” Trans. 14th SMiRT, Lyon, France.

Lee, R.C., 1996, “Investigation of Nonlinear Dynamic Soil Properties at the Savannah River Site,” Westinghouse Savanna River Site Report, WSRC-TR-96-0062, Rev.0.

Lysmer, J., et al., 1981, “SASSI – A System for Analysis of Soil-Structure Interaction,” Report No. UCB/GT/81-02, Geotechnical Engineering, University of California, Berkeley.

Lysmer, J., et al., 1999, “SASSI2000 – Theoretical Manual,” Revision 1, Geotechnical Engineering, University of California, Berkeley.

McGuire, R.K., Silva, W.J., Costantino, C.J., October 2001, “Technical Basis for Revision of Regulatory Guidance on Design Ground Motions: Hazard and Risk Consistent Ground Motion Spectra Guidelines,” NUREG/CR-6728, Risk Engineering Inc. for U.S. Nuclear Regulatory Commission.

Naito, Y, et al., 2001, “Model Test on Dynamic Cross Interaction of Adjacent Buildings in Nuclear Power Plants – Field Test,” Trans. 16th SMiRT, Session K15/1, Washington DC.

Nasuda, T., et al., 1991, “Embedment Effect on Soil-Structure Interaction,” Trans. 11th SMiRT, Vol. K1, K06/1, pp. 111-116, Tokyo, Japan.

NUREG-0800, Revision 2, 1989, “Standard Review Plan,” Office of Nuclear Reactor Regulation, U.S. Nuclear Regulatory Commission.

Seed, H.B. and Idriss, I.M., 1969, “The Influence of Soil Conditions on Ground Motions During Earthquakes,” J. Soil Mech. Found. Engin. Div., ASCE, 94:93-137.

Suzuki, A. et al., 2001, “Evaluation of Seismic Input Motions and Responses of Buildings in Nuclear Power Plants,” Proceeding of the OECD/NEA Workshop on the Engineering Characterization of Seismic Input, Brookhaven National Laboratory, Upton, New York, NEA/CSNI/R(2000)2/Volume 2.

USNRC, March 1997, "Identification and Characterization of Seismic Sources and Determination of Safe Shutdown Earthquake Ground Motion," U.S. Nuclear Regulatory Commission, Regulatory Guide 1.165.

Xu, J., et al., 1993, "Integrated Software System for Seismic Evaluations of Nuclear Power Plant Structures," The International Journal of Computers & Structures, Vol. 46, No.4, pp.717-723.

Xu, J., et al., 2001, "Identification of Free-Field Soil Properties Using NUPEC Recorded Ground Motions," Trans. 16th SMiRT, Washington, D.C., U.S.A.

Xu, J., et al., 2002, "Probabilistic Site Identification Analysis Using NUPEC Recorded Free-Field Motions," ASME - PVP, Vancouver, CA.